Annual Report
Jahresbericht

2013

Walther–Meissner–Institut
für Tieftemperaturforschung
Bayerische Akademie der Wissenschaften

Contact:

Prof. Dr. Rudolf Gross
Walther–Meißner–Institut für Tieftemperaturforschung
Bayerische Akademie der Wissenschaften
and
Lehrstuhl für Technische Physik – E23
Technische Universität München

Address:

Walther–Meißner–Str. 8	Phone:	+49 – (0)89 289 14201
D - 85748 Garching	Fax:	+49 – (0)89 289 14206
GERMANY	e–mail:	Rudolf.Gross@wmi.badw.de
	WWW–address:	http://www.wmi.badw.de

Secretary's Office and Administration:

Emel Dönertas	Phone:	+49 – (0)89 289 14202
	Fax:	+49 – (0)89 289 14206
	e–mail:	Emel.Doenertas@wmi.badw.de
		Sekretariat@wmi.badw.de
Ludwig Ossiander	Phone:	+49 – (0)89 289 14205
	Fax:	+49 – (0)89 289 14206
	e–mail:	Ludwig.Ossiander@wmi.badw.de
		Verwaltung@wmi.badw.de

Preface

Dear colleagues, friends, partners, and alumni of the Walther-Meißner-Institute for Low Temperature Research (WMI) of the Bavarian Academy for Sciences and Humanities (BAdW)!

The scientists and students of WMI are pleased to present to you their ***Annual Report 2013***. The report intends to provide you an overview on our last year's teaching and research activities, ranging from fundamental studies in solid state physics, application oriented research, and materials science to technological developments in low temperature, thin film and nanotechnology. Our research interests cover superconductivity and superfluidity, magnetism, ordering and emergent phenomena in correlated electron systems, spin electronics and spin caloritronics, as well as quantum information processing and quantum coherence in solid state systems. As every year, our Annual Report comes early to give you a timely piece of information. It is aiming to provide not only concise summaries of our ongoing research projects and their major results, but also information on our teaching activities as well as statistical data about publications, completed and ongoing Ph.D., diploma, master and bachelor theses, collaborations, funding, and recent developments in infrastructure and experimental facilities.

After the busy year 2012 with the evaluation of the Excellence Cluster ***Nanosystems Initiative Munich (NIM)***, a review of the research strategy and performance of the ***Bavarian Academy for Sciences and Humanities (BAdW)***, as well as an midterm review of the EU network ***Circuit and Cavity Quantum Electro-Dynamics (CCQED)***, the year 2013 fortunately was less demanding regarding review procedures and therefore more productive concerning the scientific research performed at WMI. Nevertheless, we have been successful also in 2013 in extending our long-term collaborative research projects. The ***Transregional Collaborative Research Center TRR 80 "From Correlations to Functionality"*** was granted funding for another four-year period from 2014 until 2017. The same ist true for the ***Priority Program SPP 1450 on "Superconductivity in Iron-Based Compounds"***, which was receiving funding for the period from 2014 to 2016. Moreover, in 2013 a new project entitled ***Exotic Superconductivity in Strongly Anisotropic Correlated Organic Metals in the Vicinity of Insulating Phases*** has been granted by the German Research Foundation (DFG), the EU Collaborative Project entitled ***"Quantum Propagating Microwaves in Strongly Coupled Environments – PROMISCE"*** had a successful midterm review, and finally our application for an International PhD School of Excellence (IDK) entitled ***"Exploring Quantum Matter (EQM)"*** within the ***Elite-Netzwerk Bayern*** was evaluated very positively. We hope that funding for this new graduate school, which we applied for together with Max-Planck Institut für Quantenoptik (MPQ), Ludwig-Maximilians Universität München (LMU) and Technische Universität München (TUM), will start early in 2014.

Our successful research in 2013 is reflected in more than 30 ISI-listed publications, new extramural funding, and fruitful collaborations with international research institutions and industry. The high international visibility of WMI is documented by more than 1300 citations of our publications in 2013 and a large number of invited presentations at national and international conferences. WMI also has organized national and international workshops and conferences, in this way further promoting its scientific visibility. One of the most important assets of WMI is the large number or talented and dedicated students, working in meanwhile crowded laboratories and offices. In this year, the total number of student helpers, bachelor, master/diploma and PhD students was exceeding 50 and thus reaching a new all-time record value. In 2013, 19 bachelor, 8 master/diploma and 4 PhD theses were completed, while 14 master/diploma and 18 PhD students are still ongoing with their work. Without any doubt, our successful research would not be possible without the dedicated and hard work of all scientific and technical staff as well as doctorate, diploma/master and bachelor students. In the same way, an important prerequisite of success in science is the continuous support by

various funding agencies. In this context we gratefully acknowledge financial support from the BAdW, the DFG, the Bavarian Ministry for Science and Arts, the BMBF and the EU. A further key to our success in research is the recruitment of outstanding, scientifically independent group leaders with complementary research interests and technical expertise, a process which is supported and monitored by the scientific advisory board of WMI. We are strongly committed to support and promote young scientists in their career.

Success in science also has some negative aspects. Carrying out a large number or research projects results in a considerable increase of the basic running costs not covered by third-party funding. Hence, although we succeeded to keep the third-party funding at a high level of about 40% of our full cost budget since several years, the budget situation of WMI is becoming increasingly difficult and no longer financially viable. This unfortunate development is mainly caused by the rapid increase of costs for energy. For example, at WMI the costs for electricity increased by a factor of about four within the last 10 years at an almost constant full cost budget. For 2014, we will have to pay probably 150 kEuro only for the so-called EEG-Umlage. The consequences are missing investments in the technical infrastructure and replacements of important instruments. It is high time that the Bavarian Ministry for Science and Arts takes appropriate measures to keep up the international competitiveness of WMI.

I hope that our Annual Report 2013 inspires your interest in WMI. I take this opportunity to thank all the colleagues, guests, students, post–docs and cooperating partners, who contributed to our research and teaching activities within the last year, and last but not least all our friends and sponsors for their interest, trust and continuous support.

Rudolf Gross

Garching, December 2013

the majority of the WMI team members

Contents

The Walther–Meißner–Institute

General Information

The Walther–Meißner–Institute for Low Temperature Research (WMI) is operated by the Commission for Low Temperature Research of the Bavarian Academy of Sciences and Humanities (BAdW). The commission was founded in 1946 on Walther Meißner's initiative, who was president of BAdW from 1946 to 1950. The Commissions (Research Groups) of the Academy are set up in order to carry out long–term projects, which are too ambitious for the lifetime or capacity of any single researcher, or which require the collaboration of specialists in various disciplines. At present, the Bavarian Academy of Sciences and Humanities consists of 36 Commissions with more than 300 employees.

The Commission for Low Temperature Research of the BAdW started its research activities in 1946 in the Herrsching barracks. After the retirement of Walther Meißner in 1952, Heinz Maier-Leibnitz, who followed Walther Meißner on the Chair for Technical Physics of the Technische Universität München, became the new head of the Commission for Low Temperature Research. In 1967, the commission moved to the Garching research campus after the construction of the new "Zentralinstitut für Tieftemperaturforschung" (ZTTF) was completed (director: Prof. Heinz Maier-Leibnitz, technical director: Prof. Franz Xaver Eder). Until 1972, the theory group of the Institute Laue Langevin was hosted at the ZTTF. In 1980, Prof. Dr. Klaus Andres became the new director of the ZTTF again associated with the Chair for Technical Physics (E23) at the Technische Universität München, followed by Prof. Dr. Rudolf Gross in 2000. In 1982, the ZTTF was renamed into Walther-Meißner-Institute for Low Temperature Research (WMI) on the occasion of Walther Meißner's 100. birthday.

As already mentioned, it is a long tradition that WMI hosts the Chair for Technical Physics (E 23) of the Technische Universität München (TUM) with the director of the WMI being a full professor at the Faculty of Physics of TUM. However, there are also close ties with the Ludwig-Maximilians-Universität (LMU). Between 2004 and 2010, WMI hosted a scanning probe division with the head of this division being a professor at the Ludwig-Maximilians-Universität (LMU). In this way a tight collaboration has been established between WMI and research groups of both Munich universities, joining technological and human resources in the fields of experimental and theoretical solid-state and condensed matter physics, low temperature techniques, materials science as well as thin film and nanotechnology. Noteworthy, the WMI supplies liquid helium to more than 25 research groups at both Munich universities and provides the technological basis for low temperature research.

Research Activities

The research activities of the Walther–Meißner–Institute are focused on low temperature solid-state and condensed matter physics (see reports below). The research program is devoted to both **fundamental** and **applied research** and also addresses **materials science, thin film and nanotechnology** aspects. With respect to **basic research** the main focus of the WMI is on

- superconductivity and superfluidity,
- magnetism, spin transport, spin mechanics and spin caloritronics,
- quantum phenomena and quantum coherence in mesoscopic systems and nanostructures,
- circuit-quantum electrodynamics and circuit-nanomechanics,
- ordering and emergent phenomena in correlated electron systems,
- and the general properties of metallic systems at low and very low temperatures.

The WMI also conducts **applied research** in the fields of

- solid-state quantum information processing systems,
- superconducting and spintronic devices,
- oxide electronics,
- multi-functional and multiferroic materials,
- and the development of low and ultra low temperature systems and techniques.

With respect to **materials science, thin film and nanotechnology** the research program is focused on

- the synthesis of superconducting and magnetic materials,
- the single crystal growth of oxide materials,
- the thin film technology of complex oxide heterostructures including multifunctional and multiferroic material systems,
- and the fabrication of superconducting, magnetic, and hybrid nanostructures.

The WMI also develops and operates systems and techniques for low and ultra–low temperature experiments. A successful development have been dry mK-systems that can be operated without liquid helium by using a pulse-tube refrigerator for precooling. Meanwhile, these systems have been successfully commercialized by the company VeriCold Technologies GmbH at Ismaning, Germany, which was taken over by Oxford Instruments in 2007. As further typical examples we mention a nuclear demagnetization cryostat for temperature down to below 100 µK, or very flexible dilution refrigerator inserts for temperatures down to about 20 mK mK fitting into a 2 inch bore. These systems have been engineered and fabricated at the WMI. Within the last years, several dilution refrigerators have been provided to other research groups for various low temperature experiments. The WMI also operates a helium liquifier with an annual capacity of well above 150.000 liters and supplies both Munich universities with liquid helium. To optimize the transfer of liquid helium into transport containers the WMI has developed a pumping system for liquid helium that is commercialized in collaboration with a company.

To a large extent the research activities of WMI are integrated into national and international research projects such as Clusters of Excellence, Collaborative Research Centers, Research Units, or EU projects. The individual research groups of WMI offer a wide range of attractive research opportunities for diploma (graduate) students, PhD students and postdoctoral fellows.

Experimental Facilities and Resources

The WMI is equipped with state of the art facilities for the preparation and characterization of superconducting and magnetic materials as well as for various low and ultra–low temperature experiments. The main experimental and technological resources of WMI are listed in the following.

Materials Preparation and Fabrication of Nanostructures

- Laser Molecular Beam Epitaxy (L-MBE) system for oxide heterostructures (equipped with in–situ RHEED, Omicron AFM/STM system, atomic oxygen/nitrogen source, infrared-laser heating system, metallization)
- molecular beam epitaxy (MBE) system for metallic systems
- UHV magnetron sputtering systems for metals (e.g. Nb, Al, NiPd, ...)

- magnetron sputtering system for oxide heteroepitaxy (equipped with four sputtering guns and an oxygen ion gun)
- reactive ion etching (RIE) system, Plasmalab 80 Plus with ICP plasma source, Oxford Instruments Plasma Technology
- ion beam etching (IBE) system equipped with a LN_2 cooled sample holder
- polishing machine for substrate preparation
- ultrasonic bonding machine
- 50 m^2 class 1000 clean room facility
- optical lithography (Süss maskaligner MJB 3 and projection lithography)
- electron beam lithography (based on Philips XL 30 SFEG scanning electron microscope and Raith Elphy Plus lithography system including a laser stage)
- four-mirror image furnace for crystal growth

Characterization

- 2–circle x–ray diffractometer (Bruker D8 Advance, sample temperature up to 1 600°C)
- high resolution 4–circle x–ray diffractometer with Göbel mirror and Ge monochromator (Bruker D8 Discover)
- scanning electron microscope with EDX analysis
- UHV room temperature AFM/STM system
- 2048 u high resolution mass spectrometer (Fa. Pfeiffer, cross-beam ion source, SEM)
- Low Energy Electron Diffraction (SPECTA-LEED, Fa. Omicron)
- two Raman spectroscopy systems (1.5 to 300 K, in-situ sample preparation)
- SQUID magnetometer (Quantum Design, 1.5 to 700 K, up to 7 T)
- several high field magnet systems (up to 17 T Tesla) with variable temperature inserts
- 7 T split coil magnet systems with optical access and variable temperature insert
- 3D vector magnet (2/2/6 Tesla) with variable temperature inserts
- experimental set–ups for the measurement of noise including low noise SQUID amplifiers and signal analyzers
- high-frequency network analyzers (up to 40 GHz) and various microwave components (sources, mixers, circulators, attenuators) for the determination of high frequency parameters
- ultra-sensitive microwave receiver for state tomography of quantum microwaves (dual path method with FPGA signal processing)
- high-frequency cryogenic probing station (up to 20 GHz, $T > 4$ K)
- magnetooptical Kerr effect (MOKE) system
- ferromagnetic resonance (FMR) system

Low temperature systems and techniques

- 5 K-Scanning Tunneling Microscope (low temperature STM, Fa. Omicron)
- several ^{3}He/^{4}He dilution refrigerator inserts for temperatures down to 10 mK
- "dry" mK-cooler based on a dilution refrigerator with pulse-tube precooling
- "dry" dilution refrigerator with a base temperature of about 10 mK equipped with a 3D vector magnet (1/1/6 Tesla)
- ultra–low temperature facility for temperatures down to below 100 µK based on a nuclear demagnetization cryostat
- experimental set–ups for the measurement of specific heat, magnetization, thermal expansion as well as electrical and thermal transport properties as a function of temperature, magnetic field and pressure

Joint Research Projects

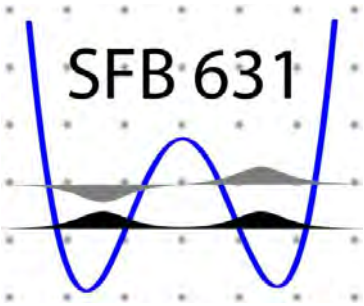

SPP 1285

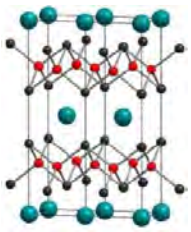

SPP 1458

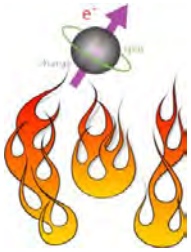

SPP 1538

The Collaborative Research Center 631

F. Deppe, R. Gross, H. Hübl, A. Marx[1]

The **Collaborative Research Center 631 (SFB 631) on Solid State Quantum Information Processing** was established in 2003 and extended for a second and a third four-year funding in 2007 and 2011, respectively. The third funding period will last until June, 2015.

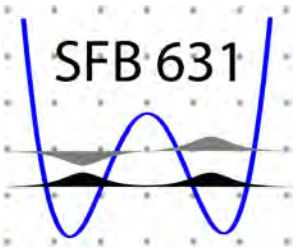

Since the start of SFB 631 a decade ago, quantum information science has developed into a fascinating and one of the most rapidly growing fields of science and technology. It resides at the interface between physics, mathematics, computer and materials science, and engineering. It is concerned with both fundamental questions and technological developments, aiming at the realization of a useful quantum information hardware.

At WMI, the study of the physics of solid state quantum systems has developed into a key research field. Besides superconducting quantum circuits, the research activities of WMI meanwhile include also quantum spin systems and mechanical systems, as well as systems combining different degrees of freedom in quantum hybrid structures. Our research within SFB 631 does not only provide the foundations of quantum information systems and quantum technology, but also addresses key fundamental questions regarding quantum coherence, quantum dynamics and decoherence processes in solid state quantum systems. Furthermore, it requires extremely sensitive measurements at low and ultra-low temperatures and therefore perfectly fits to the research profile of WMI.

The research effort of SFB 631 is highly collaborative and interdisciplinary. To cover the broad spectrum of fundamental and application oriented questions related to solid state quantum information systems in a comprehensive way, SFB 631 joins research activities from quantum information theory, experimental and theoretical solid state physics, quantum optics, materials science, and nanotechnology. Today, within SFB 631 research groups from the Bavarian Academy of Sciences and Humanities (BAdW), the TU Munich (TUM), the Ludwig-Maximilians-University (LMU), the Max-Planck-Institute for Quantum Optics (MPQ), as well as Augsburg and Regensburg University are collaborating in 17 research projects. At present, SFB 631 joins more than 30 principal investigators and more than 60 Ph.D. and diploma students, as well as a large number of postdocs and guest scientists. WMI is one of the main actors, not only being involved in the three projects A3 (Gross, Hübl, Marx), A8 (Gross, Marx, Deppe) and C3 (Hübl), but also providing the coordination of the center from the beginning (spokesman: Rudolf Gross).

Within the project A3 on *Superconducting Quantum Circuits as Basic Elements for Quantum Information Processing* and project A8 on *Cavity Quantum Electrodynamics with Superconducting Devices*, the research program of WMI within SFB 631 is focusing on the fabrication and study of superconducting quantum information circuits. This includes the fabrication of superconducting flux qubits in which quantum mechanical superposition states of clockwise and counter-clockwise circulating persistent currents are used for the realization of solid state qubits. A particular development of WMI is the realization of flux qubits with tunable gap which offer more flexibility in circuit design [1]. These qubits are coupled to superconducting microwave resonators. In this way fascinating quantum electrodynamic experiments with deliberately designed artificial solid state atoms become possible. Since such experiments are

[1]This work is supported by the German Research Foundation through SFB 631.

completely analogous to quantum optical experiments on natural atoms in optical resonators, this prospering new field is called circuit quantum electrodynamics (circuit QED). Here, particular goals are the strong and ultra-strong coupling [2] of superconducting qubits to high-quality superconducting microwave resonators, the generation and detection of non-classical microwave states (e.g. Fock or squeezed states), the development of dispersive readout and quantum non-demolition measurements, and the entanglement of superconducting qubits via multiple resonators. Regarding these research goals the WMI team closely collaborates with the theory groups at LMU (von Delft), the University of Augsburg (Hänggi), the Universidad del País Vasco - Euskal Herriko Unibertsitatea at Bilbao (Solano), and the Instituto de Física Fundamental at Madrid (Garcia-Ripoll), as well as the experimental groups at the NTT Basic Research Laboratories (Semba) and the Nano Electronics Research Laboratories at NEC Corporation, Japan (Nakamura, Tsai, Yamamoto). The research work within SFB 631 is also closely linked to the activities within Research Area I of the Cluster of Excellence *Nanosystems Initiative Munich (NIM)* (see pp. 15–18).

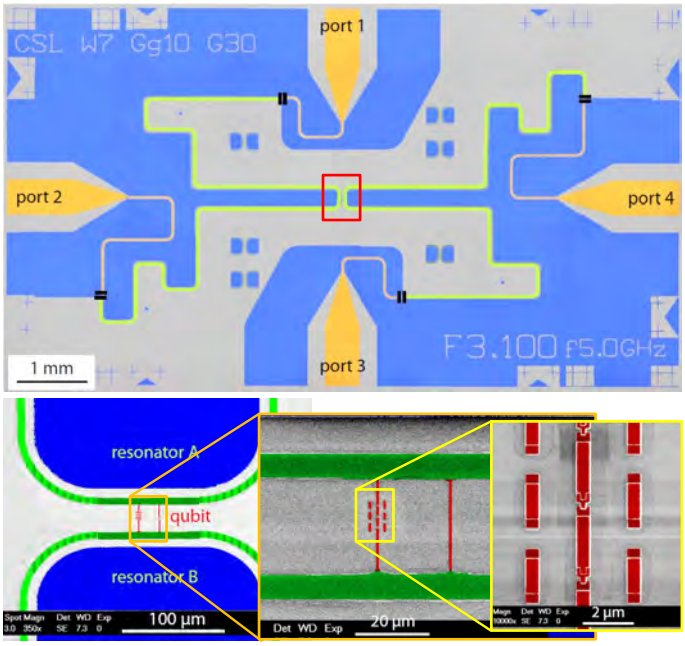

Figure 1: Top: Optical micrograph showing the circuit design of a superconducting quantum switch. Bottom: Parts of the coupling region marked in the upper subfigure by the red rectangle shown on an enlarged scale. The green structures represent the inner conductors of the two coplanar waveguide resonators, the red ones the galvanically coupled qubit loop with the three Al/AlO_x/Al Josephson junctions.

Analogous to the field of cavity quantum electrodynamics (cavity QED), in circuit QED the interaction between light and matter is studied. In 2013, we could realize a central element of superconducting circuit QED, a so-called quantum switch [3, 4] providing tunable and switchable coupling between two superconducting resonators via a superconducting flux quantum bit (see report by A. Baust *et al.*, pp. 33–35). The coupling of the two resonators via a single flux qubit allows for the realization of a tunable coupling which depends on the qubit state. Most importantly, the two resonators can be completely decoupled by setting the magnetic flux through the qubit such that the dynamical coupling just compensates for the geometric coupling, yielding effective zero coupling between the two resonators. The quantum switch circuit also can be used to create entangled quantum states. We successfully implemented a quantum switch consisting of two superconducting coplanar stripline resonators and a flux qubit, all fabricated on the same chip. Spectroscopy measurements demonstrated the switching between the coupled and the decoupled state. The setup allowed us to achieve an on-off ratio sufficient for many applications in quantum information systems. As shown in the report by A. Baust *et al.* (see pp. 33–35), we also could perform time domain experiments on the quantum switch, making the switchable coupling directly observable. In this way we could provide direct experimental evidence for the expected switching behavior, as the transfer of energy from one into another resonator controlled by the qubit state could be directly observed.

In circuit QED architectures with multiple qubits and resonators, meanwhile quantum logic gates have been successfully realized [5, 6]. However, while the requirements for such digital

quantum computing circuits are still enormous, analog quantum simulation with circuit QED systems appears to be a technologically less demanding, and therefore interesting goal. In analog quantum simulations, one mimics the Hamiltonian of a system of interest with a circuit offering a higher degree of controllability than the original system. In this context, one specific proposal is to strongly couple nonlinear resonators to explore Bose-Hubbard physics in the driven-dissipative regime [7, 8]. For such experiments, a scalable approach to tunable coupling between the resonators is strongly desirable. As shown by the report of Wulschner *et al.* (see pp. 65–66), we achieved promising experimental progress in this direction. We successfully fabricated two LC microwave resonators coupled via an RF SQUID [9], representing basic building blocks of superconducting quantum simulators.

After having demonstrated for the first time path entanglement of propagating quantum microwaves using superconducting circuits and quantum signal recovery techniques [11–13], we successfully realized squeezed coherent states with a flux-driven Josephson parametric amplifier (see Ref. [10] and report by L. Zhong *et al.*, pp. 67–68). Josephson parametric amplifiers (JPAs) are promising devices to achieve low-noise amplification. In the non-degenerate mode, JPAs behave like linear amplifiers with noise temperature approaching the standard quantum limit dictated by the Heisenberg uncertainty relation. In the degenerate mode, JPAs are phase sensitive amplifiers which can amplify a signal quadrature with a noise temperature below the standard quantum limit of linear amplifiers, and at the same time squeeze another quadrature below the vacuum fluctuations. In this way, JPAs allowed us to study the squeezing physics of propagating quantum microwaves. We used the dual-path state reconstruction method developed at WMI [11–13] and applied it to the study of squeezed coherent states generated by a flux-driven JPA [10]. Moreover, we successfully analyzed the noise properties of a flux-driven parametric amplifier with the WMI dual-path state reconstruction method (see Refs. [12–14] and report by L. Zhong *et al.*, pp. 69–70)

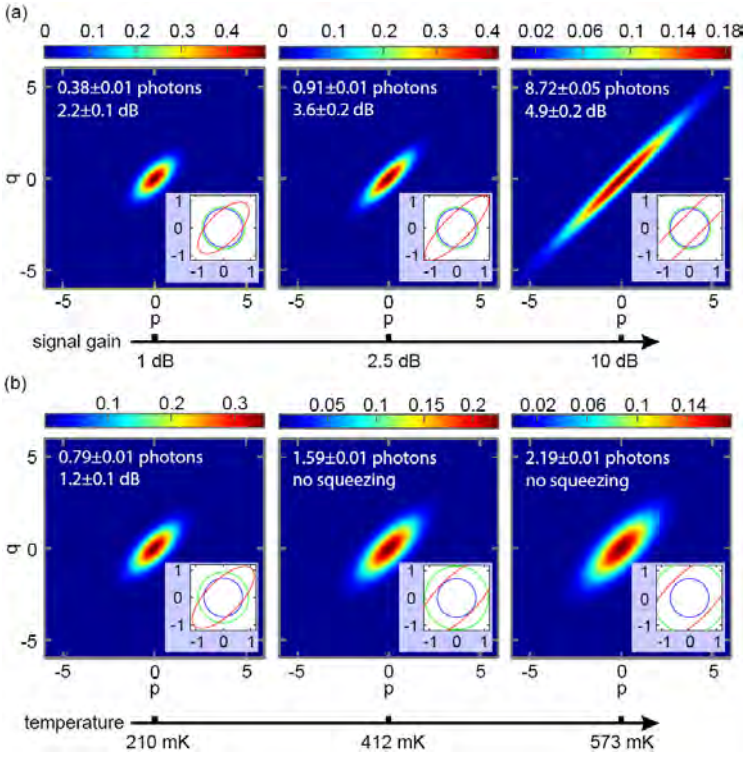

Figure 2: Reconstructed Wigner functions (color map) of squeezed vacuum and squeezed thermal states incident at the input port of the microwave beam splitter. p and q are dimensionless quadrature variables spanning the phase space. The insets show the $1/e$-contours of the ideal vacuum (blue), the experimental vacuum or thermal states (green), and the squeezed vacuum or squeezed thermal states (red). (a) Constant 30 dB-attenuator temperature of 50 mK. (b) Constant signal gain of 1 dB. Reprinted from Ref. [10].

In a fruitful collaboration with the Finley group at Walter Schottky Institute, we deposited NbN thin films by DC magnetron sputtering on [100] GaAs substrates, optimized their quality, and demonstrated their use for efficient single photon detection in the near-infrared [15]. Meanwhile the superconducting single photon detectors (SSPDs) have been successfully used for the efficient on-chip time resolved detection of quantum dot emission. The quantum light emitted by the self-assembled InGaAs quantum dots (QDs) was routed into the optical modes

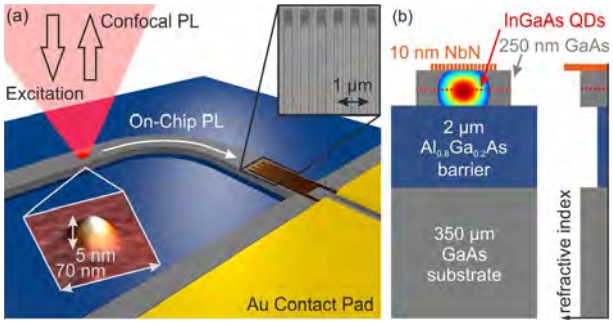

Figure 3: (a) Self assembled InGaAs quantum dots embedded in a GaAs ridge waveguide are excited using a helium neon laser. The light emitted by the quantum dots is detected either in a confocal geometry or guided along the waveguide and evanescently coupled into a NbN SSPD. (b) Layer structure of the sample as prepared by molecular beam epitaxy and reactive magnetron sputtering. Reprinted from Ref. [16].

of a GaAs ridge waveguide and detected on-chip via evanescent coupling to the NbN SSPD [16].

We also considerably extended the experimental facilities for ultra low-noise experiments on superconducting quantum circuits. As shown in the report by J. Goetz *et al.* (see pp. 75–76) the new dilution refrigerator in the Quantum Laboratory K04 has been improved regarding cooling power. Furthermore, a new liquid helium dewar and measurement equipment has been installed, allowing now for demanding experiments on superconducting quantum circuits. The setting up of a new cryogen-free dilution refrigerator with a pulse tube refrigerator (PTR) precooling and a large sample stage in the Quantum Laboratory K21 is approaching completion. All components for the 1 K-stage and for the dilution circuit have been fabricated in the WMI workshop and the wiring for thermometry down to the mixing chamber plate has been installed (see report by A. Marx *et al.*, pp. 77–78).

References

[1] M. J. Schwarz, J. Goetz, Z. Jiang, T. Niemczyk, F. Deppe, A. Marx, and R. Gross. Gradiometric flux qubits with tunable gap. arXiv:1210.3982 (2012).
[2] T. Niemczyk, F. Deppe, H. Huebl, E. P. Menzel, F. Hocke, M. J. Schwarz, J. J. Garcia-Ripoll, D. Zueco, T. Hummer, E. Solano, A. Marx, and R. Gross, Nat Phys **6**, 772–776 (2010).
[3] E. Hoffmann. *Experiments on Two-Resonator Circuit Quantum Electrodynamics: A Superconducting Quantum Switch*. Ph.D. thesis, TU München (2013).
[4] M. Mariantoni, F. Deppe, A. Marx, R. Gross, F. Wilhelm, and E. Solano, Phys. Rev. B **78**, 104508 (2008).
[5] E. Lucero, R. Barends, Y. Chen, J. Kelly, M. Mariantoni, A. Megrant, P. O. Malley, D. Sank, A. Vainsencher, J. Wenner, T. White, Y. Yin, A. N. Cleland, and J. M. Martinis, Nature Phys. **8**, 719–723 (2012).
[6] A. Fedorov, L. Steffen, M. Baur, M. P. da Silva, and A. Wallraff, Nature **481**, 170–172 (2011).
[7] M. Leib, and M. J. Hartmann, New J. of Phys. **12**, 093031 (2010).
[8] M. Leib, F. Deppe, A. Marx, R. Gross, and M. J. Hartmann, New Journal of Physics **14**, 075024 (2012).
[9] B. Peropadre, D. Zueco, F. Wulschner, F. Deppe, A. Marx, R. Gross, and J. Garcia-Ripoll, Phys. Rev. B **87**, 134504 (2013).
[10] L. Zhong, E. P. Menzel, R. D. Candia, P. Eder, M. Ihmig, A. Baust, M. Haeberlein, E. Hoffmann, K. Inomata, T. Yamamoto, Y. Nakamura, E. Solano, F. Deppe, A. Marx, and R. Gross, New Journal of Physics **15**, 125013 (2013).
[11] E. P. Menzel, R. Di Candia, F. Deppe, P. Eder, L. Zhong, M. Ihmig, M. Haeberlein, A. Baust, E. Hoffmann, D. Ballester, K. Inomata, T. Yamamoto, Y. Nakamura, E. Solano, A. Marx, and R. Gross, Phys. Rev. Lett. **109**, 250502 (2012).
[12] E. P. Menzel, F. Deppe, M. Mariantoni, M. A. Araque Caballero, A. Baust, T. Niemczyk, E. Hoffmann, A. Marx, E. Solano, and R. Gross, Phys. Rev. Lett. **105**, 100401 (2010).
[13] E. P. Menzel. *Propagating Quantum Microwaves: Dual-path State Reconstruction and Path Entanglement*. Dissertation, Technische Universität München (2013).
[14] R. Di Candia, E. P. Menzel, L. Zhong, F. Deppe, A. Marx, R. Gross, and E. Solano. Dual-Path Methods for Propagating Quantum Microwaves. Accepted for publication in New J. of Phys., arXiv:1308.3117 (2013).
[15] G. Reithmaier, J. Senf, S. Lichtmannecker, T. Reichert, F. Flassig, A. Voss, R. Gross, and J. J. Finley, Journal of Applied Physics **113**, 143507 (2013).
[16] G. Reithmaier, S. Lichtmannecker, T. Reichert, P. Hasch, K. Mueller, M. Bichler, R. Gross, and J. J. Finley, Scientific Reports **3**, – (2013).

The Cluster of Excellence "Nanosystems Initiative Munich – NIM"

F. Deppe, S.T.B. Gönnenwein, R. Gross, H. Hübl, A. Marx[1]

The excellence cluster ***Nanosystems Initiative Munich (NIM)*** comprises internationally recognized expertises in all relevant research areas of nanosciences, ranging from quantum nanophysics to the creation and study of nanosystems for biophysics and the life sciences. NIM's overall scientific vision is to integrate nanometer sized building blocks as well as bio-molecular assemblies into entire functional systems.

NIM was launched in 2006. The first six-year funding period of NIM ended in October 2012. After an intermediate evaluation, NIM was granted a further five-year funding period until end of 2017. NIM joins research groups from LMU Munich, TU Munich, WMI, the University of Augsburg, the Munich University of Applied Science, the Max-Planck-Institutes for Biochemistry and Quantum Optics, and the Deutsches Museum. NIM's future research activities are organized in five research areas (RAs) as shown in the figure: RA I – ***Quantum Nanophysics***, RA II – ***Hybrid Nanosystems***, RA III – ***Nanosystems for Energy Conversion***, RA IV – ***Biomolecular Nanosystems***, and RA V – ***Biomedical Nanotechnologies***. At WMI, several scientists (Deppe, Gönnenwein, Gross, Hübl, Marx) actively contribute to the ambitious research program of the second funding period of NIM. The physics of quantum nanosystems is one of the main future research directions of NIM, in perfect agreement with the focus of several research activities at WMI. The major contributions of WMI are to RA I: ***Quantum Nanophysics*** and RA II: ***Hybrid Nanosystems***. Research area I is coordinated by R. Gross of WMI.

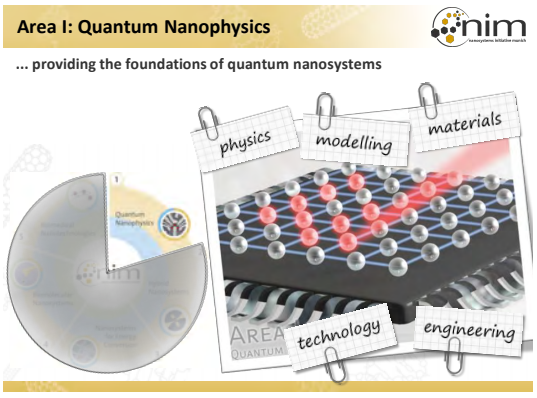

The scientific program of ***Research Area I*** is focused on quantum nanosystems. It aims at the modeling and understanding of such nanosystems on a quantum level. The modelling and understanding of nanosystems on a quantum level is a key prerequisite for their application in hybrid devices, energy conversion systems as well as in biomolecular and biomedical systems. The scientific program of research area I addresses this fundamental problem by systematically studying quantum systems based on solid state nanostructures and tailor-made meso-scale many body systems realized in optical lattices.

A particular objective of the WMI activities within RA I is the systematic study of the interaction between nanoscale solid state quantum systems and the modes of electromagnetic fields on a single quantum level. To this end, we could realize strong coupling between the magnetic

[1]This work is supported by the German Excellence Initiative via the Nanosystems Initiative Munich (NIM).

excitations of a ferrimagnetic systems (magnons) and those of a superconducting microwave resonator (photons) (see Ref. [1] and report by J. Lotze *et al.*, pp. 54–56). In this field the research activities within NIM are closely linked to those of SFB 631 described already above (see pp. 11–14). The WMI research activities also aim at the study of pure spin currents in the quantum regime. It is planned to perform spin pumping experiments in ferromagnet/normal metal or antiferromagnet/normal metal structures in the limit of mK temperatures and single microwave photons. A number of successful experiments in this direction already have been performed (see Refs. [2–6] and report by M. Schreier *et al.*, pp. 60–62).

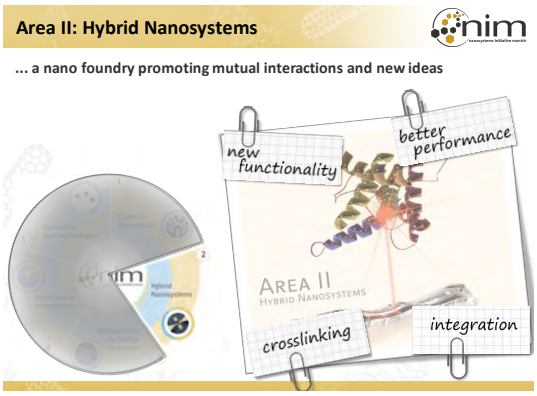

The ***Research Area II*** on Hybrid Nanosystems is NIM's main nanofoundry, where a great variety of solid state and nano-bio-systems are fabricated by advanced top-down and smart bottom-up approaches. Within RA II, WMI investigates the interaction of light with magnonic excitations using near-field and nano-optical effects (in collaboration with Grundler, TUM). Metallic nanostructures integrated into magnetic devices are used to locally enhance the light-induced electrical field due to plasmonic effects and to extend the wavevector spectrum by exploiting evanescent waves. Also, the coupling of magnonic and phononic modes is investigated in ferromagnetic/ferroelectric hybrid devices (in a cooperation with Krenner/Wixforth, University of Augsburg, and Weig, University of Konstanz). We already have shown that in such devices a surface acoustic wave (SAW) propagating in the ferroelectric induces local, radio-frequency, elastic strains in the adjacent ferromagnet [7]. This allows to elastically drive magnetization dynamics, and makes hypersound ferromagnetic resonance experiments with submicron spatial resolution possible. Recently, we have demonstrated magnetoelastic coupling between the mechanical modes of a Si_3N_4 nanobeam and the magnetic degrees of freedom of a Co film deposited on it.

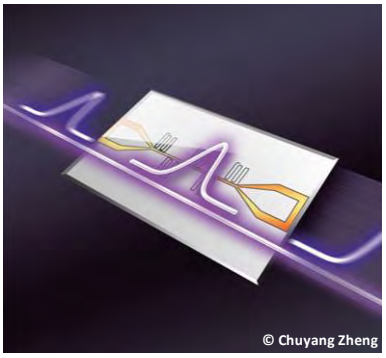

A successful new research field started at WMI some years ago is nanomechanics. In a collaboration with E. Weig, University of Konstanz, and T. Kippenberg, EPFL Lausanne, we have successfully fabricated electro-mechanical nanosystems consisting of a Si_3N_4/Nb nanobeam coupled to a high quality factor superconducting microwave resonator (see Refs. [8–10] and report by H. Huebl *et al.*, pp. 36–38). These hybrid systems combine two platforms that have traditionally been studied in separate contexts: Superconducting microwave circuits are essentially printed circuit boards that operate at very high frequencies (10 GHz) and low temperatures (0.05 K above absolute zero). In recent years, these circuits have been established as one of the most promising candidates for future quantum information processors, due to their excellent coherence, operation speed and scalability. Nanomechanical oscillators, on the other hand, have been under physicists' scrutiny for the yet unexplored quantum aspects of their vibrational motion, probing the laws of quantum mechanics in an unprecedentedly literal sense. We could realize a coupling between the microwave field and the vibration of a nanomechanical beam in an on-chip platform of finger nail size. The coupling proceeds by a tiny capacitance change in the circuit induced by the motion of the nanomechanical beam. By analogy with phenomena known in atomic and optical physics, we found that the nanomechanical oscillator can mediate interference between microwaves, resulting in interesting features such as electro-mechanically induced transparency (EMIT) [8] and ab-

sorption (EMIA) [9, 10], and can be exploited to control the propagation of microwave signals. In particular, we could create spectrally extremely sharp transmission windows (linewidth 10 Hz) for microwave radiation, which are accompanied by very long delays on the order of 10 milliseconds [8–10]. We also addressed more subtle questions with regard to the possible temporal dynamics of the control that have been debated among experts, and found full agreement with their expectations [8, 10]. Another important result was that our system is capable of operating in a regime in which decoherence, a potentially detrimental effect for the processing of quantum information, is not a critical issue. In summary, we developed a platform to manipulate wave propagation in a fully integrated architecture without the need of photon detection and regeneration. Its implications extend to the field of quantum computing and quantum information processing.

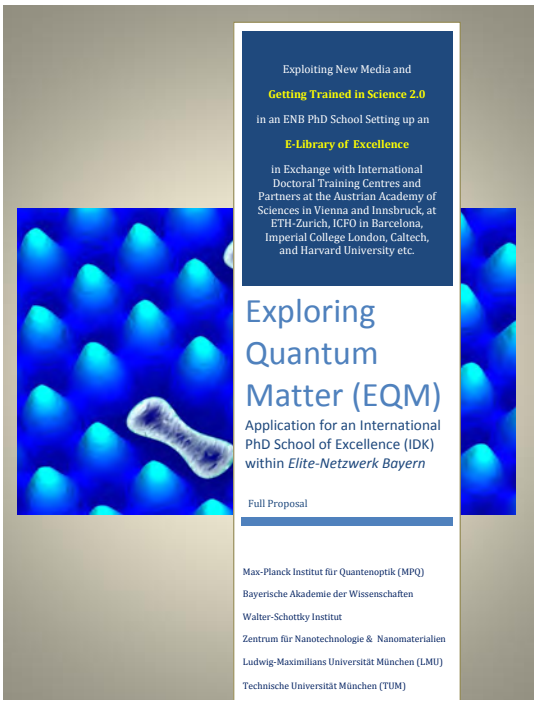

In order to unite the unique competences in quantum physics in Munich and extend them into an international excellence network of doctoral training centres with partners at the Austrian Academy of Science in Vienna and Innsbruck, at ETH Zurich, ICFO Barcelona, Imperial College London, Caltech, and Harvard, we applied for an International PhD School of Excellence (IDK) entitled ***"Exploring Quantum Matter (EQM)"*** within Elite-Netzwerk Bayern in 2013. The proposal has been evaluated very positively and the final decision on funding will be made in January 2014. The participating institutions are Max-Planck Institut für Quantenoptik (MPQ), Walther-Meißner-Institut of BAdW, Walter-Schottky Institut, Ludwig-Maximilians Universität München (LMU), and Technische Universität München (TUM). Exploring Quantum Matter from few-body interactions to artificial many-body systems will provide a common research focus to unite the competences of leading research groups in Munich in an interdisciplinary, professional and unified manner: quantum many-body systems will be studied in experimental and theoretical physics, material science, mathematics, computer science, and chemistry.

The particular focus of WMI within the applied International PhD School of Excellence will be ***"Scalable networks of solid-state quantum circuits"***, which are becoming increasingly attractive for quantum simulations. For example, networks of nonlinear superconducting transmission line resonators or optical nanocavities can be used as scalable quantum simulators for the Bose-Hubbard Hamiltonian. The resonators are made nonlinear by a controllable coupling to superconducting or semiconductor quantum bits, thereby forming harmonic oscillators with tunable Kerr nonlinearity. Networks of these entities would be particularly well suited for accessing the strongly correlated regime and for investigating quantum many-body dynamics of interacting particles under the influence of driving and dissipation. Solid state quantum circuits with multiple drives are another attracting system. E.g., superconducting quantum bits strongly coupled to a resonator field mode and subjected to multiple classical drives can be used for quantum simulations of relativistic quantum physics (e.g. dynamics of the Dirac equation, Klein paradox). The key advantage is the controllability of the relevant physical parameters via the strength of the longitudinal and two transverse drives. Moreover, quantum bits with two-tone multiple drives can be used for quantum simulation of strong and ultra-strong coupling dynamics.

References

[1] H. Huebl, C. W. Zollitsch, J. Lotze, F. Hocke, M. Greifenstein, A. Marx, R. Gross, and S. T. B. Goennenwein, Phys. Rev. Lett. **111**, 127003 (2013).

[2] H. Nakayama, M. Althammer, Y.-T. Chen, K. Uchida, Y. Kajiwara, D. Kikuchi, T. Ohtani, S. Geprägs, M. Opel, S. Takahashi, R. Gross, G. E. W. Bauer, S. T. B. Goennenwein, and E. Saitoh, ArXiv e-prints (2012). arXiv:1211.0098 [cond-mat.mtrl-sci].

[3] S. T. Goennenwein, and G. E. Bauer, Nature Nanotechnology **7**, 145–147 (2012).

[4] M. Weiler, M. Althammer, F. D. Czeschka, H. Huebl, M. S. Wagner, M. Opel, I.-M. Imort, G. Reiss, A. Thomas, R. Gross, and S. T. B. Goennenwein, Phys. Rev. Lett. **108**, 106602 (2012).

[5] F. D. Czeschka, L. Dreher, M. S. Brandt, M. Weiler, M. Althammer, I.-M. Imort, G. Reiss, A. Thomas, W. Schoch, W. Limmer, H. Huebl, R. Gross, and S. T. B. Goennenwein, Phys. Rev. Lett. **107**, 046601 (2011).

[6] M. Weiler, L. Dreher, C. Heeg, H. Huebl, R. Gross, M. S. Brandt, and S. T. B. Goennenwein, Phys. Rev. Lett. **106**, 117601 (2011).

[7] M. Weiler, H. Huebl, F. S. Goerg, F. D. Czeschka, R. Gross, and S. T. B. Goennenwein, Phys. Rev. Lett. **108**, 176601 (2012).

[8] X. Zhou, F. Hocke, A. Schliesser, A. Marx, H. Huebl, R. Gross, and T. J. Kippenberg, Nat. Phys. **9**, 179 (2013).

[9] F. Hocke, X. Zhou, A. Schliesser, T. J. Kippenberg, H. Huebl, and R. Gross, New J. Phys. **14**, 123037 (2012).

[10] F. Hocke. *Microwave Circuit-electrodynamics in a Nanomechanical Hybrid System*. Dissertation, Technische Universität München (2013).

Second Funding Period for the DFG Transregional Collaborative Research Center TRR 80 "From Correlations to Functionality"

R. Hackl [1]

In November 2013 the Senate of the German Research Foundation (DFG) decided to support the Transregional Collaborative Research Center TRR 80 "From Correlations to Functionality" for another four years in the period from 2014 until 2017. The TRR 80 is a collaboration between the University Augsburg (UA) as a lead institution, the Technical University Munich (TUM), the Ludwig-Maximilians University (LMU), and the Walther-Meißner-Institute (WMI). The first funding period (2010–2013) was very successful and productive yielding more than 200 publications.

The objective is to find new materials having electronic correlations and offering opportunities for functionalities. An important example is the interface of different insulating materials exhibiting metallic conduction or even superconductivity. Also the introduction of defects and other inhomogeneities into correlated metals or metal oxides often yields new and unexpected properties that can be used for future applications. The situation is comparable to that of semiconductor research some 50 years ago when the transition from the observation of new properties over the deliberate modification of the materials to a wealth of applications occurred.

The TRR 80 is a collaboration between materials scientists, experimentalists, and theorists. It is planned to exploit the enormous possibilities of materials engineering proceeding from single crystal growth and thin film deposition to heteroepitaxy and atomically precise structures. Many of the properties are not understood yet and need in-depth experimental studies and theoretical modeling. The projects of the TRR 80 comprise state of the art preparation techniques, a large variety of innovative experimental tools, and various theory projects covering analytical and the most advanced numerical techniques.

The WMI contributes with a spectroscopy project which is intended to improve the spatial resolution of light scattering experiments by more than an order of magnitude bridging the gap between the diffraction limit of visible light and scanning tunneling techniques. This is achieved by placing a metallic tip with a typical apex radius of 5 nm into the focus of the laser, bring it close to the sample surface, and use the near field enhancement of the tip for reducing the scattering volume by three to six orders of magnitude. In this way lattice and transport properties can be studied on length scales of order 10 nm relevant for most of the new materials of interest for the TRR 80.

[1] The work is supported by the DFG via the Transregional Collaborative Research Center TRR 80.

Six Years of Research in the DFG Priority Program SPP 1285 "Semiconductor Spintronics"

M. Althammer, S. Geprägs, S. T. B. Goennenwein, R. Gross, M. Opel [1]

The use of electron and hole spins for future semiconductor devices is in the focus of current research. Key prerequisites for the development of novel device concepts for spin electronics and spin optoelectronics are the realization of an effective injection of spin-polarized charge carriers, as well as the thorough understanding of the transport, manipulation, and detection of the spin degree of freedom. To promote research in this field, the German Research Foundation (DFG) started a 6-year Priority Program entitled *Semiconductor Spintronics (SPP 1285)* in July 2007. The general scientific objectives of this program were defined as (i) the efficient injection of spin polarized electrons using para- and ferromagnetic semiconductors and ferromagnetic metal clusters, (ii) the transport of electron spins across interfaces and large distances, (iii) the direct manipulation of the orientation of electron spins, (iv) the study of spin-spin-interactions, (v) the development of concepts for spintronics and spin-optoelectronics, and (vi) the study of basic principles of spin-based quantum information processing in semiconductors.

The priority program SPP 1285, consisting of three 2-year funding periods, was supporting 33 single projects in basic and applied research all over Germany. The WMI has been participating in this program from the very beginning in 2007. With our project entitled *Spin Injection, Spin Transport, and Controllable Ferromagnetism in Transition Metal-Doped ZnO*, the WMI was granted funding for all three terms (2007–2009, 2009–2011, and 2011–2013). The key objectives of our project included (i) the fabrication of high-quality epitaxial ZnO thin films and heterostructures as well as $[\mathrm{ZnO/ferromagnet}]_n$ digital alloys tailored to the needs of spin (opto)electronic devices, (ii) the investigation of the spin coherence time in ZnO by optical pump & probe experiments, (iii) the optical study of electrical spin injection and spin transport in ferromagnet/ZnO heterostructures, and finally (iv) the investigation of the spin dephasing via all-electrical transport experiments in ZnO-based, vertical spin valve heterostructures. Our work in this project resulted in 9 publications in peer-reviewed journals [1–9]. Furthermore, 3 PhD students [10–12]. Moreover, 6 diploma or master students finished their theses at the WMI which were fully or to a large extent linked to or funded by this project.

In close collaboration with various project partners in SPP 1285, we have comprehensively investigated the material system ZnO, making extensive use of our thin film fabrication labs. With funding from the priority program, we equipped our existing ultra-high vacuum laser molecular beam epitaxy (laser-MBE) system with (i) an upgraded flexible ultra-violet laser beam optics allowing for the precise variation of the laser fluence, (ii) an upgraded infrared laser heating system allowing for both high substrate temperatures in UHV environment and rapid temperature changes, and (iii) a new radical source for atomic oxygen and nitrogen [7]. We have optimized the deposition parameters for doped and undoped ZnO single thin films, ZnO buffer layers, and ZnO-based multilayer structures. The detailed structural characterization by X-ray and transmission electron microscopy (TEM) analysis showed (see Fig. 1(a)) that epitaxial ZnO thin films with high structural quality can be achieved on (0001)-oriented Al_2O_3 substrates, in spite of the large lattice mismatch of 18% [7]. We have also realized the heteroepitaxial growth of ZnO based multilayers as a prerequisite for spin transport experiments and the fabrication of spintronic devices [6, 7]. Our research project aimed at the magnetic properties and the possibility of dilute magnetic doping with transition metal ions

[1]This work is supported by the German Research Foundation via the Priority Program SPP 1285 (project number GR 1132/14).

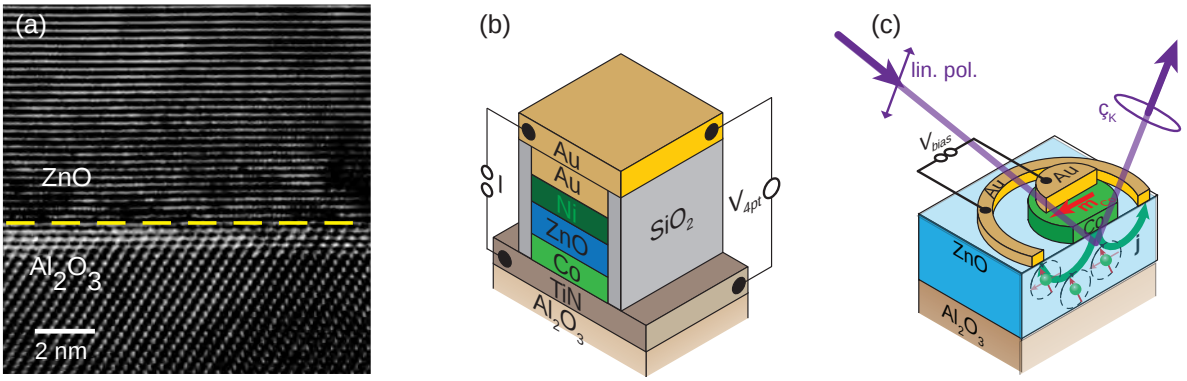

Figure 1: (a) High-resolution transmission electron microscopy image of an epitaxial ZnO thin film on Al_2O_3. (b) Cross-sectional view of a ZnO based spin-valve junction for the all-electrical study of spin transport across ZnO. (c) Illustration of the mesa structure and the measurement setup for electrical injection/optical detection.

on the one hand side and spin coherence and spin dephasing properties on the other. The latter becomes important for semiconductor spintronic devices in view of the injection, transport, manipulation, and detection of spin-polarized carriers. Our results are in detail summarized in Ref. [8]. In the following, we only give a short overview over the main aspects.

During the past ten years, there have been broad research efforts aiming at the realization of room-temperature ferromagnetism in ZnO by suitable transition metal (TM) doping. From theory, ferromagnetism was predicted for dilute magnetic doping with Mn oder Co. Although a large number of publications reported the observation of ferromagnetic-like behavior for ZnO:TM, those studies mostly did not take into account the possible formation of spurious secondary phases. We have grown several series of differently doped thin films (TM = Mn, Co, Cu, ...), homoepitaxially on ZnO and heteroepitaxially on $ScAlMgO_4$ or Al_2O_3 substrates. In a very detailed and systematic study for ZnO:Co combining integral and element-specific techniques, we discovered no indication for carrier-mediated itinerant ferromagnetism [2]. In contrast, phase-pure, crystallographically excellent ZnO:Co thin films were found to be uniformly paramagnetic. Superparamagnetism arised only when phase separation or defect formation occurred and always stemmed from nanometer-sized metallic precipitates [5]. Other thin-film compounds like ZnO:(Li,Ni) and ZnO:Cu did also not exhibit any indication of ferromagnetism. So, dilute magnetic doping of ZnO, initially considered a success story, turned out to be more difficult than expected. The early positive reports have to be re-considered in the light of element-specific, microscopic techniques applied to such "ferromagnetic" transition metal-doped oxide materials.

Although it seems to be impossible to realize room-temperature ferromagnetism in ZnO, the small spin-orbit coupling and correspondingly large spin coherence length makes ZnO suitable for transporting or manipulating spins in thin film spintronic devices. In close collaboration with project no. 6 ("Coherent spin transport in semiconductors", B. Beschoten & G. Güntherodt, RWTH Aachen), we have carefully investigated the spin-coherence in ZnO thin films by applying both optical and electrical injection/detection schemes. From the first optical pump/optical probe experiment, we revealed a long ($\simeq$ 15 ns) and a short component ($\simeq$ 2 ns) for the spin dephasing time in our ZnO thin films at low temperatures [9]. We attributed the long component to electrons localized at donors (presumably Al) as it was only seen in optical pump/probe experiments. The short one, however, was also observed for electrical "pumping" and therefore should represent the behavior of mobile charge carriers in ZnO. This assumption was confirmed in a second all-electrical magnetotransport measurement utilizing vertical Co/ZnO/Ni spin valve structures (Fig. 1(b)). We successfully created and detected a spin-polarized ensemble of electrons and demonstrated the transport of this spin information across several nanometers in ZnO [6]. From a detailed analysis applying

a two-spin channel model with spin-dependent interface resistances, we have derived a spin lifetime of 2.6 ns for these itinerant spins at low temperatures [6]. All these data agreed well with the results of our third combined electrical pump/optical probe experiment (Fig. 1(c)) where we found a spin dephasing time of $\simeq 1$ ns [8].

References

[1] A. Nielsen, A. Brandlmaier, M. Althammer, W. Kaiser, M. Opel, J. Simon, W. Mader, S. T. B. Goennenwein, and R. Gross, Appl. Phys. Lett. **93**, 162510 (2008).

[2] M. Opel, K.-W. Nielsen, S. Bauer, S. Goennenwein, J. Cezar, D. Schmeisser, J. Simon, W. Mader, and R. Gross, Eur. Phys. J. B **63**, 437–444 (2008).

[3] D. Venkateshvaran, W. Kaiser, A. Boger, M. Althammer, M. S. R. Rao, S. T. B. Goennenwein, M. Opel, and R. Gross, Phys. Rev. B **78**, 092405 (2008).

[4] D. Venkateshvaran, M. Althammer, A. Nielsen, S. Geprägs, M. S. Ramachandra Rao, S. T. B. Goennenwein, M. Opel, and R. Gross, Phys. Rev. B **79**, 134405 (2009).

[5] A. Ney, M. Opel, T. C. Kaspar, V. Ney, S. Ye, K. Ollefs, T. Kammermeier, S. Bauer, K.-W. Nielsen, S. T. B. Goennenwein, M. H. Engelhard, S. Zhou, K. Potzger, J. Simon, W. Mader, S. M. Heald, J. C. Cezar, F. Wilhelm, A. Rogalev, R. Gross, and S. A. Chambers, New J. Phys. **12**, 013020 (2010).

[6] M. Althammer, E.-M. Karrer-Müller, S. T. B. Goennenwein, M. Opel, and R. Gross, Appl. Phys. Lett. **101**, 082404 (2012).

[7] M. Opel, S. Geprägs, M. Althammer, T. Brenninger, and R. Gross. Laser molecular beam epitaxy of ZnO thin films and heterostructures. Accepted for publication in J. Phys. D: Appl. Phys., arXiv:1307.1616 (2014).

[8] M. Opel, S. T. B. Goennenwein, M. Althammer, K.-W. Nielsen, E.-M. Karrer-Müller, S. Bauer, K. Senn, C. Schwark, C. Weier, G. Güntherodt, B. Beschoten, and R. Gross. Zinc Oxide - From Dilute Magnetic Doping to Spin Transport. Accepted for publication in Phys. Stat. Sol. B, arXiv:1309.5857 (2014).

[9] S. Kuhlen, R. Ledesch, R. de Winter, M. Althammer, S. T. B. Goennenwein, M. Opel, R. Gross, T. A. Wassner, M. S. Brandt, and B. Beschoten. Unambiguous determination of spin dephasing times in ZnO. Submitted for publication in Phys. Stat. Sol. B, arXiv:1309.6600 (2014).

[10] K.-W. Nielsen. *Ursache der magnetischen Kopplung in Kobalt-dotiertem ZnO*. Phd thesis, TU München (2008).

[11] A. Nielsen. *Magnetit – ein Material für die Spinelektronik*. Phd thesis, TU München (2009).

[12] M. K. Althammer. *Spin-transport-phenomena in metals, semiconductors, and insulators*. Phd thesis, TU München (2012).

Second Funding Period for the DFG Priority Program SPP 1458 "Superconductivity in Iron-Based Compounds"

R. Hackl [1]

In June 2013 the German Research Foundation (DFG) decided to support the Priority Program SPP 1450 ***"Superconductivity in Iron-Based Compounds"*** for another three years until 2016. The funding includes support for approximately 25 research groups in Germany and enables them to organize one workshop, two international conferences, and several mini-workshops for the participating students. One of the coordinators (R.H.) is affiliated with the Walther-Meißner-Institute (WMI) and is principal investigator of the project ***"Raman study of the interrelation of electron dynamics and phase transitions in iron-based superconductors"*** (HA 2071/7-2).

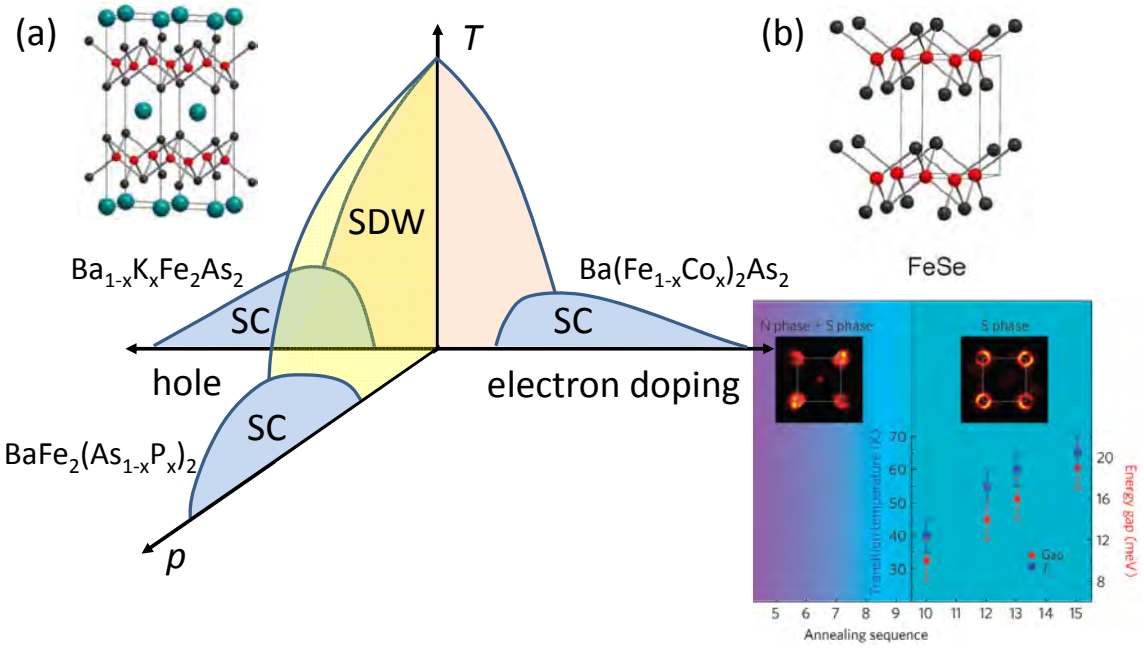

Figure 1: Phase diagrams and Fermi surface in Fe-based materials. (a) Schematic phase diagrams for different control parameters in 122 compounds (upper left inset). All three elements in ternary 122 compounds can be substituted. In $(Ba_{1-x}K_x)Fe_2As_2$ it is justified to speak of doping since the valencies of Ba and K are uniquely defined. In $Ba(Fe_{1-x}Co_x)_2As_2$ the valence of Co is debated [1] while in $BaFe_2(As_{1-x}P_x)_2$ the substitution is clearly isovalent. The phase diagram of $BaFe_2(As_{1-x}P_x)_2$ is almost identical to that obtained with applied pressure [2]. (b) Evolution of the Fermi surface and the spectroscopic gap in mono-layer FeSe (upper right inset) [3]. As deposited the layer is insulating and has Fermi surfaces around the center and the corner of the Brillouin zone. After several annealing steps (horizontal axis) the central Fermi surface vanishes gradually and a gap is found in the photoemission spectra up to maximally 65 K.

The priority program focuses on the basic physical properties of the iron-based superconductors (FeSC). Due to their band structure having Fermi surfaces in high symmetry points which can be tuned by substitution and applied pressure the FeSC are laboratories for fundamental studies of unconventional Cooper pairing. The system $BaFe_2As_2$ offers four different routes for exploring the phase diagram [Fig. 1 (a)]: (i) substitution of Ba^{2+} by K^+ clearly having a doping effect [4], (ii) substitution of Fe by Co where the doping is less evident [1, 5], and (iii) isovalent substitution of As by P [6] which is by and large equivalent to (iv) applied hydrostatic pressure [2]. In all cases the Fermi surfaces yield to the changes of the electron

[1] The work is supported by the German Research Foundation (DFG) via the Priority Program SPP 1458 (project HA 2071/7-2).

count and the structure. In addition, the various substitutions influence the mean free path of the carriers in different ways since they are at different distances from the relevant Fe layers. However, in all cases the shapes of the Fermi surfaces have a crucial influence on the superconducting and magnetic properties. This influence becomes particularly clear in the chalcogenide FeSe [Fig. 1 (b)]. Here, a single layer FeSe on buffered $SrTiO_3$ shows spectroscopic evidence of superconductivity if the Fermi surface is tuned so as to solely encircle the corners of the Brillouin zone. Then a gap is found in the photoemission spectra which closes at approximately 65 K in samples that underwent appropriate annealing protocols and reaches roughly $6k_BT_c$ at low temperature [3]. If transport and magnetization measurements can corroborate the conjectures from photoemission spectroscopy mono-layer FeSe would break the current record of SmFeAsO reaching 56 K [7] and bring the chalcogenides closer to the center of future activities.

The project at the WMI focuses on electronic properties in both the magnetic and the superconducting state. One of the new developments is the detwinning device for the system $Ba(Fe_{1-x}Co_x)_2As_2$ which undergoes a structural phase transition for $x \leq 0.065$. In detwinned samples the properties in the spin-density-wave (SDW), phase which is established a few degrees below the structural transition, can be studied with light polarizations parallel and perpendicular to the SDW ordering vector, returning clear anisotropies in both the electronic and lattice properties. In addition, the evolution of nematic fluctuations as one of the putative driving forces of the phase transitions and even superconductivity can be studied in more detail. The superconducting response in $(Ba_{1-x}K_x)Fe_2As_2$ allows insight into the momentum dependence of the pairing potential $V_{\mathbf{k},\mathbf{k}'}$ via excitonic modes inside the gap (contribution by T. Böhm in this Annual Report). These modes which were predicted by Bardasis and Schrieffer [8] and studied in some detail in the context of light scattering [9–11], facilitate the quantification of anisotropies in the pairing potential and were found to be the litmus test for competing *s*- and *d*-wave ground states in the FeSCs [12–14]. Hence the Raman experiment can contribute to tracking down the changes in $V_{\mathbf{k},\mathbf{k}'}$ as a function of the Fermi surface topology.

References

[1] H. Wadati, I. Elfimov, and G. A. Sawatzky, Phys. Rev. Lett. **105**, 157004 (2010).
[2] E. Colombier, S. L. Bud'ko, N. Ni, and P. C. Canfield, Phys. Rev. B **79**, 224518 (2009).
[3] S. He, J. He, W. Zhang, L. Zhao, D. Liu, X. Liu, D. Mou, Y.-B. Ou, Q.-Y. Wang, Z. Li, L. Wang, Y. Peng, Y. Liu, C. Chen, L. Yu, G. Liu, X. Dong, J. Zhang, C. Chen, Z. Xu, X. Chen, X. Ma, Q. Xue, and X. J. Zhou, Nat. Mater. **12**, 605 (2013).
[4] M. Rotter, M. Tegel, and D. Johrendt, Phys. Rev. Lett. **101**, 107006 (2008).
[5] A. S. Sefat, R. Jin, M. A. McGuire, B. C. Sales, D. J. Singh, and D. Mandrus, Phys. Rev. Lett. **101**, 117004 (2008).
[6] J. G. Analytis, J.-H. Chu, R. D. McDonald, S. C. Riggs, and I. R. Fisher, Phys. Rev. Lett. **105**, 207004 (2010).
[7] K. Ishida, Y. Nakai, and H. Hosono, J. Phys. Soc. Jpn **78**, 062001 (2009).
[8] A. Bardasis, and J. R. Schrieffer, Phys. Rev. **121**, 1050–1062 (1961).
[9] A. Zawadowski, J. Ruvalds, and J. Solana, Phys. Rev. A **5**, 399–421 (1972).
[10] M. V. Klein, and S. B. Dierker, Phys. Rev. B **29**, 4976 (1984).
[11] H. Monien, and A. Zawadowski, Phys. Rev. B **41**, 8798 (1990).
[12] D. J. Scalapino, and T. P. Devereaux, Phys. Rev. B **80**, 140512 (2009).
[13] F. Kretzschmar, B. Muschler, T. Böhm, R. Hackl, H.-H. Wen, V. Tsurkan, J. Deisenhofer, and A. Loidl. Fermiology and pairing in iron-based superconductors. In **WMI Annual Report**, 53 (2012).
[14] F. Kretzschmar, B. Muschler, T. Böhm, A. Baum, R. Hackl, H.-H. Wen, V. Tsurkan, J. Deisenhofer, and A. Loidl, Phys. Rev. Lett. **110**, 187002 (2013).

The DFG Priority Program SPP 1538 "Spin Caloric Transport"

S. T. B. Goennenwein, R. Gross, M. Schreier, S. Meyer, J. Lotze, M. Weiler, M. Althammer, H. Huebl, M. Opel, S. Geprägs [1]

The field of *spin caloritronics* addresses the impact of the spin degree of freedom on the thermally driven transport properties of solid state systems [1]. A few years ago, the notion emerged that spin caloritronic phenomena are much more than spin-dependent replica of the well-established, thermo-galvanic effects. One key insight from the ensuing research activities is that spin-dependent entropy transport does not necessarily require mobile charge carriers. Rather, entropy transport also is possible via spin excitations (magnons), resulting in a new set of spin caloritronic phenomena such as the *spin Seebeck effect* [2] or the *spin Nernst effect* [3]. Since magnons are present in conductive ferromagnets just as well as in so-called magnetic insulators – i.e., in electrically insulating materials exhibiting long-range ferromagnetic or ferrimagnetic order – the new spin caloritronic effects just mentioned will be present in particular also in magnetic insulators. In contrast, the conventional, charge-based thermo-galvanic effects must vanish in these materials, since magnetic insulators do not contain mobile charges. Magnon-based spin caloritronic effects thus indeed are qualitatively different from the long-known, charge-based thermo-galvanic phenomena.

To stimulate research activities on spin caloric phenomena, the German Research Foundation (DFG) has launched the Priority Program SPP 1538 entitled ***Spin Caloric Transport (SpinCaT)*** in 2011. The aim of SPP 1538 is to develop the new research field of spin-related caloric effects. The Walther-Meißner-Institute (WMI) participates in this program with the project ***Spin-dependent Thermo-galvanic Effects***. As the first three-year funding period will end in mid 2014, we have already submitted a renewal proposal for the second three year funding period. One focus of our spin caloric transport research activities is on spatially resolved spin caloritronic experiments. As detailed in Ref. [4], we use a focused laser beam to generate a local thermal gradient in magnetic thin films or hybrid heterostructures, and investigate the resulting spin caloritronic responses [5]. This technique in particular enables spatially resolved spin Seebeck effect measurements in magnetic insulator/normal metal hybrids. We have pursued and extended this approach, taking advantage of the excellent yttrium iron garnet ($Y_3Fe_5O_{12}$, YIG) thin films grown via laser-MBE in house at WMI [6]. This year, we have substantiated the spatially resolved spin Seebeck experiments by a detailed calculation of the thermal profiles arising in YIG/normal metal hybrids upon laser illumination [7, 8]. We furthermore have quantitatively compared the magnitude of the spin Seebeck effect observed experimentally in these structures with related, magnon-current based phenomena, namely the spin pumping effect and the spin Hall magnetoresistance [9]. In the second line of experiments, we have extensively investigated the spin Hall magnetoresistance that we recently discovered in YIG/Pt-type hybrid structures [5, 10–12]. As discussed in more detail in the contribution by Meyer *et al.* on page 57, the spin Hall magnetoresistance arises from the interplay between charge currents flowing in the normal metal (Pt) with magnon currents (spin currents) flowing in the magnetic insulator (YIG), and thus is closely related to the thermally driven magnon currents observed in spin Seebeck measurements in these structures. It also is important to emphasize that our spin caloritronic experiments viz. their theoretical

[1] This work is supported by the German Research Foundation via Priority Program SPP 1538 (project number GO 944/4-1).

interpretation are performed in close collaboration with the groups of Prof. E. Saitoh and Prof. G. E. W. Bauer from the Institute for Materials Research, Tohoku University, Sendai, Japan, as well as with collaboration partners within SPP 1538.

Currently, we work towards time-resolved spin Seebeck effect experiments in our YIG/Pt hybrid structures, aiming to identify the microscopic mechanisms responsible for the effect. Another important line of work deals with the fabrication and investigation of magnetic insulators exhibiting a magnetic compensation point, such as gadolinium iron garnet ($Gd_3Fe_5O_{12}$) or dysprosium iron garnet ($Dy_3Fe_5O_{12}$). At a certain temperature (the compensation temperature), the magnetic moments of the different magnetic sublattices in these materials cancel out exactly. The materials then behave like antiferromagnets in many aspects, enabling exploratory studies of spin caloritronic phenomena in this regime.

References

[1] G. E. W. Bauer, E. Saitoh, and B. J. van Wees, Nat. Mater. **11**, 391–399 (2012).

[2] K. Uchida, J. Xiao, H. Adachi, J. Ohe, S. Takahashi, J. Ieda, T. Ota, Y. Kajiwara, H. Umezawa, H. Kawai, G. E. W. Bauer, S. Maekawa, and E. Saitoh, Nat. Mater. **9**, 894–897 (2010).

[3] K. Tauber, M. Gradhand, D. V. Fedorov, and I. Mertig, Phys. Rev. Lett. **109**, 026601 (2012).

[4] M. Weiler, M. Schreier, M. Althammer, S. Meyer, H. Huebl, M. Opel, S. Geprägs, R. Gross, S. T. B. Goennenwein, I.-M. Imort, G. Reiss, and A. Thomas. Spin and Charge Currents in Magneto-thermal Landscapes. In **WMI Annual Report**, 68 (2012).

[5] M. Weiler, M. Althammer, F. D. Czeschka, H. Huebl, M. S. Wagner, M. Opel, I.-M. Imort, G. Reiss, A. Thomas, R. Gross, and S. T. B. Goennenwein, Phys. Rev. Lett. **108**, 106602 (2012).

[6] M. Althammer, M. S. Wagner, J. Lotze, H. Huebl, S. T. B. Goennenwein, and M. Opel. Epitaxial Yttrium-Iron-Garnet (YIG) Thin Films. In **WMI Annual Report**, 75 (2011).

[7] M. Schreier, A. Kamra, M. Weiler, J. Xiao, G. E. W. Bauer, R. Gross, and S. T. B. Goennenwein, Phys. Rev. B **88**, 094410 (2013).

[8] M. Schreier, N. Roschewsky, E. Dobler, S. Meyer, H. Huebl, R. Gross, and S. T. B. Goennenwein, Appl. Phys. Lett. **103**, 242404 (2013).

[9] M. Weiler, M. Althammer, M. Schreier, J. Lotze, M. Pernpeintner, S. Meyer, H. Huebl, R. Gross, A. Kamra, J. Xiao, Y.-T. Chen, H. Jiao, G. E. W. Bauer, and S. T. B. Goennenwein, Phys. Rev. Lett. **111**, 176601 (2013).

[10] H. Nakayama, M. Althammer, Y.-T. Chen, K. Uchida, Y. Kajiwara, D. Kikuchi, T. Ohtani, S. Geprägs, M. Opel, S. Takahashi, R. Gross, G. E. W. Bauer, S. T. B. Goennenwein, and E. Saitoh, Phys. Rev. Lett. **110**, 206601 (2013).

[11] M. Althammer, S. Meyer, H. Nakayama, M. Schreier, S. Altmannshofer, M. Weiler, H. Huebl, S. Geprägs, M. Opel, R. Gross, D. Meier, C. Klewe, T. Kuschel, J.-M. Schmalhorst, G. Reiss, L. Shen, A. Gupta, Y.-T. Chen, G. E. W. Bauer, E. Saitoh, and S. T. B. Goennenwein, Phys. Rev. B **87**, 224401 (2013).

[12] Y.-T. Chen, S. Takahashi, H. Nakayama, M. Althammer, S. T. B. Goennenwein, E. Saitoh, and G. E. W. Bauer, Phys. Rev. B **87**, 144411 (2013).

The EU Marie Curie Initial Training Network "Circuit and Cavity Quantum Electrodynamics (CCQED)"

F. Deppe, R. Gross, A. Marx [1]

The key objective of the european network ***Circuit and Cavity Quantum Electro-Dynamics (CCQED)*** is to investigate the coupling between light and matter at its most fundamental level, where one or a few atoms strongly interact with a single mode of the electromagnetic field stored in a resonator containing a small number of photons. This research area, named *Cavity Quantum Electrodynamics*, has been at first investigated with real atoms coupled to microwave or optical photons. However, the recent years showed that the very same physics can be studied in a solid-state architecture, nicknamed *Circuit Quantum Electrodynamics*, where now artificial atoms made of Josephson junctions are coupled to on-chip superconducting resonators. Both fields made spectacular progress in the past years, with a remarkable diversity of demonstrated physical effects. To list a few, milestones include the direct observation of the quantum jumps of microwave light, the deterministic generation and tomography of arbitrary quantum states of a resonator by superconducting quantum bits, the evidence of the lamb shift in a solid-state system, the generation of nonlinear photonics with one atom, and the realization of feedback schemes on single atoms triggered by the detection of single photons.

In 2011, the european network ***Circuit and Cavity Quantum Electro-Dynamics (CCQED)*** has been granted 3.5 Million Euros by the European Union through a Marie Curie Action within the Seventh Framework Program Initial Training Network ITN-People-2010. The aim of CCQED is to bridge two communities in physics, in the academic and private sectors, to share, pursue and diffuse within Europe the benefits of collaborations in the science of elementary quanta. CCQED involves 10 research centres and 3 companies, representing the cutting edge of research in the quantum electrodynamics of fundamental systems in Europe. The network trains 12 early stage researchers (Ph.D. students) and 2 experienced researchers (postdocs). They focus on establishing bonds between solid-state and quantum optics physics, strengthening the communication between theory and experiment, and establishing links between fundamental and applied research. Prominent scientists and industry leaders contribute to the schools and workshops. Special attention is given to the development of complementary skills, such as communication, presentation, project planning, and management. The WMI contributes with its expertise on the design, fabrication, and measurement of superconducting quantum circuits. In particular, the focus lies on the exploration of quantum correlations in the important microwave frequency domain.

At the WMI, we perform experimental studies on propagating microwaves generated using superconducting quantum circuits in a cryogenic environment [1–3]. We demonstrated switchable coupling between two niobium transmission line resonators (TLR) mediated by a superconducting flux qubit [4, 5]. For fixed coupling, we investigated the distributed coupling [6] and developed a layout for scalable chains of TLR [7, 8]. Transmission measurements yielded consistent parameters for up to three coupled TLR. These experiments are the basis for more elaborate studies on thermal entanglement, entanglement scaling laws, and, more generally, analog quantum simulations. Furthermore, we measured propagating squeezed microwave light generated by a flux-driven Josephson parametric amplifier. We can consistently detect squeezing [9] by using either a single path and sideband mixing or a beam splitter and dual-path state tomography [1–3, 10]. In the latter case, we demonstrated entanglement with

[1] This work is supported by the EU projects CCQED.

respect to the two beam splitter output paths. Based on this work, we plan teleportation with continuous-variable quantum microwaves.

From September 09 to 13, 2013, ***CCQED*** has organized the ***International Conference on Resonator QED***. It took place at the Kardinal Wendel Haus close to the English Garden in Munich-Schwabing (organizers: Peter Domokos (Wigner), Rudolf Gross (WMI), Gerhard Rempe (MPQ) & Tatjana Wilk (MPQ)). It was focussing on (i) single atom cavity QED, (ii) multi-atom cavity QED, (iii) circuit QED, (iv) photonic crystal cavity QED, (v) quantum information processing with CCQED systems, (vi) cavity optomechanics, (vii) hybrid circuit or cavity QED systems, and (viii) QED without cavity. With more than 140 participants from all over the world, the conference was a major and very successful event. The final programme comprised 6 tutorials, 28 invited talks, 18 contributed talks and 57 posters. The local CCQED network partners (Max-Planck-Institute for Quantum Optics and Walther-Meißner-Institute) opened doors for a tour through their laboratories. Moreover, the CCQED industry partners invited conference attendees to visit their facilities or offer to meet their experts. To disseminate research on quantum optics and circuit QED to a broader public, CCQED organized an evening with a public lecture by Nobel laureate in physics, Serge Haroche on 11^{th} September at the Ehrensaal of the Deutsches Museum. Subsequently, a panel discussion (presented by Jeanne Rubner, Bayerischer Rundfunk) on "Research & Innovation" with guests from research, politics and industry examined the link between basic research and innovation. The event attracted more than 150 participants.

The EU small or medium-scale focused research project "Quantum Propagating Microwaves in Strongly Coupled Environments (PROMISCE)"

F. Deppe, R. Gross, A. Marx [2]

The EU Collaborative Project entitled ***Quantum Propagating Microwaves in Strongly Coupled Environments – PROMISCE*** is funded by the FET-Open Initiative of the EU 7^{th} Framework Program since early 2012. It studies the dynamics of microwave photons in quantum circuits, including their interaction with superconducting qubits, transmission lines and quantum metamaterials. The aim of ***PROMISCE*** is to provide the foundations for a novel research field: propagating quantum microwave technologies in strongly and ultrastrongly coupled environments. It emerged from the challenging and controversial idea that microwave photons can interact strongly among each other and with their environment, even in the absence of confining cavities. ***PROMISCE*** combines two major innovative and interdisciplinary components. The first one, propagating quantum microwave photonics, focuses on the generation, control, and

[2]This work is supported by the EU project PROMISCE.

detection of quantum microwave beams and photons using superconducting quantum circuits. The second one aims at the exploration of interactions between propagating quantum microwaves and their potential for quantum information processing. The ultimate goal of PROMISCE is to merge the possibilities of all-optical quantum computing with superconducting circuits. The result should be quantum networks [7, 8] that perform useful tasks such as scalable quantum gates or quantum simulation of condensed matter and field quantum theory problems [11].

The research efforts at WMI employ superconducting quantum circuits to explore novel paths in engineering strong and ultrastrong controlled interactions [12] between propagating microwave photons and their environment as well as among photons themselves. To this end, we aim at the development and understanding of microwave beam splitters [6, 13], which are an essential component in the manipulation of propagating photons and in particular for the implementation of single-qubit gates in travelling qubits. Recently, we have witnessed the development of tunable beam splitters in the optical regime, a novel tool which allows one to dynamically control those single qubit gates. Within PROMISCE we develop microwave beam splitters with a similar degree of tunability. Another research direction within PROMISCE is the development of a deterministic single photon source, which can be realized either by a reliably controlled superconducting qubit in a leaky cavity or a superconducting qubit in an open line with some transverse driving. As WMI is an early player in the field of quantum propagating microwave, it contributes with pronounced experimental expertise to PROMISCE.

References

[1] E. P. Menzel, R. Di Candia, F. Deppe, P. Eder, L. Zhong, M. Ihmig, M. Haeberlein, A. Baust, E. Hoffmann, D. Ballester, K. Inomata, T. Yamamoto, Y. Nakamura, E. Solano, A. Marx, and R. Gross, Phys. Rev. Lett. **109**, 250502 (2012).

[2] E. P. Menzel, F. Deppe, M. Mariantoni, M. A. Araque Caballero, A. Baust, T. Niemczyk, E. Hoffmann, A. Marx, E. Solano, and R. Gross, Phys. Rev. Lett. **105**, 100401 (2010).

[3] E. P. Menzel. *Propagating Quantum Microwaves: Dual-path State Reconstruction and Path Entanglement*. Dissertation, Technische Universität München (2013).

[4] E. Hoffmann. *Experiments on Two-Resonator Circuit Quantum Electrodynamics: A Superconducting Quantum Switch*. Ph.D. thesis, TU München (2013).

[5] M. Mariantoni, F. Deppe, A. Marx, R. Gross, F. Wilhelm, and E. Solano, Phys. Rev. B **78**, 104508 (2008).

[6] B. Peropadre, D. Zueco, F. Wulschner, F. Deppe, A. Marx, R. Gross, and J. Garcia-Ripoll, Phys. Rev. B **87**, 134504 (2013).

[7] M. Leib, and M. J. Hartmann, New J. of Phys. **12**, 093031 (2010).

[8] M. Leib, F. Deppe, A. Marx, R. Gross, and M. J. Hartmann, New Journal of Physics **14**, 075024 (2012).

[9] L. Zhong, E. P. Menzel, R. D. Candia, P. Eder, M. Ihmig, A. Baust, M. Haeberlein, E. Hoffmann, K. Inomata, T. Yamamoto, Y. Nakamura, E. Solano, F. Deppe, A. Marx, and R. Gross, New Journal of Physics **15**, 125013 (2013).

[10] R. Di Candia, E. P. Menzel, L. Zhong, F. Deppe, A. Marx, R. Gross, and E. Solano. Dual-Path Methods for Propagating Quantum Microwaves. Accepted for publication in New J. of Phys., arXiv:1308.3117 (2013).

[11] D. Ballester, G. Romero, J. J. Garcia-Ripoll, F. Deppe, and E. Solano, Phys. Rev. X **2**, 021007 (2012).

[12] T. Niemczyk, F. Deppe, H. Huebl, E. P. Menzel, F. Hocke, M. J. Schwarz, J. J. Garcia-Ripoll, D. Zueco, T. Hummer, E. Solano, A. Marx, and R. Gross, Nat Phys **6**, 772–776 (2010).

[13] M. Haeberlein, D. Zueco, P. Assum, E. Hoffmann, B. Peropadre, J. Garcia-Ripoll, E. Solano, F. Deppe, A. Marx, and R. Gross. Fast microwave beam splitters from superconducting resonators. Submitted for publication, arXiv:1302.0729 (2013).

Basic Research

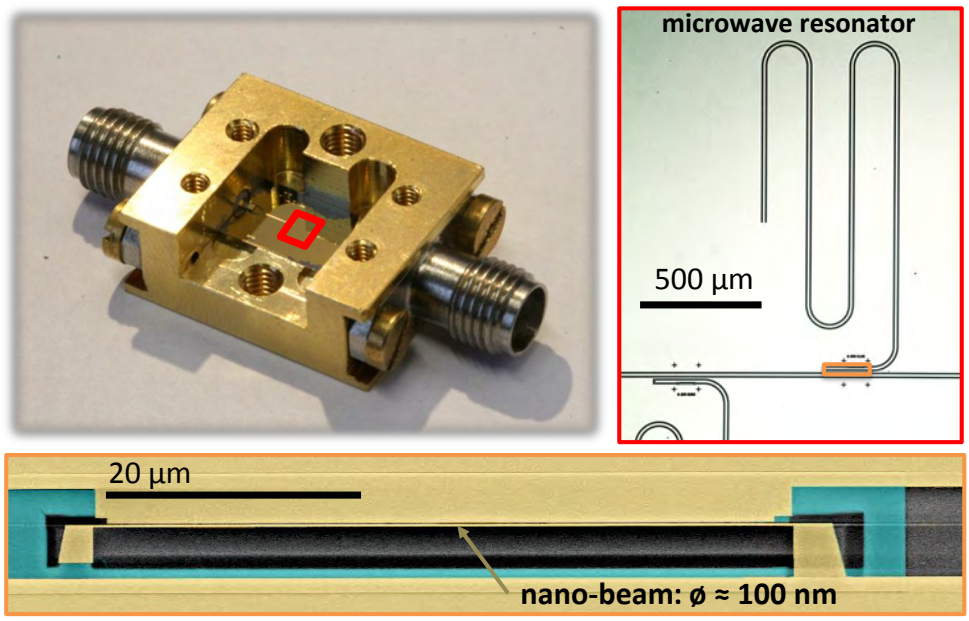

Microwave box (top left) containing a chip with several superconducting coplanar waveguide resonators (top right). The image at the bottom shows an enlarged view of one end of a microwave resonator, where an about 100 nm wide Si_3N_4/Nb nanobeam is coupled to the ground plane of the resonator.

Time-domain Experiments on the Quantum Switch

A. Baust, E. Hoffmann, M. Haeberlein, P. Eder, H. Huebl, E. Menzel, F. Deppe, A. Marx, R. Gross[1]
D. Zueco[2], *J.-J. Garcia-Ripoll*[3], *E. Solano*[4]

During the last decade, superconducting coplanar waveguide resonators and quantum bits (qubits) have not only proven to provide a highly flexible toolbox for the realization of experiments giving deep insight into light-matter interaction physics [1, 2], but are also very promising building blocks for future quantum computing and quantum simulation architectures. However, the successful realization of the latter will not only require to increase the number of qubits and resonators used in the setup, but will also require tunable and switchable coupling between these building blocks.

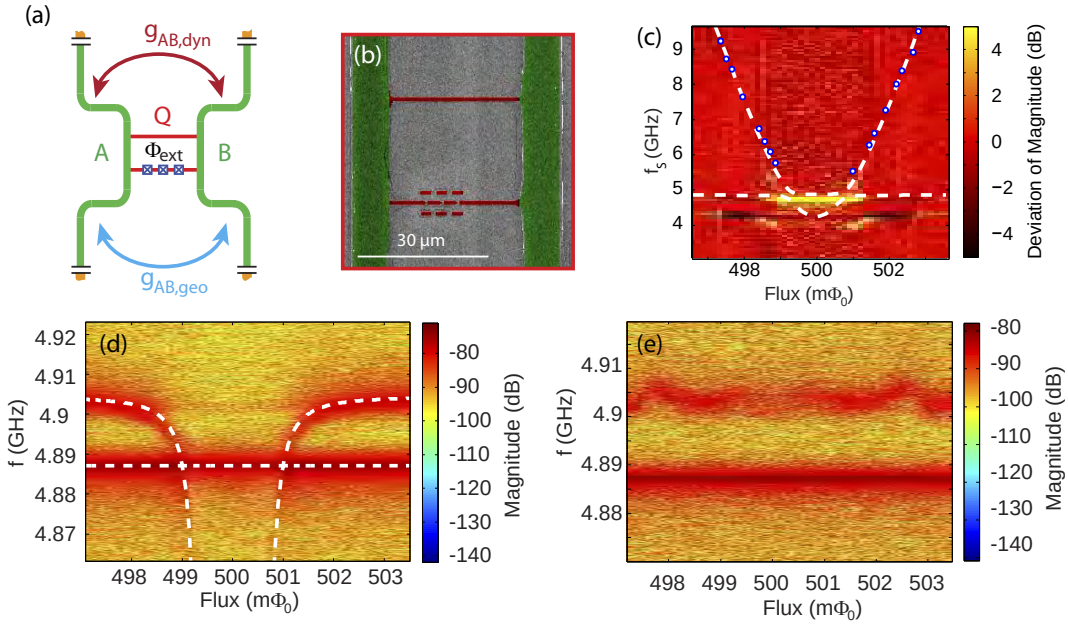

Figure 1: (a) Sketch of the quantum switch with the qubit Q coupled to the resonators A and B. The coupling between the resonators is determined by the dynamical and geometric coupling rates. (b) False-color SEM micrograph of the flux qubit (red) coupled galvanically to the resonators (green). (c) Qubit parameters are extracted from a two-tone spectroscopy measurement. (d) Transmission measured through one of the resonators depending on the magnetic flux and frequency with the qubit in the ground state. The crossings defining the switch setting conditions between the two resonant modes are observed. (e) Same transmission measurement for a driven qubit. No crossing between the modes is observed, indicating that the coupling between the resonators is present independent of the applied magnetic flux. (a)-(e) These figures are taken from Ref. [3].

Our approach to realize tunable coupling between two microwave resonators is the *quantum switch* [4] which consists of a three-Josephson-junction flux qubit coupled galvanically to two half-wave resonators, cf. Fig. 1(a-b). In this setup, two coupling mechanisms between the resonators have to be considered. The *geometric coupling* g_{geo} is determined solely by the circuit

[1]This work is supported by the German Research Foundation via SFB 631, the German Excellence Initiative via NIM, the EU Marie Curie Initial Training Network CCQED and the EU Specific Targeted Research Program PROMISCE.

[2]CSIC-Universidad de Zaragoza, Spain.
[3]IFF-CSIC, Madrid, Spain.
[4]Universidad del Pais Vasco UPV/EHU and Ikerbasque, Spain. E.S. acknowledges financial support by PROMISCE, SCALEQIT, UPV/EHU UFI 11/55 Basque Government IT 472-10 and Spanish MINECO FIS2012-36673-C03-02.

layout, the *dynamical coupling* g_{dyn} depends on the qubit state and on the qubit transition frequency which can be tuned by applying an external magnetic flux to the qubit loop. The magnetic flux can be adjusted such that the dynamical coupling compensates the geometric coupling, yielding zero coupling between the two resonators (defining the *switch setting conditions*). For a detailed description of the quantum switch, we refer to Refs. [3, 5].

The qubit parameters are extracted from two-tone spectroscopy as shown in Fig. 1(c). In Fig. 1(d), the transmission through one of the two resonators depending on the magnetic flux applied to the qubit loop is shown. As expected for coupled harmonic oscillators, two modes can be observed. The frequency of the upper mode depends on the magnetic flux and crosses the lower mode at the switch setting conditions. However, when the qubit is driven, the coupling between the two resonators is present independent of the applied flux, cf. Fig. 1(e). These spectroscopic measurements already indicate that the coupling between the resonators can be switched on and off by driving the qubit or varying the magnetic flux.

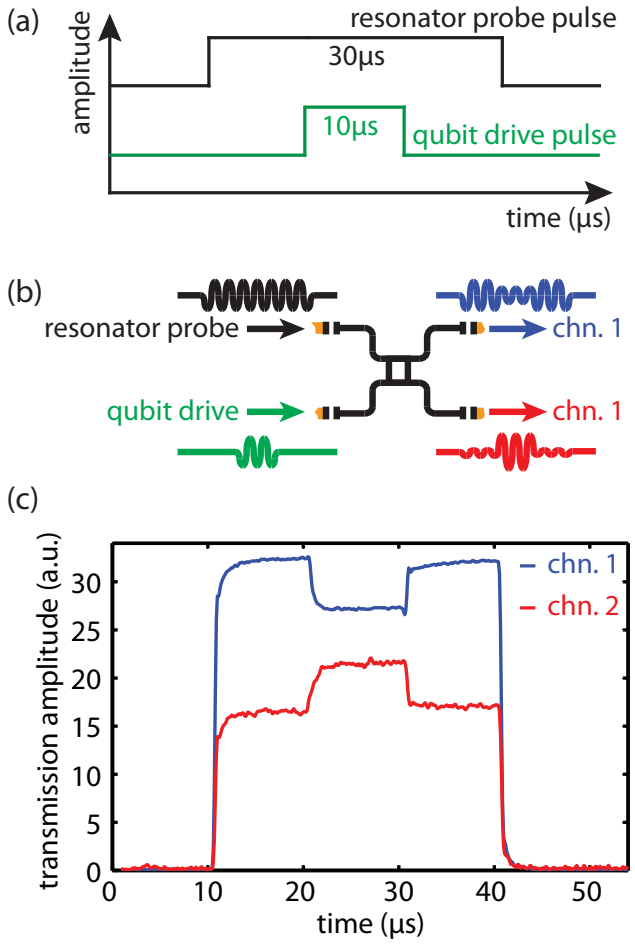

Figure 2: (a) Pulse pattern for the time-domain probe of the quantum switch. The resonator probe pulse has a length of 30 µs. The qubit drive pulse is delayed by 10 µs and is 10 µs long. (b) When the qubit is driven, a decrease in the output signal of the probed resonator is expected as energy is transferred into the second resonator. Simultaneously, an increase in the second resonator output signal is expected. (c) Measured time traces of the output signals of the two resonators. Decrease (chn. 1) and increase (chn. 2) in the resonator output signals are observed as expected when the qubit drive is switched on.

Here, we report on a time domain experiment making the switchable coupling directly observable. To this end, we have set a flux corresponding to the switch setting condition and have applied a probe pulse (length $\tau_{\mathrm{res}} = 30\,\mu\mathrm{s}$) to one of the resonators at the frequency of the lower mode $\omega_{\mathrm{res}} = 4.888\,\mathrm{GHz}$. Only 10 µs after applying the resonator probe pulse, a strong 10 µs driving pulse is applied to the qubit, switching the coupling between the resonators on. A schematic of the pulse sequence is depicted in Fig. 2(a-b). The output signals of both resonators are detected time-resolved using an FPGA-enhanced A/D-converter. The results are shown in Fig. 2(c). After switching on the qubit drive, the output signal level of the resonator where the drive pulse is applied decreases, whereas it increases for the other resonator. This result represents a direct experimental evidence for the expected switching behavior as the transfer of energy from one into another resonator controlled by the qubit state can be observed.

However, for an ideal quantum switch, one would expect that at the switch setting condition the output signal level for the second resonator is zero when the qubit is in the ground state. Nevertheless, in our case a finite output signal level can be observed. We ascribe this finding to the fact that, due to the galvanic coupling, more than two resonant modes are present in our sample (data

not shown), giving rise to an additional coupling channel between the two resonators. While the origin of these additional modes has yet to be understood in full detail, the data shown here still provide experimental evidence for tunable and switchable coupling between two coplanar waveguide resonators.

References

[1] A. Wallraff, D. I. Schuster, A. Blais, L. Frunzio, R.-S. Huang, J. Majer, S. Kumar, S. M. Girvin, and R. J. Schoelkopf, Nature **431**, 162–167 (2004).
[2] T. Niemczyk, F. Deppe, H. Huebl, E. P. Menzel, F. Hocke, M. J. Schwarz, J. J. Garcia-Ripoll, D. Zueco, T. Hummer, E. Solano, A. Marx, and R. Gross, Nat Phys **6**, 772–776 (2010).
[3] E. Hoffmann. Tunable Coupling Between Two Resonators Controlled by a Flux Qubit - The Quantum Switch. In **WMI Annual Report**, pp. 49–50 (2012).
[4] M. Mariantoni, F. Deppe, A. Marx, R. Gross, F. Wilhelm, and E. Solano, Phys. Rev. B **78**, 104508 (2008).
[5] E. Hoffmann. *Experiments on Two-Resonator Circuit Quantum Electrodynamics: A Superconducting Quantum Switch*. Ph.D. thesis, TU München (2013).

Switching Dynamics of Electromechanically Induced Transparency

H. Huebl, F. Hocke, A. Marx, R. Gross [1]
X. Zhou, A. Schliesser, T. J. Kippenberg [2,3]

In the field of optomechanics, a light field trapped in an optical resonator dynamically interacts with a mechanical degree of freedom, enabling cooling and amplification of mechanical motion. This concept of light-matter interaction can be transferred to the microwave (MW) regime combining superconducting MW circuits with nanometer-sized mechanical beams, establishing the class of circuit nano-electromechanics. [1–9]. In this realm, a range of optomechanical phenomena can be explored. Amongst them are the transduction of the displacement of the mechanical oscillator on the microwave properties with a sensitivity below the level of the mechanical zero-point motion, the implementation of microwave sideband cooling to the quantum ground state, and electromechanical amplification of microwave signals [1, 10]. Additionally, spectroscopy of the coupled microwave-mechanical system leads to interference effects such as the electromechanically induced absorption and transparency [1, 2, 11, 12]. Those are important steps towards for the realization of advanced protocols including quantum state transfer from the microwave to the mechanical domain [7, 10–14], fast sideband cooling [15], and routing of classical and quantum microwave signals.

In the following, we consider only the case of red-detuning ($\Delta = -\Omega_m$) [1, 2] (cf. Fig. 1). In this case, a strong drive tone at ω_d close to the lower motional sideband of the superconducting microwave cavity is applied to the system, while a second, much weaker tone probes the modified cavity resonance at frequency $\omega_p = \omega_d + \Omega$. The simultaneous presence of the drive and the probe tones results in a force oscillating at $\Omega = \omega_p - \omega_d$. If this difference frequency is close to the mechanical resonance frequency, $\Omega \simeq \Omega_m$, a coherent oscillation of the mechanical system is induced. As a consequence of this oscillation, Stokes and anti-Stokes fields build up at $\omega_d \pm \Omega_m$ around the strong driving field. Additionally, the microwave resonator acts as a narrow-band filter for these fields. If the system is in the resolved-sideband regime, i.e. if the mechanical frequency Ω_m exceeds the linewidth κ_c of the microwave cavity, the Stokes line at $\omega_d - \Omega_m < \omega_c$ is strongly suppressed because it is off-resonant with the cavity, whereas the anti-Stokes line at $\omega_d + \Omega_m \simeq \omega_c$ is enhanced. Moreover, since the anti-Stokes scattered field is degenerate with the probe field sent to the cavity, it can lead to destructive interference of the two fields, preventing the build-up of an intra-cavity probe field. In consequence, we expect an increased "transparency" of the cavity transmission (cf. inset of Fig. 1).

To this end, we investigate the nano-electromechanical hybrid device outlined in Refs. [1, 2] comprised of a superconducting niobium microwave resonator with a resonance frequency of $\omega_c/(2\pi) = 6.07\,\mathrm{GHz}$ and a linewidth of $\kappa_c/(2\pi) = 742\,\mathrm{kHz}$ and a double layer Si_3N_4/Nb nanobeam with dimensions of $60\,\mu\mathrm{m} \times 140\,\mathrm{nm} \times 200\,\mathrm{nm}$, a mechanical resonance frequency $\Omega_m/(2\pi)) = 1.45\,\mathrm{MHz}$, and a linewidth of $\Gamma_m/(2\pi) = 9\,\mathrm{Hz}$. This system thus resides in the resolved sideband regime as $\Omega_m > \kappa_c$. The experiments are performed in a dilution refrigerator at approximately 170 mK to reduce the initial thermal equilibrium phonon occupancy in the mechanical nanobeam. At an even lower temperature, of approximately 30 mK, we observe an increase in the quality factor to 0.6×10^6. These temperatures are far below the superconducting transition temperature of Nb (9.2 K) and the thermal excitation of the microwave cavity is significantly suppressed, as $\hbar\omega_c/k_B = 288\,\mathrm{mK}$, where $\hbar$ is the reduced Planck constant and k_B is the Boltzmann constant.

[1]The authors acknowledge financial support from the German Excellence Initiative via the "Nanosystems Initiative Munich'" (NIM).

[2]École Polytechnique Fédérale de Lausanne (EPFL), CH-1015 Lausanne, Switzerland

[3]T.J.K acknowledges support by the ERC grant SIMP and X.Z. by the NCCR of Quantum Engineering. Samples were grown and fabricated at the Center of MicroNanotechnology (CMi) at EPFL.

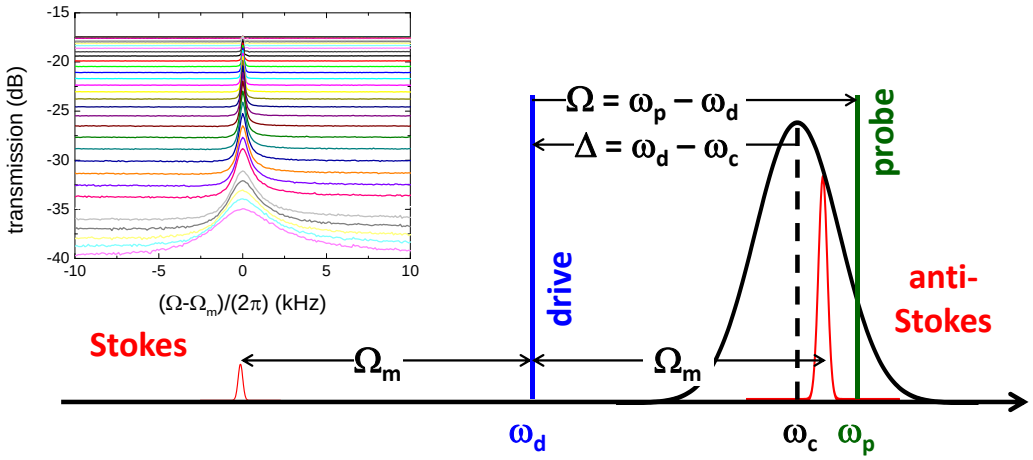

Figure 1: Microwave excitation configuration and electromechanically induced transparency. The drive tone and the probe tone are adjusted to the frequencies ω_d and ω_p, respectively. To detect electromechanically induced transparency, the drive tone is set to the red sideband configuration $\omega_d = \omega_c - \Omega_m$ and the probe tone is swept over the anti-Stokes line. The inset shows the resulting transmission spectra for increasing drive powers. Here, a transparency feature arises and broadens for high drive powers due to the increased effective mechanical damping rate Γ_{eff}.

To access the switching dynamics of the device, we modulate the drive tone and investigate the response of the probe beam in the time domain. Note, that the system's response can be limited both by the dynamics of the mechanical mode amplitude and by the pump field. Figure 2(a) shows the pulse sequence employed to experimentally investigate the dynamics. The continuous wave probe tone is set to the frequency $\omega_p = \omega_d + \Omega_m$ and the drive tone set to ω_d is modulated. Using a sufficiently long pulse, we prepare the system in a steady state situation. After this, we pulse the drive tone with a 50% duty cycle and a pulse length of $T_{on/off}$.

We find, that the transmission displayed in Fig. 2(b) for short pulse times $T_{on/off}$ follows the modulation of the pump tone and is determined by the characteristic time constant of the microwave cavity κ_c. This reveals a counterintuitive regime where the relevant time constant is substantially faster than the slowest time constant of the problem (that is, the inverse effective mechanical damping rate, Γ_m). For longer $T_{on/off}$ we find, that the mechanical damping rate Γ_m is at play as shown in Fig. 2(c). During longer "off" configurations, the mechanical oscillation relaxes towards its equilibrium position at the rate of the intrinsic damping rate Γ_m, so when the pump is switched back on, the mechanical oscillation amplitude is not identical to the steady state configuration present at the end of the preparation pulse. As a consequence, the transparency feature increases back towards its steady state value at a rate of the effective damping rate Γ_{eff}, leading to a recovery to a finite probe transmission. Thus, continuous switching is possible if the loss in the mechanical amplitude due to damping between the successive pump pulses is compensated within the switching period. Note, that in the "on" state, the transparency window amplitude depends significantly on the mechanical oscillation amplitude (see Fig. 2(b) and (c) in combination with the inset in Fig. 1). Extending the demonstrated temporal control in conjunction with probe pulses allows storage of the probe field through conversion into a coherent excitation of the mechanical oscillator [16].

To summarize, we have demonstrated that electromechanically induced transparency can be used in electromechanical systems to manipulate the transmission of a microwave signal in a fully integrated architecture without the need of photon detection and regeneration. Interestingly, the switching can be faster than the timescale of the mechanical oscillator's energy decay rate, a feature which is also of interest for the implementation of narrow switchable filters in the microwave domain. Combining the system with the powerful advances in the generation

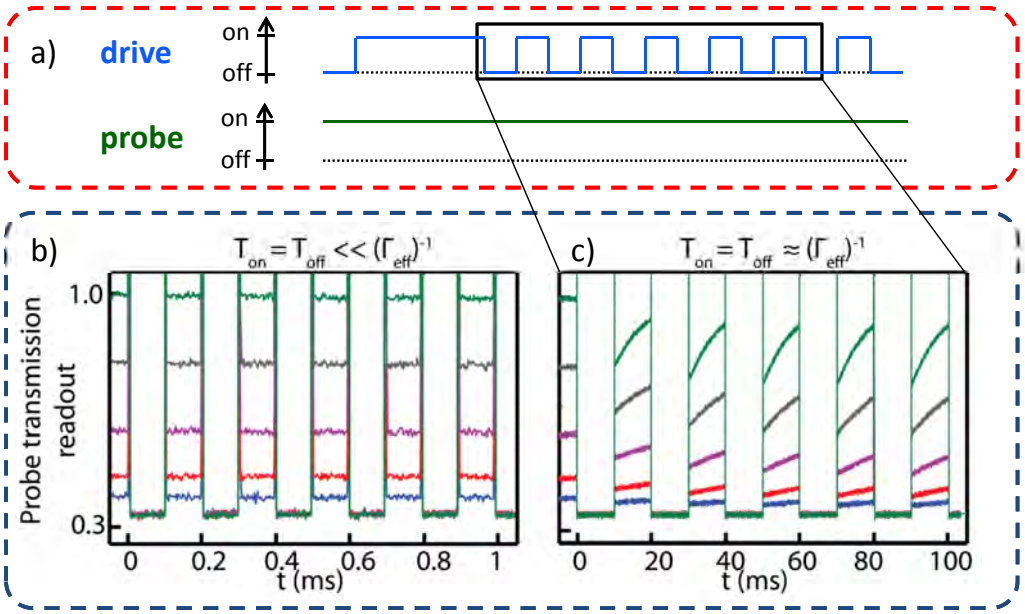

Figure 2: Dynamic response of the transparency feature for pulsed drive tone excitation. The frequencies are configured as outlined in Fig. 1. Panel a) displays the drive pulse sequence sent to the nano-electromechanical device. The probe tone is operated in a continuous wave operation. Panel b) shows the transmission of the system for the on and off times ($T_{on/off}$) short as compared to $(\Gamma_{eff})^{-1}$. Evidently, the system responds on much shorter timescales comparable with the inverse cavity decay rate $(\kappa_c)^{-1}$ and is not limited by Γ_{eff}. For longer $T_{on/off}$ we find, that the mechanical system relaxes during the off period of the pulse, cf. panel (c). Subsequently, when the pulse is switched on again, the system reaches for its steady state value with the effective mechanical damping rate Γ_{eff}.

and detection of single microwave photons may allow for the control over the propagation of non-classical states using the electromechanical architecture. Moreover, it provides the basis for the complete storage and retrieval of a microwave quantum state in long-lived mechanical excitations.

References

[1] F. Hocke, X. Zhou, A. Schliesser, T. J. Kippenberg, H. Huebl, and R. Gross, New J. Phys. **14**, 123037 (2012).
[2] X. Zhou, F. Hocke, A. Schliesser, A. Marx, H. Huebl, R. Gross, and T. J. Kippenberg, Nat. Phys. **9**, 179 (2013).
[3] F. Marquardt, and S. M. Girvin, Physics **2**, 40 (2009).
[4] M. Aspelmeyer, S. Gröblacher, K. Hammerer, and N. Kiesel, J. Opt. Soc. Am. B **27**, A189–A197 (2010).
[5] C. A. Regal, and K. W. Lehnert, J. Phys.: Conf. Ser. **264**, 012025 (2011).
[6] M. Aspelmeyer, P. Meystre, and K. Schwab, Phys. Today **65**, 29–35 (2012).
[7] J. D. Teufel, D. Li, M. S. Allman, K. Cicak, A. J. Sirois, J. D. Whittaker, and R. W. Simmonds, Nature **471**, 204–208 (2011).
[8] T. A. Palomaki, J. W. Harlow, J. D. Teufel, R. W. Simmonds, and K. W. Lehnert, Nature **495**, 210–214 (2013).
[9] T. A. Palomaki, J. D. Teufel, R. W. Simmonds, and K. W. Lehnert, Science **342**, 710 (2013).
[10] F. Massel, T. T. Heikkilaä, J.-M. Pirkkalainen, S. U. Cho, H. Saloniemi, P. J. Hakonen, and M. A. Sillanpää, Nature **480**, 351–354 (2011).
[11] S. Weis, R. Rivière, S. Deléglise, E. Gavartin, O. Arcizet, A. Schliesser, and T. J. Kippenberg, Science **330**, 1520–1523 (2010).
[12] A. H. Safavi-Naeini, T. P. M. Alegre, J. Chan, M. Eichenfield, M. Winger, Q. Lin, J. T. Hill, D. E. Chang, and O. Painter, Nature **472**, 69–73 (2011).
[13] O. Romero-Isart, A. C. Pflanzer, M. L. Juan, R. Quidant, N. Kiesel, M. Aspelmeyer, and J. I. Cirac, Phys. Rev. A **83**, 013803 (2011).
[14] E. Verhagen, S. Delèglise, S. Weis, A. Schliesser, and T. J. Kippenberg, Nature **482**, 63–67 (2012).
[15] X. Wang, S. Vinjanampathy, F. W. Strauch, and K. Jacobs, Phys. Rev. Lett. **107**, 177204 (2011).
[16] T. A. Palomaki, J. W. Harlow, J. D. Teufel, S. R. W., and K. W. Lehnert, Nature **495**, 210 (2013).

Analysis of the Subdominant *d*-Wave Pairing Channel in Iron-based Superconductors

T. Böhm [1], *F. Kretzschmar, R. Hackl* [2]
A.F. Kemper [3], *T.P. Devereaux* [4]

The investigation of the pairing state in iron-based superconductors (FeSC) is of fundamental interest not only for explaining the pairing there but also for studying unconventional superconductivity in general. Taking the FeSC $Ba_{0.6}K_{0.4}Fe_2As_2$ it was found that the s_{+-} state is favored due to the nesting between the central hole bands and the electron bands [1, 2]. However, since the electron bands reside on high symmetry positions the coupling between them is also appreciable and may even be comparable in magnitude to that between the electron and hole bands.

To gain insight into this topic, Raman experiments were performed on optimally doped $Ba_{0.6}K_{0.4}Fe_2As_2$ [3]. It was observed that both couplings affect the Raman spectra in a way that can be described quantitatively with a theoretical model. The experimental data together with the results of the model are presented in Fig. 1. The figure shows difference spectra in the symmetries A_{1g}, B_{2g} and B_{1g} referring to the 1 Fe Brillouin zone. This selection enables one to assign a symmetry to the observed features. For all symmetries the spectra are showing a redistribution of spectral weight from low to high energies because of the opening of the superconducting gap upon cooling [4]. The narrow peak at 140 cm^{-1} only exists in B_{1g}, so this mode has $x^2 - y^2$ symmetry. The superconductivity is assigned to the dominant s_{+-} coupling between the electron and hole bands and the *d*-wave mode to the subdominant coupling between the electron bands, which forms an exciton-like Bardasis-Schrieffer [5–8] mode in an orthogonal symmetry.

A quantitative analysis should now prove these assumptions and reveal properties of both the superconducting gaps and the excitonic mode. The theoretical model is based on a realistic band structure as derived from LDA

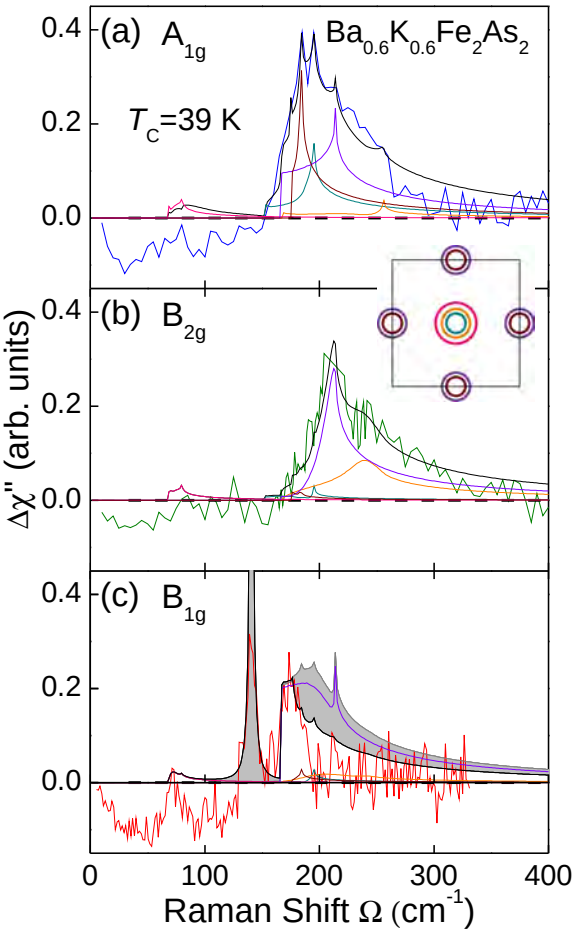

Figure 1: Raman spectra and fits for $Ba_{0.6}K_{0.4}Fe_2As_2$. In order to get the response $\Delta\chi''$, the Raman response in the normal state at 45 K is subtracted from the response in the superconducting state at 8 K. The inset shows a sketch of the bands in the 1 Fe zone to identify the response from each band and their contribution to the complete fit (black). The grey shaded area in B_{1g} is the spectral weight that is shifted from the pair breaking region into the excitonic mode.

[1] Part of the work was performed as visiting researcher at Stanford University during the period December 4, 2012 until May 15, 2013. Since September 2013 support came from the DFG (German Research Foundation) via the priority program SPP1458 (Project number HA 2071/7-2).
[2] The work was supported by the DFG via the Transregional Collaborative Research Center TRR 80.
[3] Lawrence Berkeley National Laboratory, 1 Cyclotron Road, Berkeley, CA 94720, USA
[4] SIMES, SLAC National Accelerator Laboratory, 2575 Sand Hill Road, Menlo Park, CA 94025, USA

calculations [9, 10] containing five bands as seen in the inset of Fig. 1. To reproduce the Raman response arising from superconductivity a **k**-dependent gap $\Delta_n(\mathbf{k})$ was assigned to each band n [11]. In order to apply the theory to the experiment one starts with the B_{2g} spectrum since this one is free from excitonic modes as in B_{1g} and screening effects as in A_{1g}. The response in this symmetry results predominantly from the gap on the outer electron band (purple) being twice as intense as that from the middle hole band (orange). With these gaps fixed, the missing ones can be set using the A_{1g} spectrum. The black curve shows the full response and is in good agreement with experiment. The gaps are visualized in Fig. 2.

All gaps have small anisotropies and nearly the same magnitude except for that on the outer hole band. The Fermi surface of this band has a larger cross section than the other hole bands and thus it is not nested similarly well as the others. Consequently the magnitude of the gap is smaller. The structure of the gaps and their magnitude is in good agreement with ARPES measurements [10, 12].

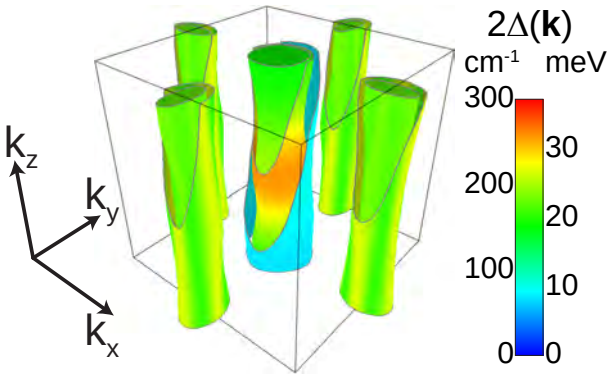

Figure 2: Color-coded magnitudes of the band dependent gaps $\Delta_n(\mathbf{k})$ at the Fermi momentum. The color scale shows a k_z-dependence with maxima at k_z=0 for the gaps at the hole bands and an angular dependence with maxima along k_x and k_y for those at the electron bands.

To reproduce the B_{1g} spectrum, the effect of the d-wave coupling must be included. This is based on the theoretical work of Scalapino and Devereaux [6]. Due to the small gap anisotropy on the outer electron band the B_{1g} spectrum without the effect of the $d_{x^2-y^2}$-wave channel would have a maximum at approximately $190\,\mathrm{cm}^{-1}$ and a shoulder at $170\,\mathrm{cm}^{-1}$. If the d-wave coupling is switched on, the spectral weight is drained from the maximum into the excitonic mode. The relative strength of the d and s channels explains the energy of the collective mode and the transfer of spectral weight.

This opens the possibility that an increase of the d-wave beyond the s-wave coupling strength could lead to a superconductor with the full d-wave symmetry. One can think of enhancing the influence of the electron bands by electron doping and simultaneously reducing the nesting condition by a mismatch of the electron and hole bands. This is in agreement with a proposal on the basis of FLEX calculations [13], where the s-wave coupling dominates for hole and low electron doping while the d-wave coupling prevails for a high electron doping.

References

[1] A. D. Christianson *et al.*, Nature **456**, 930–932 (2008).
[2] I. I. Mazin *et al.*, Phys. Rev. B **82**, 180502 (2010).
[3] F. Kretzschmar *et al.*, Phys. Rev. Lett. **110**, 187002 (2013).
[4] M. V. Klein, and S. B. Dierker, Phys. Rev. B **29**, 4976–4991 (1984).
[5] A. Bardasis, and J. R. Schrieffer, Phys. Rev. Lett. **7**, 472–472 (1961).
[6] D. J. Scalapino, and T. P. Devereaux, Phys. Rev. B **80**, 140512 (2009).
[7] A. Zawadowski, J. Ruvalds, and J. Solana, Phys. Rev. A **5**, 399–421 (1972).
[8] H. Monien, and A. Zawadowski, Phys. Rev. B **41**, 8798–8810 (1990).
[9] S. Graser *et al.*, Phys. Rev. B **81**, 214503 (2010).
[10] M. Yi *et al.*, Phys. Rev. B **80**, 024515 (2009).
[11] G. R. Boyd, T. P. Devereaux, P. J. Hirschfeld, V. Mishra, and D. J. Scalapino, Phys. Rev. B **79**, 174521 (2009).
[12] K. Nakayama *et al.*, EPL (Europhysics Letters) **85**, 67002 (2009).
[13] H. Ikeda, R. Arita, and J. Kuneš, Phys. Rev. B **81**, 054502 (2010).

Phase Fluctuations, Gauge Invariance and the Anderson–Higgs Mechanism in Non–Centrosymmetric Superconductors

Dietrich Einzel and Nikolaj Bittner

Abstract. We formulate a microscopic gauge–invariant theory for the order parameter collective modes applicable to the recently discovered non–centrosymmetric superconductors (NCS) in the clean limit. Besides the gauge mode $\omega_{\rm G}$, common to all superconductors, we can specify a new massive collective mode, which usually occurs in context with phase fluctuations in ordinary two–band superconductors, the so–called *Leggett mode* $\omega_{\rm L}$, for the first time in NCS. Given the existence of these two order parameter collective modes $\omega_{\rm G}$ and $\omega_{\rm L}$ in NCS, we show, that they are both required to ensure the charge conservation law. Moreover we study the electromagnetic response of the pair condensate, which immediately allows for the identification of the condensate plasma mode $\omega_{\rm P}$. The long–range Coulomb interaction is seen to distinguish between the order parameter collective modes $\omega_{\rm G}$ and $\omega_{\rm L}$ with respect to their participation in the Anderson–Higgs mechanism: like in ordinary two–band superconductors, $\omega_{\rm G}$ gets shifted to $\omega_{\rm P}$, whereas $\omega_{\rm L}$ is seen to remain unaffected.

Introduction. The order parameter of conventional and unconventional superconductors is usually classified in terms of either spin singlet (even parity) or spin triplet (odd parity) by the Pauli exclusion principle. A necessary prerequisite for such a classification is, however, the existence of an inversion center. Something of a stir has been caused by the discovery of the bulk superconductors $CePt_3Si$ (tetragonal) and $Li_2Pd_xPt_{3-x}B$ (cubic), without inversion symmetry, to give only two examples, which initiated extensive theoretical and experimental studies. The antisymmetric spin–orbit coupling (ASOC) caused by the absence of an inversion center implies (i) the lifting of the Kramers degeneracy associated with the splitting into a two–band structure and (ii) the possibility of a superposition of singlet and triplet contributions to the energy gap matrix. When applied to NCS, the microscopic BCS description of ordinary two–band superconductors has thus to be generalized to include the singlet–triplet mixture of the NCS energy gap matrix. For a comprehensive review of the physics of NCS, the reader is referred to the book entitled *Non–centrosymmetric superconductors* [1] and references therein. In this letter we focus on the order parameter collective modes in NCS associated with the phase dynamics. We provide for the first time expressions for the gauge mode frequency $\omega_{\rm G}$, the frequency of Leggett's collective mode $\omega_{\rm L}$ as well as for the frequency $\omega_{\rm P}$ of the condensate plasma mode. The interplay of these collective modes is studied in connection with the electromagnetic response of the pair condensate, with special emphasis on the participation of the collective modes in the Anderson–Higgs mechanism [2, 3].

Equilibrium description of NCS. The model Hamiltonian for noninteracting electrons in a non-centrosymmetric crystal reads

$$\hat{\mathcal{H}} \;=\; \sum_{\mathbf{k}\sigma\sigma'} \hat{c}^{\dagger}_{\mathbf{k}\sigma} \left[\xi_{\mathbf{k}}\delta_{\sigma\sigma'} + \boldsymbol{\gamma}_{\mathbf{k}}\cdot\boldsymbol{\tau}_{\sigma\sigma'}\right] \hat{c}_{\mathbf{k}\sigma'}\,, \tag{1}$$

where $\xi_{\mathbf{k}}$ represents the bare band dispersion, $\sigma,\sigma' = \uparrow,\downarrow$ label the spin state and $\boldsymbol{\tau}$ are the Pauli matrices. The second term describes an ASOC with a vectorial coupling $\boldsymbol{\gamma}_{\mathbf{k}}$. In NCS two important classes of ASOCs are realized which reflect the underlying point group $\mathcal{G}$ of the crystal. We shall particularly be interested in the tetragonal point group C_{4v} (application to $CePt_3Si$, for example) and the cubic point group $O(432)$ (applicable to the system $Li_2Pd_xPt_{3-x}B$). For $\mathcal{G} = C_{4v}$ the ASOC reads $\boldsymbol{\gamma}_{\mathbf{k}} = \mathrm{fl}_{\perp}(\hat{\mathbf{k}}\times\hat{\mathbf{e}}_z) + \mathrm{fl}_{\parallel}\hat{k}_x\hat{k}_y\hat{k}_z(\hat{k}_x^2 - \hat{k}_y^2)\hat{\mathbf{e}}_z$. In the purely two-dimensional case ($\mathrm{fl}_{\parallel} = 0$) one recovers what is known as the *Rashba interaction*. For the cubic point group $\mathcal{G} = O(432)$ $\boldsymbol{\gamma}_{\mathbf{k}}$ reads $\boldsymbol{\gamma}_{\mathbf{k}} =$

$\mathrm{fl}_1\hat{\mathbf{k}} - \mathrm{fl}_3\left[\hat{k}_x(\hat{k}_y^2+\hat{k}_z^2)\hat{\mathbf{e}}_x + \hat{k}_y(\hat{k}_z^2+\hat{k}_x^2)\hat{\mathbf{e}}_y + \hat{k}_z(\hat{k}_x^2+\hat{k}_y^2)\hat{\mathbf{e}}_z\right]$. Diagonalizing the Hamiltonian, one finds the eigenvalues $\xi_{\mathbf{k}\mu} = \xi_{\mathbf{k}} + \mu|\boldsymbol{\gamma}_{\mathbf{k}}|$, which physically correspond to the lifting of the Kramers degeneracy between the two spin states at a given $\mathbf{k}$ and hence establish the two–band structure characteristic of NCS metals. Sigrist and co-workers have shown that the presence of the ASOC generally allows for an admixture of a spin–triplet order parameter to a spin–singlet pairing gap. This implies that we can write down the following ansatz for the energy gap matrix in spin space $\Delta_{\mathbf{k}\sigma\sigma'} = [(\Delta_s(T)\mathbf{1} + \mathbf{d}_{\mathbf{k}}(T)\cdot\boldsymbol{\tau})i\tau^y]_{\sigma\sigma'}$ where $\Delta_s(T)$ and $\mathbf{d}_{\mathbf{k}}(T)$ reflect the singlet and triplet part of the pair potential, respectively. It is then easy to see that the ASOC is not destructive for triplet pairing, if one assumes $\mathbf{d}_{\mathbf{k}} \parallel \boldsymbol{\gamma}_{\mathbf{k}}$. This results in the following ansatz for the gap function on both bands $\mu = \pm 1$ in terms of a singlet (Δ_s) and a triplet (Δ_t) amplitude:

$$\Delta_{\mathbf{k}\mu} \;=\; \Delta_s(T) + \mu\Delta_t(T)f_{\mathbf{k}}\;;\; f_{\mathbf{k}} = |\boldsymbol{\gamma}_{\mathbf{k}}| / \left\langle|\boldsymbol{\gamma}_{\mathbf{p}}|\right\rangle_{\mathrm{FS}} \geq 0\,. \tag{2}$$

The gaps $\Delta_s(T)$ and $\Delta_t(T)$ are solutions of the following set of coupled self–consistency equations ($g_{\mathbf{p}\nu}$: Gor'kov pair amplitude):

$$\Delta_{\mathbf{k}\mu} \;=\; \sum_{\mathbf{p}\nu}\Gamma^{\mu\nu}_{\mathbf{kp}}g_{\mathbf{p}\nu}\;;\; g_{\mathbf{p}\nu} = -\theta_{\mathbf{p}\nu}\Delta_{\mathbf{p}\nu}\;;\; \theta_{\mathbf{p}\nu} = \frac{1}{2E_{\mathbf{p}\nu}}\tanh\frac{E_{\mathbf{p}\nu}}{2k_{\mathrm{B}}T}\,, \tag{3}$$

into which the two–gap weak–coupling model pairing interaction $\Gamma^{\mu\nu}_{\mathbf{kp}} = -\left\{\Gamma_s + \Gamma_t\mu\nu f_{\mathbf{k}}f_{\mathbf{p}} - \Gamma_m\left(\mu f_{\mathbf{k}} + \nu f_{\mathbf{p}}\right)\right\}\Theta(\epsilon_0 - |\xi_{\mathbf{k}\mu}|)\Theta(\epsilon_0 - |\xi_{\mathbf{p}\nu}|)$ enters. This model interaction is governed by the pairing interaction matrix $\boldsymbol{\lambda}$ ($\lambda_\alpha = N(0)\Gamma_\alpha, \alpha = s,t,m$) with the aid of which the equilibrium gap equation assumes the compact form

$$\begin{aligned}\left\{-\boldsymbol{\lambda}^{-1} + \begin{pmatrix}\Xi_0 & \Xi_1\\ \Xi_1 & \Xi_2\end{pmatrix}\right\}\cdot\begin{pmatrix}\Delta_s\\ \Delta_t\end{pmatrix} &= \begin{pmatrix}0\\0\end{pmatrix} \\ \boldsymbol{\lambda} &= \begin{pmatrix}\lambda_s & -\lambda_m\\ -\lambda_m & \lambda_t\end{pmatrix};\; \boldsymbol{\lambda}^{-1} = \frac{1}{|\boldsymbol{\lambda}|}\begin{pmatrix}\lambda_t & \lambda_m\\ \lambda_m & \lambda_s\end{pmatrix}.\end{aligned} \tag{4}$$

Here we have defined $\Xi_n = \sum_{\nu=\pm1}\left\langle\theta_{\hat{\mathbf{p}}\nu}\left(\nu f_{\mathbf{p}}\right)^n\right\rangle_{\mathrm{FS}}$ with the index FS denoting the Fermi surface average. Note that in the absence of the off–diagonal elements $\gamma_{\mathrm{ncs}} = \Xi_1 - \lambda_m/|\lambda|$ the respective gap equations for the singlet and triplet components are decoupled. Therefore we expect new physics to emerge from the fact that $\gamma_{\mathrm{ncs}} \neq 0$ (cf. Eq. (13)). In addition to the (off–diagonal) Gor'kov amplitude $g_{\mathbf{k}\mu}$, the equilibrium situation is further specified by the Bogoliubov–Valatin quasiparticle (BVQP) distribution function $\nu(E_{\mathbf{k}\mu}) = [\exp(E_{\mathbf{k}\mu}/k_{\mathrm{B}}T)+1]^{-1}$ and the diagonal distribution function $n_{\mathbf{k}\mu} = u^2_{\mathbf{k}\mu}\nu(E_{\mathbf{k}\mu}) + v^2_{\mathbf{k}\mu}\nu(-E_{\mathbf{k}\mu})$, where $u_{\mathbf{k}\mu}$ and $v_{\mathbf{k}\mu}$ denote the usual coherence factors. In addition we need to define the two energy derivatives $\Phi_{\mathbf{k}\mu} = -\partial n_{\mathbf{k}\mu}/\partial\xi_{\mathbf{k}\mu}$ and $y_{\mathbf{k}\mu} = -\partial\nu(E_{\mathbf{k}\mu})/\partial E_{\mathbf{k}\mu}$.

Electromagnetic condensate response. We turn now to the description of a non–equilibrium situation which, for the time being, is characterized only by a scalar electromagnetic potential $\Phi(\mathbf{q},\omega)$. In addition there exists a charge fluctuation term $\propto \delta n$, which accounts for the action of the long–range Coulomb interaction $V_{\mathbf{q}} = 4\pi e^2/\mathbf{q}^2$ within the RPA, so that $\delta\xi_0 = e\Phi(\mathbf{q},\omega) + V_{\mathbf{q}}\delta n(\mathbf{q},\omega)$ with $\delta n = \sum_{\mathbf{p}\nu}\delta n_{\mathbf{p}\nu}$. Here $\delta n(\mathbf{q},\omega)$ represents the total density response of the system to $\delta\xi_0$. The perturbation $\delta\xi_0$ causes both density (δn) and current ($\mathbf{j} = \sum_{\mathbf{p}\nu}\mathbf{v}_{\mathbf{p}\nu}[\delta n_{\mathbf{p}\nu} + \Phi_{\mathbf{p}\nu}\delta\xi_0]$) fluctuations. Moreover, $\delta\xi_0$ induces fluctuations $\delta g_{\mathbf{k}\mu}$ of the Gor'kov pair amplitude, as well as both amplitude ($\lambda = +1$) and phase ($\lambda = -1$) fluctuations of the order parameter $\delta\Delta^{(\lambda)}_{\mathbf{k}\mu} = \frac{1}{2}[\delta\Delta_{\mathbf{k}\mu} + \lambda\delta\Delta^*_{-\mathbf{k}\mu}]$. In what follows, we wish to focus on the phase fluctuations and decompose $\delta\Delta^{(-)}_{\mathbf{k}\mu}$ into singlet ($\delta\Delta^{(-)}_s$) and triplet ($\delta\Delta^{(-)}_t$) contributions, analogous to Eq. (2), according to

$$\delta\Delta^{(-)}_{\mathbf{k}\mu} = \delta\Delta^{(-)}_s + \mu f_{\mathbf{k}}\delta\Delta^{(-)}_t\,. \tag{5}$$

This order parameter dynamics can be obtained from a straightforward variation of Eq. (3) [4]

$$\delta\Delta^{(-)}_{\mathbf{k}\mu} \;=\; \sum_{\mathbf{p}\nu}\Gamma^{\mu\nu}_{\mathbf{k}\mathbf{p}}\delta g^{(-)}_{\mathbf{p}\nu} \;\;;\;\; \delta g^{(-)}_{\mathbf{k}\nu} + \theta_{\mathbf{k}\mu}\delta\Delta^{(-)}_{\mathbf{k}\mu} = \omega\lambda_{\mathbf{k}\mu}\delta\xi_0 - [\omega^2 - (\mathbf{q}\cdot\mathbf{v}_{\mathbf{k}\mu})^2]\lambda_{\mathbf{k}\mu}\frac{\delta\Delta^{(-)}_{\mathbf{k}\mu}}{2\Delta^{(-)}_{\mathbf{k}\mu}}\,. \quad (6)$$

Here we have defined the condensate response or Tsuneto function:

$$\lambda_{\mathbf{k}\mu} \;=\; 4\Delta^2_{\mathbf{k}\mu}\frac{\theta_{\mathbf{k}\mu}[\omega^2 - (\mathbf{q}\cdot\mathbf{v}_{\mathbf{k}\mu})^2] + \Phi_{\mathbf{k}\mu}(\mathbf{q}\cdot\mathbf{v}_{\mathbf{k}\mu})^2}{(\mathbf{q}\cdot\mathbf{v}_{\mathbf{k}\mu})^2[\omega^2 - 4\xi^2_{\mathbf{k}\mu}] - \omega^2[\omega^2 - 4E^2_{\mathbf{k}\mu}]}\,. \quad (7)$$

The physical significance of the Tsuneto function lies in the sum rule, which generates the so–called *condensate density* $\chi_{\rm P0} = \sum_{\mathbf{p}\mu}\lambda_{\mathbf{p}\mu} = N_{\rm F}\sum_{\nu\pm1}\langle\lambda_{\hat{\mathbf{p}}\nu}\rangle_{\rm FS}$. The total particle density δn can be shown to obey the conservation law

$$\omega\delta n - \mathbf{q}\cdot\mathbf{j} = \sum_{\mathbf{p}\nu}\lambda_{\mathbf{p}\nu}\left\{\left[\omega^2 - (\mathbf{q}\cdot\mathbf{v}_{\mathbf{p}\nu})^2\right]\frac{\delta\Delta^{(-)}_{\mathbf{k}\mu}}{2\Delta_{\mathbf{p}\nu}} - \omega\delta\xi_0\right\} = 0 \quad (8)$$

only, if all phase fluctuation modes of the order parameter in Eq. (6) are properly accounted for. The result for the diagonal phase space density response function $\delta n_{\mathbf{k}\mu}$ reads [4]:

$$\delta n_{\mathbf{k}\mu} \;=\; \left(\frac{\eta^2_{\mathbf{k}}\varphi_{\mathbf{k}}}{\omega^2 - \eta^2_{\mathbf{k}}} - \lambda_{\mathbf{k}}\right)\delta\xi_0 + \omega\lambda_{\mathbf{k}\mu}\frac{\delta\Delta^{(-)}_{\mathbf{k}\mu}}{2\Delta_{\mathbf{k}\mu}} \approx -\lambda_{\mathbf{k}}\delta\xi_0 + \omega\lambda_{\mathbf{k}\mu}\frac{\delta\Delta^{(-)}_{\mathbf{k}\mu}}{2\Delta_{\mathbf{k}\mu}}\,, \quad (9)$$

where in the second equality of Eq. (9) we have ignored the quasiparticle contributions $\propto \varphi_{\mathbf{k}\mu} = \Phi_{\mathbf{k}\mu} - \lambda_{\mathbf{k}\mu}$ to the response. Hence the quantity $\delta n_{\rm P}$, which involves exclusively the Tsuneto function $\lambda_{\mathbf{k}\mu}$,

$$\delta n_{\rm P} = -\chi_{\rm P0}\delta\xi_0 + \omega\sum_{\mathbf{p}\nu}\lambda_{\mathbf{p}\nu}\frac{\delta\Delta^{(-)}_{\mathbf{p}\nu}}{2\Delta_{\mathbf{p}\nu}} = \chi^{(0)}_{\rm P}\delta\xi_0\,, \quad (10)$$

and the function $\chi^{(0)}_{\rm P}$ describes the condensate response of the NCS system alone. We expect that the frequency and wave–vector dependence of $\chi^{(0)}_{\rm P}(\mathbf{q},\omega)$ contains the information on the relevant order parameter collective modes in NCS. Defining $a = \omega^2_{{\rm G}\mathbf{q}} + \omega^2_{{\rm L}\mathbf{q}}$ and $b = \omega^2_{{\rm G}\mathbf{q}}\omega'^2_{{\rm L}\mathbf{q}}$, we find:

$$\chi^{(0)}_{\rm P} = \chi_{\rm P0}\frac{\omega^2_{{\rm G}\mathbf{q}}[\omega^2 - \omega'^2_{{\rm L}\mathbf{q}}]}{\omega^4 - a\omega^2 + b}\,. \quad (11)$$

The physical significance of these frequencies lies in the interpretation of $\omega^2_{{\rm G}\mathbf{q}}$ as the *gauge*, *Anderson–Bogoliubov* or *Nambu–Goldstone* mode of NCS

$$\omega^2_{{\rm G}\mathbf{q}} \;=\; \frac{\sum_{\nu=\pm}\langle\lambda_{\hat{\mathbf{p}}\nu}(\mathbf{q}\cdot\mathbf{v}_{\mathbf{p}\nu})^2\rangle_{\rm FS}}{\sum_{\nu=\pm}\langle\lambda_{\hat{\mathbf{p}}\nu}\rangle_{\rm FS}} \quad (12)$$

as well as of $\omega^2_{{\rm L}\mathbf{q}}$ ($\omega'^2_{{\rm L}\mathbf{q}}$) as *Leggett's collective mode* of NCS

$$\omega^2_{{\rm L}\mathbf{q}} = \omega^2_{\rm L} + \mathcal{O}(\mathbf{q}^2) \approx \omega'^2_{{\rm L}\mathbf{q}} \;\;;\;\; \omega^2_{\rm L} = 4\gamma_{\rm ncs}\frac{\lambda_0\Delta_s^2 + \lambda_2\Delta_t^2 + 2\lambda_1\Delta_s\Delta_t}{\lambda_0\lambda_2 - \lambda_1^2}\,. \quad (13)$$

Here the definitions $\lambda_n = \Delta_s\Delta_t\sum_{\nu=\pm1}\left\langle\lambda_{\hat{\mathbf{p}}\nu}(\nu f_{\mathbf{p}})^n/\Delta^2_{\mathbf{p}\nu}\right\rangle_{\rm FS}$ have been used. The analysis of the roots of $\omega^4 - a\omega^2 + b = [\omega^2 - \omega^2_+][\omega^2 - \omega^2_-]$ immediately leads to $\omega^2_+ = \omega^2_{{\rm L}\mathbf{q}} + \mathcal{O}(\mathbf{q}^4)$

and $\omega_-^2 = \omega_{\mathrm{G}\mathbf{q}}^2 + \mathcal{O}(\mathbf{q}^4)$. Let us now turn to the renormalization of $\chi_{\mathrm{P}}^{(0)}$ by the long–range Coulomb interaction. The observation

$$V_{\mathbf{q}}\chi_{\mathrm{P}}^{(0)} = \frac{\omega_{\mathrm{P}}^2\left[\omega^2 - \omega_{\mathrm{L}\mathbf{q}}'^2\right]}{\omega^4 - a\omega^2 + b} \;\; ; \;\; \omega_{\mathrm{P}}^2(\hat{\mathbf{q}}) = \frac{4\pi n e^2}{m}\sum_\nu 3\left\langle \lambda_{\hat{\mathbf{p}}\nu}(\hat{\mathbf{q}}\cdot\hat{\mathbf{p}})^2\right\rangle_{\mathrm{FS}} \tag{14}$$

allows for the identification of $\omega_{\mathrm{P}}^2(\hat{\mathbf{q}})$ as an *anisotropic condensate plasma frequency* of NCS. Using the abbreviations $A = \underline{\omega_{\mathrm{P}}^2(\hat{\mathbf{q}}) + \omega_{\mathrm{G}\mathbf{q}}^2} + \omega_{\mathrm{L}\mathbf{q}}^2$ and $B = \underline{(\omega_{\mathrm{P}}^2(\hat{\mathbf{q}}) + \omega_{\mathrm{G}\mathbf{q}}^2)}\omega_{\mathrm{L}\mathbf{q}}'^2$, the full density response assumes a form reminiscent of Eq. (11):

$$\delta n_{\mathrm{P}} = \chi_{\mathrm{P}} e\Phi \;\; ; \;\; \chi_{\mathrm{P}} = \chi_{\mathrm{P}}^{(0)}/(1 - V_{\mathbf{q}}\chi_{\mathrm{P}}^{(0)}) = \chi_{\mathrm{P}0}\frac{\omega_{\mathrm{G}\mathbf{q}}^2[\omega^2 - \omega_{\mathrm{L}\mathbf{q}}'^2]}{\omega^4 - A\omega^2 + B}\,. \tag{15}$$

The full condensate density response, also manifested in the condensate dielectric function $\epsilon_{\mathrm{P}} = 1 - V_{\mathbf{q}}\chi_{\mathrm{P}}^{(0)} = (\omega^4 - A\omega^2 + B)/(\omega^4 - a\omega^2 + b)$, is seen to display what is referred to as the *Anderson–Higgs mechanism* in the theory of NCS, which consists in the shift of the gauge mode to the plasma frequency ($\omega_{\mathrm{P}\mathbf{q}}^2 = \omega_{\mathrm{P}}^2(\hat{\mathbf{q}}) + \omega_{\mathrm{G}\mathbf{q}}^2$), as indicated in the underlined parts of the coefficients A and B. The analysis of the roots of $\omega^4 - A\omega^2 + B = [\omega^2 - \Omega_+^2][\omega^2 - \Omega_-^2]$ leads to $\Omega_+^2 = \omega_{\mathrm{P}\mathbf{q}}^2 + \omega_{\mathrm{L}\mathbf{q}}^2 - \omega_{\mathrm{L}\mathbf{q}}'^2 + \mathcal{O}(\mathbf{q}^4)$ and $\Omega_-^2 = \omega_{\mathrm{L}\mathbf{q}}'^2 + \mathcal{O}(\mathbf{q}^4)$. We may therefore state that the Leggett mode, although being related to the phase dynamics of the NCS order parameter, remains unaffected by the long–range Coulomb interaction and hence does not participate in the Anderson–Higgs mechanism. It should be emphasized that a similar result has been found for the case of ordinary two–band superconductors [5].

Conclusions. In summary, we have presented for the first time a comprehensive, gauge–invariant description of the order parameter collective modes (related to fluctuations of the phase) in NCS systems. The relevant modes are found to be (i) the gauge mode $\omega_{\mathrm{G}\mathbf{q}}$, (ii) the Leggett mode $\omega_{\mathrm{L}\mathbf{q}}$ ($\omega_{\mathrm{L}\mathbf{q}}'$) and (iii) the condensate plasma mode $\omega_{\mathrm{P}}(\hat{\mathbf{q}})$. In spite of the more complex singlet/triplet mixture of the NCS order parameter, the gauge mode and the plasma frequency have a form similar to the ones derived for ordinary two–band superconductors. The Leggett mode, on the other hand, looks different when compared with its ordinary two–gap counterpart [5]. The validity of the charge conservation law could be proved by accounting for *both* order parameter collective modes $\omega_{\mathrm{G}\mathbf{q}}$ and $\omega_{\mathrm{L}\mathbf{q}}$. The superconducting analogue to the Higgs mechanism [3] in particle physics could be shown to be at work, in which only the gauge mode participates $\omega_{\mathrm{G}\mathbf{q}}^2 \to \omega_{\mathrm{P}\mathbf{q}}^2$, whereas the Leggett mode does not. Future activities will include (i) the solution of the gap equation (4), (ii) a comprehensive numerical analysis of the wave–vector and temperature dependence of $\omega_{\mathrm{G}\mathbf{q}}$ and $\omega_{\mathrm{L}\mathbf{q}}$ ($\omega_{\mathrm{G}\mathbf{q}}'$) for different crystal symmetries ($O(432)$, C_{4v}, ...) and (iii) a careful investigation of the exotic case of a *massless* Leggett mode in the limit $\gamma_{\mathrm{ncs}} \to 0$, which might simulate the existence of two distinct gauge modes in NCS.

References

[1] E. Bauer, and M. Sigrist (eds.) *Non–centrosymmetric superconductors*, Vol. 847 of *Lecture Notes in Physics* (Springer, Heidelberg, 2012).
[2] P. W. Anderson, Phys. Rev. **130**, 439–442 (1963).
[3] P. Higgs, Phys. Rev. Lett. **13**, 508–509 (1964).
[4] For a review of BCS–Nambu kinetic theory see chapter 7 of ref. [1].
[5] A. J. Leggett, Prog. Theor. Phys. **36**, 901–930 (1966).

Phonon Anomalies at the Helimagnetic Phase Transition in MnSi

H.-M. Eiter, P. Jaschke, R. Hackl [1]
A. Bauer, M. Gangl, C. Pfleiderer [2,3]

MnSi is a magnetic material crystallizing in the non-centrosymmetric B20 structure. The broken inversion symmetry gives rise to spin-orbit coupling and the formation of spin helices below the ordering temperature $T_C = 29\,\mathrm{K}$. The competition between the exchange and the Dzyaloshinskii-Moriya interactions leads to additional ordering phenomena such as the celebrated Skyrmion phase [4] or non-Fermi-liquid phases at high pressure [5]. Recently, the transition at T_C was shown to be of the first order [6], raising, among other things, the question as to the involvement of the lattice.

In our light scattering study we looked in some detail at the temperature and symmetry dependence of the phonons. The results for the E phonons are compiled in Fig. 1. We do not show the full spectra but rather the line widths and the phonon positions as derived from Voigt fitting profiles emulating the convolution of a Gaussian (resolution) and a Lorentzian (homogeneous width) line shape. This is necessary since, due to the high crystal quality, the intrinsic line widths of the phonons are close to the resolution of $2\,\mathrm{cm}^{-1}$. While the line widths decrease smoothly with temperature the phonon positions show various anomalies around and below T_C. Since the anomalies disappear in a magnetic field of 4 T larger than the critical field [4], they can be associated with the helimagnetic transition.

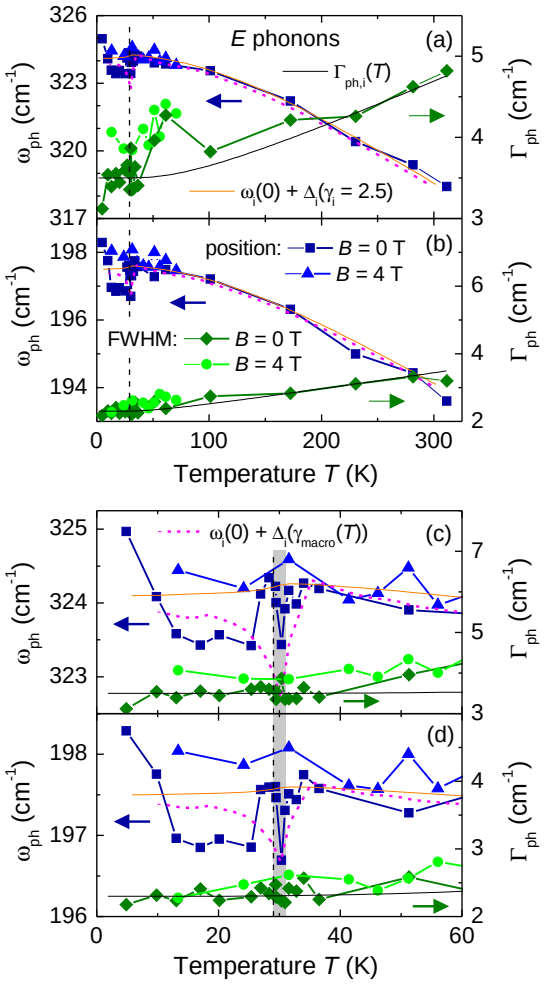

Figure 1: Temperature dependence of the E phonons in MnSi. Shown are the frequencies (left scale) and widths (right scale) of the two strongest lines for (a,b) the full temperature range and (c,d) low temperature. The linewidth can be described by the model of anharmonic decay [1] (black lines). The frequency change originates in the thermal expansion and can be described by a constant Grüneisen parameter $\gamma_i = 2.5$ above 35 K (orange line). The dip in the phonon frequency right above T_C (dashed vertical line) in the fluctuation disordered regime [2, 3] (shaded) can be mimicked using thermodynamic parameters (dashed magenta line). In a magnetic field of 4 T (triangles and circles), the phonon anomalies disappear.

The line widths of all phonons (including the T_2 modes) can be well described by symmetric anharmonic decay [1] in the entire temperature range studied (black solid curves). However, the anharmonic decay is insufficient to explain the shift of the phonons. The major contribution rather comes from the expansion of the lattice. Clearly various effects contribute to the coefficient of thermal expansion $\alpha(T)$ including the normal anharmonic processes and magnetostriction. The experimental results for $\alpha(T)$ directly indicate that the phase transition has

[1] The work was supported by the DFG via project HA 2071/5 in the coordinated program PAK 405.
[2] Physik-Department E21, Technische Universität München, 85748 Garching
[3] The work was supported by the DFG via project PF 393/10-1 in the coordinated program PAK 405. Current support comes from the European Commission via the ERC grant 291079 TOPFIT.

a substantial impact on the lattice [7–9]. An influence of magnetism can be detected up to 200 K [2, 8]. While we cannot disentangle the various contributions completely, we study the role of the Raman-active phonons.

The contribution of a phonon mode i to the volume change is given by the microscopic Grüneisen parameter $\gamma_i = -\partial(\ln\omega_i)/\partial(\ln V)$. If we assume that γ_i is temperature independent, the equation can be integrated [10], yielding a relation between the shift $\Delta_i(T)$ and $\alpha(T) \propto V(T)$,

$$\Delta_i(T) = \omega_i(0)\left\{\exp\left[-3\gamma_i\int_0^T \alpha(T')dT'\right] - 1\right\}. \quad (1)$$

Using the data for $\alpha(T)$ from the literature [9] and setting $\gamma_i = 2.5$, the orange curves in Fig. 1 are obtained being in agreement with the Raman results at $T > 35$ K. Around T_C and below, the phonon anomalies are not reproduced at all, for instance, the dip in the frequency above T_C which is clearly resolved in Fig. 1 (c) and (d). Therefore we reexamine the thermodynamic data [11, 12] and use it to calculate [13] the macroscopic Grüneisen parameter γ_{macro}. Below 50 K, γ_{macro} is strongly temperature dependent while it saturates at 2.5 above. First, this justifies the choice of γ_i and, second, if γ_{macro} is substituted tentatively[4] for γ_i in Eq. (1) the dip above T_C is by and large reproduced. Yet, the recovery of the phonon energies at T_C and the renormalization below have no correspondence. As shown in detail in Fig. 2 for the two strongest E and T_2 phonons, the energy dip above T_C vanishes after subtraction of $\Delta_i(T)$ leaving behind a substantial anomaly at T_C and a softening below. Obviously, the phonons reproduce the magnetostriction effects in the paramagnetic phase down to approximately 35 K and possibly even in the fluctuation regime. In the vicinity of the phase transition and below volume effects cannot account for the phonon anomaly but the phonons may couple directly to the spin order.

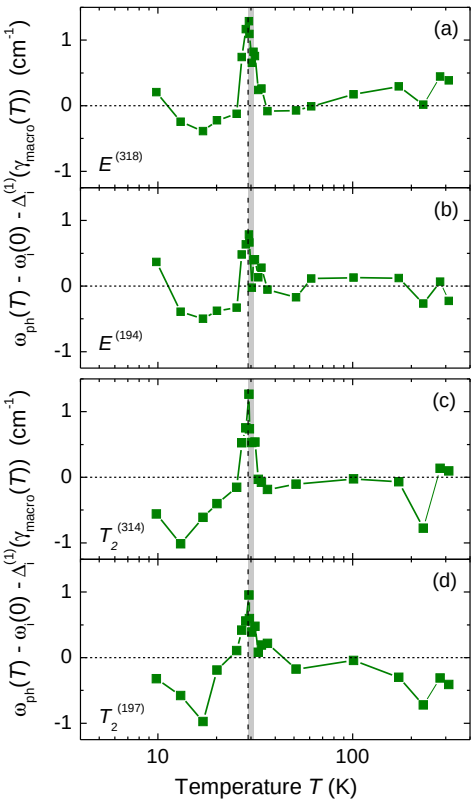

Figure 2: Difference between the experimental phonon energies $\omega_{\text{ph}}(T)$ of the four strongest lines and those calculated via Eq. (1) using $\gamma_{\text{macro}}(T)$. Note the logarithmic temperature scale. The anomaly at T_C has no correspondence in the thermodynamic properties.

References

[1] P. G. Klemens, Phys. Rev. **148**, 845–848 (1966).
[2] Y. Ishikawa, Y. Noda, Y. J. Uemura, C. F. Majkrzak, and G. Shirane, Phys. Rev. B **31**, 5884–5893 (1985).
[3] B. Roessli, P. Böni, W. E. Fischer, and Y. Endoh, Phys. Rev. Lett. **88**, 237204 (2002).
[4] S. Mühlbauer *et al.*, Science **323**, 915–919 (2009).
[5] C. Pfleiderer, P. Böni, T. Keller, U. K. Rößler, and A. Rosch, Science **316**, 1871–1874 (2007).
[6] M. Janoschek *et al.*, Phys. Rev. B **87**, 134407 (2013).
[7] E. Fawcett, J. Maita, and J. Wernick, Intern. J. Magnetism **1**, 29–34 (1970).
[8] M. Matsunaga, Y. Ishikawa, and T. Nakajima, J. Phys. Soc. Jpn. **51**, 1153–1161 (1982).
[9] S. M. Stishov *et al.*, J. Phys.: Condens. Matter **20**, 235222 (2008).
[10] C. Postmus, J. R. Ferraro, and S. S. Mitra, Phys. Rev. **174**, 983–987 (1968).
[11] A. E. Petrova, and S. M. Stishov, J. Phys.: Condens. Matter **21**, 196001 (2009).
[12] A. Bauer, M. Garst, and C. Pfleiderer, Phys. Rev. Lett. **110**, 177207 (2013).
[13] N. W. Ashcroft, and N. D. Mermin. *Solid State Physics* (CBS Publishing Asia LTD., 1988).

[4] Eq. (1) is justified only for constant γ, and $\gamma_{\text{macro}} = 2.5$ holds only for $T > 50$ K.

Fermi surface transformation in the electron-doped cuprate superconductor $Nd_{2-x}Ce_xCuO_4$ detected by high-field Hall effect studies

T. Helm, W. Biberacher, A. Erb, M. V. Kartsovnik, and R. Gross [1]
S. Lepault, C. Proust[2]

In order to clarify the mechanism responsible for the high-temperature superconductivity in superconducting (SC) cuprates one needs to know the exact nature of the underlying "normal", i.e. nonsuperconducting state. This long-standing issue, however, remains largely controversial. Even in the relatively simple case of electron-doped cuprates $Ln_{2-x}Ce_xCuO_4$ (Ln = Nd, Pr, Sm, La), where the SC state emerges in direct neighbourhood of a commensurate antiferromagnetic (AF) ordering, there is no consensus as to whether the two states coexist and, if yes, then to which extent [1]. A promising approach to resolving this issue is high-field magnetotransport studies, which recently proved extremely useful for exploring the electronic state in cuprates [2–4]. In particular, for the electron-doped system $Nd_{2-x}Ce_xCuO_4$ (NCCO) the quantum oscillations of magnetoresistance (Shubnikov-de Haas, SdH, effect) observed in the magnetic-breakdown regime have given a compelling evidence of a symmetry-broken state persisting in the overdoped range all the way up to the edge of the SC dome on the x-T phase diagram [3, 5].

Interestingly, the SdH effect was observed on the optimally doped and a range of overdoped compositions of NCCO, whereas no oscillations have been found in underdoped samples. This can hardly be attributed to the crystal quality. On the contrary, from the crystal growth point of view a higher crystal quality is expected the lower the doping level [6, 7]. Fig. 1 shows the amplitude of the slow SdH oscillations (full circles) plotted along with the SC critical temperature T_c (grey line) against Ce concentration x. Going from higher to lower doping, the oscillation amplitude grows, in accord with the increasing superlattice potential [3], till $x = 0.15$. It slightly reduces but still remains sizable at optimal doping $x_{opt} = 0.145$. However, a further decrease of x by just 0.5% leads to a dramatic drop of the amplitude below the resolution level. At the same time the effective cyclotron mass (stars in Fig. 1), extracted from the T-dependence of the oscillations amplitude, grows with an increasing rate, as x approaches x_{opt}. Such a behavior is reminiscent of the diverging effective mass effect found in heavy fermion compounds in the vicinity of a quantum critical point [8]. This suggests a significant change in the electronic system of NCCO occurring very close to optimal doping. In the absence of quantum oscillations below x_{opt}, one can try to employ another magnetotransport quantity, namely, the Hall resistivity for

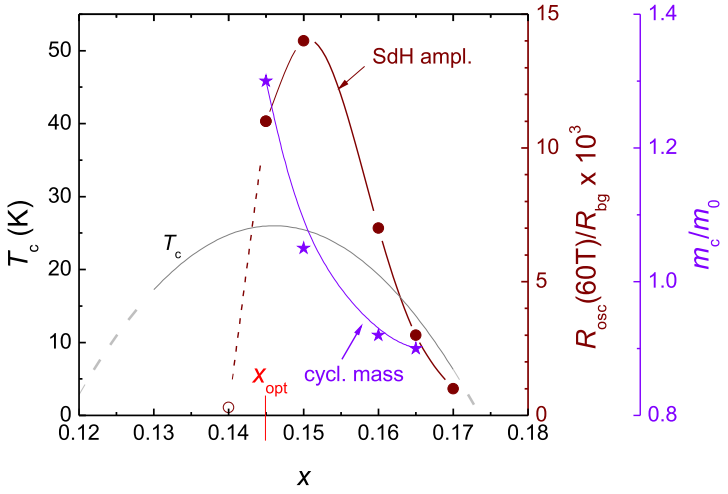

Figure 1: The superconducting critical temperature (grey line), Shubnikov-de Haas amplitude (circles), and effective cyclotron mass (in the free electron mass units, stars) plotted versus Ce concentration x in NCCO single crystals.

[1]The work was supported by the German Research Foundation grant GR 1132/15. The pulsed field experiment was supported by EuroMagNET II under the EU Contract No. 228043.
[2]Laboratoire National des Champs Magnétiques Intenses (LNCMI), CNRS, Toulouse, France

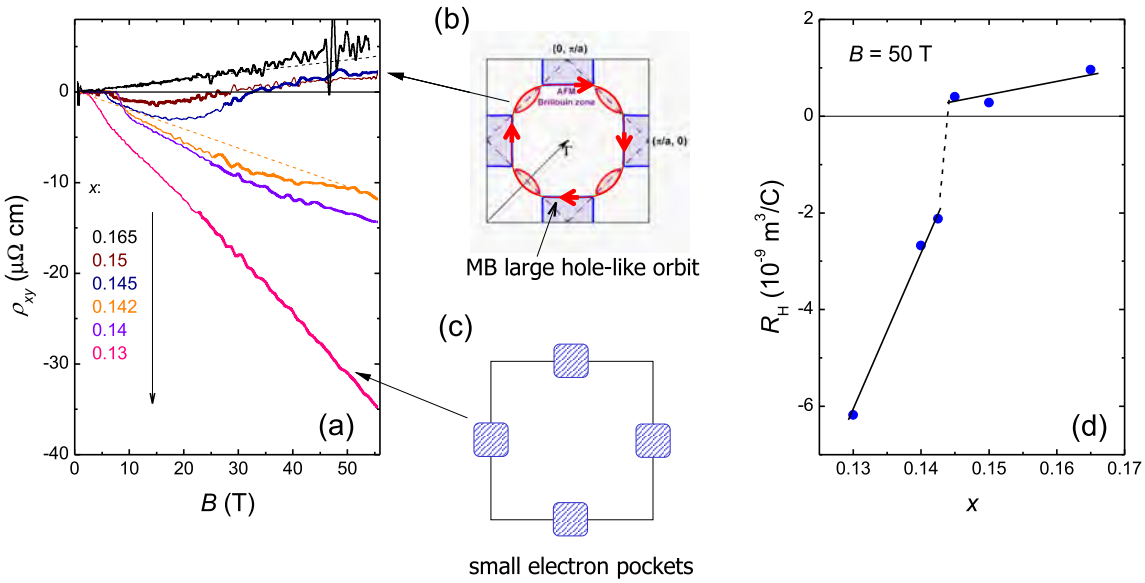

Figure 2: (a) Field-dependent Hall resistivity $\rho_{xy}(B)$ measured on NCCO samples with different Ce concentration x at $T = 2\,\mathrm{K}$ in pulsed magnetic fields. (b) Reconstructed Fermi surface of overdoped NCCO as implied by SdH [3, 5] and Hall effect (present work) experiments. The red line with arrows shows a MB cyclotron orbit encompassing both the hole (red) and electron (blue) Fermi pockets. (c) Pertinent Fermi surface of strongly underdoped ($x \sim 0.13$) NCCO yielding a large negative Hall resistivity. (d) Hall coefficient $R_\mathbf{H} = \rho_{xy}/B$ calculated from the data in (a) at $B = 50\,\mathrm{T}$.

tracking this change.

Hence we have carried out a pulsed-field experiment on the Hall effect in NCCO crystals with different Ce concentrations around x_{opt}. Examples of the field-dependent Hall resistivity $\rho_{xy}(B)$ measured at low temperatures ($T = 2\,\mathrm{K}$) are presented in Fig. 2(a). The overdoped, $x = 0.165$, sample shows a weak positive signal, linearly growing with field. It is consistent with the behavior expected in the magnetic breakdown (MB) regime, when the Hall effect is governed by the large hole-like cyclotron orbit shown by the red line in Fig. 2(b). As the Ce concentration approaches the optimal level $x_{\mathrm{opt}} = 0.145$ [6, 7], the MB field increases to $B_0 \simeq 20\,\mathrm{T}$. At $B < B_0$, small electron- and hole-like orbits on the reconstructed Fermi surface provide competing contributions to the Hall conductivity, resulting to a weak negative $\rho_{xy}(B)$. At $B > B_0$, the signal turns up, crosses zero, and eventually assumes a linear positive slope corresponding to the strong MB regime. For $x < x_{\mathrm{opt}}$, the Hall resistivity is negative, indicating the dominant contribution of small electron Fermi pockets, see Fig. 2(c).

Most interestingly, the behavior of the Hall resistivity is found to change abruptly upon crossing the optimal doping level: the weak positive slope observed at high fields for $x \geq x_{\mathrm{opt}}$ is replaced by a highly negative signal showing no sign of saturation at the highest fields, as soon as the Ce concentration is reduced by just $\approx 0.3\%$ below x_{opt}.[3] To emphasize this change, Fig. 2(d) shows the x dependence of the Hall coefficient $R_\mathbf{H} = \rho_{xy}/B$ at $B = 50\,\mathrm{T}$. One clearly observes a sharp step right below x_{opt}, revealing a considerable transformation in the electronic system.

Taking into account the large negative value of R_H and the absence of MB in the underdoped samples, it is natural to associate the transformation with a large energy gap emerging on a part of the Fermi surface and an accompanied suppression of the hole-like charge carriers. While the exact microscopic origin of this transformation is still to be clarified, it is remarkable

[3] A weak curvature of the $\rho_{xy}(B)$ dependence at fields between 20 and 50 T can be attributed to an unavoidable finite distribution width (typically $\leq 0.3\%$) of Ce concentration through the sample volume. Note that at fields $B > 50\,\mathrm{T}$, $\rho_{xy}(B)$ acquires a linear slope extrapolating to zero, cf. the dashed orange straight line in Fig. 2(a).

that it occurs exactly at the doping level corresponding to the maximum SC critical temperature. Further studies of magnetotransport properties such as magnetoresistance anisotropy, Nernst and Seebeck effects as well as magnetization and NMR experiments on high-quality NCCO crystals around optimal doping level are expected to elucidate the origin of the detected transformation and its impact on superconductivity in electron-doped cuprates.

References

[1] N. P. Armitage, P. Fournier, and R. L. Greene, Rev. Mod. Phys. **82**, 2421–2487 (2010).
[2] L. Taillefer, J. Phys.: Condens. Matter **21**, 164212 (2009).
[3] M. V. Kartsovnik, T. Helm, C. Putzke, F. W.-F. I. Sheikin, S. Lepault, C. Proust, D. Vignolles, N. Bittner, W. Biberacher, A. Erb, J. Wosnitza, and R. Gross, New J. Phys. **13**, 015001 (2011).
[4] B. Vignolle, D. Vignolles, M.-H. Julien, and C. Proust, C. R. Phys. **14**, 39–52 (2013).
[5] T. Helm, M. V. Kartsovnik, I. Sheikin, M. Bartkowiak, F. Wolff-Fabris, N. Bittner, W. Biberacher, M. Lambacher, A. Erb, J. Wosnitza, and R. Gross, Phys. Rev. Lett. **105**, 247002 (2010).
[6] M. Lambacher. *Crystal growth and normal state transport of electron doped high temperature superconductors*. Phd thesis, TU München (2008).
[7] M. Lambacher, T. Helm, M. Kartsovnik, and A. Erb, Eur. Phys. J. Special Topics **188**, 61–72 (2010).
[8] P. Gegenwart, Q. Si, and F. Steglich, Nat. Phys. **4**, 186–197 (2008).

Quantum and Classical Magnetoresistance Oscillations in an Organic Superconductor in the Proximity of the Mott transition

M. V. Kartsovnik, W. Biberacher [1]
V. N. Zverev,[2] *I. Sheikin,*[3] *N. D. Kushch* [4]

One of the most interesting of recently synthesized crystalline organic conductors is the bifunctional layered compound κ-$(BETS)_2Mn[N(CN)_2]_3$ [1]. On the one hand, it exhibits a nontrivial interplay between the magnetism of paramagnetic Mn^{2+} ions in the insulating anion layers and itinerant spins of the conduction system in the molecular BETS layers, involved in a metal-insulator (MI), most likely Mott transition at 20 K [2]. On the other hand, it displays a competition and coexistence of the magnetically ordered insulating and superconducting states [1, 3] typical of strongly correlated materials of current interest such as high-T_c superconductors. Remarkably, due to very small energy scales corresponding to the competition, it is possible to tune the ground state by a small variation of pressure: an ambient-pressure insulator becomes a superconductor at $P \approx 500$ bar [3].

To understand the influence of the insulating ordering instability on the normal charge carriers and on Cooper pairing, it is very important to know the properties of the Fermi surface and their dependence on the proximity to the insulating state. Magnetoresistance effects, in particular, the Shubnikov-de Haas (SdH) effect and angle-dependent magnetoresistance oscillations (AMRO) are known to be very powerful methods of Fermi surface studies in organic metals [4]. Therefore, we have carried out high-field magnetoresistance studies of κ-$(BETS)_2Mn[N(CN)_2]_3$ under pressure $P = 1.7$ kbar. This pressure places the compound into the metallic domain of the $T - P$ phase diagram but rather close to the Mott-insulating region.

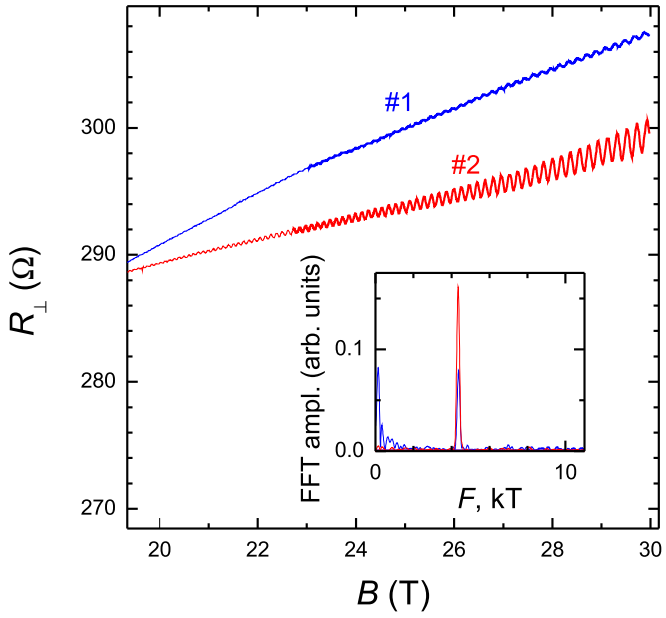

Figure 1: Shubnikov-de Haas oscillations in the interlayer magnetoresistance of two samples of κ-$(BETS)_2Mn[N(CN)_2]_3$. The inset shows the corresponding fast Fourier transform spectra.

We have found both Shubnikov-de Haas (SdH) oscillations and semiclassical angle-dependent magnetoresistance oscillations (AMRO) which provided a direct access to the Fermi surface of the compound. The frequency of the SdH oscillations (Fig. 1), $F \approx 4300$ T, corresponds to the area of the first Brillouin zone, in agreement with the results of theoretical calculations, taking into account the magnetic breakdown effect. The effective cyclotron mass $m_c \approx 7.4 m_0$ (where m_0 is the free electron mass) is notably higher than in cognate κ-type salts, indicating a strong influence of electron correlations.

[1] The work was supported by the German Research Foundation grant No. KA 1652/4-1; the high field measurements were supported by the LNCMI-CNRS, member of the European Magnetic Field Laboratory (EMFL).
[2] Institute of Solid State Physics, Chernogolovka, Russia
[3] Laboratoire National des Champs Magnétiques Intenses (LNCMI), CNRS, Grenoble, France
[4] Institute of Problems of Chemical Physics, Chernogolovka, Russia

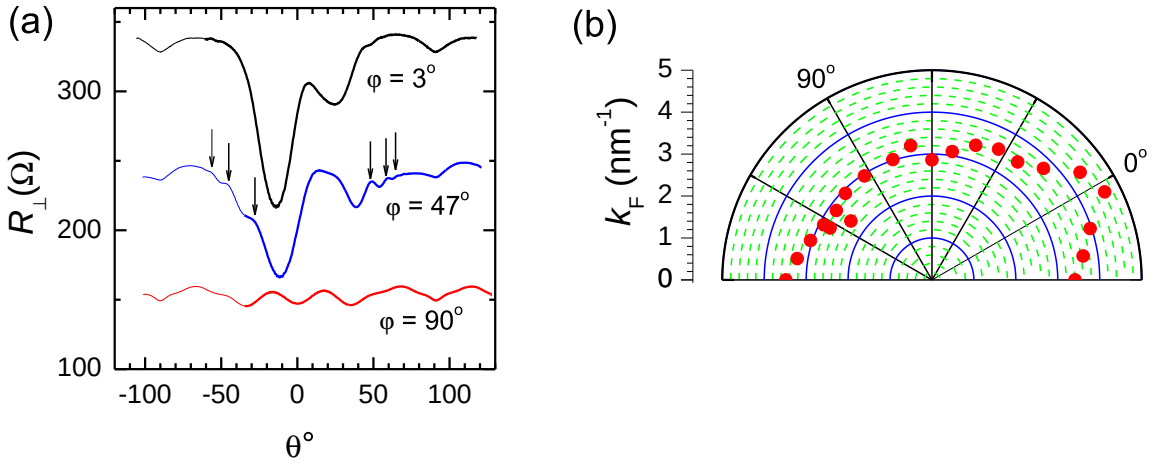

Figure 2: (a) Interlayer resistance at 28 T as a function of the angle θ between the magnetic field direction and the normal to layers, at different fixed azimuthal angles φ. Arrows point to the AMRO features at $\varphi = 47°$. (b) Polar plot of the in-plane Fermi wave vector k_F determined from the φ-dependence of the AMRO period.

A series of field sweeps at different sample orientations was made in search of the spin-zero effect. The latter is an effect of commensurability between the Landau level spacing and Zeeman splitting occurring at certain field orientations [5]. We have succeeded in finding two spin-zeros. However, their positions turn out to be surprisingly asymmetric with respect to the normal to conducting layers. Moreover, our tentative measurements have not revealed any higher-order spin-zeros up to rather large tilt angles. These results suggest a nontrivial magnetic state of the conduction electrons.

Besides the fast SdH oscillations, the magnetoresistance has revealed a few slow features which may also be related to the magnetic state.

Fig. 2(a) shows the interlayer resistance at $B = 28$ T as a function of polar angle θ between the field direction and the normal to conducting layers. The rotation axis is labeled by the azimuthal angle φ. In a wide range of azimuthal orientations clear AMRO features periodic in the $\tan\theta$-scale are observed, as, e.g., indicated by arrows for the $\varphi = 47°$ curve. From the φ-dependence of the AMRO period the size and shape of the relevant Fermi surface has been determined, see Fig. 2(b), which turn out to be consistent with the SdH data above.

Besides the conventional AMRO, the $R(\theta)$ dependence exhibits features [particularly pronounced in the $\varphi = 90°$ curve in Fig. 2(a)], which are not periodic in $\tan\theta$. Taking into account the aforementioned anomalous behavior of spin-zeros and field-dependent magnetoresistance background, it is tempting to associate the new features with magnetic properties of the present material in the vicinity of the Mott-insulating state. More detailed studies of the magnetoresistance, particularly of the effect of field orientation, should elucidate whether the observed anomalies originate from the Mott instability or are related to exchange interaction with localized d-electron spins in the anion layers.

References

[1] N. D. Kushch, E. B. Yagubskii, M. V. Kartsovnik, L. I. Buravov, A. D. Dubrovskii, A. N. Chekhlov, and W. Biberacher, J. Am. Chem Soc. **130**, 7238 (2008).
[2] O. M. Vyaselev, M. V. Kartsovnik, W. Biberacher, L. V. Zorina, N. D. Kushch, and E. B. Yagubskii, Phys. Rev. B **83**, 094425 (2011).
[3] V. N. Zverev, M. V. Kartsovnik, W. Biberacher, S. S. Khasanov, R. P. Shibaeva, L. Ouahab, L. Toupet, N. D. Kushch, E. B. Yagubskii, and E. Canadell, Phys. Rev. B **82**, 155123 (2010).
[4] M. V. Kartsovnik, Chem. Rev **104**, 5737–5781 (2004).
[5] D. Shoenberg. *Magnetic Oscillations in Metals* (Cambridge University Press, Cambridge, 1984).

Low-temperature phase diagram of κ-$(BETS)_2FeCl_4$

M. Kunz, W. Biberacher, K. Neumaier, M.V. Kartsovnik [1]
N.D. Kushch [2]

In the last years bifunctional organic compounds showing quasi-two-dimensional metallic conduction with strong correlation effects and magnetic ordering are studied intensively. Of special interest among these materials is the family $(BETS)_2FeX_4$ with X being Cl or Br. These compounds can crystallize in two modifications called κ and λ differing from each other by the structure of the molecular layer. At low temperatures all these materials show a transition into an antiferromagnetic (AFM) state. While λ-$(BETS)_2FeCl_4$ becomes Mott-insulating at the AFM transition, the κ compounds remain metallic. In κ-$(BETS)_2FeBr_4$ the AFM transition takes place at the Néel temperature $T_N = 2.5\,K$. It further shows a superconducting (SC) transition at 1.1 K. This compound was studied extensively in the past years with several reports on the low-temperature phase diagram, see e.g. [1]. A similar behavior is reported for κ-$(BETS)_2FeCl_4$. It shows the transition to the AF state at $T_N \approx 0.45\,K$ and a possible SC transition below 200 mK [2]. But up to now there exists no data on the low-temperature phase diagram. The SC transition was observed in ac-susceptibility measurements but not seen in resistance. We have performed a detailed analysis of the low temperature phase diagram of κ-$(BETS)_2FeCl_4$ by measuring the interlayer resistance in magnetic fields down to 25 mK.

For this experiment plate-like samples of κ-$(BETS)_2FeCl_4$ were contacted for interlayer magnetoresistance measurements and cooled down in a dilution refrigerator equipped with a 2-axes vector magnet. The samples used showed a metallic behavior of resistance on cooling with the resistance ratio $R(300\,K)/R(0.5\,K) \approx 5000$. In Fig. 1 the temperature dependence of the resistance for low temperatures is plotted. The resistance drop at ~ 460 mK is caused by the transition into the AFM state. This resistance drop is supposed to be caused by reduced scattering of the conduction electrons due to the magnetic ordering [2]. The sample remains metallic at the transition and the slope is even increased below T_N. The deviation from a linear dependence below 200 mK might be the first hint for superconductivity, however no clear SC transition was found for determination of the critical fields.

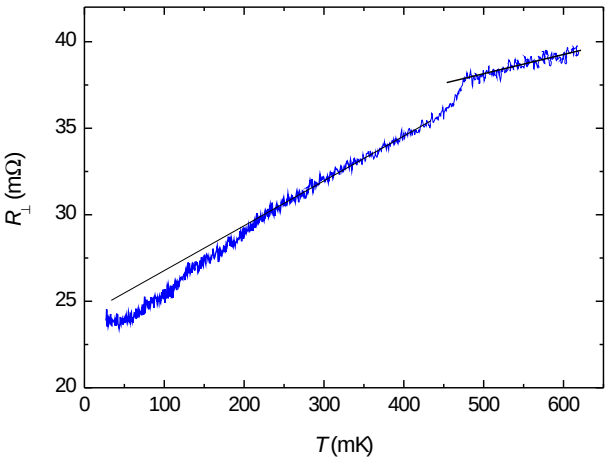

Figure 1: Temperature dependence of the interlayer resistance of κ-$(BETS)_2FeCl_4$ below 0.6 K.

The resistance drop at the AFM transition has made it possible to track the behavior of the AFM phase boundary by just doing resistance measurements. Therefore a series of magnetic field sweeps at different constant temperatures and temperature sweeps at different constant fields were performed. This was done with magnetic field aligned parallel to each of the principal crystal axes. The resulting phase boundaries can be seen in Fig. 2 (note the different scales). The filled/empty symbols represent points taken from temperature/field sweeps.

The black diamonds in Fig. 2 represent the transition for the magnetic field aligned parallel to the b-axis (perpendicular to the conducting layers), which is the hardest axis for the AFM ordering. The AFM state is suppressed by a magnetic field of $B \approx 1.3\,T$ at 160 mK. Interestingly,

[1] This work was supported by the German Research Foundation by grant number KA 1652/4-1.
[2] Institute of Problems of Chemical Physics, 142432 Chernogolovka, Russia

the AFM state is apparently enhanced in small magnetic fields. At about 150 mT we find an increase in T_N by ~ 5 mK in comparison with the zero field value.

For a magnetic field along the *c*-axis (black triangles) the transition temperature is not enhanced by the field and already decreases notably at 400 mT. Measurements at higher fields along this axis were not possible due to the weak horizontal coil of our vector magnet but are planned for the near future.

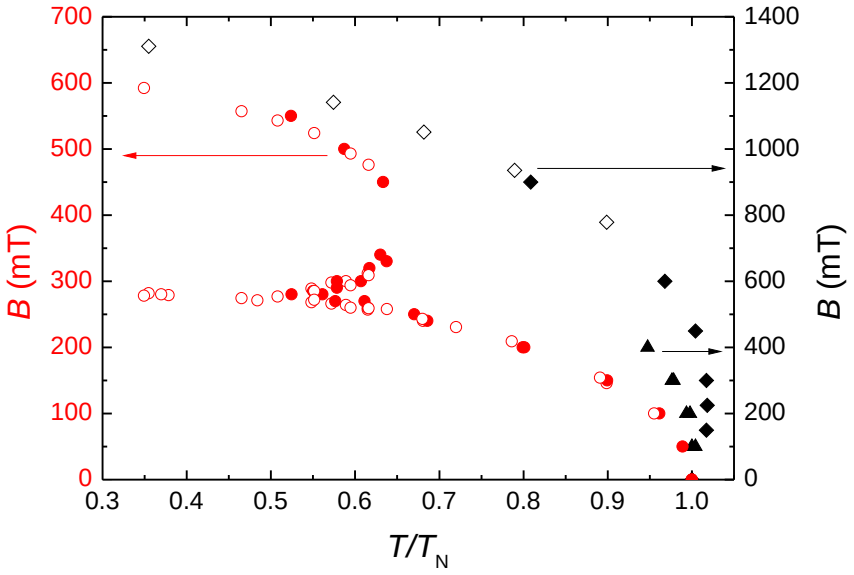

Figure 2: Phase diagram of κ-$(BETS)_2FeCl_4$ for different field directions. Symbols are explained in the text.

The AFM phase boundary changes dramatically, if the field is applied parallel to the *a*-axis, which is the easy axis of the AFM ordering, as shown by the red circles in Fig. 2. Here the transition temperature is decreased strongly already at rather low fields and, at temperatures below 300 mK ($\approx 0.65\,T_N$), another phase line appears. In field sweeps below this temperature two or, in a narrow temperature interval, even three phase transitions are visible. At low temperatures the system undergoes a spin-flop transition where the AFM spin orientation changes by 90°, which is supposed to be a first order phase transition. The second AFM phase is suppressed at approximately twice the spin-flop field. Going to higher temperatures, there exists a bicritical point at $T \approx 0.55\,T_N$ above which there is no first order phase transition any more, but up to $T \approx 0.65\,T_N$ the spin-flopped AFM state can still be accessed due to a reentrant transition. The phase diagram found for the fields along the *a*-axis looks as a textbook example for uniaxial antiferromagnets along the easy axis [3]. To the best of our knowledge, this behavior was not reported for any other organic AFM metal including the sister compound κ-$(BETS)_2FeBr_4$ [1].

In conclusion, the AFM in κ-$(BETS)_2FeCl_4$ shows an interesting behavior in a magnetic fiel applied parallel to the different crystal axes. For fields perpendicular to the conducting layers a small enhancment of the transition temperature at low fields is observed, which, if real, has not be explained yet. For fields parallel to the easy axis a spin-flopped AFM phase appears, which has been theoretically predicted but, to our knowledge, not seen in experiments on organic crystals yet.

References

[1] T. Konoike, S. Uji, T. Terashima, M. Nishimura, S. Yasuzuka, K. Enomoto, H. Fujiwara, B. Zhang, and H. Kobayashi, Phys. Rev. B **70**, 094514 (2004).

[2] T. Otsuka, A. Kobayashi, Y. Miyamoto, J. Kiuchi, S. Nakamura, N. Wada, E. Fujiwara, H. Fujiwara, and H. Kobayashi, J. Solid State Chem. **159**, 407–412 (2001).

[3] L. Landau, and E. Lifshitz. *Electrodynamics of Continuous Media*, Vol. 8 of *A Course of Theoretical Physics* (Pergamon Press, 1984), 2nd edn.

Spin pumping in the strong coupling regime

J. Lotze, H. Huebl, M. Greifenstein, S. Geprägs, R. Gross, S. T. B. Goennenwein [1]

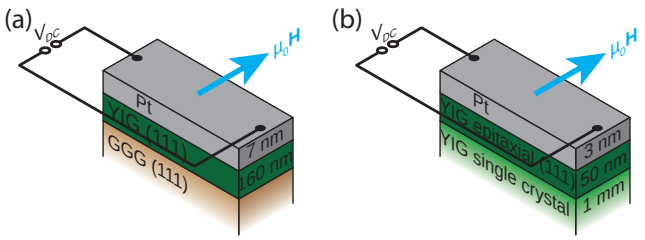

Figure 1: (a) Sample #1: a 160 nm thick YIG film grown on a gadolinium gallium garnet (GGG) substrate and covered by a 7 nm thick Pt layer. (b) Sample #2: a bulk YIG crystal covered by a YIG epilayer, followed by a thin Pt layer. In both cases, the external magnetic field is applied in the film plane and the DC voltage is measured perpendicularly to the magnetic field.

Ferromagnetic resonance (FMR) is a powerful tool for the spectroscopy of ferromagnetic materials. The microwave radiation used to excite FMR is usually enhanced by placing the sample in a resonant cavity. The experiments then are carried out at fixed frequency, while sweeping the magnetic field [1]. In the interpretation of FMR measurements, the resonant cavity mode and the FMR mode of the magnetic sample are thought of as separate entities, not influencing each other. This is a valid approximation in the weak coupling regime, where the coupling between cavity photons and magnons in the sample is small. However, this coupling critically depends on the amount of material in the cavity: the effective coupling between the cavity and the magnetic system is $g_{eff} = g_0\sqrt{N}$, where g_0 is the coupling of the cavity to a single spin, and N is the number of spins in the sample [2]. With a sufficiently large sample, this allows us to reach the strong coupling regime in which $g_{eff}^2 > \kappa\gamma$, where κ, γ are the relaxation rates of the cavity and spin system, respectively. Analogously to the the formation of a molecule from two atoms, the photonic and magnonic states then hybridize and photon-magnon superposition states are created. This is accompanied by a characteristic anticrossing of the dispersion lines of the cavity and FMR modes, according to

$$\omega_{1,2} = \omega_r + \frac{\Delta}{2} \pm \sqrt{\Delta^2 + 4g_{\mathrm{eff}}^2}\,, \tag{1}$$

where $\Delta = \omega_\mathrm{r} - \omega_\mathrm{FMR} = g_S\mu_\mathrm{B}(B - B_\mathrm{FMR})/\hbar$ is the field dependent detuning [3].

Furthermore, in a ferromagnet/normal metal (FM/NM) bilayer, the resonant excitation of the magnetization creates a spin angular momentum flow – a spin current – from FM to the NM in the so-called spin pumping mechanism [4]. This enables the independent and simultaneous measurement of the photonic and the magnonic character of such a hybridized state in a spin pumping experiment: for the measurement of the photonic character the microwave reflection at the cavity entrance is detected, while the magnonic character is accessible by measuring the DC voltage created by the spin current in the NM through the inverse spin Hall effect [5].

We could show that spin pumping experiments indeed are possible in both the weak and the strong coupling regime. We simultaneously measured the FMR and spin pumping signals of two different samples in a resonant cavity as a function of microwave frequency as well as magnetic field: the first (sample #1) is a 160 nm thin film of ferromagnetic yttrium iron garnet (YIG), grown by pulsed laser deposition on a gadolinium gallium garnet substrate and subsequently covered with a 7 nm film of platinum (Fig. 1 (a)). Since the FM layer in this sample is thin, the coupling to the mode of the resonant cavity is expected to be small. Conversely, in sample #2, a platinum film is evaporated onto a piece of single crystal YIG with

[1] This work is supported by the German Research Foundation (DFG) via the project SPP 1538 "Spin Caloric Transport" and the German Excellence Initiative via the Nanosystems Initiative Munich (NIM).

dimensions $1 \times 5 \times 1\,\mathrm{mm}^3$ (Fig. 1 (b)). This increase in volume of the ferromagnet is expected to enhance the coupling by a factor of 100 relative to sample #1.

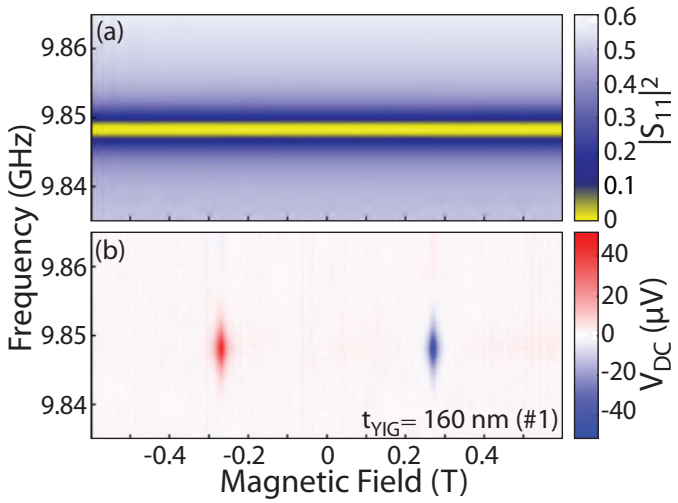

Figure 2: Sample #1: (a) microwave reflection $|S_{11}|^2$ as a function of magnetic field and microwave frequency presented in a false color plot. (b) DC voltage, measured simultaneously, in a false color plot.

The experiments were performed in a microwave cavity operating at 9.848 GHz. A magnetic field of up to ± 1 T was applied in the film plane. The microwave radiation used to excite the cavity and spin system was provided by a vector network analyzer (VNA) connected to the cavity. The FMR was detected by measuring the microwave reflection S_{11} with the VNA. For measuring the spin pumping voltage, DC leads were connected to the sample perpendicularly to the magnetic field (Fig. 1). It was recorded by the auxiliary port of the VNA after preamplification. In this way it is possible to measure both FMR and spin pumping quickly and simultaneously.

In Fig. 2 (a), the microwave reflection $|S_{11}|^2$ is shown as a function of magnetic field and microwave frequency as a false color plot for sample #1. A horizontal line at the resonant frequency of the cavity is clearly visible. The resonance frequency is in this case clearly independent of the applied magnetic field. This is not the case for the spin pumping voltage, also shown as a function of magnetic field and microwave frequency in Fig. 2 (b): at the magnetic field values of ± 0.27 T, which are satisfying the ferromagnetic resonance condition, a spin current into the normal metal is excited resulting in a DC voltage clearly apparent as nearly vertical lines. The DC voltage changes sign with the inversion of the magnetic field direction as is expected from a inverse spin Hall generated voltage. This result clearly shows the system to be in the weak coupling regime, as both the cavity and the FMR modes are essentially unperturbed, straight lines.

In contrast, Fig. 3 shows the strongly coupled case resulting from a measurement of sample #2. Panel (a) shows the microwave reflection measured as a function of microwave frequency

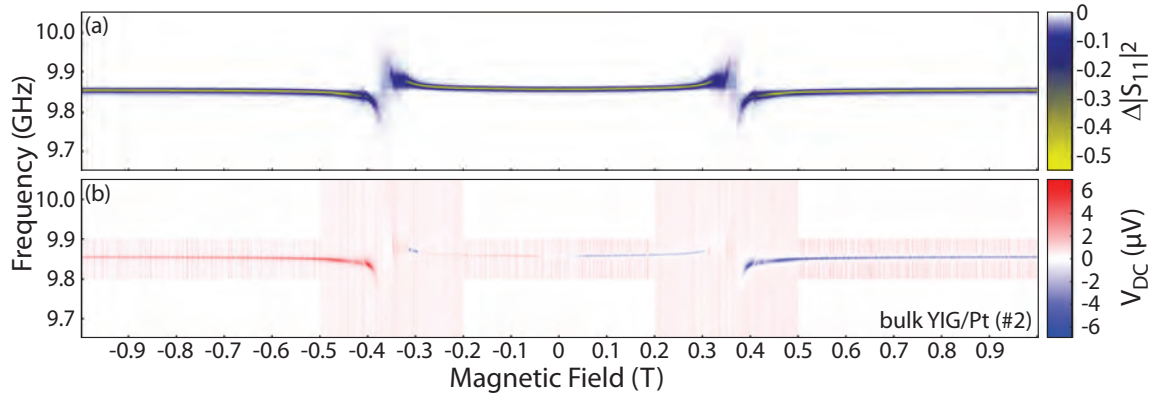

Figure 3: Sample #2: (a) microwave reflection $|S_{11}|^2$ as a function of magnetic field and microwave frequency presented in a false color plot. (b) DC voltage, measured simultaneously, in a false color plot.

and magnetic field as a false color plot. Around the ferromagnetic resonance conditions clear anticrossings between the dispersions of the cavity and the FMR modes can be seen, reflecting the much stronger coupling between the cavity and the magnetic system as compared to sample #1. In addition several bulk spin wave modes are visible, which also couple to the microwave cavity. This pattern is reproduced in Fig. 3 (b), where the measured DC voltage as a function of microwave frequency and magnetic field is shown. This voltage changes sign on magnetic field inversion, as is expected for a inverse spin Hall voltage. However, the spin pumping mechanism cannot account for the DC voltages generated far away from the anticrossing fields, due fact that the excitation at those field values is overwhelmingly "photon-like". The DC voltage in the strong coupling limit thus appears to be much richer as compared to the weak coupling case.

In conclusion, we have demonstrated the ability to record a spin pumping voltage at the same time as the FMR, as a function of both magnetic field and microwave frequency. Our thin film sample shows the expected behavior for the weak coupling limit in both FMR and spin pumping signals. For the strongly coupled case, the FMR is shows the expected anticrossing. The DC signal follows that anticrossing, showing that spin pumping measurements in the strong coupling regime are indeed possible.

References

[1] C. Poole. *Electron Spin Resonance: A Comprehensive Treatise on Experimental Techniques/Second Edition*. Dover books on physics (Dover Publ., 1983).
[2] D. Walls, and G. Milburn. *Quantum Optics*. SpringerLink: Springer e-Books (Springer, 2008).
[3] H. Huebl, C. W. Zollitsch, J. Lotze, F. Hocke, M. Greifenstein, A. Marx, R. Gross, and S. T. B. Goennenwein, Phys. Rev. Lett. **111**, 127003 (2013).
[4] Y. Tserkovnyak, A. Brataas, and G. E. W. Bauer, Phys. Rev. Lett. **88**, 117601 (2002).
[5] E. Saitoh, M. Ueda, H. Miyajima, and G. Tatara, Appl. Phys. Lett. **88**, 182509 (2006).

Spin Hall Magnetoresistance – A Spin-Current Mediated Non-Local Magnetoresistance Effect –

S. Meyer, M. Althammer, M. Schreier, S. Geprägs, M. Opel, R. Gross, S.T.B. Goennenwein [1] *H. Nakayama,*[2] *E. Saitoh,*[3] *Y.-T. Chen,*[4] *G.E.W. Bauer* [5]

Magnetoresistive effects are utilized in a broad variety of applications ranging from magnetic sensors to the read heads of hard disk drives. *Magnetoresistive* hereby refers to characteristic changes of the resistivity of an electrical conductor, induced (and thus also controllable) via magnetic degrees of freedom. Large magnetoresistive effects arise in ferromagnetic metals and corresponding heterostructures, since the charge carriers in these structures propagate through magnetically ordered media and therefore interact strongly with magnetic degrees of freedom. In a recent international collaboration, we have observed and modeled a new type of magnetoresistance [1–4]. In this so-called spin Hall magnetoresistance (SMR), the charge transport and the magnetic properties are confined to spatially disjunct regions, respectively. More specifically, the SMR arises in hybrid bilayers consisting of a paramagnetic normal metal (NM) deposited onto an electrically insulating magnetic material, usually referred to as a ferromagnetic insulator (FMI). In contrast to conventional magnetoresistive effects, in SMR, the magnetic properties of the magnetic insulator (through which no charge current is flowing) characteristically influence the charge transport through the normal metal (which does not exhibit long-range magnetic order). In this sense, the SMR thus is a 'non-local' magnetoresistive effect.

We attribute the SMR to *pure spin currents* propagating across the FMI/NM interface. In other words, angular momentum is transported across the FMI/NM interface into the FMI, while charge transport only takes place in the NM. The SMR arises in a two-step process: A charge current $\mathbf{J_q}$ flowing in the NM [cf. Fig. 1(a)] induces a spin current $\mathbf{J_s}$ with a spin polarization $\mathbf{s}$ via the spin Hall effect (SHE) [5]. If the spin current, spin polarization $\mathbf{s}$ and the magnetization $\mathbf{M}$ of the FMI are not collinear [cf. Fig. 1(a)], $\mathbf{J_s}$ can propagate across the FMI/NM interface into the FMI due to spin transfer torque effects. This outflow of spin current corresponds to a dissipation channel for

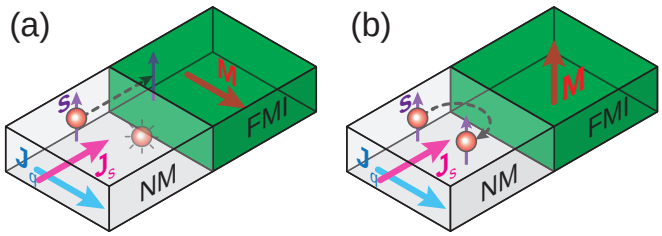

Figure 1: Graphical illustration of the spin Hall magnetoresistance (SMR) in normal metal (NM)/ferromagnetic insulator (FMI) hybrid structures. A charge current $\mathbf{J_q}$ (blue arrow) flowing in the normal metal is converted into a spin current $\mathbf{J_s}$ (magenta arrow) with spin polarization $\mathbf{s}$ (violet arrow) via the SHE. At the FMI/NM interface, the spin current is absorbed or reflected, depending on the relative orientation of the magnetization $\mathbf{M}$ in the FMI (red arrow) and the spin current spin polarization $\mathbf{s}$. (a) If $\mathbf{M}$ is perpendicular to $\mathbf{s}$, it is possible to transfer angular momentum via the spin torque effect, and the spin current gets absorbed by the FMI, effectively increasing the NM resistivity. (b) For a collinear alignment of $\mathbf{M}$ and $\mathbf{s}$, no angular momentum transfer is possible, such that the spin current cannot propagate into the FMI.

[1]Financial support by the German Research Foundation via SPP 1538 (project no. GO 944/4-1) and the Nanosystems Initiative Munich (NIM) is gratefully acknowledged.

[2]Institute for Materials Research, Tohoku University, Sendai 980-8577, Japan.

[3]Institute for Materials Research and WPI Advanced Institute for Material Research, Tohoku University, Sendai 980-8577, Japan; CREST, Japan Science and Technology Agency, Sanbancho, Tokyo 102-0075, Japan, and The Advanced Science Research Center, Japan Atomic Energy Agency, Tokai 319 - 1195, Japan.

[4]Kavli Insitute of Nanoscience, Delft University of Technology, 2628 CJ Delft, The Netherlands.

[5]Kavli Insitute of Nanoscience, Delft University of Technology, 2628 CJ Delft, The Netherlands, and Institute for Materials Research, Tohoku University, Sendai 980-8577, Japan.

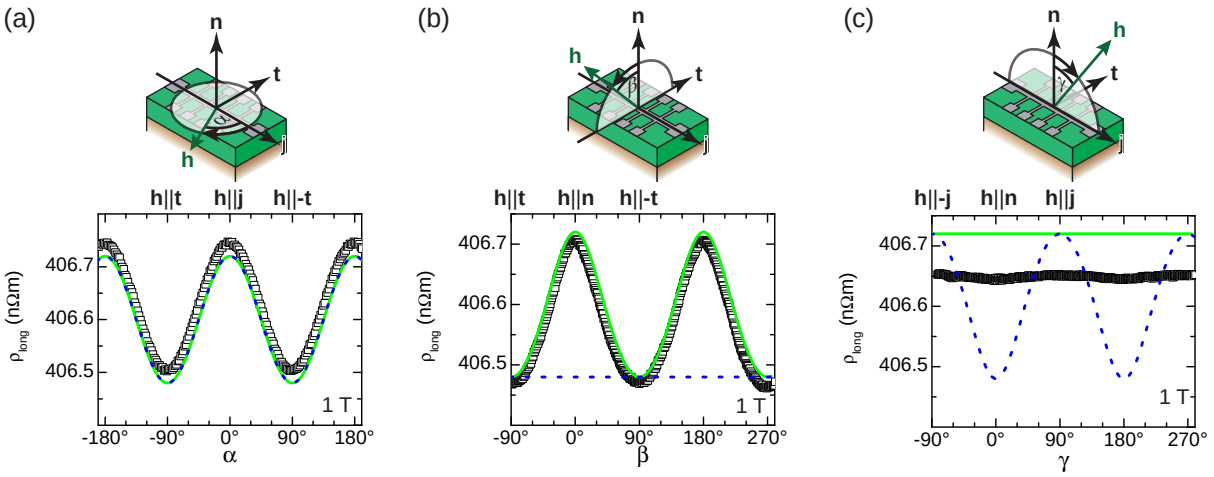

Figure 2: SMR data measured on a YIG (54 nm)/Pt (7 nm) hybrid structure at $T = 300\,\mathrm{K}$ and $\mu_0 H = 1\,\mathrm{T}$: (a) Evolution of the sheet resistivity ρ_{long} as a function of the magnetic field orientation **h** for an in-plane rotation of the external magnetic field. (b) Dependence of ρ_{long} on magnetic field orientation β, rotating **H** around the current flow direction. (c) Angular evolution of ρ_{long} for magnetic field rotation around **t**. The rotation angles α, β and γ are shown in the sketches above the experimental data (the arrows indicate positive direction). The green lines depict a simulation of the data using the SMR model [Eq.(1)], while the dashed blue lines are a simulation with the AMR model, Eq. (2).

the charge transport in NM. In contrast, if **s** and **M** are collinear [cf. Fig. 1(b)], no angular momentum transfer across the interface is possible. The spin current is then reflected at the FMI/NM interface and converted back into a charge current via the inverse spin Hall effect (ISHE) [6], such that there is no spin current-related charge transport dissipation channel in this case. Taken together, the **M** orientation in the FMI thus determines the amount of spin current across the FMI/NM interface, which in turn affects the magnitude of the charge current in the normal metal. In this way, a magnetoresistance in the normal metal arises, governed by the magnetic properties of the ferromagnetic insulator – without any charge current flowing through the magnetically ordered material.

The SMR can be quantitatively modeled in a diffusive spin transport picture, as described in more detail in Ref. [4]. We here only quote that this analysis yields

$$\rho_{\mathrm{long}} = \rho_0 + \rho_1 \, (\mathbf{m} \cdot \mathbf{t})^2 \tag{1}$$

for the sheet resistivity ρ_{long} of the NM film, as a function of the magnetization orientation $\mathbf{m} = \mathbf{M}/M$ in the FMI. The unit vector **t** is in the NM film plane, perpendicular to the direction **j** of charge current (see Fig. 2). The SMR described by Eq. (1) is qualitatively different from the conventional anisotropic magnetoresistance (AMR) of a polycrystalline, metallic ferromagnet, which obeys

$$\rho_{\mathrm{long}} = \rho_0 + \Delta\rho \, (\mathbf{m} \cdot \mathbf{j})^2 . \tag{2}$$

This suggests that magnetotransport experiments as a function of **m** orientation allow to distinguish the SMR effect from AMR.

We experimentally tested the ideas outlined above, using yttrium iron garnet (YIG) thin films as the FMI, and Pt as the NM. The YIG films were grown via pulsed laser deposition onto gadolinium gallium garnet substrates, and covered with a polycrystalline Pt thin film in situ, without breaking the vacuum. Subsequently, the samples were patterned into Hall-bar mesa structures for magnetotransport experiments. Figure 2 shows magnetization orientation dependent resistance measurements, recorded at room temperature while rotating an external magnetic field **H** with a magnitude $\mu_0 H = 1\,\mathrm{T}$ around the film normal **n** (angle α), around the direction **j** of current (angle β), and around the transverse direction **t** (angle γ) [3, 7]. The

green lines in Fig. 2 depict the magnetoresistance expected for SMR according to Eq. (1), while the dashed blue lines show the behavior expected for AMR, Eq. (2). Clearly, our experimental data is in excellent qualitative as well as quantitative agreement with the SMR theory, while conventional AMR cannot explain the observed magnetoresistance. In particular, we thus can exclude magnetoresistive effects in a spin-polarized metallic layer in Pt, induced at the YIG/Pt interface due to the magnetic proximity effect [8], as the origin of the magnetoresistance in our YIG/Pt samples. This notion is further corroborated by X-ray magnetic circular dichroism measurements [9]. Let us also mention that the excellent agreement between SMR theory and experiment is not limited to the sheet resistivity ρ_{long}. Rather, the SMR model also quantitatively accounts for the transverse magnetoresistance (misleadingly often called planar Hall effect in the literature), as well as the anomalous Hall-effect type magnetogalvanic voltages observed in our YIG/Pt hybrids. We furthermore could show that the SMR exists not only in YIG/Pt hybrids, but also in YIG/Au/Pt, YIG/Cu/Pt, Fe_3O_4/Pt, and $NiFe_2O_4$/Pt heterostructures [3]. These results establish the SMR as a universal and robust effect, giving straightforward access to spin transport parameters such as the spin diffusion length and the spin Hall angle in the normal metal. Moreover, the SMR effect is quantitatively consistent with other spin-current related phenomena, in particular spin pumping and the spin Seebeck effect, as discussed in more detail in Ref. [10].

In summary, we have experimentally observed and theoretically modeled a novel magnetoresistance effect, which is based on pure spin current flow across a FMI/NM interface. This so-called spin Hall magnetoresistance is determined by the transmission viz. the reflection of a pure spin current at a FMI/NM interface, depending on the orientation of the magnetization in the magnetic insulator with respect to the spin current spin polarization in the normal metal. Although no charge current can penetrate into the magnetic insulator, its magnetic properties nevertheless characteristically impact the charge transport in the adjacent normal metal. SMR experiments allow to quantify the spin transport parameters in the normal metal, and provide important complementary information for spin caloritronics experiments in ferromagnet/normal metal hybrid structures.

References

[1] M. Weiler, M. Althammer, F. D. Czeschka, H. Huebl, M. S. Wagner, M. Opel, I. Imort, G. Reiss, A. Thomas, R. Gross, and S. T. B. Goennenwein, Phys. Rev. Lett. **108**, 106602 (2012).

[2] H. Nakayama, M. Althammer, Y.-T. Chen, K. Uchida, Y. Kajiwara, D. Kikuchi, T. Ohtani, S. Geprägs, M. Opel, S. Takahashi, R. Gross, G. E. W. Bauer, S. T. B. Goennenwein, and E. Saitoh, Phys. Rev. Lett. **110**, 206601 (2013).

[3] M. Althammer, S. Meyer, H. Nakayama, M. Schreier, S. Altmannshofer, M. Weiler, H. Huebl, S. Geprägs, M. Opel, R. Gross, D. Meier, C. Klewe, T. Kuschel, J.-M. Schmalhorst, G. Reiss, L. Shen, A. Gupta, Y.-T. Chen, G. E. W. Bauer, E. Saitoh, and S. T. B. Goennenwein, Phys. Rev. B **87**, 224401 (2013).

[4] Y.-T. Chen, S. Takahashi, H. Nakayama, M. Althammer, S. T. B. Goennenwein, E. Saitoh, and G. E. W. Bauer, Phys. Rev. B **87**, 144411 (2013).

[5] J. E. Hirsch, Phys. Rev. Lett. **83**, 1834–1837 (1999).

[6] E. Saitoh, M. Ueda, H. Miyajima, and G. Tatara, Appl. Phys. Lett. **88**, 182509 (2006).

[7] W. Limmer, M. Glunk, J. Daeubler, T. Hummel, W. Schoch, R. Sauer, C. Bihler, H. Huebl, M. S. Brandt, and S. T. B. Goennenwein, Phys. Rev. B **74**, 205205 (2006).

[8] Y. M. Lu, Y. Choi, C. M. Ortega, X. M. Cheng, J. W. Cai, S. Y. Huang, L. Sun, and C. L. Chien, Phys. Rev. Lett. **110**, 147207 (2013).

[9] S. Geprägs, S. Meyer, S. Altmannshofer, M. Opel, F. Wilhelm, A. Rogalev, R. Gross, and S. T. B. Goennenwein, Appl. Phys. Lett. **101**, 262407 (2012).

[10] M. Weiler, M. Althammer, M. Schreier, J. Lotze, M. Pernpeintner, S. Meyer, H. Huebl, R. Gross, A. Kamra, J. Xiao, Y.-T. Chen, H. Jiao, G. E. W. Bauer, and S. T. B. Goennenwein, Phys. Rev. Lett. **111**, 176601 (2013).

Magnon, phonon and electron temperature profiles and the spin Seebeck effect in magnetic insulator/normal metal hybrid structures

M. Schreier, M. Weiler, S. Meyer, M. Althammer, M. Opel, S. Geprägs, R. Gross, S. T. B. Goennenwein [1]
A. Kamra[2], *J. Xiao*[3,4], *G. E. W. Bauer*[5,6]

The spin Seebeck effect [1, 2] (SSE) allows to generate pure spin currents from thermal excitations. While the spin Seebeck effect itself has been experimentally established [1–9], an agreement between experiments and theory [10, 11] has proven elusive. In experimental publications the average *temperature gradient* across the entire sample is usually quoted, while the thermodynamic state (local temperature profile) at the interface at which the spin current is generated, could not be measured yet. According to the spin Seebeck theory, however, the knowledge of the actual *temperature difference* ΔT_{me} between the magnon and the electron systems at the ferromagnet/normal metal interface is crucial, since ΔT_{me} determines the magnitude of the spin current [10]. The temperature difference ΔT_{me} arises due to different thermal properties and boundary conditions for the magnons, phonons and electrons in the ferromagnet/normal metal hybrids used in experiments. The phonon (T_p), electron (T_e) and magnon (T_m) temperature profiles in a substrate/ferromagnet/normal metal multilayer structure are schematically depicted in Fig. 1. As detailed in this report, the temperature profiles can show discontinuities at the material interfaces due to interface properties such as the Kapitza resistance [12]. Temperature profiles are not easily measurable for a non-equilibrium situation in which magnon, phonon, and electron temperatures differ. To date, an in depth analysis and interpretation of experimental spin Seebeck effect data is possible only by modeling the magnon, phonon, and electron temperature profiles based on the relevant material parameters. Especially for magnetic insulators the determination of the phonon temperature T_p profile is of central importance in this approach [13, 14].

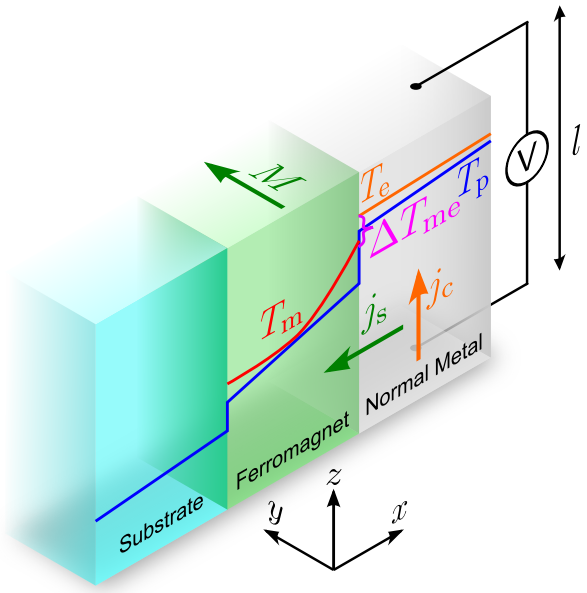

Figure 1: In the (longitudinal) spin Seebeck effect a difference ΔT_{me} between the temperature T_m of the magnons in a ferromagnet (FM) and the temperature T_e of the electrons in a normal metal (NM) causes a spin current j_s between the ferromagnet and the normal metal that is converted into a charge current $\boldsymbol{j}_c \propto j_s \hat{\boldsymbol{x}} \times \hat{\boldsymbol{s}}$ by the inverse spin Hall effect, where $\hat{\boldsymbol{s}} = -\boldsymbol{M}/|\boldsymbol{M}|$ is the polarization vector of the spin current and $\boldsymbol{M}$ is the magnetization vector.

[1] Financial support from the German Research Foundation via SPP 1538 "Spin Caloric Transport", Project No. GO 944/4-1, and the German Excellence Initiative via the Nanosystems Initiative Munich (NIM) is gratefully acknowledged.

[2] Kavli Institute of Nanoscience, Delft University of Technology, Delft, The Netherlands.
[3] Department of Physics and State Key Laboratory of Surface Physics, Fudan University, Shanghai, China.
[4] Supported by the National Natural Science Foundation of China (No. 11004036, No. 91121002).
[5] Kavli Institute of Nanoscience, Delft University of Technology, Delft, The Netherlands
Institute for Materials Research and WPI-AIMR, Tohoku University, Sendai, Japan.
[6] Supported by the German Research Foundation via SPP 1538 "Spin Caloric Transport", Project No. GO 944/4-1 and BA 2954/1-1, FOM (Stichting voor Fundamenteel Onderzoek der Materie), EU-ICT-7 "MACALO", the ICC-IMR, Grand-in-Aid for Scientific Research (Kakenhi) A 25247056.

We have modeled and calculated the phonon, electron and magnon temperature profiles in ferromagnet/normal metal hybrid structures, by solving the heat transport equations with appropriate boundary conditions utilizing three-dimensional finite element (3D FEM) solvers (COMSOL[7]). Details can be found in Ref. [15]. In particular, we explicitly take into account the heat current carried by the pumped spin current through the interface. For the sake of simplicity, we here limit the discussion to hybrids based on the ferrimagnetic insulator yttrium iron garnet ($Y_3Fe_5O_{12}$, YIG). The magnon temperature calculations are based on the work by Sanders and Walton [14] and Xiao *et al.* [10], that we extensively use with a focus on ultrathin films in which interfacial effects become important for the thermal transport. The T_p, T_e, and T_m profiles thus obtained yield the temperature difference ΔT_{me} at the magnetic insulator/normal metal interfaces, from which the spin Seebeck voltage can be inferred [10]. The voltages thus calculated agree well with our spatially resolved longitudinal spin Seebeck effect measurements [6, 15].

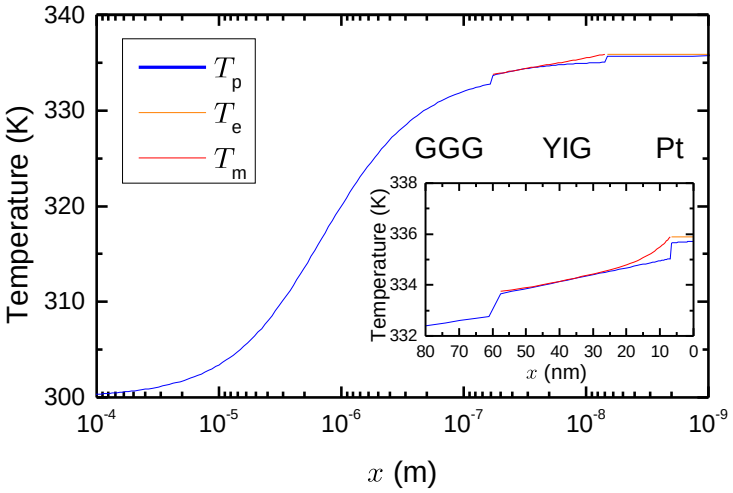

Figure 2: Phonon, electron and magnon temperature distributions along the optical axis of the laser beam at 10 mW laser power in a GGG(500 µm)/YIG(54 nm)/Pt(7 nm) sample calculated via 3D FEM for the entire sample. The inset shows the thin film region.

Figure 2 shows the phonon, electron, and magnon temperature profiles induced by local laser illumination (laser heating) [6] along the film normal x. The phonon temperature (blue line) shows pronounced jumps at the interfaces between the individual layer, stemming from interfacial thermal resistances. This also affects electron and magnon temperature due to their strong coupling with the phonons. Thereby, the inclusion of interfacial thermal resistance leads to a substantial increase in ΔT_{me} by about an order of magnitude. Nevertheless, we find that the coupling between electrons and magnons across the YIG/Pt interface is strong enough as to almost eliminate ΔT_{me} which is of the order of only a few millikelvins. The strong interaction between electrons and magnons is caused by the energy (heat) transport associated with the spin current, leading to the spin Seebeck effect.

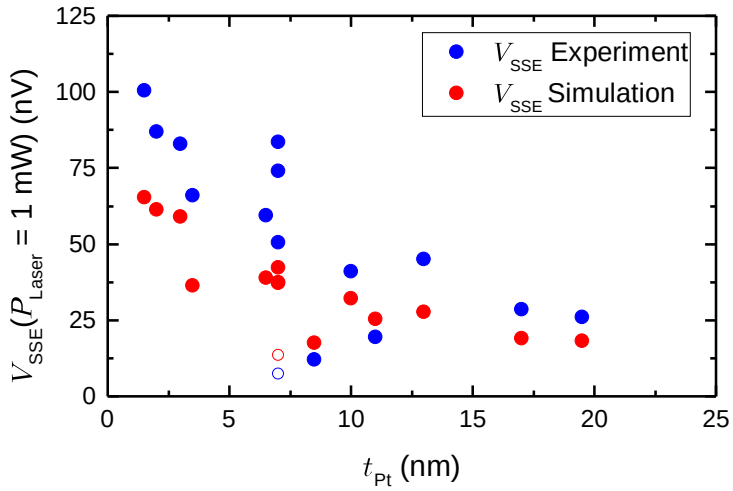

Figure 3: Comparison of the observed and computed spin Seebeck voltages under local laser heating. The open circles depict the sample with an additional gold layer between the platinum and the YIG. A good agreement between theory and experiment is found.

Figure 3 shows a comparison between the voltages measured experimentally in our local

[7]COMSOL Multiphysics® 4.3a

laser heating setup [6, 16] and theoretical values obtained from our simulations for different YIG/Pt heterostructures of varying layer thicknesses. For a YIG(54 nm)/Pt(7 nm) sample, for example, a voltage $V_{\mathrm{SSE}} = 74\,\mathrm{nV}$ is observed in experiment for $P_{\mathrm{laser}} = 1\,\mathrm{mW}$ at the sample surface. This compares reasonably well to the $V_{\mathrm{SSE}} = 37\,\mathrm{nV}$ that we obtain from our simulation. This agreement is not limited to this particular sample as can be seen in Fig. 3. Generally the calculated ΔT_{me} seem to be somewhat underestimated, possibly owing to the magnon property parameters used [15].

In summary, our detailed temperature profile calculations together with the spin Seebeck effect theory [10] allow us to quantitatively reproduce the spin Seebeck voltages observed in our experiments. Our model calculations in particular show that thermal coupling between the magnons in the ferromagnet and the electrons in the normal metal notably affects the magnon temperature in the ferromagnet, an issue widely neglected in the literature so far.

References

[1] K. Uchida, S. Takahashi, K. Harii, J. Ieda, W. Koshibae, K. Ando, S. Maekawa, and E. Saitoh, Nature **455**, 778–781 (2008).
[2] K. Uchida, H. Adachi, T. Ota, H. Nakayama, S. Maekawa, and E. Saitoh, Appl. Phys. Lett. **97**, 172505 (2010).
[3] K. Uchida, J. Xiao, H. Adachi, J. Ohe, S. Takahashi, J. Ieda, T. Ota, Y. Kajiwara, H. Umezawa, H. Kawai, G. E. W. Bauer, S. Maekawa, and E. Saitoh, Nat. Mater. **9**, 894–897 (2010).
[4] K. Uchida, T. Nonaka, T. Ota, and E. Saitoh, Applied Physics Letters **97**, 262504 (2010).
[5] C. M. Jaworski, J. Yang, S. Mack, D. D. Awschalom, J. P. Heremans, and R. C. Myers, Nat. Mater. **9**, 898–903 (2010).
[6] M. Weiler, M. Althammer, F. D. Czeschka, H. Huebl, M. S. Wagner, M. Opel, I.-M. Imort, G. Reiss, A. Thomas, R. Gross, and S. T. B. Goennenwein, Phys. Rev. Lett. **108**, 106602 (2012).
[7] D. Meier, T. Kuschel, L. Shen, A. Gupta, T. Kikkawa, K. Uchida, E. Saitoh, J.-M. Schmalhorst, and G. Reiss, Phys. Rev. B **87**, 054421 (2013).
[8] D. Qu, S. Y. Huang, J. Hu, R. Wu, and C. L. Chien, Phys. Rev. Lett. **110**, 067206 (2013).
[9] T. Kikkawa, K. Uchida, Y. Shiomi, Z. Qiu, D. Hou, D. Tian, H. Nakayama, X.-F. Jin, and E. Saitoh, Phys. Rev. Lett. **110**, 067207 (2013).
[10] J. Xiao, G. E. W. Bauer, K. Uchida, E. Saitoh, and S. Maekawa, Phys. Rev. B **81**, 214418 (2010).
[11] H. Adachi, J.-i. Ohe, S. Takahashi, and S. Maekawa, Phys. Rev. B **83**, 094410 (2011).
[12] P. L. Kapitza, Journal of Physics **4**, 181–210 (1941).
[13] M. I. Kaganov, I. M. Lifshitz, and L. V. Tanatarov, Sov. Phys. JETP **4**, 173–178 (1957).
[14] D. J. Sanders, and D. Walton, Phys. Rev. B **15**, 1489–1494 (1977).
[15] M. Schreier, A. Kamra, M. Weiler, J. Xiao, G. E. W. Bauer, R. Gross, and S. T. B. Goennenwein, Phys. Rev. B **88**, 094410 (2013).
[16] M. Schreier. *Spatially resolved spin Seebeck experiments*. Master's thesis, Technische Universität München (2012).

Application–Oriented Research

Superconducting Microwave Resonators with Tunable Coupling

F. Wulschner, J. Goetz, E. P. Menzel, F. Deppe, A. Marx, R. Gross [1]

In circuit quantum electrodynamics (QED), Josephson-junction based quantum two level systems (qubits) and superconducting microwave resonators are the fundamental building blocks. In contrast to quantum-optical cavity QED, the large effective dipole moment of superconducting qubits allows for the coupling between qubit and resonator to reach the strong or even the ultra-strong regime [1]. In circuit QED architectures with multiple qubits and resonators, quantum logic gates have been successfully realized [2, 3]. However, while the requirements for such digital quantum computing are still enormous, analog quantum simulation with circuit QED systems appears to be a technologically less demanding and therefore attracts increasing interest. In analog quantum simulations, one mimics the Hamiltonian of a system of interest with a circuit offering a higher degree of controllability than the original system. In this context, one specific proposal is to strongly couple nonlinear resonators to explore Bose-Hubbard physics in the driven-dissipative regime [4, 5]. For such experiments, a scalable approach for the realization of tunable coupling between the resonators is strongly desirable. In this report, we present preliminary experimental data in this direction: two LC microwave resonators are coupled via an RF SQUID [6].

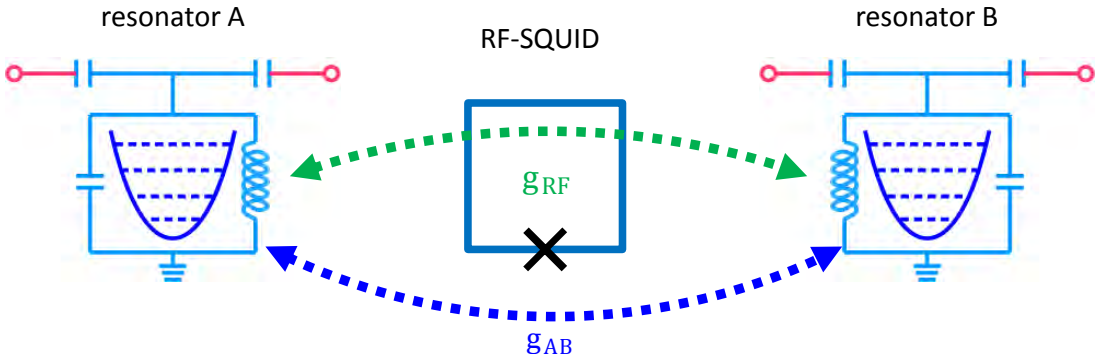

Figure 1: Circuit schematic. The black cross marks the Josephson junction intersecting the RF SQUID loop. Both junction and loop are fabricated using niobium technology. The coupling capacitors at the resonator input and output allow for transmission measurements through the superconducting resonators representing harmonic *LC* oscillators. The sample is mounted inside a dilution refrigerator and cooled to 50 mK.

A schematic of the experiment is shown in Fig. 1. The RF SQUID is positioned at a current antinode of the fundamental mode of both microwave resonators. In a simplified model, we can treat the RF SQUID as a tunable mutual inductance which can change both sign and magnitude depending on the operation point of the RF SQUID. In an experiment, the latter can be controlled by applying a magnetic flux Φ to the RF SQUID loop. Hence, the RF SQUID can mediate a flux-tunable second-order coupling, $g_{\mathrm{RF}} \cos(2\pi\Phi/\Phi_0)$, between the two resonators. This can be used to balance the geometric coupling g_{AB} caused by the physical proximity of the resonators and the resulting overlap of their electromagnetic fields. Another important point is that due to the size of the used RF SQUID loop, in our setup the currents circulating around the RF SQUID loop generate sizable magnetic fields which cannot be neglected. The backaction of these fields onto the RF SQUID is commonly described by the screening parameter β_L. All in all, one finds the resonator-resonator coupling [7]

[1] We acknowledge support by the German Research Foundation via SFB 631, the German Excellence Initiative via NIM, and the EU projects CCQED and PROMISCE.

$$g = g_{\mathrm{AB}} + g_{\mathrm{RF}} \frac{\cos(2\pi\Phi/\Phi_0)}{1+\beta_L \cos(2\pi\Phi/\Phi_0)} \tag{1}$$

For $\beta_L > 1$, the RF SQUID has multiple metastable operation points, which is undesirable for a well-controlled coupling mechanism. However, a small β_L reduces g_{RF} because it implies a small loop size and/or a small critical current of the RF SQUID junction. Therefore, we choose β_L smaller than, but close to unity. We can clearly see the tunable coupling in the transmission measurement through one of the resonators shown in Fig. 2. In particular, the spacing between the two normal modes is reduced near half a flux quantum in the RF SQUID loop. As the next step, we plan to optimize the circuit parameters such that we can completely decouple the resonators. Such an improved device has potential applications in analog quantum simulations and quantum information processing with propagating microwave photons. A further interesting aspect is to drive the coupling at a high frequency. This should allow for the observation of squeezing and parametric amplification as proposed in Ref. [8].

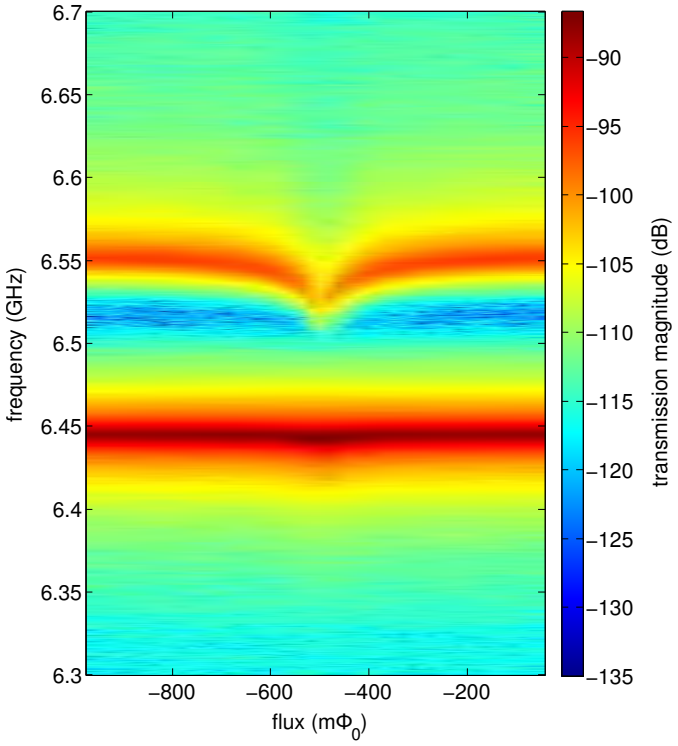

Figure 2: Transmission magnitude (color code) as a function of probing frequency and applied flux through the RF SQUID loop.

References

[1] T. Niemczyk, F. Deppe, H. Huebl, E. P. Menzel, F. Hocke, M. J. Schwarz, J. J. Garcia-Ripoll, D. Zueco, T. Huemmer, E. Solano, A. Marx, and R. Gross, Nature Phys. **6**, 772–776 (2010).
[2] E. Lucero, R. Barends, Y. Chen, J. Kelly, M. Mariantoni, A. Megrant, P. O. Malley, D. Sank, A. Vainsencher, J. Wenner, T. White, Y. Yin, A. N. Cleland, and J. M. Martinis, Nature Phys. **8**, 719–723 (2012).
[3] A. Fedorov, L. Steffen, M. Baur, M. P. da Silva, and A. Wallraff, Nature **481**, 170–172 (2011).
[4] M. Leib, and M. J. Hartmann, New J. of Phys. **12**, 093031 (2010).
[5] M. Leib, F. Deppe, A. Marx, R. Gross, and M. J. Hartmann, New. J. of Phys. **14**, 075024 (2012).
[6] B. Peropadre, D. Zueco, F. Wulschner, F. Deppe, A. Marx, R. Gross, and J. Garcia-Ripoll, Phys. Rev. B **87**, 134504 (2013).
[7] M. S. Allman, F. Altomare, J. D. Whittaker, K. Cicak, D. Li, A. Sirois, J. Strong, J. D. Teufel, and R. W. Simmonds, Phys. Rev. Lett. **104**, 177004 (2010).
[8] L. Tian, M. S. Allman, and R. W. Simmonds, New J. of Phys. **10**, 115001 (2008).

Squeezed Coherent States with Flux-Driven Josephson Parametric Amplifier

L. Zhong, E. P. Menzel, P. Eder, A. Baust, M. Haeberlein, E. Hoffmann, F. Deppe, A. Marx, R. Gross [1,2]

Josephson parametric amplifiers (JPAs) [1, 2] are promising devices to achieve low-noise amplification. In the non-degenerate mode, JPAs behave like linear amplifiers with noise temperature approaching the standard quantum limit dictated by the Heisenberg uncertainty relation. In the degenerate mode, JPAs are phase sensitive amplifiers which can amplify a single signal quadrature with a noise temperature below the standard quantum limit of linear amplifiers, and at the same time squeeze another quadrature below the vacuum fluctuations. Hence, JPAs allow us to study the squeezing physics of propagating quantum microwaves. Here, we first describe the dual-path state reconstruction method [3, 4], and use it to investigate squeezed coherent states generated by a flux-driven JPA [5].

The dual-path state reconstruction setup is shown in Fig. 1. In our experiment, the signal is generated by a flux-driven JPA with a vacuum or a coherent state at the input. We first split the signal using a microwave beam splitter. During this process, vacuum fluctuations produced by a broadband 50 Ω load are added. At the two beam splitter output ports, we first amplify the signals and then downconvert them to an intermediate frequency using IQ-mixers. The resulting orthogonal quadrature signals, $I_{1,2}$ and $Q_{1,2}$, are then digitized by four analog-to-digital-converters (ADCs), and processed in real time by a field programmable gate array (FPGA) logic. Based on the beam splitter relations and on independence of the noise contributions from the two detection paths, we get access to all moments of the annihilation and creation operators of the signal mode and noise contributions up to the fourth order.

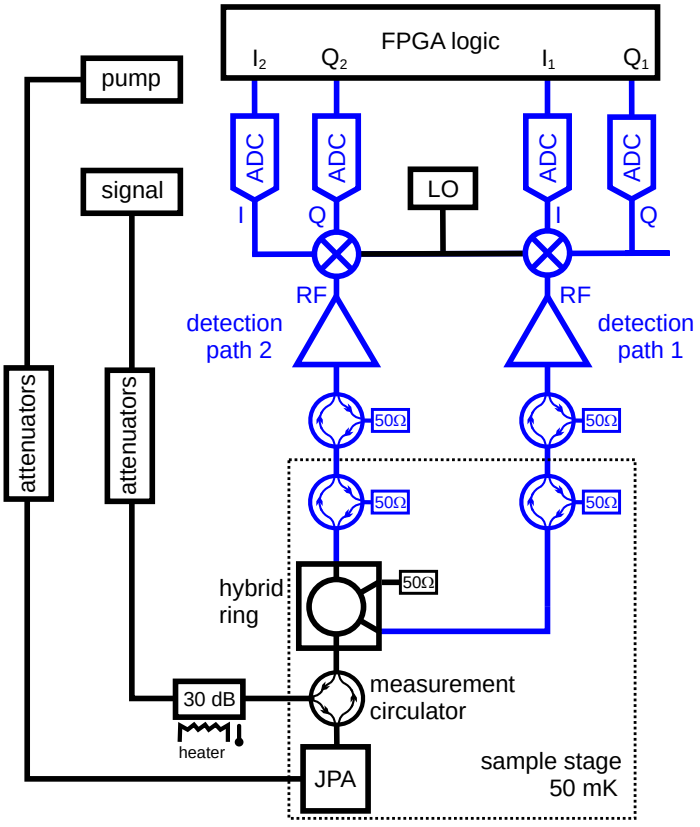

Figure 1: Simplified schematic of the dual path setup [5].

There are two ways to obtain a squeezed coherent state. Starting from the vacuum $|0\rangle$, one can either perform a squeeze operation $\hat{S}(\xi)$ followed by a displacement operation $\hat{D}(\alpha)$ or do the operations the other way round. Here, $\xi \equiv r\exp(\varphi)$ denotes the complex squeeze parameter and α the complex displacement parameter. We define the coherent phases Θ with respect to

[1]We acknowledge financial support from the German Research Foundation via SFB 631, the German excellence initiative via NIM, and the EU projects CCQED and PROMISCE.
[2]We thank C. Probst, K. Neumaier and K. Uhlig for providing their expertise in cryogenic engineering.

a reference plane at the beam splitter input and θ with respect to a reference plane at the JPA input. We further call $\gamma \equiv -\varphi/2$ the anti-squeezed angle. For the former method, the final displacement of the squeezed coherent state only depends on the displacement operation and is independent of the squeeze factor r. However, the displacement of the squeezed coherent state obtained from the second method depends on both the displacement and the squeezing operations. When the anti-squeezed quadrature is parallel to the displacement direction of a coherent state, the final displacement of the squeezed coherent state is maximum.

In Fig. 2, we present an analysis on squeezed coherent states generated with the second method and detected with the dual-path setup. By fixing the anti-squeezing angle of squeezed vacuum states γ at 0°, 45°, 90°, and 135° and rotating the phase Θ of the coherent signal, we map out the dependence of the displacement of a squeezed coherent state on γ and θ. The squeezed vacuum states are centered at the origin, and the coherent states are located on a circle about the origin. When rotating the phase of the JPA coherent input signal, the squeezed coherent state moves mainly along the γ-direction. The displacement of the squeezed coherent states reaches its maximum when $\gamma = \theta + 2n \times 90°$, where $n \in \mathbb{Z}$. To fit to theory, we need to shift the reference plane of the coherent state from the beam splitter input with phase Θ to the JPA input with phase θ. We retrieve $\Delta\Theta = 6.2 \pm 0.2°$ and a squeezing factor $r = 1.8 \pm 0.1$.

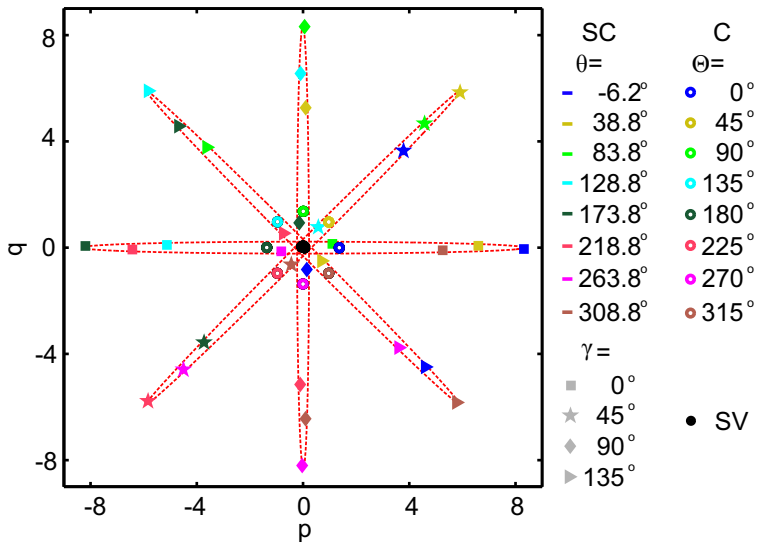

Figure 2: Experimental displacement for squeezed vacuum (SV), coherent (C), and squeezed coherent (SC) states [5]. The displacement is the center of the individual state and in phase space given by its first moment. p and q are the phase space variables.

In summary, we use the dual-path state reconstruction method to study the physics of squeezed coherent microwaves. More detailed information is available from Ref. [5].

References

[1] F. Mallet, M. A. Castellanos-Beltran, H. S. Ku, S. Glancy, E. Knill, K. D. Irwin, G. C. Hilton, L. R. Vale, and K. W. Lehnert, Phys. Rev. Lett. **106**, 220502 (2011).

[2] T. Yamamoto, K. Inomata, M. Watanabe, K. Matsuba, T. Miyazaki, W. D. Oliver, Y. Nakamura, and J. S. Tsai, Appl. Phys. Lett. **93**, 042510 (2008).

[3] E. P. Menzel, F. Deppe, M. Mariantoni, M. Á. Araque Caballero, A. Baust, T. Niemczyk, E. Hoffmann, A. Marx, E. Solano, and R. Gross, Phys. Rev. Lett. **105**, 100401 (2010).

[4] E. P. Menzel, R. Di Candia, F. Deppe, P. Eder, L. Zhong, M. Ihmig, M. Haeberlein, A. Baust, E. Hoffmann, D. Ballester, K. Inomata, T. Yamamoto, Y. Nakamura, E. Solano, A. Marx, and R. Gross, Phys. Rev. Lett. **109**, 250502 (2012).

[5] L. Zhong, E. P. Menzel, R. D. Candia, P. Eder, M. Ihmig, A. Baust, M. Haeberlein, E. Hoffmann, K. Inomata, T. Yamamoto, Y. Nakamura, E. Solano, F. Deppe, A. Marx, and R. Gross, New Journal of Physics **15**, 125013 (2013).

Noise Properties of a Flux-Driven Josephson Parametric Amplifier in the Degenerate Mode

L. Zhong, E. P. Menzel, P. Eder, A. Baust, M. Haeberlein, E. Hoffmann, F. Deppe, A. Marx, R. Gross [1]

Recently, we have witnessed a revival of the interest in Josephson parametric amplifiers (JPA) due to their excellent noise properties. The latter allow for applications in the realm of microwave quantum photonics [1] ranging from ultra-low-noise amplification, tomography of propagating quantum microwaves [2], single-shot readout of superconducting flux qubits [3] to the generation of squeezed states [4] and continuous-variable path entanglement [5]. The latter work can be perceived as as first step on the way to implementation of continuous-variable quantum communication protocols. In this report, we analyze the noise properties of a flux-driven parametric amplifier [6] with the dual-path state reconstruction method [7, 8], which has been developed at the WMI. For details on the operation principle of a JPA and on the dual-path setup, we refer the reader to contribution by Zhong et al. in this annual report (see pp. 67–68) and to our annual report of 2010 [9], respectively.

We operate the JPA in the degenerate mode, where the signal and idler modes occur at the same frequency and interfere. Our operation frequency is 5.637 MHz. Depending on the phase difference between these modes, this interference is constructive or destructive, resulting in amplification or deamplification. In other words, the amplification is phase-sensitive. In Fig. 1, we show the output of the JPA as a function of the temperature T_{att} of the thermal fluctuations at the input (see Ref. [4] for further technical details). For any quadrature X, the variance $(\Delta X_{\mathrm{out}})^2$ at the output of an amplifier is related to the variance $(\Delta X_{\mathrm{in}})^2$ at the input via the relation

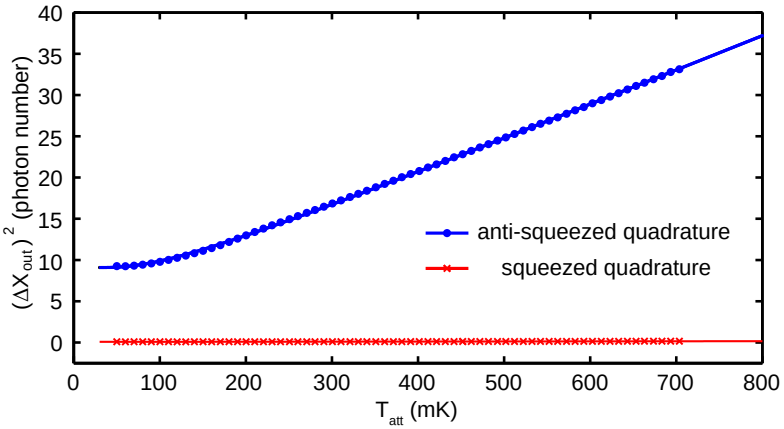

Figure 1: Anti-squeezed and squeezed quadrature variance as a function of the noise source temperature T_{att}. The lines are fits to the data represented by the symbols.

$$(\Delta X_{\mathrm{out}})^2 = G_X\,(\Delta X_{\mathrm{in}})^2 + (\Delta X_{\mathrm{noise}})^2\,. \tag{1}$$

Here, G_X is the power gain for the quadrature X and $(\Delta X_{\mathrm{noise}})^2$ is the noise added by the amplifier referred to its output. We calculate $(\Delta X_{\mathrm{in}})^2$ from the temperature of the noise source and model the cable losses between the noise source output and the JPA input with beam splitters to account for temperature gradients. The variances of the squeezed thermal state at the JPA output, $(\Delta X_{\mathrm{out}})^2$, is obtained by the dual-path reconstruction method [4]. The results are summarized in Tab. 1. We observe a variance of 0.14 ± 0.01 photons (referred to the input) for the noise added by our JPA to the anti-squeezed quadrature. This value is clearly below

[1] This work is supported by German Research Foundation via SFB 631, German Excellence Initiative via NIM, and the EU projects CCQED and PROMISCE.

Table 1: Results of the dual-path analysis of the JPA gain and the noise along the squeezed (sq) and anti-squeezed (anti) quadratures. The error bars describe the statistical error obtained from the fitting procedure. $(\Delta X_{\mathrm{noise}})^2$ is given in units of photon number.

X	G_X (dB)	$(\Delta X_{\mathrm{noise}})^2$	$(\Delta X_{\mathrm{noise}})^2 / G_X$
sq	-11.7 ± 0.3	0.06 ± 0.01	–
anti	13.7 ± 0.1	–	0.14 ± 0.01

the standard quantum limit for a single quadrature of a phase-insensitive amplifier, which is 0.25 photons for our quadrature definition. The relevant noise number for the use of the JPA as a squeezer is the noise it adds to the squeezed quadrature at the JPA output, which is 0.06 photons.

In summary, we have verified that our JPA, when operated as a phase-sensitive device, adds less noise to the amplified quadrature than an ideal phase-insensitive amplifier. This property is of utmost importance for high efficiency photon detection, state tomography and quantum communication applications in the microwave domain.

References

[1] Y. Nakamura, and T. Yamamoto, IEEE Photon. J. **5**, 0701406 (2013).

[2] F. Mallet, M. A. Castellanos-Beltran, H. S. Ku, S. Glancy, E. Knill, K. D. Irwin, G. C. Hilton, L. R. Vale, and K. W. Lehnert, Phys. Rev. Lett. **106**, 220502 (2011).

[3] Z. R. Lin, K. Inomata, W. D. Oliver, K. Koshino, Y. Nakamura, J. S. Tsai, and T. Yamamoto, Appl. Phys. Lett. **103**, 132602 (2013).

[4] L. Zhong, E. P. Menzel, R. D. Candia, P. Eder, M. Ihmig, A. Baust, M. Haeberlein, E. Hoffmann, K. Inomata, T. Yamamoto, Y. Nakamura, E. Solano, F. Deppe, A. Marx, and R. Gross, New Journal of Physics **15**, 125013 (2013).

[5] E. P. Menzel, R. Di Candia, F. Deppe, P. Eder, L. Zhong, M. Ihmig, M. Haeberlein, A. Baust, E. Hoffmann, D. Ballester, K. Inomata, T. Yamamoto, Y. Nakamura, E. Solano, A. Marx, and R. Gross, Phys. Rev. Lett. **109**, 250502 (2012).

[6] T. Yamamoto, K. Inomata, M. Watanabe, K. Matsuba, T. Miyazaki, W. D. Oliver, Y. Nakamura, and J. S. Tsai, Appl. Phys. Lett. **93**, 042510 (2008).

[7] E. P. Menzel, F. Deppe, M. Mariantoni, M. Á. Araque Caballero, A. Baust, T. Niemczyk, E. Hoffmann, A. Marx, E. Solano, and R. Gross, Phys. Rev. Lett. **105**, 100401 (2010).

[8] R. Di Candia, E. P. Menzel, L. Zhong, F. Deppe, A. Marx, R. Gross, and E. Solano. Dual-Path Methods for Propagating Quantum Microwaves. Accepted for publication in New J. of Phys., arXiv:1308.3117 (2013).

[9] A. Baust, E. P. Menzel, T. Niemczyk, E. Hoffmann, M. Häberlein, F. Deppe, A. Marx, R. Gross, K. Inomata, T. Yamamoto, and Y. Nakamura. Characterization of a Flux-Driven Josephson Parametric Amplifier. In **WMI Annual Report**, 34–35 (2010).

Materials, Thin Film and Nanotechnology, Experimental Techniques

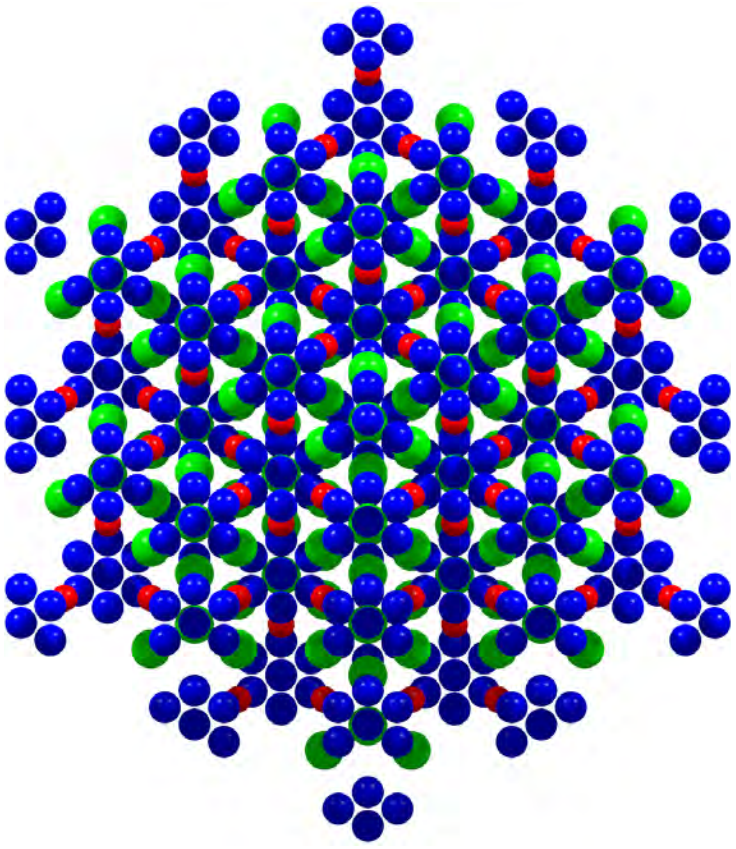

The *A*-227 pyrochlore structure of $Nd_2Ir_2O_7$. View along the (111) direction (red: Nd^{3+}, green: Ir^{4+}, blue: O^{2-}).

Pyrochlore Iridates: Candidates for the Realization of Weyl Nodes?

S. Geprägs, A. Wörfel, M. Lammel, A. Habel, K. Helm-Knapp, M. Opel, R. Gross

Pyrochlore iridates $A_2Ir_2O_7$ (A = Y or rare earth ion) offer a promising playground for the study of strong spin-orbit coupling, electronic correlations, and band topology effects. Novel phases such as axial or topological insulators have been predicted for these compounds [1]. In particular, $Nd_2Ir_2O_7$ is proposed to exhibit Weyl semimetal nodes [2] where two non-degenerated bands touch each other, creating a local linear dispersion in analogy to graphene. However, these nodes occur inside a fully three-dimensional solid and are topologically protected, making Weyl states absolutely robust to perturbations [3].

In the cubic pyrochlore iridates, the magnetic A^{3+} and Ir^{4+} ions reside on two distinct interpenetrating sublattices of corner-sharing tetrahedra (see insets of Fig. 1) [4]. Due to the threefold rings in the two sublattices, the magnetic interaction is highly frustrated. With increasing ionic radius of the A^{3+} ion, different ground states of $A_2Ir_2O_7$ were observed in the pioneering work of Matsuhira *et al.* [5]. While for $Pr_2Ir_2O_7$ the ground state is metallic, a metal-insulator transition (MIT) was observed for heavier rare earth ions like A = Nd, Sm, or Eu at low temperatures. This MIT is accompanied by a bifurcation of the magnetic susceptibility under field-cooled (FC) and zero field-cooled (ZFC) conditions, suggesting the existence of a magnetic long-range ordered state for temperatures $T < T_{MIT}$ [6]. However, recently a different temperature dependence of the electric resistivity as well as the remanent magnetization was reported for $Nd_2Ir_2O_7$ [7, 8].

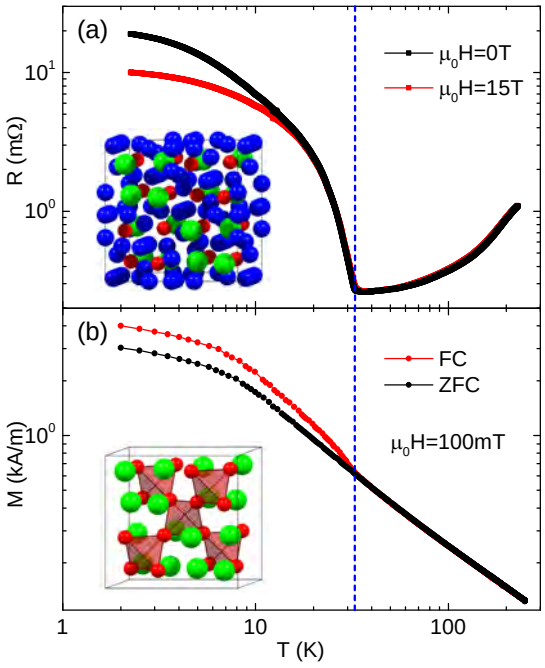

Figure 1: Temperature dependence of (a) the electric resistance measured at different magnetic fields and (b) the magnetization recorded at $\mu_0 H = 100\,\mathrm{mT}$ under zero field-cooled (ZFC) and field-cooled (FC) conditions for polycrystalline $Nd_2Ir_2O_7$. The metal-to-insulator transition at $T \simeq 33\,\mathrm{K}$ is marked by the blue dashed line. The inset in (a) shows the crystallographic unit cell of the pyrochlore structure (red: Nd, green: Ir, blue: O). The corner-sharing tetrahedra of the Nd^{3+} ions are highlighted in the inset of (b).

To resolve this discrepancy, we fabricated polycrystalline bulk samples of $Nd_2Ir_2O_7$ by a standard solid state reaction, using Nd_2O_3 and Ir powder as starting materials. The stoichiometric mixture was reacted at temperatures between 900°C and 1125°C with several intermediate grindings. From X-ray diffraction, no parasitic phases were detected. The lattice constant of bulk $Nd_2Ir_2O_7$ was determined by Nelson-Riley extrapolation to $a = (1.0376 \pm 0.0001)\,\mathrm{nm}$, which is comparable to literature values [7]. The temperature dependence of the electric resistance was measured using a standard van der Pauw geometry. Figure 1(a) reveals a clear MIT at around $T_{MIT} \simeq 33\,\mathrm{K}$. Furthermore, a negative magnetoresistance was detected for temperatures $T < T_{MIT}$. From SQUID magnetometry, the magnetization as a function of temperature differs for $T < T_{MIT}$, depending on zero field-cooled or field-cooled conditions (cf. Fig. 1(b)). These results point to the presence of a magnetic long-range order below T_{MIT}, confirming the initial measurements by Matsuhira *et al.* [5]. However, the origin of the MIT is still unclear and has to be investigated in the future.

Measurements of the optical conductivity by Ueda *et al.* [9] revealed that $Nd_2Ir_2O_7$ is indeed

close to a Weyl semimetal state, but still behaves like a Mott insulator at low temperatures. To stabilize such a Weyl semimetal state in $Nd_2Ir_2O_7$, one might take advantage of epitaxial strain in thin film samples. One prominent example is HgTe which shows a transition from a normal to a topological insulator when strained. For the first time in literature, we report here on epitaxial $Nd_2Ir_2O_7$ thin films deposited on single crystalline Y:ZrO_2 (YSZ) substrates by pulsed laser deposition from a stoichiometric, polycrystalline target [10]. The growth parameters were optimized with respect to the crystalline properties of the $Nd_2Ir_2O_7$ thin films. Optimum growth was obtained for a substrate temperature of 750°C, an oxygen atmosphere of 25×10^{-3} mbar, and a laser fluence of $2\,J/cm^2$.

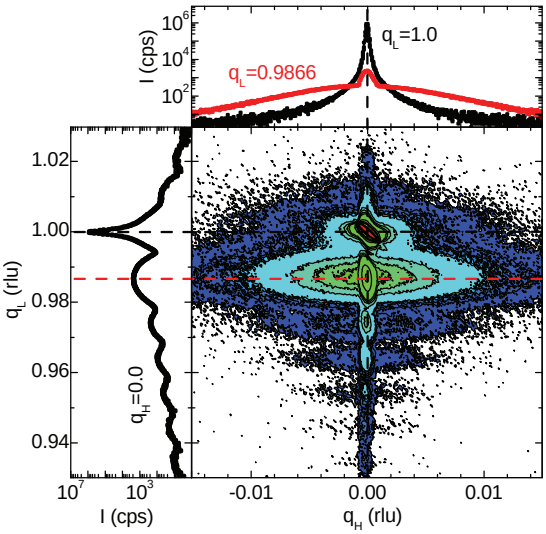

Figure 2: Reciprocal space map and corresponding q-scans of a 27.5 nm thick $Nd_2Ir_2O_7$ film on a YSZ substrate around the YSZ(111) reflection.

The structural properties of the thin film samples were investigated by high-resolution X-ray diffractometry. Figure 2 displays diffraction scans around the YSZ(111) reflection from a 27.5 nm thick $Nd_2Ir_2O_7$ thin film. Obviously, the reciprocal space map as well as the corresponding q_L-scan at $q_H = 0.0$ depicted in the left panel of Fig. 2 reveal a high crystalline quality, since finite thickness fringes are visible over the whole investigated reciprocal space, demonstrating an excellent coherent growth. Furthermore, the thin film exhibits a low mosaic spread which can be quantified by the full width at half maximum (FWHM) of the q_H-scan measured at $q_L = 0.9866$ rlu, shown in the upper panel of Fig. 2. A value of FWHM $= 6.809 \times 10^{-4}$ rlu is obtained, corresponding to 0.04° for standard ω rocking curve scans. Thus, the X-ray diffraction measurements indicate a coherent growth with low interface and surface roughness. The latter is further evidenced by atomic force microscopy measurements (not shown here) which reveal a surface roughness of only 0.7 nm (rms value).

In forthcoming experiments, we will systematically investigate the magnetic and magnetoelectric transport properties as a function of the strain state in $Nd_2Ir_2O_7$ thin films. To this end, the key objective is to possibly tune the ground state of $Nd_2Ir_2O_7$ from a Mott insulator state to a Weyl semimetal.

References

[1] X. Wan, A. M. Turner, A. Vishwanath, and S. Y. Savrasov, Phys. Rev. B **83**, 205101 (2011).
[2] G. Chen, and M. Hermele, Phys. Rev. B **86**, 235129 (2012).
[3] L. Lu, L. Fu, J. D. Joannopoulos, and M. Soljacic, Nature Photon. **7**, 294–299 (2013).
[4] J. S. Gardner, M. J. P. Gingras, and J. E. Greedan, Rev. Mod. Phys. **82**, 53–107 (2010).
[5] K. Matsuhira, M. Wakeshima, Y. Hinatsu, and S. Takagi, J. Phys. Soc. Jpn. **80**, 094701 (2011).
[6] K. Tomiyasu, K. Matsuhira, K. Iwasa, M. Watahiki, S. Takagi, M. Wakeshima, Y. Hinatsu, M. Yokoyama, K. Ohoyama, and K. Yamada, J. Phys. Soc. Jpn. **81**, 034709 (2012).
[7] S. M. Disseler, C. Dhital, T. C. Hogan, A. Amato, S. R. Giblin, C. de la Cruz, A. Daoud-Aladine, S. D. Wilson, and M. J. Graf, Phys. Rev. B **85**, 174441 (2012).
[8] S. M. Disseler, S. R. Giblin, C. Dhital, K. C. Lukas, S. D. Wilson, and M. J. Graf, Phys. Rev. B **87**, 060403 (2013).
[9] K. Ueda, J. Fujioka, Y. Takahashi, T. Suzuki, S. Ishiwata, Y. Taguchi, and Y. Tokura, Phys. Rev. Lett. **109**, 136402 (2012).
[10] M. R. Lammel. *$Nd_2Ir_2O_7$: A new Weyl semimetal?* Bachelor thesis, TU München (2013).

Progress in the WMI Quantum Laboratory K04

J. Goetz, F. Wulschner, J. Höß, K. Neumaier, C. Probst, F. Deppe, A. Marx, R. Gross [1]

Last year, we reported on first cool-downs of a new liquid helium-precooled dilution refrigerator designed for experiments on superconducting quantum circuits. The new fridge is set up in the WMI Quantum Laboratory K04 [1]. In 2013, the systems has been completed and optimized. Here, we report on the improvement of the cooling power as well as the installation of a new liquid helium dewar and measurement equipment (see Fig. 1). These steps have lead to first successful experiments (see report by F. Wulschner *et al.*, pp. 65–66).

Figure 1: Photograph of the dilution refrigerator with the new dewar during the experiment.

By installing a suitable bypass between the exhaust of the turbomolecular pump and the mechanical prepump we have improved the cooling power of the new dilution refrigerator. By this simple measure we avoid to pump through the gas handling system with its large flow impedance. This impedance reduction results in a lower pressure at the output of the distillation line which allows for a larger ^{3}He throughput. With this improvement, the cooling power of the mixing chamber was increased by a factor of almost two to 140 µW at 100 mK.

Additionally, we have equipped the cryostat with eight coaxial measurement lines down to the mixing chamber stage suitable for microwave frequencies. These lines are thermally anchored at 4 K, 1.5 K, the still plate (200 mK), and the sample stage. We use low-loss silver-coated copper-clad steel cables from room temperature to the 4 K-stage. As a consequence, the helium consumption increases by 5 l per day. From the 4 K stage to the sample stage, we use phosphor bronze cables with niobium center conductor. Currently, four of the lines are used as attenuated input lines and four as output lines. The latter are passing a series of cold circulators and four ultra low-noise high electron mobility transistor (HEMT) amplifiers. In this way, we can mount up to four samples simultaneously to the sample stage. For the future it is planned to expand the number of input lines to be able to set up more complex experiments.

To provide more space at the sample stage, a larger vacuum pot is used. In this way, we can extend the length of the sample stage from 5 cm to approximately 30 cm (see Fig. 2). In this

[1] We acknowledge financial support from the German Research Foundation via SFB 631, the German Excellence Initiative via NIM, and the EU projects CCQED and PROMISCE.

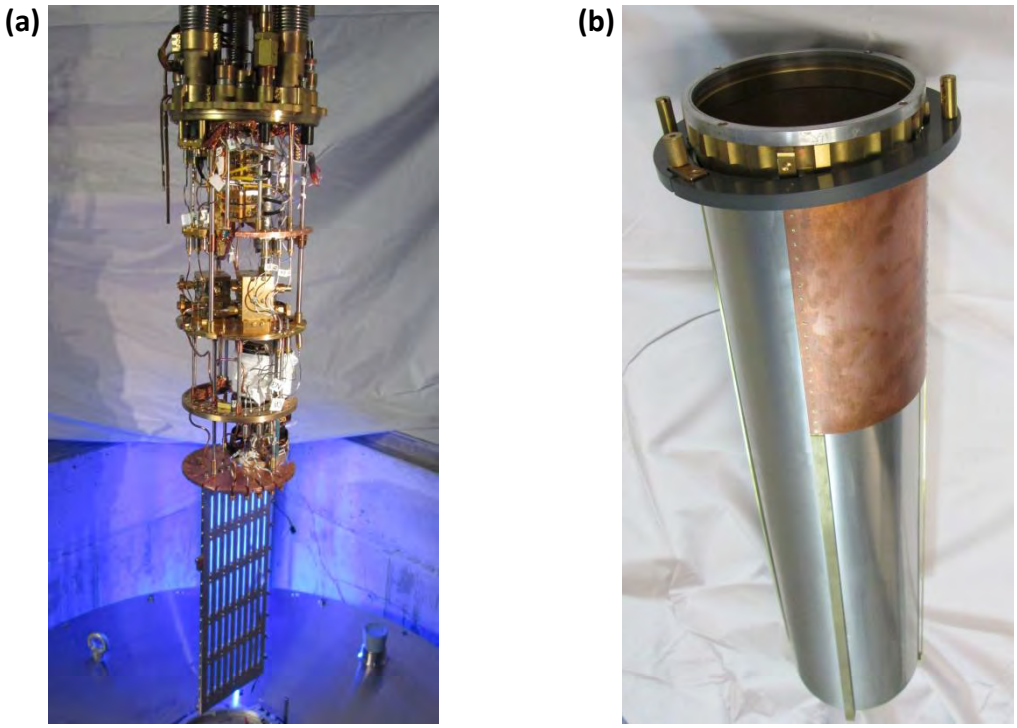

Figure 2: (a) Fridge insert from 4 K down to the sample stage, including eight coaxial microwave measurement lines. **(b)** The new vacuum pot with a cryoperm magnetic shielding.

context, we have also installed a larger helium dewar. The latter is a Cryogenic Ltd. stainless steel cryostat with a ^{4}He volume of 89 l. As a consequence, the time between two refills now exceeds nine days and hence allows for more than week-long continuous measurement sessions.

With the improved version of the dilution refrigerator and measurement equipment we already performed several successful cool-downs which resulted in first experimental data. These include the analysis of the tunable coupling between two superconducting transmission line resonators (see report by F. Wulschner *et al.*, pp. 65–66) and studies on quality factors of transmission line resonators. These experiments will be continued in the next cool-downs. Altogether, we have completed a powerful new measurement setup for superconducting quantum circuits which has been designed, engineered, fabricated, assembled and tested at WMI.

References

[1] J. Goetz, M. J. Schwarz, F. Wulschner, J. Höß, K. Neumaier, C. Probst, F. Deppe, A. Marx, and R. Gross. Building of a New Dilution Refrigerator in a WMI Quantum Science Laboratory. In **WMI Annual Report**, 89–90 (2012).

Cryogen-free Dilution Fridge with Large Sample Stage – It is cold!

A. Marx, J. Höß, and K. Uhlig [1]

To further develop our activities on quantum effects in the microwave regime we have started out setting up a new cryogen-free refrigerator with a pulse tube refrigerator (PTR) [1] and with a large sample stage in the WMI Quantum Laboratory K21 (cf. last year's report [2]). This refrigerator features large diameters of all temperature stages providing extensive space for advanced quantum experiments based on a large number of bulky microwave components. Here, we report on the progress in the construction of this refrigerator and the first successful cooldowns of this cryostat to base temperature. The main components of the refrigerator are the PTR, a 1 K-stage and a dilution unit. The two stages of the PTR cool the incoming ^{4}He and the ^{3}He/^{4}He mixture as well as a radiation shield at each stage. To provide sufficiently high cooling power near 1 K to cool microwave components and cables, this refrigerator has been equipped with a novel 1 K-stage [3]. All components for the 1 K-stage and for the dilution circuit have been fabricated in the WMI workshop (cf. Fig. 1). The wiring for thermometry down to the mixing chamber plate has been installed.

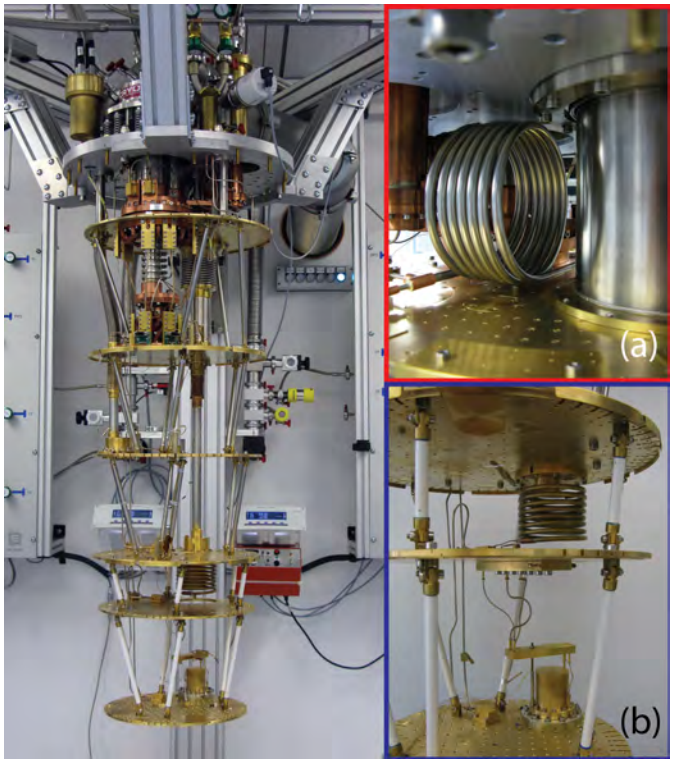

Figure 1: Photographs of the fully operational new cryogen-free dilution refrigerator. **(a)** Improved counterflow heat exchanger in the ^{4}He precooling circuit. In **(b)** the concentric tube and two step heat exchangers as well as the mixing chamber can bee seen from top to bottom.

The dilution refrigerator is precooled by a dedicated ^{4}He circuit consisting of a counterflow heat exchanger (hx) for the incoming ^{4}He and hxs on each temperature stage (two hxs on the first PTR stage, one large hx at the second PTR stage and one hx on each lower temperature stage) [4]. The ^{4}He is circulated by a membrane compressor starting with a pressure of 4 bar at room temperature. During cooldown, the ^{4}He gas flow is cooled in heat exchangers at the first and the second stages of the PTR and then the gas stream cools the 1 K-stage, the still, the counterflow heat exchangers and the mixing chamber. The original design of the counterflow hx for the incoming ^{4}He soon turned out to be not efficient enough and was replaced by an optimized version with thrice the length of the initial one (cf. Fig. 1(a)). Precooling the refrigerator from room temperature to below 5 K takes around 32 h for non-optimized values of ^{4}He flow rate in the precooling circuit. Next, the precooling circuit has to be carefully evacuated before starting the condensation process to avoid the formation of a superfluid film thermally shorting the lowest temperatures stages.

Sufficiently high cooling power near 1 K to cool microwave components and cables was one

[1] We acknowledge financial support by the German Research Foundation through SFB 631, the German Excellence Initiative through the Nanosystems Initiative Munich (NIM), and the EU projects CCQED and PROMISCE.

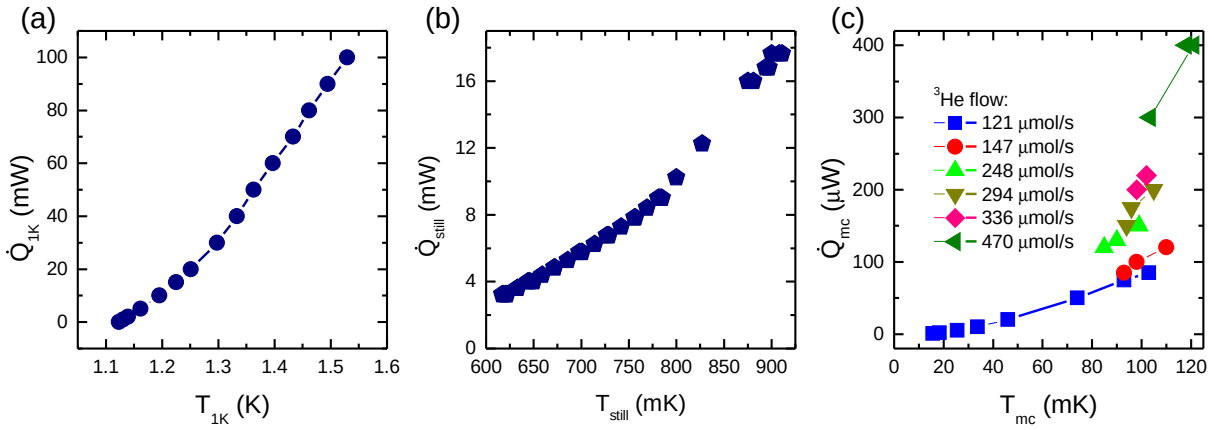

Figure 2: Cooling capacity at different stages of the refrigerator. (a) Cooling power $\dot{Q}_{1K}$ of the 1 K-stage as a function of the temperature T_{1K} of the 1 K-stage. (b) Cooling capacity $\dot{Q}_{still}$ of the distillation vs. still temperature T_{still}. (c) Cooling power $\dot{Q}_{mc}$ of the mixing chamber as a function of the temperature T_{mc} inside the mixing chamber for different values of the ^{3}He flow rates.

important aspect in designing the refrigerator. Therefore the refrigerator is equipped with a 1 K-stage operating in a closed cycle. This 1 K-stage is also used to condense the incoming ^{3}He/^{4}He mixture. The flow circuits of the ^{4}He and the ^{3}He/^{4}He mixture are not coupled. The incoming ^{4}He is precooled to 3 K at the second PTR stage. After further cooling in a counterflow hx in the 1 K pumping line the liquid ^{4}He accumulates in a vessel. The experimentally determined cooling power of the 1 K-stage is depicted in Fig. 2(a). With the present setup (rotary pump of 80 m^3/h) a refrigeration capacity of up to 100 mW could be reached.

The dilution unit consists of a continuous heat exchanger, two step heat exchangers and a mixing chamber with a diameter of 40 mm and a height of 55 mm as shown in Figs. 1(b) and 3. Figure 2(b) shows the still cooling power which can be as large as 18 mW at 900 mK in the present configuration at a ^{3}He flow rate $\dot{n}_3 \sim 510\,\mu$mol/s which is limited by the pressure of the incoming ^{3}He flow. The minimum base temperature of the refrigerator is below 11 mK [5]. We have determined the temperature dependent cooling power $\dot{Q}_{mc}$ for different ^{3}He flow rates (cf. Fig. 2(c)). The cooling power at 100 mK was determined to 300 μW at the maximum ^{3}He flow rate. At 116 mK a cooling power of 400 μW was observed (this temperature is often used to define the cooling power of commercial dilution refrigerators).

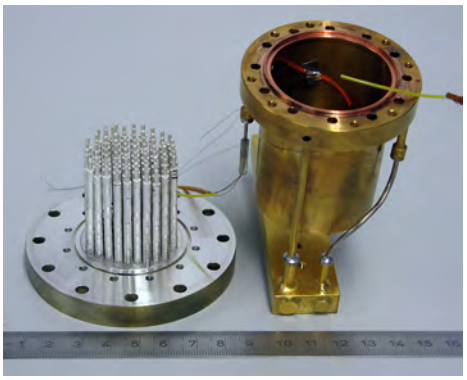

Figure 3: Mixing chamber.

In the next step the refrigerator will be equipped with microwave lines, cold amplifiers and other microwave components for experiments towards quantum simulation and quantum information processing systems.

References

[1] Cryomech Inc., Syracuse, N.Y., model PT410-RM, www.cryomech.com.
[2] A. Marx, J. Höß, and K. Uhlig. Cryogen-free Dilution Refrigerator with Large Sample Stage. In **WMI Annual Report**, 91 (2012).
[3] K. Uhlig, Cryocoolers **17**, 471 (2012).
[4] K. Uhlig. Dry Fridge Continued. In **WMI Annual Report**, 58 (2005).
[5] Thermometers kindly provided by K. Neumaier, Karl.Neumaier@wmi.badw-muenchen.de.

Vibrations in a Dry Fridge: Surprise, surprise!

K. Uhlig

In most experiments at mK temperatures dilution refrigerators (DR) are used. Most modern DRs are precooled by two stage pulse tube cryo-coolers (PTC) because of their ease of use and cost effectiveness [1]. A frequently asked question on these so-called cryogen-free DRs concerns the vibrations of the PTC and how they affect the dilution process. This question cannot be answered easily. Naively one might think that if the PTC of a DR is turned off temporarily, the mixing chamber (MC) would go to a lower temperature and from this temperature drop the heat leak into the MC would be calculable. However, it turns out that once the PTC of a dry fridge is turned off, the dilution circuit gets out of balance quite quickly before the MC has the time to respond to the small heat leak caused by the vibrations of the PTC.

In previous work [2] we have measured the vibrational heat leak by using the equation for the cooling power $\dot{Q}$ of a MC:

$$\dot{Q} = \dot{n}_3 * (96 * T_m^2 - 12 * T_n^2)\,. \qquad (1)$$

Here $\dot{n}_3$ is the ^{3}He flow rate, T_m is the temperature of the MC and T_n is the temperature of the ^{3}He at the inlet of the MC [3]. We measured T_m and T_n at various values of $\dot{n}_3$ and thus were able to derive a value for the spurious heat leak. The finding was that the heat leak was small, below 0.1 µW.

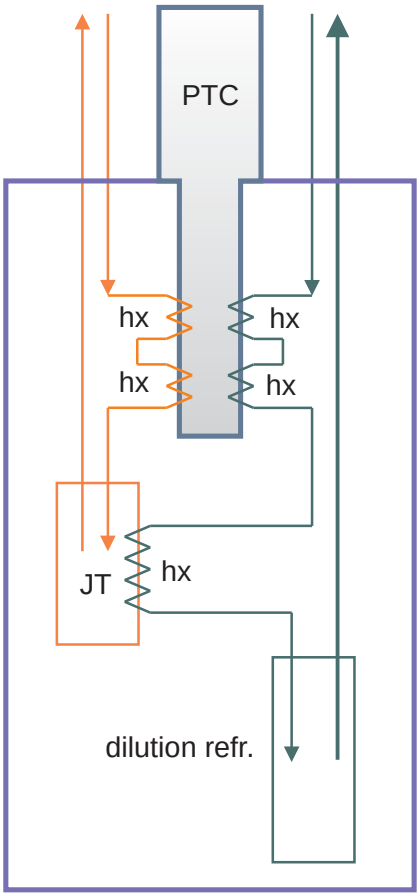

Figure 1: Schematic sketch of our DR. It consists of three components, the PTC, a ^{4}He-1K-loop and a dilution unit (hx = heat exchanger).

In the present version of our DR, the flange of the PTC is bolted directly to the top flange of the cryostat with no vibration damper in between. The two cooling stages of the PTC, however, are thermally connected to the DR by soft copper braided ropes to block vibrations. We use a small PTC (0.5 W @ 4 K) to keep vibrations low [4], contrary to commercial DRs where usually bigger PTCs (1 W or 1.5 W @ 4 K) are installed.

Unlike commercial DRs, ours is equipped with a ^{4}He Joule-Thomson loop [5, 6] which condenses the ^{3}He stream of the dilution circuit after pre-cooling by the PTC (Fig.1). When the vessel of the condenser is filled up with liquid ^{4}He, it can be run in a single cycle mode for over 15 minutes with the PTC turned off. During this time span the DR is pre-cooled by the JT-loop alone, and the MC has plenty of time to reach its new base temperature.

From Eq. (1) we see that the refrigeration power of the MC is about $\propto T_m^2$. Thus, $dT_m \propto \frac{dQ}{T_m}$ which means that T_m is most sensitive to a small heat leak at the lowest MC temperature possible. Our DR with a base temperature of 4.3 mK is well suited for this experiment.

For thermometry we use a CMN (Cerium Magnesium Nitrate) thermometer where the susceptibility χ follows the Curie-Weiss-law. Its temperature resolution is highest at the lowest temperatures. It is approximately given by $\frac{d\chi}{dT} \propto -\frac{1}{(T-\Delta)^2} \simeq -1/T^2$ (with the Weiss constant $\Delta \sim 1.5$ mK).

In our experiment, the DR was operated at its base temperature, the vessel of the condenser filled with ^{4}He, and then the PTC turned off. Very surprisingly, there was no cooling effect of the MC within the resolution of our thermometer. With use of Eq. (1) and assuming a vibrational heat leak $\dot{Q} = 10\,\mu W$, we would expect a temperature drop of the MC of 0.1 mK which would be well within the resolution of the CMN thermometer. So we conclude that the vibrational heat leak in our DR is below an unexpectedly low value of 10 µW. Presumably the vibrational heat leak depends on the construction of the cryostat. In our DR, it seems that by improving the heat exchangers of the dilution unit even lower base temperatures would be attainable.

References

[1] K. Uhlig, J. Phys. Conf. Ser. **400**, 052039 (2012).
[2] K. Uhlig, Cryogenics **44**, 53–57 (2004).
[3] F. Pobell. *Matter and Methods at Low Temperatures* (Springer, 2006), 3rd edn.
[4] Cryomech Inc., Syracuse, N.Y.; http://www.cryomech.com.
[5] K. Uhlig, Adv. Cryog. Eng. **57B**, 1823–1829 (2011).
[6] K. Uhlig. Cryogen-free Dilution Refrigerator with 1K Stage. In **Cryocoolers**, Vol. 17, Pp. 471–477 (ICC Press, Boulder, CO, 2012).

Experimental Facilities

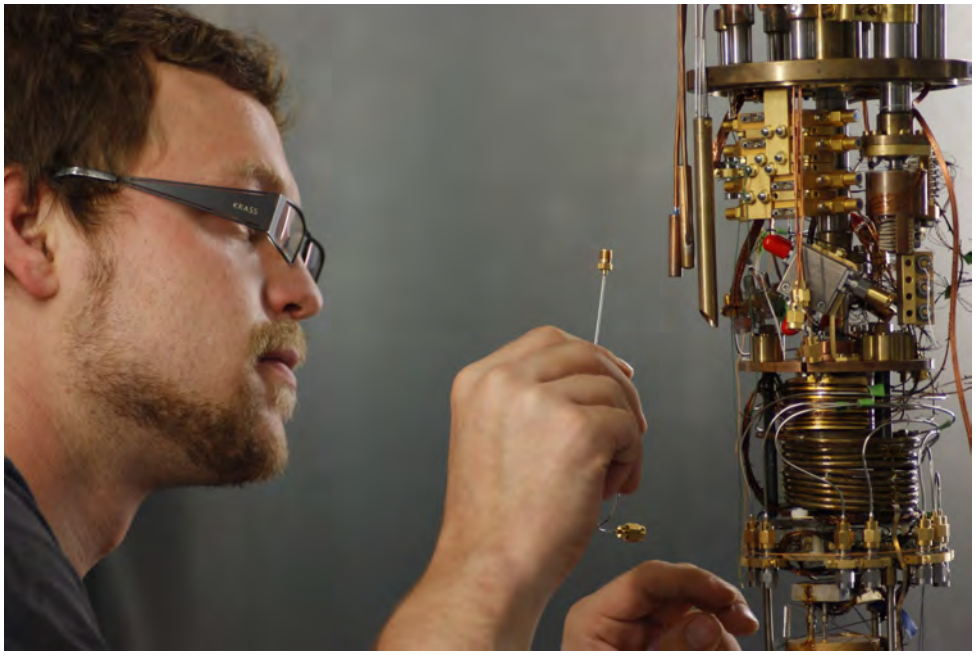

Overview of Key Experimental Facilities and Infrastructure

In the following basic information on the key experimental facilities and components of the technical infrastructure installed at the Walther-Meißner-Institute (WMI) is given.

UHV Laser-MBE

The WMI operates an UHV Laser-Molecular Beam Epitaxy (L-MBE) system for the growth of complex oxide heterostructures. The system has been designed to meet the special requirements of oxide epitaxy. The UHV cluster tool consists of the following main components:

- central transfer chamber;
- load-lock chamber with a heater system for substrate annealing;
- laser deposition chamber with a KrF excimer laser, *in-situ* reflection high energy electron diffraction (RHEED) system, laser substrate heating system, and atomic oxygen/nitrogen source; the RHEED system has been modified to allow for the operation at high oxygen partial pressure up to 0.5 mbar;
- surface characterization chamber with UHV scanning atomic force microscope (Omicron);
- metallization chamber with a four heart electron gun system and a liquid nitrogen cooled sample stage. The sample holder can be tilted for shadow evaporation.

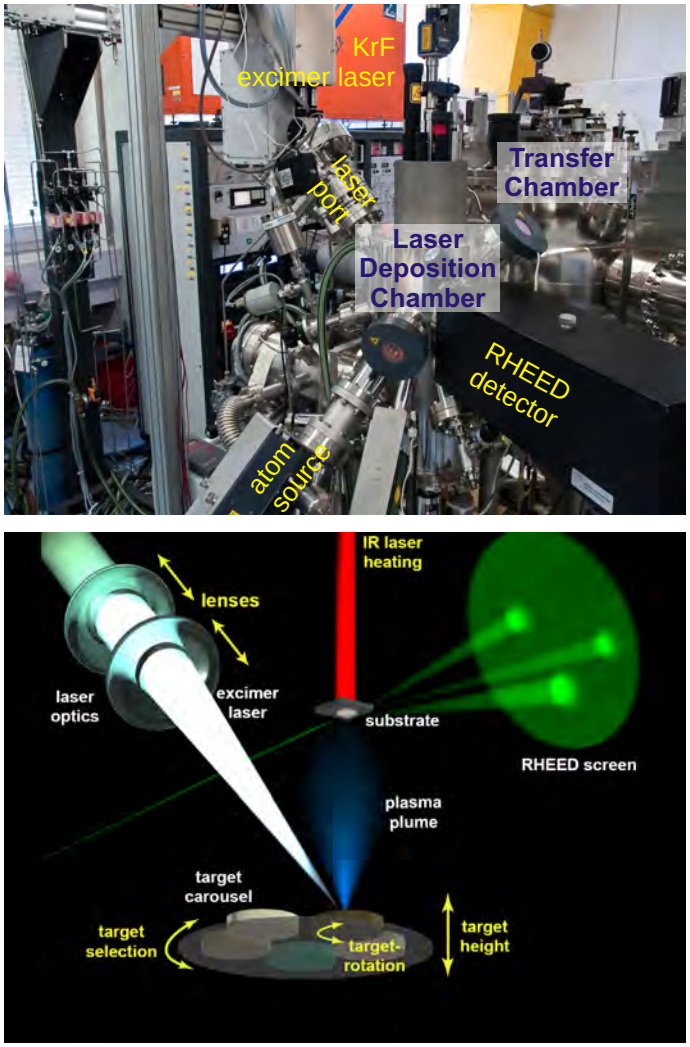

Figure 1: Top: UHV laser-molecular beam epitaxy system. Bottom: principle of the deposition process.

The system is used for the growth of complex oxide heterostructures consisting of superconducting, ferromagnetic, ferroelectric, and semiconducting materials such as high-temperature superconductors, doped manganites, (double) perovskites, magnetite, zinc oxide, rare earth iron garnets, pyrochlore iridates, etc.

The original laser molecular beam epitaxy system (laser-MBE) designed already in 1995/96 has been continuously upgraded and modified until now. In particular, the substrate heating system and the temperature control unit were changed from a resistive radiation heater to an infrared laser heating system (see Fig. 3, left) including a pyrometer for determining the sample temperature. In addition, a source for atomic oxygen and nitrogen has been installed. The main advantage of the new heating system is that only the substrate is heated while the surrounding parts are hardly affected (Fig. 3, right). In this way one can achieve a substantially better vacuum at temperatures well above 1000 °C. The achievable substrate temperature is limited by the melting point and the size of the substrate material (approx. 1410 °C for a $5 \times 5\,\mathrm{mm}^2$ silicon substrate). The laser heating system has already been successfully used for removing the amorphous silicon oxide layer from the surface of silicon substrates at 1150 °C.

Figure 2: Pulsed Laser Deposition (PLD): When the pulse of the UV laser (KrF excimer laser, 248 nm) hits the target, the target material is ablated and the so-called laser "plume" containing highly excited atoms and molecules is formed.

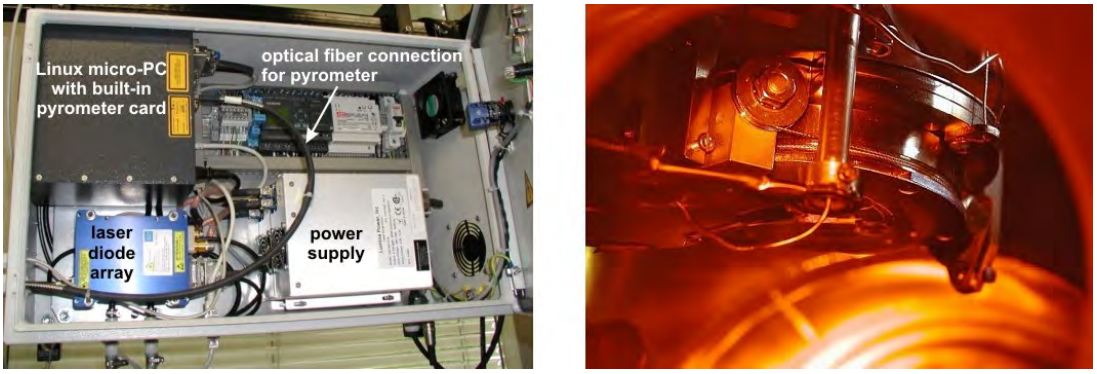

Figure 3: Components of the laser heating system: The substrate is heated using an IR diode laser head that is located in a separate box far away from the deposition chamber (left). The laser light is brought to the substrate (right) via an optical fiber.

We have further developed and installed a home-made telescope zoom optics for the pulsed UV laser light, consisting of in total five lenses on sliding lens holders allowing for a movement over a total distance of 1200 mm. The lens holders are attached to independent stepper motors, each connected to a controller providing an accurate positioning precision. The controllers are driven via a PC, thus allowing for a full automation of the lens system itself. With this telescope zoom optics we are able to change the area of the UV laser spot on the target, resulting in an accessible range of laser fluences from $\rho_\mathrm{L} = 0.5\,\mathrm{J/cm}^2$ to $5\,\mathrm{J/cm}^2$. To maintain a stable laser fluence at the target, we have installed a so-called *intelligent* window (PVD Products) at the laser entrance port combining two unique features. First, it keeps the inner side of the entrance window free of coatings by blocking the ablated plasma plume via a rotatable disc consisting of UV grade fused silica. Second, an insertable mirror positioned in the light path after the disc allows to guide the incoming UV laser pulse through a side window, where its energy is determined by a pyroelectric detector. These measures help to improve the deposition processes by accurately monitoring ρ_L as one of the most critical process parameters.

UHV Electron Beam Evaporation System

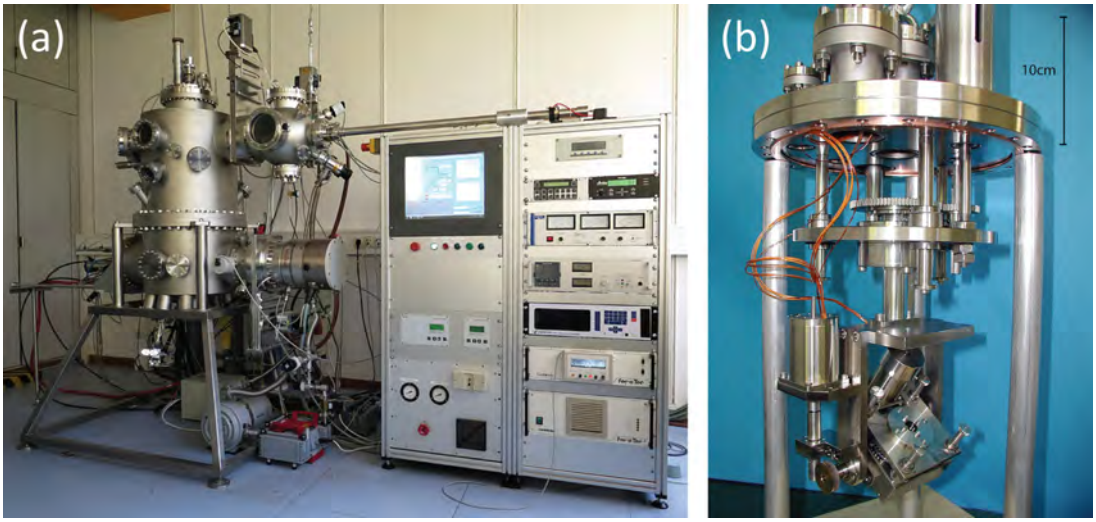

Figure 4: (a) Photograph of the UHV electron beam evaporation system. (b) Manipulator with UHV stepping motors for automated and precise sample tilt and options for rotation.

The UHV metal MBE system allows for the growth of high quality metallic thin films by electron beam evaporation and molecular beam epitaxy. The system is optimized for the fabrication of superconducting persistent current qubits by aluminum shadow evaporation. It is equipped with an improved substrate holder allowing for multi-angle shadow evaporation. The main components of the system are:

- UHV system with a process chamber with a base pressure of $\sim 1 \times 10^{-8}$ mbar pumped by a 1000 l/s turbo molecular pump with magnetic suspension of the rotor adequate for corrosive gases.
- Load-lock chamber equipped with a magnetic transfer system (push-pull positioner) for sample transfer without breaking the vacuum in the process chamber.
- Downstream pressure control by an adaptive pressure controlled gate valve.
- Electron beam evaporator with six 8 cm^3 crucibles embedded in a linearly movable water cooled rail providing six different materials.
- Film thickness measurement and closed loop evaporation rate control by a quartz crystal microbalance in combination with the evaporation controller.
- Effusion cell for molecular beam epitaxy processes.
- Ion sputtering gun for in-situ sample cleaning
- Manipulator with UHV stepping motors for automated and precise sample tilt and options for rotating and cooling the sample.

A precise and reproducible tilt of the sample is realized by a sample manipulator with process specific degrees of freedom. The downstream pressure control allows for a fast adjustment and precise control of the oxygen partial pressure. This is crucial for a well-defined oxidation process of the Josephson junctions barriers. The entire process can be performed fully automated via a touch screen and is controlled by a LabView program. Up to six effusion cells can be optionally added to the system allowing for further materials. The manipulator allows for further degrees of freedom that can be used to align the sample to the effusion cells, the ion sputtering gun and to measuring equipment such as ellipsometry or RHEED.

Single Crystal Growth and Synthesis of Bulk Materials

Transition metal oxides are of great interest due to their various interesting physical properties (e.g. high temperature superconductivity, colossal magnetoresistance, ferroelectricity, nonlinear optical properties etc.) and their high potential for applications. Therefore, the WMI operates a laboratory for the synthesis of bulk materials and single crystals of transition metal oxides. Besides various chamber- and tube furnaces a four-mirror image furnace is used for the crystal growth of various oxide systems. With this furnace crystals of many different compounds of the high temperature superconductors and various other transition metal oxides have been grown as single crystals using the traveling solvent floating zone technique. The furnace consists basically of 4 elliptical mirrors with a common focus on the sample rod and with halogen lamps in their other focus. By irradiation of the focused light the sample rod is locally heated and eventually molten. The molten zone can be moved up and down along the entire sample rod under simultaneous rotation. Due to the anisotropic growth velocity a preferential growth of those grains with the fastest growth velocity along the pulling direction is obtained and the formerly polycrystalline rod is transformed into a single crystal. Single crystal growth can be performed with this furnace at maximum temperatures up to 2200 °C in the pressure range from 10^{-5} mbar up to 10 bar and in oxidizing, reducing as well as inert atmosphere.

Figure 5: The four-mirror image furnace installed at the crystal laboratory of the WMI. Crystals can be grown by the floating zone and traveling solvent floating zone techniques at temperatures up to 2200 °C and pressures up to 10 bar.

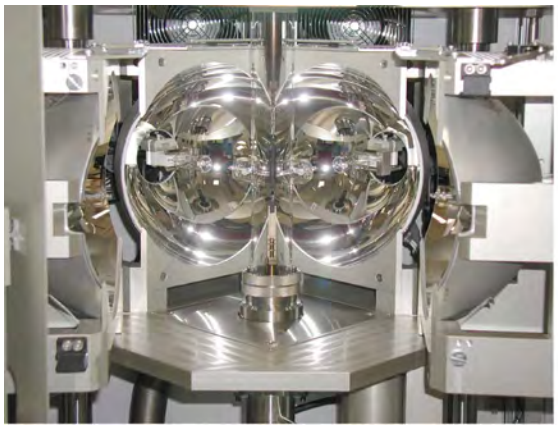

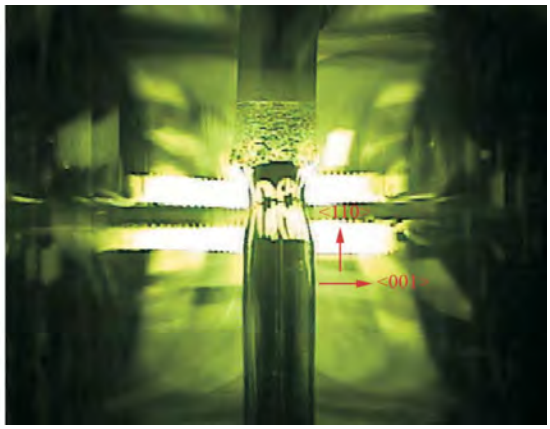

Figure 6: Left: Central part of the image furnace with four elliptical mirrors. In the center one can see the quartz tube with a polycrystalline rod. Right: View on the molten zone of $Pr_{2-x}Ce_xCuO_4$ (melting point: 1280 °C) obtained by a CCD camera.

The X-ray diffraction systems

For X-ray analysis the Walther-Meissner-Institute operates two X-ray diffractometers (Bruker D8 Advance and D8 Discover). The two-circle system is used for powder diffraction. In this system the samples can be heated in oxygen atmosphere up to 1600 °C. It is equipped with a Göbel mirror and an area detector to save measuring time. The second system is a high resolution four-circle diffractometer that can be used for reciprocal space mappings. It is equipped with a Göbel mirror and an asymmetric two-fold Ge monochromator and allows for the texture analysis of thin film superlattices and single crystalline materials. In both systems measurements can be carried out fully computer controlled.

Beside these two Bruker X-ray systems a Laue camera for single crystal analysis and a Debye-Scherrer camera are available.

Figure 7: The two-circle X-ray diffractometer Bruker D8 Advance.

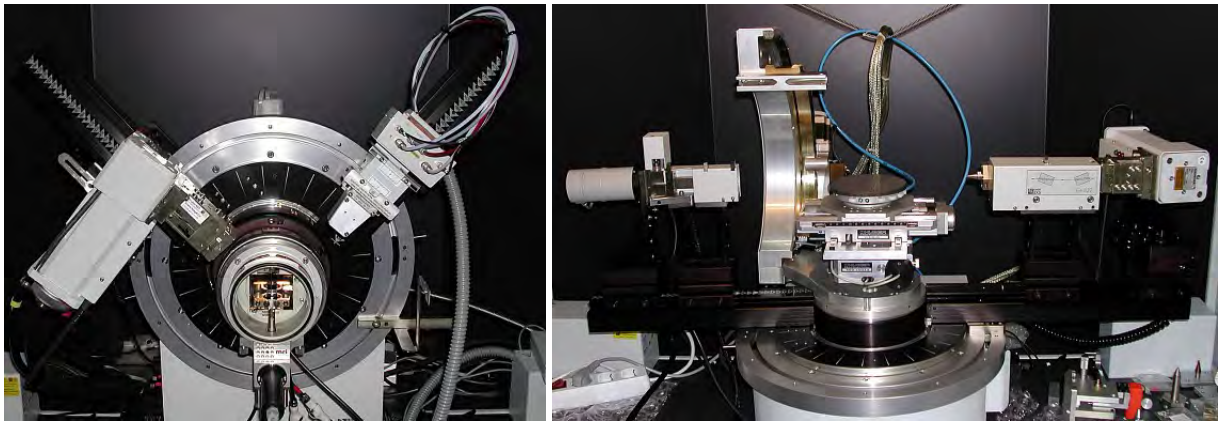

Figure 8: Left: High temperature sample holder of the D8 Advance system. Right: Four-circle high resolution X-ray diffractometer Bruker D8 Discover.

Figure 9: Quantum Design SQUID magnetometer.

The SQUID magnetometer

For the analysis of the magnetic properties of materials, a Quantum Design SQUID magnetometer system (Fig. 9) is operated at the WMI. The SQUID magnetometer allows for measurements in the temperature regime from 1.8 to 400 K and provides excellent sensitivity particularly in the low field regime. Due to the excellent sensitivity of the system, thin film samples with a very small sample volume can be analyzed. The SQUID magnetometer is equipped with a superconducting solenoid allowing for a maximum field of 7 T. At present, the magnetometer is used for the characterization of magnetic and superconducting materials (both in bulk and thin film form). Examples are the cuprate high temperature superconductors, the doped manganites, magnetite, the double perovskites, magnetic semiconductors, or multiferroics.

The High Field Laboratory

Transport and thermodynamic properties of samples are often studied as a function of the applied magnetic field. For such measurements several superconducting magnets are available at the WMI. Two of them (8/10 and 15/17 Tesla magnet system) are located in the high magnetic field laboratory in the basement of the WMI. The magnet systems are installed below the floor level to facilitate the access to the top flange and the change of the sample sticks. The magnet systems are decoupled from the building to avoid noise due to mechanical vibrations. A variety of sample holders can be mounted allowing for e.g. sample rotation during the measurement. For standard sample holders the accessible temperature regime is 1.5 K $< T <$ 300 K. However, also ^{3}He/^{4}He dilution refrigerator inserts ($T >$ 20 mK) or high temperature units ($T <$ 700 K) can be mounted. All measurements are fully computer controlled (by the use of the LabView software tool) allowing for remote control and almost continuous measurements.

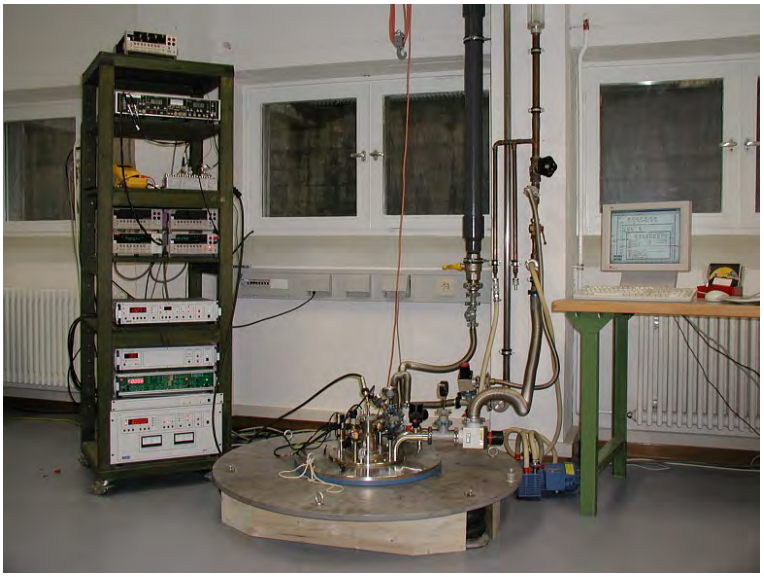

Figure 10: High field laboratory with Oxford 17 T magnet system.

Since 2012, a 3D vector magnet with variable temperature insert, allowing for 2 T in-plane and 6 T out-of-plane magnetic fields is available for thermal and electrical transport experiments. A further 3D vector magnet allowing for 1 T in-plane and 6 T out-of-plane magnetic fields is

installed in the WMI Quantum Laboratories as part of a cryogen-free dilution system (see page 93).

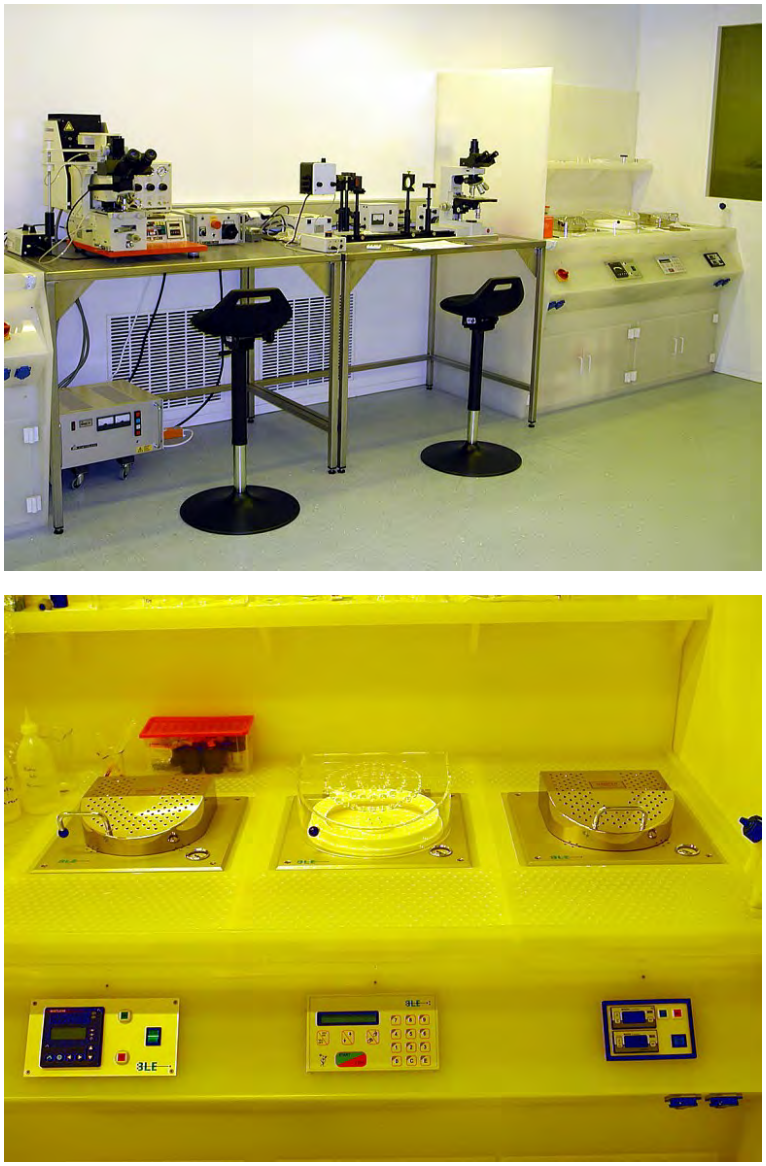

Figure 11: Top: Part of the clean room facility with optical lithography equipment and clean room benches. Bottom: Resist coater and hot plates.

The Clean Room Facility

For the fabrication of nanostructures and superconducting as well as spintronic devices the WMI operates a class 1000 clean room facility with an area of about 50 m^2. This clean room facility has been put into operation at the WMI within the year 2001. The clean room is subdivided into two parts for photolithography and electron beam lithography, respectively. The clean room facility is equipped with the standard tools for photolithography such as resist coaters, hot plates, wet benches, a Karl Süss MJB3 mask aligner and an optical projection lithography system. The technical infrastructure for the clean room is located in the basement of the WMI directly below the clean room area.

Since 2005 the clean room also is equipped with a reactive ion etching system, Plasmalab 80 Plus with ICP plasma source (Oxford Instruments Plasma Technology).

Electron Beam Lithography

The Electron Beam Lithography System is installed in the second part of the clean room facility. It consists of a Philips XL 30 SFEG scanning electron microscope (SEM) with a Raith Elphy Plus electron beam lithography system and a laser interferometer table for precise stitching of writing fields.

The SEM is equipped with a hot field emitter and typically provides a beam diameter of less than 1.5 nm at $\geq$ 10 keV or about 2.5 nm at 1 keV. The lithography unit allows the fabrication of nanostructures down to about 10 nm. We have realized the controlled fabrication of metallic strip patterns with a strip width of about 20 nm. The electron beam lithography is used for the fabrication of nanostructures in metallic and oxide systems required for the study of quantum effects in mesoscopic samples.

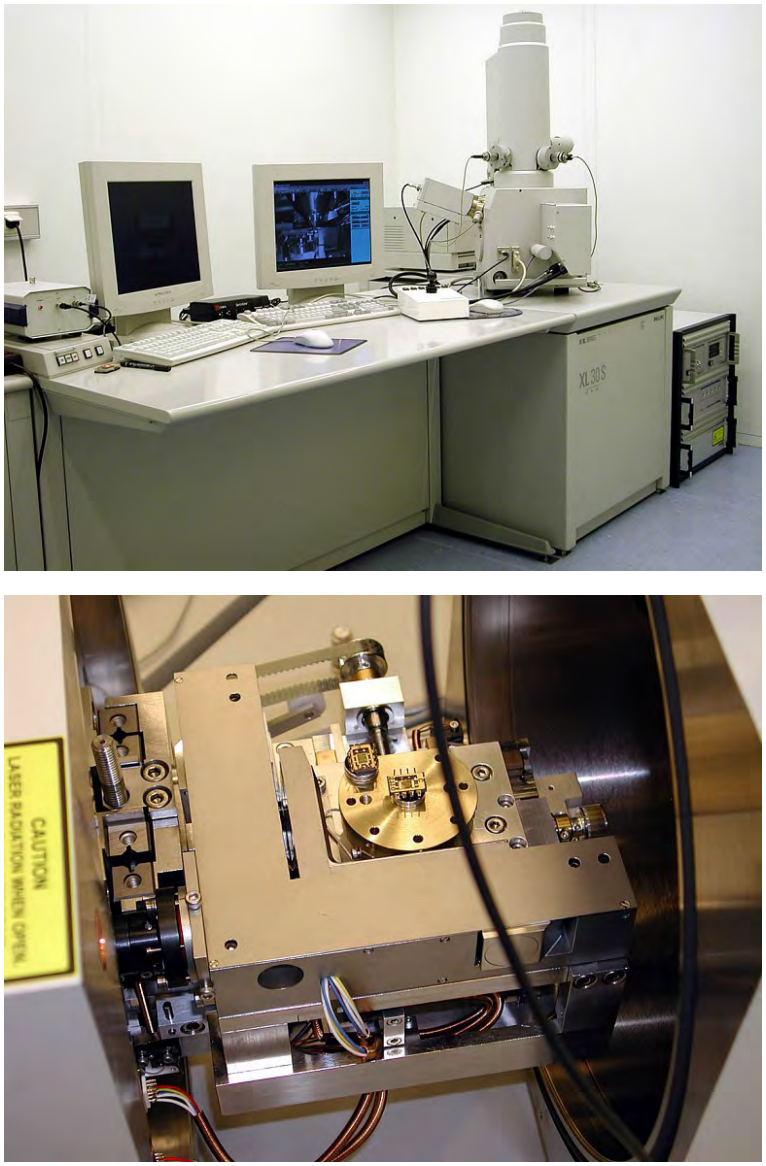

Figure 12: Top: Philips XL 30 SFEG Scanning Electron Microscope with Raith Elphy Plus Lithography System. Bottom: Raith Laser Stage.

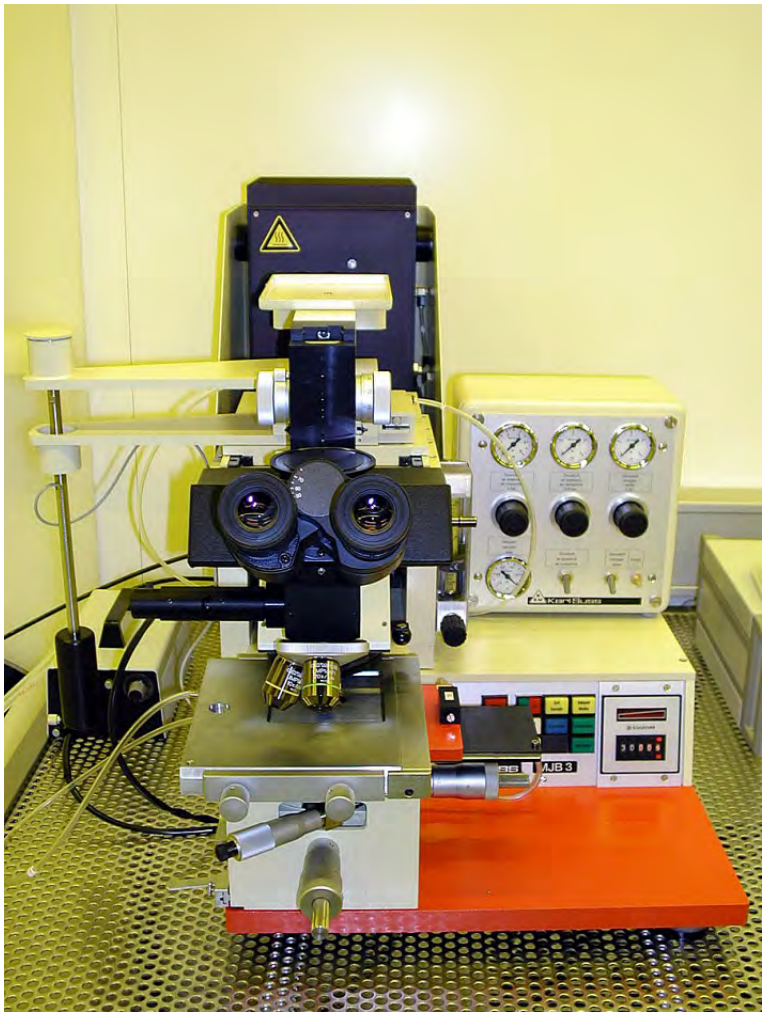

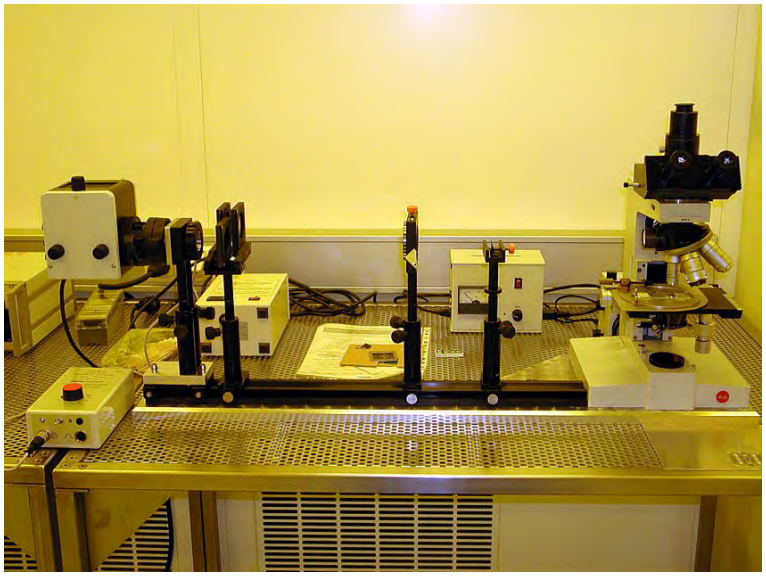

Figure 13: Top: Süss MJB 3 maskaligner for optical lithography. Bottom: Optical projection lithography based on an optical microscope.

Optical Lithography

For photolithography, a Karl Süss MJB 3 maskaligner or an optical microscope based projection system are used. The maskaligner operates in the 1 : 1 soft or hard contact mode and uses chromium metal masks. In the projection system the mask pattern is demagnified by a factor of 5 to 100. Therefore, cheap foil masks can be used. With both systems microstructures with a lateral dimension down to 1 µm can be fabricated.

Low and Ultra-Low Temperature Facilities

At the WMI, we have constructed the first dilution refrigerator with pulse tube pre-cooling for ultra-low temperature experiments. This type of refrigerator works without cryo-liquids, and thus is a lot more practical, more economical and more reliable than cryostats with liquid helium pre-cooling. These days, all major cryo-engineering companies are offering commercial versions of this Millikelvin cooler, and these so-called "dry" refrigerators outsell conventional refrigerators by a wide margin. The general construction concept of most manufacturers is unchanged from our original prototype, where the refrigerator consists of three basic components. The first cooling stage is a commercial pulse tube cryocooler which reaches a base temperature of 2.5 K. The second stage is a Joule-Thomson stage, and the last stage is a dilution refrigeration stage, where the lowest temperature of the cryostat is about 0.01 K (Fig. 14).

Figure 14: The "dry" dilution refrigerator of the WMI.

Figure 15: Low-temperature unit of a WMI dilution refrigerator ready to go into a cryostat.

Figure 16: Two mixing chamber mounting plates with silver sponges. Those are needed to overcome the thermal resistance (Kapitza resistance) between the liquid ^{3,4}He and the mounting plate of the mixing chamber. To fabricate the mounting of the sponge (square pins embedded in the sponge) a spark erosion technique has been employed.

In many low temperature applications high refrigeration capacities are required. Our design allows for a high circulation rate of ^{3}He which in the end determines the cooling power of a dilution refrigerator. Presently our "dry" fridge reaches a refrigeration capacity of 700 µW at a temperature of the mixing chamber of 0.1 K, seven times the cooling power of the WMI nuclear demagnetization cryostat. Goals of our present work are a further increase of cooling power and a lower base temperature of the dry dilution refrigerator. For a more detailed report, please see page 77.

A smaller version of our cryogen-free fridge has become commercially available by *Oxford Instruments* (formerly *VeriCold Technologies, Ismaning*). It has a refrigeration capacity of 250 µW

at a mixing chamber temperature of 0.1 K (Fig. 15).

The WMI also develops and fabricates dilution refrigerator inserts for temperatures down to about 20 mK. The inserts fit into all cryogenic systems (e.g. superconducting magnets) having a two inch bore. They allow fast sample change and rapid cool down cycles of less than five hours. The dilution refrigerator inserts are engineered and fabricated in-house and are also provided to other low temperature laboratories for ultra-low temperature experiments.

Millikelvin Temperatures in Combination with 3D Vector Magnetic-Fields

Figure 17: The dilution refrigerator with the 3D vector magnet located in the Quantum Laboratories.

Part of the Quantum Laboratories at the Walther-Meißner-Institut is a cryogen-free dilution refrigerator equipped with a 3D vector magnet allowing for 1 T in-plane and 6 T out-of-plane magnetic fields. Additional microwave coaxial lines allow for the microwave spectroscopy up to 18 GHz under these experimental conditions.

Scientifically, several directions in the field of fundamental light-matter interaction are envisaged:

(i) Circuit quantum electrodynamics (circuit QED), where superconducting qubits form hybrids with microwave resonators. These experiments are time consuming, because quantum effects arise in the limit of low excitation numbers. Hereby, challenging requirements are imposed on the detection systems allowing to detect microwave signals in the attowatt regime.

(ii) Storage of quantum states. One possibility is the transfer of the quantum information contained in photons to long-lived spin states. Additionally, exchange coupled systems or ferromagetic systems come into focus, because the effective coupling strength scales with the square-root of the number of spins contributing. In general, we study the light-matter interaction with long-lived spin systems and integrate superconducting quantum circuits.

(iii) Spin systems. Here, the investigations are not limited to paramagnetic spin systems, but will be extended to exchange coupled (ferro-) magnetic systems. Hereby, magnetization damping can be investigated as a function of temperature, frequency and magnetic field direction.

(iv) Circuit electro-mechanical hybrid systems consisting of a nanomechanical element coupled to a superconducting microwave resonator. In this context, sideband cooling of the mechanical system into its ground state and pulsed spectroscopy of hybrid system are performed and will be extended.

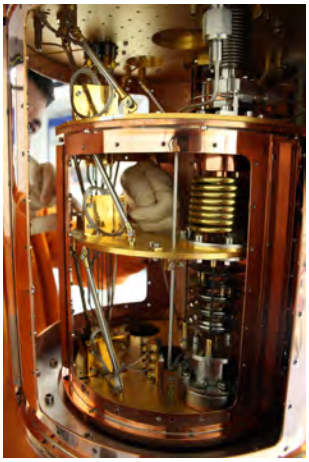

Figure 18: Inside of the dilution system. The windows of the 4 K and the still shield are removed providing access to the low temperature stages.

WMI Millikelvin Facilities for Experiments with Superconducting Quantum Circuits

The research on superconducting quantum circuits at the WMI focuses mainly on systems sensitive to externally applied flux (flux qubits), circuit QED systems where flux qubits are coupled to transmission line resonators, squeezing physics in flux driven Josephson parametric amplifiers, and propagating quantum microwaves (e.g., quantum state reconstruction methods). In order to further develop our activities on quantum effects in the microwave regime, additional cryogenic capacities at millikelvin temperatures have been established. In addition to sufficient cooling power, the specifications for these cryostats are mainly dictated by the dimensions (typically a few centimeters in each direction) of bulky microwave components such as circulators or microwave switches.

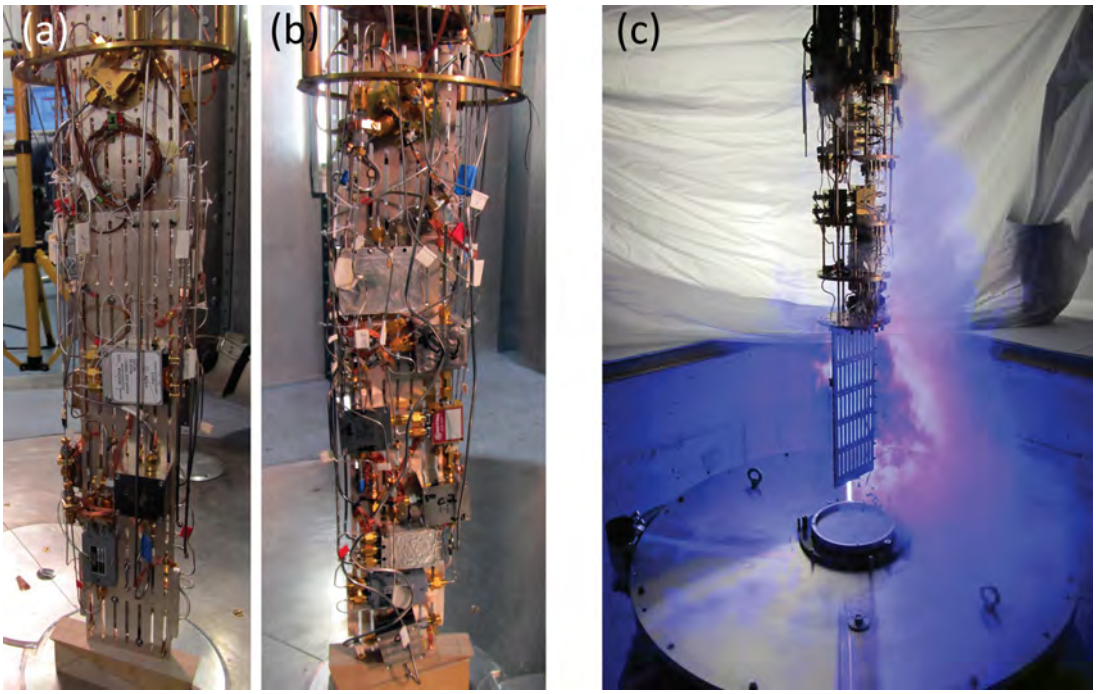

Figure 19: Liquid-helium precooled dilution refrigerators for experiments with superconducting quantum circuits. (a), (b) Back and front sides of the sample stage of the K12-refrigerator equipped with four circuit QED experiments. The height of the silver rod is 50 cm. (c) Sample stage and dewar of the dilution refrigerator in the quantum laboratory K04.

Two liquid-helium precooled dilution refrigerators are available for experiments with superconducting quantum circuits. The dilution refrigerator in laboratory K12 provides a sample space with a cylindrical volume with 11 cm diameter 55 cm height. The refrigerator is equipped with four microwave amplifiers at the 4 K-stage, seven broadband input lines and 80 twisted pair DC lines. This allows for mounting four experiments simultaneously to avoid idle times by interleaved measurements (see Fig. 19(a) and (b)). The base temperature of this refrigerator is 20 mK.

A new liquid-helium precooled dilution refrigerator for experiments with superconducting quantum circuits has been set up in the quantum laboratory K04. To provide enough space at the sample stage we have installed a Cryogenic Ltd. stainless steel dewar with a ^{4}He volume of 89 l. The time between two refills exceeds nine days. The cryostat is equipped with 16 coaxial measurement lines suitable for microwave frequencies down to the mixing chamber stage and low-noise cryogenic high electron mobility transistor (HEMT) amplifiers. Presently up to four samples can be mounted simultaneously to the sample stage. By expanding the number of input lines in the near future a more complex experiment can be set up. The cooling power of the mixing chamber at 100 mK was determined to reach 140 µW.

A new cryogen-free dilution refrigerator with a pulse tube refrigerator (PTR) and with a large sample stage has been set up in the quantum laboratory K21 using the longstanding experience in dry dilution refrigerators at the WMI. This refrigerator features large diameters (tens of centimeters) of all temperature stages providing extensive space for advanced quantum experiments. The main components of the refrigerator are the PTR, a 1 K-stage and a dilution unit. The two stages of the PTR cool the incoming ^{4}He and the ^{3}He/^{4}He mixture as well as one radiation shield at each stage. To provide sufficiently high cooling power near 1 K to cool microwave components and cables, this refrigerator has been equipped with a 1 K-stage operating in a closed cycle. A refrigeration capacity of the 1 K-stage of up to 100 mW could be reached. The dilution refrigerator is precooled by a dedicated ^{4}He circuit. The minimum base temperature of the refrigerator is below 11 mK. The cooling power at 100 mK was determined to reach 300 µW at the maximum ^{3}He flow rate.

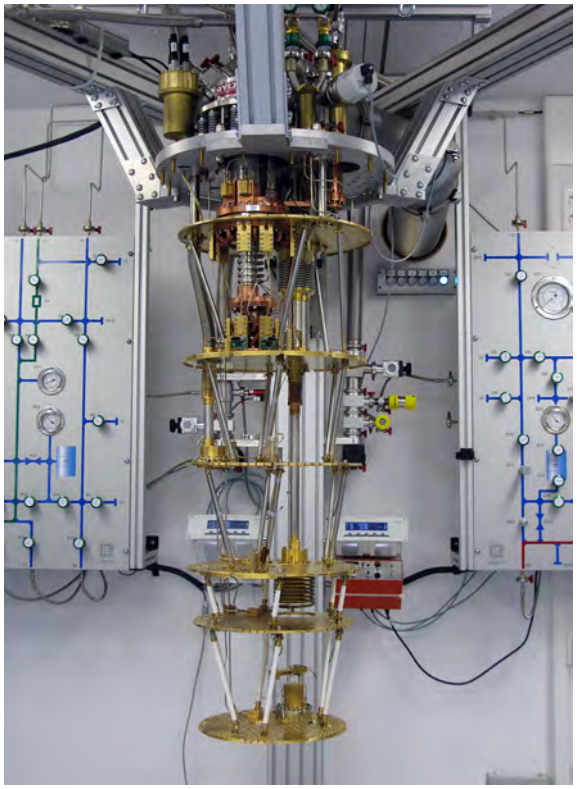

Figure 20: Dry dilution refrigerator with a large sample space.

Publications

1. **Alternative route to charge density wave formation in multiband systemss**
H.-M. Eiter, M. Lavagnini, R. Hackl, E.A. Nowadnick, A.F. Kemper, T.P. Devereaux, J.-H. Chu, J.G. Analytis, I.R. Fisher, L. Degiorgi
PNAS **110**, 64-69 (2013).

2. **Tunable Coupling Engineering Between Superconducting Resonators: From Sidebands to Effective Gauge Fields**
Borja Peropadre, David Zueco, Friedrich Wulschner, Frank Deppe, Achim Marx, Rudolf Gross, and Juan José García-Ripoll
Phys. Rev. B **87**, 134504 (2013).

3. **Slowing, advancing and switching of microwave signals using circuit nanoelectromechanics**
X. Zhou, F. Hocke, A. Schliesser, A. Marx, H. Huebl, R. Gross, and T. J. Kippenberg
Nature Physics **9**, 179-184 (2013).

4. **Der Mann, mit dem die Kälte kam – Walther Meißner und die Tieftemperaturphysik in Deutschland**
W. Buck, D. Einzel, R. Gross
Physik Journal **12**, No. 5, 37–41 (2013).

5. **Cryogen-free dilution refrigerator with 1 K-stage**
Kurt Uhlig
Cryocoolers **17**, 471 (2013).

6. **Optimisation of NbN thin films on GaAs substrates for in-situ single photon detection in structured photonic devices**
Günther Reithmaier, Jörg Senf, Stefan Lichtmannecker, Thorsten Reichert, Fabian Flassig, Andrej Voss, Rudolf Gross, Jonathan Finley
J. Appl. Phys. **113**, 143507 (2013).

7. **High Cooperativity in Coupled Microwave Resonator Ferrimagnetic Insulator Hybrids**
Hans Huebl, Christoph Zollitsch, Johannes Lotze, Fredrik Hocke, Moritz Greifenstein, Achim Marx, Sebastian T. B. Goennenwein, and Rudolf Gross
Phys. Rev. Lett. **111**, 127003 (2013).

8. **Gradiometric flux qubits with tunable gap**
M. J. Schwarz, J. Goetz, Z. Jiang, T. Niemczyk, F. Deppe, A. Marx, R. Gross
New J. Phys. **15**, 045001 (2013).

9. **Spin Hall Magnetoresistance Induced by a Non-Equilibrium Proximity Effect**
H. Nakayama, M. Althammer, Y.-T. Chen, K. Uchida, Y. Kajiwara, D. Kikuchi, T. Ohtani, S. Geprägs, M. Opel, S. Takahashi, R. Gross, G. E. W. Bauer, S. T. B. Goennenwein, E. Saitoh
Phys. Rev. Lett. **110**, 206601 (2013).

10. **Raman-Scattering Detection of Nearly Degenerate s-Wave and d-Wave Pairing Channels in Iron-Based $Ba_{0.6}K_{0.4}Fe_2As_2$ and $Rb_{0.8}Fe_{1.6}Se_2$ Superconductors**
Florian Kretzschmar, Bernhard Muschler, Thomas Böhm, Andreas Baum, Rudi Hackl, Hai-Hu Wen, Vladimir Tsurkan, Joachim Deisenhofer, Alois Loidl
Phys. Rev. Lett. **110**, 187002 (2013).

11. **On-chip time resolved detection of quantum dot emission using integrated superconducting single photon detectors**
Günther Reithmaier, Stefan Lichtmannecker, Thorsten Reichert, Peter Hasch, Kai Müller, Max Bichler, Rudolf Gross, Jonathan J. Finley
Scientific Reports **3**, 1901 (2013).

12. **Fast microwave beam splitters from superconducting resonators**
M. Haeberlein, D. Zueco, P. Assum, T. Weißl, E. Hoffmann, B. Peropadre, J.J. Garcia-Ripoll, E. Solano, F. Deppe, A. Marx, R. Gross
arXiv:1302.0729, submitted for publication (2013).

13. **Theory of spin Hall magnetoresistance**

Yan-Ting Chen, Saburo Takahashi, Hiroyasu Nakayama, Matthias Althammer, Sebastian T. B. Goennenwein, Eiji Saitoh, Gerrit E. W. Bauer
Phys. Rev. B **87**, 144411 (2013).

14. **Quantitative Study of the Spin Hall Magnetoresistance in Ferromagnetic Insulator/Normal Metal Hybrids**
M. Althammer, S. Meyer, H. Nakayama, M. Schreier, S. Altmannshofer, M. Weiler, H. Huebl, S. Geprägs, M. Opel, R. Gross, D. Meier, C. Klewe, T. Kuschel, J.-M. Schmalhorst, G. Reiss, L. Shen, A. Gupta, Y.-T. Chen, G.E.W. Bauer, E. Saitoh, S.T.B. Gönnenwein
Phys. Rev. B **87**, 224401 (2013).

15. **Converse Magnetoelectric Effects in Fe_3O_4/$BaTiO_3$ Multiferroic Hybrids**
S. Geprägs, D. Mannix, M. Opel, S.T.B. Goennenwein, R. Gross
Phys. Rev. B **88**, 054412 (2013).

16. **Magnon, phonon, and electron temperature profiles and the spin Seebeck effect in magnetic insulator/normal metal hybrid structures**
Michael Schreier, Akashdeep Kamra, Mathias Weiler, Jiang Xiao, Gerrit E. W. Bauer, Rudolf Gross, Sebastian T. B. Goennenwein
Phys. Rev. B **88**, 094410 (2013).

17. **Localized states in the Mott insulator κ-(BEDT-TTF)$_2$Cu[N(CN)$_2$]Cl as probed by photoluminescence**
N. Drichko, R. Hackl, and J. Schlueter
Phys. Rev. B **88**, 115109 (2013).

18. **Separation of semiconducting and ferromagnetic $FeSi_2$-nanoparticles by magnetic filtering**
Willi Aigner, Sabrina Niesar, Ervin Mehmedovic, Matthias Opel, Friedrich E. Wagner, Hartmut Wiggers, Martin Stutzmann
J. Appl. Phys. **114**, 134308 (2013).

19. **Two-Fluid Description of Two-Band Superconductors**
Nikolaj Bittner and Dietrich Einzel
J. Low Temp. Phys. **174**, 184-206 (2014).

20. **Experimental test of the spin mixing interface conductivity concept**
Mathias Weiler, Matthias Althammer, Michael Schreier, Johannes Lotze, Matthias Pernpeintner, Sibylle Meyer, Hans Huebl, Rudolf Gross, Akashdeep Kamra, Jiang Xiao, Yan-Ting Chen, HuJun Jiao, Gerrit E. W. Bauer, Sebastian T. B. Goennenwein
Phys. Rev. Lett. **111**, 176601 (2013).

21. **Electrically Detected Double Electron-Electron Resonance: Exchange Interaction of ^{31}P Donors and P_{b0} Defects at the Si/SiO_2 Interface**
Max Suckert, Felix Hoehne, Lukas Dreher, Markus Kuenzl, Hans Huebl, Martin Stutzmann, Martin S. Brandt
Molecular Physics **111**, 2690-2695 (2013).

22. **Thermopower enhancement by encapsulating cerium in clathrate cages**
A. Prokofiev, A. Sidorenko, K. Hradil, M. Ikeda, R. Svagera, M. Waas, H. Winkler, K. Neumaier, and S. Paschen
Nature Mater. **12**, 1096-1101 (2013).

23. **Charge Inhomogeneity in Electron-Doped $Pr_{1.85}Ce_{0.15}CuO_4$ Determined with ^{63}Cu NMR**
Michael Jurkutat, Jürgen Haase, Andreas Erb
J. Supercond. Nov. Magn. **26**, 2685-2688 (2013).

24. **Growth of high-purity scintillating $CaWO_4$ single crystals for the low-temperature direct dark matter search experiments CRESST-II and EURECA**
A. Erb, J.-C. Lanfranchi
Cryst. Eng. Comm. **15**, 2301-2304 (2013).

25. **Squeezing with a flux-driven Josephson parametric amplifier**
L. Zhong, E. P. Menzel, R. Di Candia, P. Eder, M. Ihmig, A. Baust, M. Haeberlein, E. Hoffmann, K. Inomata, T. Yamamoto, Y. Nakamura, E. Solano, F. Deppe, A. Marx, R. Gross

New J. Phys. **15**, 125013(2013).

26. **The EDMR Microscope - Combining Conductive Atomic Force Microscopy with Electrically Detected Magnetic Resonance**
Konrad Klein, Benedikt Hauer, Benedikt Stoib, Markus Trautwein, Sonja Matich, Hans Huebl, Oleksandr Astakhov, Friedhelm Finger, Robert Bittl, Martin Stutzmann, Martin S. Brandt
Rev. Sci. Instrum. **84**, 103911 (2013).

27. **Current Heating Induced Spin Seebeck Effect**
Michael Schreier, Niklas Roschewsky, Erich Dobler, Sibylle Meyer, Hans Huebl, Rudolf Gross, Sebastian T. B. Goennenwein
Appl. Phys. Lett. **103**, 242404 (2013).

28. **Spin pumping and spin currents in magnetic insulators**
M. Weiler, G. Woltersdorf, M. Althammer, H. Huebl, S. T. B. Goennenwein
In: *Recent Advances in Magnetic Insulators - From Spintronics to Microwave Applications*, Eds. Mingzhong Wu and Axel Hoffmann, Solid State Physics **64**, 123-156 (2013).

29. **Angle-dependent spin wave resonance spectroscopy of (Ga,Mn)As films**
L. Dreher, C. Bihler, E. Peiner, A. Waag, W. Schoch, W. Limmer, S. T. B. Goennenwein, M. S. Brandt
Phys. Rev. B **87**, 224422 (2013).

30. **Festkörperphysik: Aufgaben und Lösungen**
R. Gross, A. Marx, D. Einzel
Oldenbourg Wissenschaftsverlag München (2013), ISBN 978-3-486-77134-3.

31. **Laser molecular beam epitaxy of ZnO thin films and heterostructures**
Matthias Opel, Stephan Geprägs, Matthias Althammer, Thomas Brenninger, Rudolf Gross
J. Phys. D: Appl. Phys. **47**, 034002 (2014).

32. **Interactions and Chemical Transformations of Coronene Inside and Outside Carbon Nanotubes**
Bea Botka , Melinda E. Füstös , Hajnalka M. Tóháti , Katalin Németh , Gyöngyi Klupp , Zsolt Szekrényes , Dorina Kocsis , Margita Utczás , Edit Székely , Tamás Váczi , György Tarczay , Rudi Hackl , Thomas W. Chamberlain , Andrei N. Khlobystov, and Katalin Kamarás
Small, advance online publication (2013).

33. **Strain-controlled nonvolatile magnetization switching**
Stephan Geprägs, Andreas Brandlmaier, Martin S. Brandt, Rudolf Gross, Sebastian T.B. Goennenwein
Solid State Commun., advance online publication (2013).

34. **Comment on "Pt magnetic polarization on $Y_3Fe_5O_{12}$ and magnetotransport characteristics"**
Stephan Geprägs, Sebastian T.B. Goennenwein, Marc Schneider, Fabrice Wilhelm, Katharina Ollefs, Andrei Rogalev, Matthias Opel, Rudolf Gross
arXiv:1307.4869, submitted for publication (2013).

35. **Real Time Electrical Detection of Coherent Spin Oscillations**
F. Hoehne, C. Huck, M. S. Brandt, H. Huebl
arXiv:1307.7413, submitted for publication (2013).

36. **Dual-Path Methods for Propagating Quantum Microwaves**
R. Di Candia, E. P. Menzel, L. Zhong, F. Deppe, A. Marx, R. Gross, E. Solano
New. J. Phys. **16**, 015001 (2014).

37. **Time resolved spin Seebeck effect experiments as a probe of magnon-phonon thermalization time**
Niklas Roschewsky, Michael Schreier, Akashdeep Kamra, Felix Schade, Kathrin Ganzhorn, Sibylle Meyer, Hans Huebl, Stephan Geprägs, Rudolf Gross, Sebastian T. B. Goennenwein
arXiv:1309.3986, submitted for publication (2013).

38. **Zinc Oxide - From Dilute Magnetic Doping to Spin Transport**
Matthias Opel, Sebastian T.B. Goennenwein, Matthias Althammer, Karl-Wilhelm Nielsen, Eva-Maria Karrer-Müller, Sebastian Bauer, Konrad Senn, Christoph Schwark, Christian Weier, Gernot

Güntherodt, Bernd Beschoten, Rudolf Gross
arXiv:1309.5857, accepted for publication in Physica Status Solidi B (2013).

39. **Unambiguous Determination of Spin Dephasing Times in ZnO**
Sebastian Kuhlen, Ralph Ledesch, Robin de Winter, Matthias Althammer, Sebastian T.B. Goennenwein, Matthias Opel, Rudolf Gross, Thomas A. Wassner, Martin S. Brandt, Bernd Beschoten
arXiv:1309.6600, submitted for publication (2013).

40. **Magnetic quantum oscillations in the charge-density-wave state of the organic metals α-(BEDT-TTF)$_2M$Hg(SCN)$_4$ with M = K and Tl**
M. V. Kartsovnik, V. N. Zverev, D. Andres, W. Biberacher, T. Helm, P. D. Grigoriev, R. Ramazashvili, N. D. Kushch, H. Müller
arXiv:1311.5744, submitted for publication (2013).

41. **Single crystal growth of the high temperature superconducting oxides**
Andreas Erb
to be published in: Handbook of Applied Superconductivity (Wiley-VCH, 2014).

42. **Nano- and microstructures of magnetic field guided maghemite nanoparticles in thin diblock copolymer films**
Yuan Yao, Ezzeldin Metwalli, Martin A. Niedermeier, Matthias Opel, Chen Lin, Jing Ning, Jan Perlich, Stephan V. Roth, Peter Müller-Buschbaum
ACS Applied Materials & Interfaces, submitted (2013).

43. **Dry dilution refrigerator with He-4 precool loop**
Kurt Uhlig
Adv. In Cry. Eng. **59**, submitted (2013).

The accompanying diagram shows the development of the total number of citations per year of papers published by members of WMI since 1995. This number has more than doubled within the last ten years and is exceeding 1 300 in 2013.

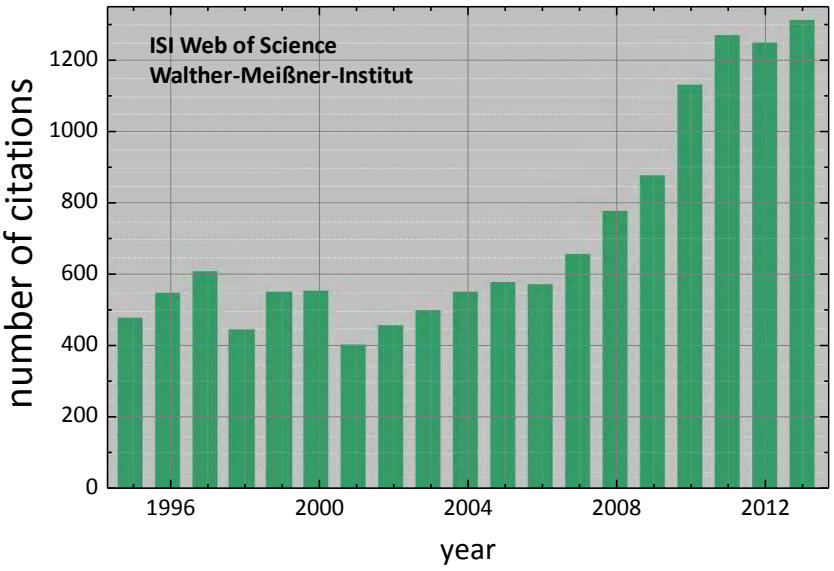

Books

Festkörperphysik

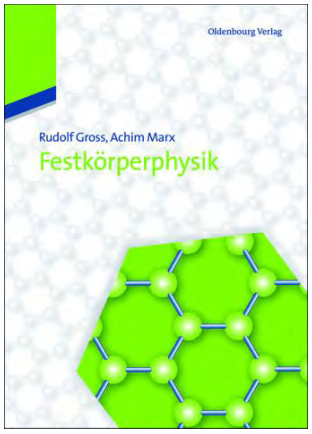

Late in 2012, the solid state physics textbook ***Festkörperphysik*** by Rudolf Gross and Achim Marx has been published by the Oldenbourg Wissenschaftsverlag München. The book was getting very positive reviews (see e.g. review by Prof. Daniel Hägele in Physik Journal **12** (2013) Nr. 10, p. 60).

The book was well received by teachers and is highly esteemed by the students. Meanwhile, the first edition with 2000 copies is almost sold out and the second edition is already in preparation.

Basic information on the book:

- Title: Festkörperphysik
- Publisher: Oldenbourg Wissenschaftsverlag München
- Published: September 19, 2012
- Presentation: hardcover, XVIII, 982 pages, with a large number of colored illustrations and tables
- Language: German
- Size: 253 mm x 170 mm x 63 mm
- Weight: 1915 g
- ISBN-13: 9783486712940
- ISBN-10: 3486712942
- Order number: 34690524, price: EUR 49,80

Festkörperphysik. Aufgaben und Lösungen

In December 2013, the supplementary book entitled ***Festkörperphysik. Aufgaben und Lösungen*** by Rudolf Gross, Achim Marx and Dietrich Einzel has been published also by the Oldenbourg Wissenschaftsverlag München. The book contains model solutions to all exercises listed at the end of the chapters of the related solid state physics textbook ***Festköperphysik***. The book is ideal for preparing for examinations and for learning on one's own

Basic information on the book:

- Title: Festkörperphysik. Aufgaben und Lösungen
- Publisher: Oldenbourg Wissenschaftsverlag München
- Published: December 18, 2013
- Presentation: paperback, XI, 309 pages, 83 black and white illustrations, 3 tables
- Language: German
- Size: 242 mm x 170 mm x 20 mm
- Weight: 1915 g
- ISBN-13: 9783486712940
- ISBN-10: 3486712942
- eISBN: 978-3-486-85896-9
- Price: EUR 25,70

Theses, Appointments, Honors and Awards, Membership in Advisory Boards, etc.

Completed and ongoing Ph.D. Theses

Completed Ph.D. Theses:

1. **Experiments on Two-Resonator Circuit Quantum Electrodynamics: A Superconducting Quantum Switch**
   Elisabeth Hoffmann, TU München, May 2013.
2. **Microwave Circuit-electrodynamics in a Nanomechanical Hybrid System**
   Fredrik Hocke, TU München, September 2013.
3. **High Magnetic Field Properties of Electron-doped Cuprate Superconductors**
   Toni Helm, TU München, September 2013.
4. **Propagating Quantum Microwaves: Dual-path State Reconstruction and Path Entanglement**
   Edwin Peter Kurt Menzel, TU München, December 2013.

Ongoing Ph.D. Theses:

5. **Wechselwirkung zwischen Spin-, Gitter- und Ladungsfreiheitsgraden in korrelierten Metallen ohne Inversionszentrum**
   Hans-Martin Eiter, TU München, since October 2008.
6. **Superconducting Flux Qubits with Tunable Gap**
   Manuel Schwarz, TU München, since June 2009.
7. **All Optical Quantum Computing**
   Max Häberlein, TU München, since December 2009.
8. **Raman-Untersuchungen an stark korrelierten Systemen mit hoher Ortsauflösung**
   Florian Kretschmar, TU München, since January 2010.
9. **Vibrational Investigations of Luminescence Molecules**
   Nitin Chelwani, TU München, since September 2010.
10. **Time-Domain Measurements on Ultra-strong-coupled Qubit-Resonator Systems**
    Alexander Baust, TU München, since October 2010.
11. **Spinabhängige thermogalvanische Effekte in ferromagnetischen Dünnschichten**
    Johannes Lotze, TU München, since April 2011.
12. **Generation and Detection of Quantum Correlations in Circuit QED Systems**
    Ling Zhong, TU München, since November 2011.
13. **Superconducting Quantum Circuits for Qunatum Electrodynamics Experiments**
    Karl Friedrich Wulschner, TU München, since January 2012.
14. **Circuit Quantum Electrodynamics Experiments with Tunable Flux Qubits**
    Jan Goetz, TU München, since January 2012.
15. **Single Excitation Transfer in the Quantum Regime: A Spin-Based Solid State Approach**
    Christoph Zollitsch, TU München, since January 2012.
16. **Untersuchung der verschiedenen Phasen eisenbasierter Supraleiter mittels Raman-Streuung**
    Andreas Baum, TU München, since April 2012.
17. **Superconducting Properties of Organic Metals in the Vicinity of Ordering Instabilities**
    Michael Kunz, TU München, since August 2012.

18. **Quantum Information Processing with Propagating Quantum Microwaves**
    Peter Eder, TU München, since November 2012.
19. **Coupled Electro-Nanomechanical Systems**
    Matthias Pernpeintner, TU München, since November 2012.
20. **Spin Transport in Ferrromagnetic Microsturctures**
    Michael Schreier, TU München, since December 2012.
21. **Spin dynamics and spin transport in solid state systems**
    Hannes Maier-Flaig, TU München, since November 2013.
22. **Circuit Quantum Electrodynamics with Three-dimensional Cavities**
    Edwar Xie, TU München, since December 2013.

The following Ph.D. students of the Walther-Meißner-Institute have finished their Ph.D. theses in 2013:

Toni Helm

Fredrik Hocke

Elisabeth Hoffmann

Edwin Menzel

Completed and ongoing Diploma, Bachelor, Master Theses

Completed Master and Diploma Theses:

1. **Optimization of Josephson Junction Nanofabrication for Superconducting Quantum Circuits**
   Franz Sterr, Diplomarbeit, TU München, March 2013.
2. **Spin Dynamics in an Antiferromagnet**
   Marc Philipp Ross, Diplomarbeit, TU München, March 2013.
3. **Development of a Time-correlated Single Photon Counting System Based on X-ray Excitation and Temporal Characterization of Ultra-fast Scintillators**
   Tobias Lamm, Masterarbeit, TU München, July 2013.
4. **Spin Hall Magnetoresistive Noise**
   Friedrich Paul Witek, Masterarbeit, TU München, August 2013.
5. **Magnetic properties of high quality single crystals of the electron underdoped cuprate superconductor $Nd_{2-x}Ce_xCuO_{4+\delta}$**
   Alma Gabriela Dorantes Palacios, LMU München, October 2013.
6. **Ferroic Emitter Devices for Spin Polarized Electron Emission**
   Stefan Hohenberger, Masterarbeit, Joint International Graduate Program Advanced Materials Science, TU München/LMU München/Universität Augsburg, November 2013.
7. **Optimized Fabrication Process for Nanoscale Josephson Junctions Used in Superconducting Quantum Circuits**
   Edwar Xie, Masterarbeit, TU München, November 2012.
8. **Design and Characterization of a Superconducting Beam Splitter for Quantum Information Processing**
   Ferdinand Loacker, Diplomarbeit, TU München, Dezember 2013.

Completed Bachelor Theses:

9. **Organic superconductor as a low-temperature pressure gauge**
   Ismail Achmed-Zade, Bachelor-Thesis, TU München, 2013.
10. **Impedanzangepasste Widerstandsmessungen bei Frequenzen im Gigahertz-Bereich**
    Korbinian Baumgärtl, Bachelor-Thesis, TU München, 2013.
11. **Vector Modulation of Microwaves for Circuit QED Experiments**
    Stefan Gantner, Bachelor-Thesis, TU München, 2013.
12. **Gap suppression in superconducting cylinders: analytic results from the Ginzburg-Landau theory**
    Luzia Höhlein, Bachelor-Thesis, TU München, 2013.
13. **Spin Hall-Magnetoresistance in FMI/NM/FMI-Trilayers**
    Dominik Irber, Bachelor-Thesis, TU München, 2013.
14. **Charakterisierung nanomechanischer Balken mittels optischer Interferometrie**
    Moritz Jung, Bachelor-Thesis, TU München, 2013.
15. **Torque Magnetometry With Quartz Tuning Forks**
    Stefan Klimesch, Bachelor-Thesis, TU München, 2013.
16. **$Nd_2Ir_2O_7$: Ein neues Weyl-Halbmetall?**
    Michaela Renate Lammel, Bachelor-Thesis, TU München, 2013.
17. **Atomic Force Microscopy on Nano-Scale Josephson Contacts**
    Dominik Martin Müller, Bachelor-Thesis, TU München, 2013.
18. **Interference Effects on Superconducting Coplanar Waveguide Structures**
    Hans Gürtner, Bachelor-Thesis, TU München, 2013.

19. **Fabrication and Characterization of $Y_3Fe_5O_{12}$/Pt/$Y_3Fe_5O_{12}$ Trilayers for Spin Current Based Experiments**
    Felix Schade, Bachelor-Thesis, TU München, 2013.
20. **Fast-Fourier-Transform-Based Electrical Noise Measurements**
    Alexander Schade, Bachelor-Thesis, TU München, 2013.
21. **Hall Effect Measurements in YIG/Pt Hybrids**
    Richard Schlitz, Bachelor-Thesis, TU München, 2013.
22. **Herstellung und Charakterisierung von $Y_3Fe_5O_{12}$-Pt Bilagen für Spinstrom basierte Experimente**
    Marc Schneider, Bachelor-Thesis, TU München, 2013.
23. **Joule Heating Induced Spin-Seebeck Effect**
    Erich Dobler, Bachelor-Thesis, TU München, 2013.
24. **Starke Kopplung in Hybridsystemen aus einem Ferrimagnet und einem supraleitenden Mikrowellenresonator**
    Christian Vogl, Bachelor-Thesis, TU München, 2013.
25. **Spitzenverstärkte Raman-Streuung (TERS)**
    Roland Richter, Bachelor-Thesis, TU München, 2013.
26. **Phononen in entzwillingtem $BaFe_2As_2$**
    Daniel Jost, Bachelor-Thesis, TU München, 2013.
27. **Untersuchung von $BaFe_2As_2$ unter dem Einfluss von uniaxialem Druck**
    Ali Özkü, Bachelor-Thesis, TU München, 2013.

Ongoing Master and Diploma Theses:

28. **Spinkaloritronik**
    Mathias Frank, Masterarbeit, TU München, since November 2012.
29. **High-field Normal State Magnetotransport Properties of Electron Doped Cuprate Superconductors**
    Vassilios Tzanos, Masterarbeit, TU München, since March 2013.
30. **Nanomechanik**
    Rasmus Holländer, TU München, since March 2013.
31. **Time-resolved Spin-Seebeck Effect**
    Niklas Roschewsky, Masterarbeit, TU München, since March 2013.
32. **Magnetoelektrische Effekte in multifunktionalen Schichtstrukturen**
    Bastian Stibbe, Diplomarbeit, TU München, since May 2013.
33. **Bestimmung thermischer Materialparameter an Dünnschicht-Solarzellen**
    Valentin Kunkel, Masterarbeit, TU München, since June 2013.
34. **Untersuchung der konkurrierenden Phasen in unkonventionellen Supraleitung**
    Andreas Walter, Masterarbeit, TU München, since October 2013.
35. **Topological Phases in Pyroclore Iridates**
    Andreas Wörfel, Masterarbeit, TU München, since October 2013.
36. **Thin Film Fabrication for Spin Current and Spin Caloritronic Experiments**
    Francesco Della Colletta, Masterarbeit, TU München, since October 2013.
37. **Magnetotransport Studies of Organic Superconductors Containing Paramagnetic Ions**
    Ludwig Schaidhammer, Masterarbeit, TU München, since November 2013.
38. **Tunable Beam Splitter: Time Domain Measurements**
    Fabian Kössel, Masterarbeit, TU München, since November 2013.
39. **Engineering the State of Light Using Gradiometric Flux Qubits with Tunable-Gap**
    Philipp Summer, Masterarbeit, TU München, since November 2013.

40. **Control of the Phonon Population in Nano-electromechanical Hybrid Systems**
Anh Tu Bohn, Masterarbeit, TU München, since November 2013.
41. **Coherent Manipulation of Phosphorus Donor Spins in Silicon at Low Temperatures**
Kai Müller, Masterarbeit, TU München, since November 2013.
42. **Spin-dependent Electronic Transport in Yttrium iron garnet**
Roland Rösslhuber, Masterarbeit, TU München, since November 2013.
43. **Chains of Tunable and Nonlinear Superconducting Resonators**
Udo Schaumburger, Masterarbeit, TU München, since December 2013.
44. **On-chip Quantum Beam-Splitter and Microwave Interferometer**
Michael Fischer, Masterarbeit, TU München, since December 2013.

Research Projects and Cooperations

A large number of our research projects are benefiting from the collaboration with external groups in joint research projects, as well as from individual collaborations, exchange programs and visitors. Most collaborations are based on joint projects, which are funded by different research organizations (see list below). A considerable number of collaborations also exists with universities, other research institutions and industry without direct financial support.

Funded Projects

A. German Research Foundation: Excellence Initiative

Cluster of Excellence "Nanosystems Initiative Munich"

1. Project Area I: *Quantum Nanophysics*
   F. Deppe, S.T.B. Gönnenwein, R. Gross, H. Huebl, A. Marx
2. Project Area II: *Hybrid Nanosystems*
   S.T.B. Gönnenwein, R. Gross, H. Huebl

B. German Research Foundation: Collaborative Research Centers

Collaborative Research Center 631: "Solid-State Quantum Information Processing: Physical Concepts and Materials Aspects"

1. Project A3: *Superconducting Quantum Circuits as Basic Elements for Quantum Information Processing*
   R. Gross, A. Marx
2. Project A8: *Cavity Quantum Electrodynamics with Superconducting Devices*
   A. Marx, R. Gross
3. Project C3: *Fundamentals of Quantum Logic Gates in Silicon*
   M. Brandt, H. Huebl, M. Stutzmann
4. Project S: *Coordination of the Collaborative Research Center*
   R. Gross

Transregional Collaborative Research Center TRR 80: "From Electronic Correlations to Functionality"

1. Project A2: *Spatially and Momentum Resolved Raman Studies of Correlated Systems*
   R. Hackl

C. German Research Foundation: Priority Programs

1. Spin-dependent thermo-galvanic effects: experiment
   within the DFG Priority Program 1538 *Spin-Caloric Transport – SpinCAT*
   S.T.B. Gönnenwein, R. Gross (Az. GO 944/4-1)
2. Project: *Raman study of electron dynamics and phase transitions in iron-pnictide compounds*
   within the DFG Priority Program 1458 *"High-Temperature Superconductivity in Iron-Pnictides"*
   R. Hackl, R. Gross, B. Büchner, D. Johrendt, C. Honerkamp (Az. HA 2071/7-1, HA 2071/7-2)

3. Project: *Spin injection, spin transport and controllable ferromagnetism in transition metal doped ZnO*
   within the DFG Priority Program 1285 *"Halbleiter-Spinelektronik"*
   R. Gross, S.T.B. Gönnenwein, M. Opel (Az. GR 1132/14-1, GR 1132/14-2, GR 1132/14-3)

D. German Research Foundation: Research Projects

1. Project: *Exotic Superconductivity in Strongly Anisotropic Correlated Organic Metals in the Vicinity of Insulating Phases*
   M. Kartsovnik, W. Biberacher, R. Gross (Az. KA 1652/4-1)
2. Project: *Doping Dependent Evolution of the Fermi Surface and Competing Ordering Phenomena in Superconducting Cuprates*
   R. Gross, M. Kartsovnik, A. Erb (Az. GR 1132/15-1)
3. Project: *Interaction Between Spin, Lattice, and Charge in Non-Centrosymmetric Correlated Metals*
   R. Hackl, R. Gross (Az. HA 2071/5-1)

E. European Union

1. EU Collaborative Project (call identifier FP7-ICT-2011-C), project title *Quantum Propagating Microwaves in Strongly Coupled Environments – PROMISCE*
   F. Deppe, A. Marx, R. Gross, Grant Agreement no. 284566
   partners: several European Universities and research facilities.
2. Marie Curie Network for Initial Training (call identifier FP7-PEOPLE-2010-ITN), project title *Circuit and Cavity Quantum Electrodynamics (CCQED)*
   R. Gross, A. Marx, F. Deppe, Grant Agreement No. PITN-GA-2010-264666
   partners: several European Universities and research facilities.
3. Marie Curie Network for Initial Training (call identifier FP7-PEOPLE-2009-ITN), project title *Cavity-confined Luminophores for Advanced Photonic Materials: A Training Action for Young Researchers (FINELUMEN)*
   R. Hackl, Grant Agreement Number PITN-GA-2008-215399
   partners: several European Universities and research facilities.

F. Bavaria California Technology Center (BaCaTeC)

1. Project: *Nematic Order and New Phases in Quantum Materials*
   R. Hackl,
   partners: Profs. Thomas Devereaux, Steve Kivelson, and Sri Raghu (Stanford University)

G. German Academic Exchange Service

1. Project-based Personnel Exchange Programme (PPP) with Serbia (project 56267076: Fe-based superconductors), collaboration with the Institute of Physics, University of Belgrade (Dr. Z.V. Popovic)
   R. Hackl

H. Others

Conferences and Workshops

The Walther-Meißner-Institute has organized/co-organized the following conferences, workshops and symposia in 2013:

International Conference on Resonator QED (September 09–13, 2013, Munich, Germany)

The conference was organized by the ***EU Marie Curie Network CCQED***. It took place at the Kardinal Wendel Haus (Mandlstraße 23, 80802 München) close to the English Garden in Munich-Schwabing. It was focussing on the following topics: (i) Single atom cavity QED, (ii) Multi-atom cavity QED, (iii) Circuit QED, (iv) Photonic crystal cavity QED, (v) Quantum information processing with CCQED systems, (vi) Cavity optomechanics, (vii) Hybrid circuit or cavity QED systems, (viii) QED without cavity. With more than 140 participants from all over the world, the conference was a major and very successful event. The final programme comprised 6 tutorials, 28 invited talks, 18 contributed talks and 57 posters. The local CCQED network partners (Max-Planck-Institute for Quantum Optics and Walther-Meißner-Institute) opened doors for a tour through their laboratories. Moreover, the CCQED industry partners invited conference attendees to visit their facilities or offer to meet their experts.

To disseminate research on quantum optics and circuit QED to a broader public, CCQED organized an evening with a public lecture by Nobel laureate in physics, Serge Haroche on 11^{th} September at the Ehrensaal of the Deutsches Museum. Subsequently, a panel discussion (presented by Jeanne Rubner, Bayerischer Rundfunk) on "Research & Innovation" with guests from research, politics and industry examined the link between basic research and innovation. The event attracted more than 150 participants.

510. Wilhelm und Else Heraeus-Seminar "Non-Magnetic Control of Spin – Fundamental Physics and Materials Design" (January 07 – 09, 2013, Bad Honnef, Germany)

The 510. WEH-Seminar was co-organized by Sebastian Gönnenwein (Walther-Meißner-Institut), Christian Heiliger (Universität Gießen), and Diemo Ködderitzsch (LMU München).

Magnetic materials play an important role in today's high tech devices, for example in hard disk drives, in magnetic sensors, or in magnetic actuators. Hereby, the magnetic properties are usually controlled or adjusted via the application of external magnetic fields. While this conventional magnetic-field control of magnetism approach is very natural and straightforward, it suffers from severe drawbacks. In particular, it is difficult to locally generate the required magnetic fields, such that the magnetic-field control of magnetism can not be scaled to modern, nm-scale devices.

In recent years, alternative schemes enabling a control of magnetic moments or spins by means of non-magnetic control parameters have emerged. These non-magnetic control of spin schemes take advantage, e.g., of electric fields, magneto-electric coupling, elastic strains, or thermal gradients the manipulate the magnetic properties. The corresponding multifunctional structures (comprising constituents with both magnetic as well as a non-magnetic functionality) offer intriguing new physics and material science insights and challenges.

The key intention of the 510. WEH-Seminar was to address and compare the main non-magnetic control of spin schemes currently investigated, and to discuss possible extensions or new concepts. In addition to the fundamental physics and theoretical concepts underlying the different approaches, materials and device considerations will play an important role. The seminar gave an overview over the rapidly developing field of non-magnetic spin control, while providing ample time for discussions and scientific networking.

Symposium on "Strong Coupling in Solid State Quantum Systems", Spring Meeting of the Condensed Matter Section of the German Physical Society (March 10 – 14, 2013, Regensburg, Germany)

Hans Hübl and Sebastian Gönnenwein of WMI organized a highly successful symposium on *Strong Coupling in Solid State Quantum Systems* within the Spring Meeting of the Condensed Matter Section of the German Physical Society.

International Miniworkshop on "Excitations in Correlated Systems and Energy Materials (ECSEM)" (July 25, 2013, Garching, Germany)

The miniworkshop was organized by Rudi Hackl of WMI to stimulate exchange between experimental and theory groups working in the field of correlated electron systems and energy materials.

Course 3 on "Physics and Electronics in Everyday Life" of the Ferienakademie 2013 (September 22 – October 04, 2013, Sarntal, Italy)

The course was hold by Rudolf Gross of WMI together with Prof. Dr. Gert Denninger, University of Stuttgart, and Prof. Dr. Klaus Mecke, University of Erlangen-Nuremberg, within the *Ferienakademie*. The Ferienakademie is jointly organized by the Technische Universität München, the University of Erlangen/Nuremberg, and the University of Stuttgart to motivate and foster highly talented students. It takes place in the Italian Alps.

Collaborations

Other collaborations without direct project funding involve:

- Stanford University, Stanford, USA (T.P. Devereaux, M. Greven, Z.-X. Shen, I. Fisher, B. Moritz)
- Universidad del País Vasco and Ikerbasque Foundation, Bilbao, Spain (E. Solano)
- Instituto de Fisica Fundamental, Madrid, Spain (Prof. Dr. J.J. Garcia-Ripoll)
- Central Research Institute of the Electric Power Industry, Tokyo, Japan (Dr. S. Ono, Dr. Y. Ando)
- Green Innovation Research Laboratories, NEC Corporation, Japan (Y. Nakamura, J.S. Tsai, K. Inomata, T. Yamamoto)
- University of Tohoku, Sendai, Japan (Gerrit E.W. Bauer, Eiji Saitoh)
- European Synchrotron Radiation Facility (ESRF), Grenoble (H. Müller, D. Mannix, F. Wilhelm, K. Ollefs)
- Materials Science Research Centre, IIT Madras, India (M.S. Ramachandra Rao)
- Raja Ramanna Centre for Advanced Technology, Indore, India (Lalit M. Kukreja)
- ETH-Zurich, Switzerland (A. Wallraff, L. Degiorgi, R. Monnier, Dr. M. Lavagnini)
- Chalmers University of Technology Gothenburg, Sweden (P. Delsing)
- MINT Center, University of Alabama (A. Gupta)
- Materials Physics Laboratory, Helsinki University of Technology, Finland (T. Heikkilä)
- Kavli Institute of NanoScience, Delft University of Technology, Delft, The Netherlands (T.M. Klapwijk, G.E.W. Bauer)
- High-Magnetic-Field Laboratory, Grenoble, France (I. Sheikin)
- High Magnetic Field Laboratory, Toulouse (C. Proust, D. Vignolles)
- B. Verkin Institute for Low Temperature Research and Engineering, Kharkov, Ukraine (V.G. Peschansky)
- Landau Institute for Theoretical Physics, Chernogolovka, Russia (P. Grigoriev)
- Clarendon Laboratory, University of Oxford, England (A. Karenowska)
- Russian Academy of Sciences, Chernogolovka, Russia (N. Kushch, A. Palnichenko)
- High Magnetic Field Laboratory, Dresden (E. Kampert, J. Wosnitza)
- National High Magnetic Field Laboratory, Tallahassee, USA (J. Brooks)
- University of Bonn, Germany (Prof. Dr. W. Mader)
- IFW Dresden, Germany (B. Büchner, J. Fink, S.V. Borisenko, M. Knupfer)
- Max-Planck-Institut für Festkörperforschung, Stuttgart (B. Keimer, L. Boeri)
- University of Tübingen, Germany (R. Kleiner, D. Kölle)
- University of Würzburg, Germany (W. Hanke, F. Assaad, C. Honerkamp, M. Potthoff)
- University of Augsburg, Germany (P. Hänggi, A. Wixforth, A. Kampf, A. Loidl, J. Deisenhofer, V. Tsurkan)
- University of Hamburg, Germany (G. Meier, W. Wurth)
- University of Leipzig, Germany (J. Haase)
- Abt. Halbleiterphysik, University of Ulm, Germany (W. Limmer)
- RWTH Aachen, Germany (G. Güntherodt, B. Beschoten)
- Georg-August-Universität, Göttingen, Germany (M. Münzenberg)
- Institut für Experimentelle und Angewandte Physik, Universität Regensburg, Germany

(Christian Back, Georg Woltersdorf)

- Universität Bielefeld, Germany (G. Reiss, A. Thomas)
- University of British Columbia, Vancouver, Canada (D. Bonn, A. Damascelli)
- Technische Universität München, Physics Department, Germany (D. Grundler, Ch. Pfleiderer, F.C. Simmel, Jean Come Lanfranchi)
- Walter Schottky Institut, TU München, Germany (G. Abstreiter, M. Stutzmann, J. Finley, M. Brandt, A. Holleitner)
- Ludwig-Maximilians-Universität München, Physics Department, Germany (J.P. Kotthaus, J. von Delft, E. Frey, J. Rädler, S. Ludwig)
- Ludwig-Maximilians-Universität München, Chemistry Department, Germany (Hubert Ebert, Diemo Ködderitzsch)
- Departamento de Fisica de la Materia Condensada, Universidad de Zaragoza, Spain (L. Morellon, J.M. de Teresa, D. Zueco)
- EPFL Lausanne, Switzerland (T. Kippenberg, H. Ronnov)
- University of New South Wales, Sydney, Australia (M. Simmons, A. Morello)
- McMaster University, Hamilton, Canada (J.P. Carbotte)
- Technische Universität Graz, Austria (E. Schachinger)
- Universität Konstanz (A. Leitenstorfer, E. Weig, J. Demsar, A. Pashkin)
- BMW Group, Munich, Germany (J. Schnagl)
- Siemens AG, CT MM 2, Munich, Germany (R. Matz, W. Metzger)
- Attocube, Munich, Germany (K. Karrai, D. Andres, E. Hoffmann)
- THEVA Dünnschichttechnik, Ismaning, Germany (W. Prusseit)
- Institut für Halbleiter- und Festkörperphysik, Johannes-Kepler-Universität Linz, Austria (A. Ney)
- Lehrstuhl für Technische Elektronik, Technische Universität München (M. Becherer)
- Institut für Angewandte Photophysik, Technische Universität Dresden (L. Eng, D. Köhler, J. Becherer)
- Jülich Centre for Neutron Science JCNS (S. Pütter)
- Université de Toulouse, Laboratoire de Physique Théorique, Toulouse, France (R. Ramazashvili)
- Lawrence Berkeley National Laboratory, Berkeley, USA (A. F. Kemper)
- University of Belgrade, Belgrade, Serbia (Z. Popovic, N. Lazarevic, D. Tanaskovic)
- University of Aveiro, Portugal (N. A. Sobolev)
- Macquarie University, MQ Research Centre for Quantum Science and Technology, Australia (J. Twamley)
- Instituto de Ciencia de Materiales de Sevilla, Spain (J. Poyato, J.L. Perez-Rodriguez)
- Research Institute for Solid State Physics and Optics, Hungarian Academy of Sciences, Budapest, Hungary (K. Kamaras, I. Tüttö, J. Balogh)
- University of Rome "La Sapienza", Rome, Italy (S. Caprara, C. Di Castro, M. Grilli)
- Hungarian Academy of Sciences, Budapest University of Technology and Economics, Budapest, Hungary (A. Virosztek, A. Zawadowski, G. Mihály)

Stays abroad

Extended visits of members of the Walther-Meißner-Institute at foreign research laboratories:

1. **Rudi Hackl**
   Stanford University and Stanford Institute for Materials and Energy Science, Stanford, USA
   24. 03. - 12. 04. 2013, 19. 06. - 03. 07. 2013
2. **Toni Helm**
   High Magnetic Field Laboratory, Toulouse, France
   07. 04. - 12. 04. 2013
3. **Toni Helm**
   High Magnetic Field Laboratory, Dresden, Germany
   29. 08. - 07. 09. 2013
4. **Mark Kartsovnik, Toni Helm, Vasilis Tzanos**
   High Magnetic Field Laboratory, Grenoble, France
   20. 04. - 29. 04. 2013
5. **Mark Kartsovnik**
   High Magnetic Field Laboratory, Grenoble, France
   08. 10. - 16. 10. 2013
6. **Vasilis Tzanos**
   High Magnetic Field Laboratory, Grenoble, France
   18. 08. - 26. 08. 2013
7. **Alexander Baust**
   NEC Corporation, Smart Energy Research Laboratories, Tsukuba, Ibaraki, Japan
   19. 08. - 18. 10. 2013

Conference Talks and Seminar Lectures

Andreas Baum

1. **Phonons in twin-free $BaFe_2As_2$**
   International Miniworkshop on "Excitations in Correlated Systems and Energy Materials (EC-SEM)" Walther-Meißner-Institut, Garching, Germany.
   25. 07. 2013
2. **Lattice dynamics in detwinned $BaFe_2As_2$ as observed via Raman scattering**
   Spring Meeting of the DPG, Regensburg, Germany.
   12. 03. 2013

Alexander Baust

1. **Tunable Coupling between Two Resonators Controlled by a Flux Qubit: the Quantum Switch**
   Spring Meeting of the DPG, Regensburg, Germany.
   13. 03. 2013
2. **Tunable Coupling between Two Resonators Controlled by a Flux Qubit: the Quantum Switch**
   APS March Meeting, Baltimore, USA.
   21. 03. 2013

Thomas Böhm

1. **Band structure and superconductivity in $Ba_{1-x}K_xFe_2As_2$**
   International Miniworkshop on "Excitations in Correlated Systems and Energy Materials (EC-SEM)", Walther-Meißner-Institut, Garching, Germany.
   25. 07. 2013
2. **Superconducting gaps and collective mode in $Ba_{0.6}K_{0.4}Fe_2As_2$ as detected in Raman spectroscopy**
   Stanford Institute for Materials and Energy Science, Stanford National Accelerator Laboratory, Stanford, USA.
   13. 05. 2013
3. **Subdominant d-wave pairing in BKFA**
   Institute of Physics, University of Belgrade, Belgrade, Serbia.
   10. – 14. 12. 2013

Nitin Chelwani

1. **Progress report on tip-enhanced Raman scattering**
   International Miniworkshop on "Excitations in Correlated Systems and Energy Materials (EC-SEM)", Walther-Meißner-Institut, Garching, Germany.
   25. 07. 2013

Frank Deppe

1. **From squeezed microwave light to path entanglement**
   Invited talk, Conference on Resonator QED, Munich, Germany.
   09. – 13. 09. 2013
2. **Tunable and switchable coupling between two superconducting transmission line resonators**
   Invited talk, NIM Workshop "Young Ideas in Nanoscience", Munich, Germany-
   19. – 20. 11. 2013

Hans-Martin Eiter

1. **Helical magnetic order in MnSi**
   International Miniworkshop on "Excitations in Correlated Systems and Energy Materials (EC-SEM)", Walther-Meißner-Institut, Garching, Germany-
   25. 07. 2013

Andreas Erb

1. **Crystal growth of superconducting and magnetically ordering oxides using the TSFZ technique**

Workshop on "Floating Zone Technique", Leibniz Institute for Solid State and Materials Research Dresden, Germany.
20. - 22. 02. 2013

2. **Growth of High-Purity $CaWO_4$ Single Crystals for the Low-Temperature Dark Matter Research Experiments CRESST and EURECA**
Collaborative Conference on Crystal Growth (3CG), Cancun, Mexico.
10. – 13. 06. 2013
3. **Crystal Growth of various Oxides using the TSFZ Technigue**
DGKK-Arbeitskreis-Treffen "Intermetallische und oxidische Systeme mit Spin und Ladungskorrelationen", Vienna, Austria.
26. – 27. 09. 2013
4. **Single crystal growth of various oxide materials for basic research and applications**
Physik-Kolloquium, Universität Leipzig, Germany.
10. 12. 2013

Stephan Geprägs

1. **Magnetoelastic and Magnetoelectric Effects in Extrinsic Multiferroic Hybrid Structures**
510. WE-Heraeus-Seminar, Bad Honnef, Germany.
06. – 09. 01. 2013

Sebastian Gönnenwein

1. **Spin Currents in Magneto-Thermal Landscapes**
12th Joint Intermag/MMM Conference, Chicago, USA-
17. 01. 2013
2. **Spin Currents in Magneto-Thermal Landscapes**
Trends in Nanoscience 2013, Kloster Irsee, Irsee, Germany-
27. 02. 2013
3. **Spin Mechanics in Ferromagnet/Ferroelectric Hybrid Structures**
March Meeting of the American Physical Society, Baltimore, USA-
20. 03. 2013
4. **Spin Current-Based Experiments in Ferromagnet/Normal Metal Hybrids**
Seminarvortrag im SFB-Kolloquium, Universität Hamburg, Germany
07. 05. 2013
5. **Experimental Test of the Spin Mixing Interface Conductivity Concept**
Spin Caloritronics V, Columbus, USA.
23. 05. 2013
6. **Spin Currents in Ferromagnet/Normal Metal Hybrids**
Quantum NanoScience Seminar, TU Delft, The Netherlands.
26. 06. 2013
7. **Spin Seebeck Experiments**
Gordon Research Conference on Spin Dynamics in Nanostructures, Hong Kong, China.
18. 08. 2013
8. **Charge and Spin Currents in Hybrid Structures**
The Kavli Institute for Theoretical Physics Program Sprintronics: Progress in Theory, Materials and Devices, UC Santa Barbara, USA.
10. 10. 2013
9. **Spin Currents in Ferromagnet/Normal Metal Hybrid Structures**
Physik-Kolloquium, Universität Dortmund, Germany.
12. 11. 2013
10. **Spin Currents in Ferromagnet/Normal Metal Hybrid Structures**
Seminar of the Institute of Condensed Matter, École Polytechnique Féderale de Lausanne, Switzerland.
27. 11. 2013

Jan Goetz

1. **Tunable gradiometric flux qubits in circuit-QED experiments**
Spring Meeting of the DPG, Regensburg, Germany.
10. - 15. 03. 2013

Rudolf Gross

1. **Quantum X-tronics: From Quantifiable to Quantum**
   R. Gross
   24. Edgar-Lüscher-Seminar, "Neues aus der Festkörperphysik"
   02 – 08 February, 2013, Klosters, Switzerland.
2. **Fermi Surfaces in Electron-Doped Cuprate Superconductors**
   R. Gross
   Invited Talk, Workshop on "Strongly Correlated Transition Metal Compounds"
   06 – 08 March, 2013, Cologne, Germany.
3. **Hochtemperatur-Supraleitung**
   R. Gross
   Invited Tutorial, 37. Edgar-Lüscher Physikseminar über "Zukunftsmaterialien"
   12 – 14 April, 2013, Zwiesel, Germany.
4. **Quantum Spin Physics with Magnetic Nanostructures**
   R. Gross
   15. 05. 2013
   Kolloquium der Fakultät für Physik, Universität Duisburg-Essen, Germany.
5. **Exploring the Quantum with Superconducting Circuits**
   R. Gross
   Invited Talk, 4. International Conference on Quantum Metrology
   15 – 17 May, 2013, Poznan, Poland.
6. **Exploring the Quantum with Superconducting Circuits**
   R. Gross
   25. 06. 2013
   Großes Physikalisches Kolloquium, Universität zu Köln, Germany.
7. **Exploring Pure Spin Currents and Quantum Spin Physics**
   R. Gross
   Plenary Talk, International Conference on Nanoscale Magnetism (ICNM-2013)
   02 – 06 September, 2013, Istanbul, Turkey.
8. **Nano- und Quantensysteme**
   R. Gross
   19. 10. 2013
   Public Lecture, Day of Open House, Garching, Germany.
9. **Superconducting Quantum Hybrid Systems**
   R. Gross
   Invited Talk, 545. WE-Heraeus-Seminar "Superconducting Proximity and Josephson Effects in Nanoscale Systems"
   19 – 22 November, 2013, Bad Honnef, Germany.
10. **Physics with Pure Spin Currents**
    R. Gross
    10. 12. 2013
    Colloquium of the Indian Institute of Technology Madras, Chennai, India.
11. **Semiconductor-Superconductor Hybrids for Circuit Nano-Electromechanics**
    R. Gross
    Invited Talk, 17^{th} International Workshop on "The Physics of Semiconductor Devices"
    10 – 13 December, 2013, Amity University, Uttar Pradesh, India.
12. **Circuit Nano-Electromechanics**
    R. Gross
    Plenary Talk, International Conference of the International Union of Materials Research Societies, IUMRS-ICA 2013
    16 – 20 December, 2013, Bangalore, India.

Rudolf Hackl

1. **A light scattering study of the evolution of pairing in Fe-based superconductors**
   Spring Meeting of the DPG, Regensburg, Germany
   14. 03. 2013

2. **Charge density wave formation in multiband systems**
   APS March Meeting, Baltimore, USA
   22. 03. 2013
3. **Collective Excitations in Superconductors and Density Wave Systems**
   Colloquium at the Stanford Institute for Materials and Energy Science, Stanford National Accelerator Laboratory, Stanford, USA.
   29. 03. 2013
4. **Fermi surface topology and superconductivity in Fe-based materials**
   International Conference on ŞQuantum in Complex Matter - SuperstripesŤ, Ischia, Italy.
   30. 05. 2013
5. **Spectroscopic evidence of coherence phenomena in superconductors**
   Invited talk at the 6th internal biennial science meeting of the MLZ, Grainau, Germany.
   12. 06. 2013
6. **Raman scattering experiments on gap and collective excitations in Fe-based superconductors**
   Invited talk, International Conference on Spectroscopic in Novel Superconductors (SNS 2013), Berkeley, USA.
   28. 06. 2013
7. **Raman scattering in high-T_c superconductors**
   Festkolloquium on the occasion of the 70th birthday of Werner Hanke and inauguration of the Willy Wien Center, Würzburg, Germany.
   19. 07. 2013
8. **Light scattering experiments in diamond anvil cells**
   MLZ Garching, Germany.
   10. 12. 2013
9. **Electronic Raman scattering and the CDW in RTe_3**
   Institute of Physics, University of Belgrade, Belgrade, Serbia.
   10. – 14. 12. 2013

Toni Helm

1. **High-field magnetotransport in electron doped High-T_c Superconductors**
   Lawrence Berkeley National Laboratory, Berkeley, USA.
   26. 04. 2013
2. **Correlations between superconductivity and symmetry-breaking instabilities in the n-doped cuprate $Nd_{2-x}Ce_xCuO_4$ probed by high-field magnetotransport**
   EMFL User Meeting, Nijmegen, The Netherlands.
   12. – 13. 06. 2013

Hans Hübl

1. **Coupling Phosphorus Donors and Microwave Resonators**
   Silicon Quantum Electronics, Grenoble, France.
   07. – 08. 02. 2013
2. **Two-tone experiments and time domain control in circuit nano-electromechanics high cooperativity in coupled microwave resonator – ferromagnetic insulator hybrids**
   APS Spring Meeting, Baltimore, USA.
   18. – 22. 03. 2013
3. **Two-tone experiments and time domain control in circuit nano-electromechanics**
   Spring Meeting of the DPG, Regensburg, Germany.
   10. – 15. 03. 2013
4. **High cooperativity in coupled microwave resonator – ferromagnetic insulator hybrids**
   GRC Spin Dynamics in Nanostructures, Hong Kong, China.
   18. – 23. 08. 2013
5. **Nano-Opto-Mechnics at Microwave Frequencies**
   Invited talk, Young Ideas in Nanoscience (NIM), Munich, Germany.
   19. – 20. 11. 2013

Mark Kartsovnik

1. **Correlation between Fermi surface transformations and superconductivity in an electron-doped high-Tc superconductors**

Invited talk, International Conference on "Quantum in Complex Matter", Superstripes 2013, Ischia, Italy.
27. 05. – 01. 06. 2013

2. **Molecular organic metals: a playground for electronic interactions and instabilities**
Invited talk, International Symposium "NANO-2013, Knowledge Society: mutual influence and interference of science and society", Chisinau, Moldova.
13. – 16. 09. 2013

Florian Kretzschmar

1. **Fluctuations and spin density wave (SDW) order in $BaFe_2As_2$**
International Miniworkshop on "Excitations in Correlated Systems and Energy Materials (ECSEM)", Walther-Meißner-Institut, Garching, Germany.
25. 07. 2013
2. **Evidence of competing s and d-wave pairing channels in iron-based superconductors**
APS March Meeting, Baltimore, USA.
21. 03. 2013
3. **Evidence of competing s and d-wave pairing channels in iron-based superconductors**
Stanford Institute for Materials and Energy Science, Stanford National Accelerator Laboratory, Stanford, USA.
28. 03. 2013

Edwin Menzel

1. **Entanglement of Continuous-Variable Quantum Microwave**
Spring Meeting of the DPG, Regensburg, Germany.
10. - 15. 03. 2013

Matthias Opel

1. **Spin Transport and Spin Dephasing in Zinc Oxide**
Spring Meeting of the DPG, Regensburg, Germany.
11. 03. 2013
2. **Absence of an induced magnetic moment in Pt on $Y_3Fe_5O_{12}$ (YIG)**
Joint European Magnetic Symposia (JEMS), Rhodos, Greece.
29. 08. 2013
3. **Electrical Spin Transport and Spin Relaxation in Zinc Oxide**
International Workshop on "Semiconductor Spintronics" & Final Meeting of the DFG Priority Program SPP 1285 "Halbleiter-Spintronik", Würzburg, Germany.
30. 09. 2013

Erwin Schuberth

1. **$YbRh_2Si_2$ at ultra-low temperatures**
Technical University, Vienna, Austria.
23. – 24. 01. 2013

Kurt Uhlig

1. **Dry dilution refrigerator with He-4 precool loop**
Cryogenic Engineering Conference 2013, Anchorage, Alaska.
19. 07. 2013

Appointments, Membership in Advisory Boards, etc.

1. **Werner Biberacher** is member of the Scientific Council of the High Magnetic Field Laboratory (LNCMI) Grenoble/Toulouse, France.
2. **Dietrich Einzel** is one of the four spokesmen of the scientific staff of the Bavarian Academy of Sciences and Humanities.
3. **Sebastian Gönnenwein** is associate member of the Cluster of Excellence *Nanosystems Initiative Munich (NIM)*.
4. **Rudolf Gross** is member of the International Advisory Committee of the International Conference M2S HTSC 2015, Geneva, Switzerland.
5. **Rudolf Gross** is member of the International Advisory Committee of the 4th International Conference on Superconductivity and Magnetism-ICSM2014, Antalya, Turkey.
6. **Rudolf Gross** is member of the Scientific Advisory Board of the Leibniz Institute for Solid-State and Materials Research, Dresden.
7. **Rudolf Gross** is member of the Kuratorium of the Physik Journal of the German Physical Society.
8. **Rudolf Gross** is member of the selection committee of the Stern-Gerlach-Medal of the German Physical Society.
9. **Rudolf Gross** is deputy spokesman of the division of *Low Temperature Physics* of the Condensed Matter Section of the German Physical Society.
10. **Rudolf Gross** is spokesman of the Collaborative Research Center 631 on *Solid State Quantum Information Processing* of the German Research Foundation.
11. **Rudolf Gross** is member of the Executive Board of the Cluster of Excellence *Nanosystems Initiative Munich (NIM)* and coordinator of the Research Area 1 on *Quantum Nanosystems*.
12. **Rudolf Gross** is member of the Board of Editors of the European Physical Journal B.
13. **Rudolf Hackl** is deputy coordinator of the DFG Priority Program SPP 1458 on "High Temperature Superconductivity in the Iron Pnictides".
14. **Rudolf Hackl** is member of the evaluation board of the neutron source Heinz Maier-Leibnitz (FRM II).
15. **Mark Kartsovnik** is member of the Selection Committee of EMFL (European Magnetic Field Laboratories) and of the International Advisory Committee of the 10th International Symposium on Crystalline Organic Metals Superconductors and Ferromagnets (ISCOM2013)

Lectures, Seminars, Courses and other Scientific Activities

Several members of Walther-Meißner-Institute give lectures and seminars at the Technische Universität München.

Lectures

Dietrich Einzel

WS 2012/2013
- Mathematische Methoden der Physik I (Mathematical Methods of Physics I)
- Übungen zu Mathematische Methoden der Physik I (Mathematical Methods of Physics I, Problem Sessions)
- WMI-Seminar über aktuelle Fragen der Tieftemperatur-Festkörperphysik (WMI Seminar on Current Topics of Low Temperature Solid-State Physics, with R. Gross, S.B.T. Gönnenwein, H. Hübl, A. Marx, M. Opel, R. Hackl)
- Seminar: Advances in Solid-State Physics (with R. Gross, M. Opel, A. Marx, S.T.B. Gönnenwein)

SS 2013
- Mathematische Methoden der Physik II (Mathematical Methods of Physics II)
- Übungen zu Mathematische Methoden der Physik II (Mathematical Methods of Physics II, Problem Sessions)
- WMI-Seminar über aktuelle Fragen der Tieftemperatur-Festkörperphysik (WMI Seminar on Current Topics of Low Temperature Solid-State Physics, with R. Gross, S.B.T. Gönnenwein, H. Hübl, A. Marx, M. Opel, R. Hackl)
- Seminar: Advances in Solid-State Physics (with R. Gross, M. Opel, A. Marx, S.T.B. Gönnenwein)

WS 2013/2014
- Mathematische Methoden der Physik I (Mathematical Methods of Physics I)
- Übungen zu Mathematische Methoden der Physik I (Mathematical Methods of Physics I, Problem Sessions)
- WMI-Seminar über aktuelle Fragen der Tieftemperatur-Festkörperphysik (WMI Seminar on Current Topics of Low Temperature Solid-State Physics, with R. Gross, S.B.T. Gönnenwein, H. Hübl, A. Marx, M. Opel, R. Hackl)
- Seminar: Advances in Solid-State Physics (with R. Gross, M. Opel, A. Marx, S.T.B. Gönnenwein)

Frank Deppe

WS 2012/2013
- Supraleitung und Tieftemperaturphysik I (Superconductivity and Low Temperature Physics I, with R. Gross)
- Übungen zu Supraleitung und Tieftemperaturphysik I (Superconductivity and Low Temperature Physics I, Problem Sessions)
- Seminar: Advances in Solid-State Physics (with R. Gross, M. Opel, A. Marx, S.T.B. Gönnenwein, D. Einzel)
- Seminar: Supraleitende Quantenschaltkreise (mit R. Gross, A. Marx) (Seminar on Superconducting Quantum Circuits)

SS 2013
- Supraleitung und Tieftemperaturphysik II (Superconductivity and Low Temperature Physics II, with R. Gross)
- Übungen zu Supraleitung und Tieftemperaturphysik II (Superconductivity and Low Temperature Physics II, Problem Sessions)
- Angewandte Supraleitung: Josephson Effekte, supraleitende Elektronik und supraleitende Quantenschaltkreise (Applied Superconductivity: Josephson Effects, Superconducting Electronics and Superconducting Quantum Circuits, with R. Gross)
- Seminar: Advances in Solid-State Physics (with R. Gross, M. Opel, A. Marx, S.T.B. Gönnenwein, D. Einzel)
- Seminar: Supraleitende Quantenschaltkreise (mit R. Gross, A. Marx) (Seminar on Superconducting Quantum Circuits)

WS 2013/2014
- Seminar: Advances in Solid-State Physics (with R. Gross, M. Opel, A. Marx, S.T.B. Gönnenwein, D. Einzel)
- Seminar: Supraleitende Quantenschaltkreise (mit R. Gross, A. Marx) (Seminar on Superconducting Quantum Circuits)

Rudolf Gross

WS 2012/2013
- Supraleitung und Tieftemperaturphysik I (Superconductivity and Low Temperature Physics I)
- Übungen zu Supraleitung und Tieftemperaturphysik I (Superconductivity and Low Temperature Physics I, Problem Sessions)
- WMI-Seminar über aktuelle Fragen der Tieftemperatur-Festkörperphysik (WMI Seminar on Current Topics of Low Temperature Solid-State Physics, with D. Einzel, S.T.B. Gönnenwein, R. Hackl, H. Hübl, A. Marx, M. Opel)
- Seminar: Advances in Solid-State Physics (with D. Einzel, S.T.B. Gönnenwein, R. Hackl, H. Hübl, A. Marx, M. Opel)
- Seminar: Superconducting Quantum Circuits (with F. Deppe, A. Marx)
- Festkörperkolloquium (Colloquium on Solid-State Physics, with D. Einzel)

SS 2013
- Supraleitung und Tieftemperaturphysik II (Superconductivity and Low Temperature Physics II)
- Übungen zu Supraleitung und Tieftemperaturphysik II (Superconductivity and Low Temperature Physics II, Problem Sessions)
- Angewandte Supraleitung: Josephson Effekte, supraleitende Elektronik und supraleitende Quantenschaltkreise (Applied Superconductivity: Josephson Effects, Superconducting Electronics and Superconducting Quantum Circuits, with F. Deppe)
- Übungen zu Angewandte Supraleitung: Josephson Effekte, supraleitende Elektronik und supraleitende Quantenschaltkreise (Applied Superconductivity: Josephson Effects, Superconducting Electronics and Superconducting Quantum Circuits, Problem Sessions, with F. Deppe)
- Seminar: Advances in Solid-State Physics (with D. Einzel, S.T.B. Gönnenwein, R. Hackl, H. Hübl, A. Marx, M. Opel)
- WMI-Seminar über aktuelle Fragen der Tieftemperatur-Festkörperphysik (WMI Seminar on Current Topics of Low Temperature Solid-State Physics, with D. Einzel, S.T.B. Gönnenwein, R. Hackl, H. Hübl, A. Marx, M. Opel)

- Seminar: Superconducting Quantum Circuits (with F. Deppe, A. Marx)
- Festkörperkolloquium (Colloquium on Solid-State Physics, with D. Einzel)
- Ferienakademie: Kurs 3 "Physik und Elektronik im Alltag" (Ferienakademie: Course 3 "Physics and Electronics in Everyday Life")

WS 2013/2014
- Physik der Kondensierten Materie I (Condensed Matter Physics I)
- Übungen zu Physik der Kondensierten Materie I (Condensed Matter Physics I, Problem Sessions, with S. Geprägs)
- WMI-Seminar über aktuelle Fragen der Tieftemperatur-Festkörperphysik (WMI Seminar on Current Topics of Low Temperature Solid-State Physics, with D. Einzel, S.T.B. Gönnenwein, R. Hackl, H. Hübl, A. Marx, M. Opel)
- Seminar: Advances in Solid-State Physics (with D. Einzel, S.T.B. Gönnenwein, R. Hackl, H. Hübl, A. Marx, M. Opel)
- Seminar: Superconducting Quantum Circuits (with F. Deppe, A. Marx)
- Festkörperkolloquium (Colloquium on Solid-State Physics, with D. Einzel)

Sebastian T.B. Gönnenwein

WS 2012/2013
- Seminar: Advances in Solid-State Physics (with R. Gross, A. Marx, M. Opel)
- Magnetismus (Magnetism)
- Übungen zu Magnetismus (Magnetism, Problem Sessions)
- WMI-Seminar über aktuelle Fragen der Tieftemperatur-Festkörperphysik (WMI Seminar on Current Topics of Low Temperature Solid State Physics, with R. Gross, D. Einzel, H. Hübl, A. Marx, M. Opel, R. Hackl)
- Seminar zu aktuellen Fragen der Magneto- und Spinelektronik (Seminar on Current Topics in Magneto and Spin Electronics, with M. Brandt, H. Hübl)

SS 2013
- Seminar: Advances in Solid-State Physics (with R. Gross, A. Marx, M. Opel)
- Spin Electronics
- Übungen zu Spin Electronics (Exercises to Spin Electronics)
- WMI-Seminar über aktuelle Fragen der Tieftemperatur-Festkörperphysik (WMI Seminar on Current Topics of Low Temperature Solid State Physics, with R. Gross, D. Einzel, H. Hübl, A. Marx, M. Opel, R. Hackl)
- Seminar zu aktuellen Fragen der Magneto- und Spinelektronik (Seminar on Current Topics in Magneto and Spin Electronics, with M. Brandt, H. Hübl)

WS 2013/2014
- Seminar: Advances in Solid-State Physics (with R. Gross, A. Marx, M. Opel)
- Magnetismus (Magnetism)
- Übungen zu Magnetismus (Magnetism, Problem Sessions)
- WMI-Seminar über aktuelle Fragen der Tieftemperatur-Festkörperphysik (WMI Seminar on Current Topics of Low Temperature Solid State Physics, with R. Gross, D. Einzel, H. Hübl, A. Marx, M. Opel, R. Hackl)

- Seminar zu aktuellen Fragen der Magneto- und Spinelektronik (Seminar on Current Topics in Magneto and Spin Electronics, with M. Brandt, H. Hübl)

Rudi Hackl

WS 2012/2013
- Seminar: Advances in Solid-State Physics (with R. Gross, S.T.B. Gönnenwein, H. Hübl, A. Marx, M. Opel)
- WMI-Seminar über aktuelle Fragen der Tieftemperatur-Festkörperphysik (WMI Seminar on Current Topics of Low Temperature Solid-State Physics, with R. Gross, S.B.T. Gönnenwein, H. Hübl, A. Marx, M. Opel, D. Einzel)

WS 2013/2014
- Low Temperature Physics and Superconductivity I (with R. Gross)
- Exercises to Low Temperature Physics and Superconductivity I
- Seminar: Advances in Solid-State Physics (with R. Gross, S.T.B. Gönnenwein, H. Hübl, A. Marx, M. Opel)
- WMI-Seminar über aktuelle Fragen der Tieftemperatur-Festkörperphysik (WMI Seminar on Current Topics of Low Temperature Solid-State Physics, with R. Gross, S.B.T. Gönnenwein, H. Hübl, A. Marx, M. Opel, D. Einzel)

Hans Hübl

WS 2012/2013
- Seminar: Spin Caloritronics and Spin Pumping
- Seminar: Advances in Solid-State Physics (with R. Gross, D. Einzel, S.T.B. Gönnenwein, A. Marx, M. Opel)
- WMI-Seminar über aktuelle Fragen der Tieftemperatur-Festkörperphysik (WMI Seminar on Current Topics of Low Temperature Solid State Physics, with R. Gross, D. Einzel, S.T.B. Gönnenwein, A. Marx, M. Opel, R. Hackl)
- Seminar zu aktuellen Fragen der Magneto- und Spinelektronik (Seminar on Current Topics in Magneto and Spin Electronics, with S.T.B. Gönnenwein, M. S. Brandt)

SS 2013
- Seminar: Spin Caloritronics and Spin Pumping
- Seminar: Advances in Solid-State Physics (with R. Gross, D. Einzel, S.T.B. Gönnenwein, A. Marx, M. Opel)
- WMI-Seminar über aktuelle Fragen der Tieftemperatur-Festkörperphysik (WMI Seminar on Current Topics of Low Temperature Solid State Physics, with R. Gross, D. Einzel, S.T.B. Gönnenwein, A. Marx, M. Opel, R. Hackl)
- Seminar zu aktuellen Fragen der Magneto- und Spinelektronik (Seminar on Current Topics in Magneto and Spin Electronics, with S.T.B. Gönnenwein, M. S. Brandt)

WS 2013/2014
- Seminar: Spin Caloritronics and Spin Pumping
- Seminar: Advances in Solid-State Physics (with R. Gross, D. Einzel, S.T.B. Gönnenwein, A. Marx, M. Opel)
- WMI-Seminar über aktuelle Fragen der Tieftemperatur-Festkörperphysik (WMI Seminar on Current Topics of Low Temperature Solid State Physics, with R. Gross, D. Einzel, S.T.B. Gönnenwein, A. Marx, M. Opel, R. Hackl)

- Seminar zu aktuellen Fragen der Magneto- und Spinelektronik (Seminar on Current Topics in Magneto and Spin Electronics, with S.T.B. Gönnenwein, M. S. Brandt)

Anton Lerf

WS 2012/2013

- Moderne Aspekte der Chemie für Physiker I (Modern Aspects of Chemistry for Physicists I)

ïż£

The WMI Seminars

The Friday Seminar – Walther-Meißner-Seminar on Current Topics in Low Temperature Physics

WS 2012/2013:

1. **Dynamics in Quantum Antiferromagnets**
   Prof. Dr. Goetz Uhrig, Lehrstuhl für Theoretische Physik I, Technische Universität Dortmund, Germany
   26. 11. 2012
2. **Exotic phases of matter: from critical metals to chiral magnets**
   Prof. Dr. Markus Garst, Institut für Theoretische Physik, Universität zu Köln, Germany
   03. 12. 2012
3. **Quantum Transport in Hybrid Nanosystems**
   Prof. Dr. Jürgen König, Fakultät für Physik, Universität Duisburg-Essen, Germany
   04. 12. 2012
4. **A Quantum Impurity Perspective on Strongly Correlated Systems**
   Prof. Dr. Walter Hofstetter, Institut für Theoretische Physik, Johann Wolfgang Goethe-Universität Frankfurt, Germany
   10. 12. 2012
5. **Progress in Quantum Monte Carlo Simulations: recent highlights and future prospects**
   Prof. Dr. Lode Pollet, Theoretische Nanophysik, LMU München, Germany
   23. 01. 2013
6. **Be Entrepreneurial! Opportunities for founders at TUM**
   Harald Jenull, UnternehmerTUM GmbH, Garching, Germany
   01. 02. 2013
7. **Raman Scattering in Multiband Systems**
   Dr. Elizabeth A. Nowadnick, Stanford Institute for Materials and Energy Sciences (SIMES), Stanford University, Stanford, USA
   08. 02. 2013
8. **Giant and reversible extrinsic magnetocaloric effects in manganite films due to strain**
   Dr. Neil D. Mathur, Department of Materials Science and Metallurgy, University of Cambridge, United Kingdom
   18. 02. 2013

SS 2013:

9. **Magnetism studies in TM-doped ZnO-based structures**
   Prof. Dr. Nikolai Sobolev, Departamento de Fisica, Universidade De Aveiro, Portugal
   26. 04. 2013
10. **Multiband, paramagnetic effects and vortices in KFe_2As_2**
    Dr. Frédéric Hardy, Karlsruher Institut für Technologie (KIT), Karlsruhe
    17. 05. 2013
11. **Superconducting Artificial Atom with Two Degrees of Freedom**
    Dr. Olivier Buisson, Institut Neel, CNRS & Université Joseph Fourier & INP-Grenoble, France
    24. 05. 2013
12. **Towards a spin-ensemble quantum memory for superconducting qubits**
    Dr. Patrice Bertet, Research Group in Quantum Electrics, Gif-sur-Yvette, France
    07. 06. 2013
13. **Geometric phases for robust quantum gates in circuit QED**
    Dr. Stefan Filipp, Laboratorium für Festkörperphysik, ETH Zürich, Switzerland
    14. 06. 2013
14. **Calculating the Electronic Structure of Materials with Strong Electronic Coulomb Correlations from First Principles? – Where do we stand?**

Prof. Dr. Silke Biermann, Centre de Physique Théorique – UMR 7644 EPFL, Lausanne, Switzerland
21. 06. 2013

15. **Fluxons for quantum circuits**
Dipl.-Phys. Kirill Fedorov, Karlsruhe Institute of Technology, Karlsruhe, Germany
21. 06. 2013
16. **Quantum corrections for low temperature electrical conductivity of $Si_xZn_{1-x}O$ thin films**
Prof. Dr. Lalit Kukreja, Laser Materials Processing Division, Raja Ramanna Centre for Advanced Technology, Indore, India
28. 06. 2013
17. **Listening to the brain with high-T_c SQUIDs**
Prof. Dr. Dag Winkler, Chalmers University of Technology, Göteborg, Sweden
05. 07. 2013
18. **Acoustic Microscopy as a Probe for Magnons**
Prof. Dr. Andrew Briggs, University of Oxford, United Kingdom
10. 07. 2013
19. **New Directions in Spin Current Research at NIST, Boulder**
Prof. Dr. Tom Silva, The National Institute of Standards and Technology Boulder, Colorado, USA
29. 07. 2013
20. **Raman scattering study in alkali-doped transition metal selenides**
Dr. Nenad Lazarevic, Institute of Physics, University of Belgrade, Serbia
05. 09. 2013
21. **Nanomechanics in the quantum regime-from quantum optics with phonons to hybrid quantum systems**
Dr. Jörg Bochmann, University of California, Santa Barbara, USA
16. 09. 2013

WS 2013/2014:

22. **Single-shot readout of superconducting flux qubit using a Josephson parametric amplifier**
Dr. Tsuyoshi Yamamoto, NEC Smart Energy Research Laboratories, NEC Corporation Tsukuba, Ibaraki, Japan
16. 10. 2013
23. **Hunds Metallicity in Iron-based Superconductors**
Dr. Markus Aichhorn, Institute of Theoretical and Computational Physics, Technische Universität Graz, Austria
08. 11. 2013
24. **Fine structure of the Kondo resonance in ultraclean carbon nanotube quantum dots**
Dr. Andreas Hüttel, Institut für Experimentelle und Angewandte Physik, Universität Regensburg, Germany
15. 11. 2013
25. **Superconducting qubits: sidebands, cavities, and vortices**
Prof. Dr. Britton Plourde, Physics Departments, Syracuse University, Syracuse, USA
22. 11. 2013

Topical Seminar on Advances in Solid State Physics – WS 2012/2013, SS 2013 and WS 2013/2014

WS 2012/2013:

1. **Preliminary discussion and assignment of topics**
R. Gross, Walther-Meißner-Institut
16. 10. 2012, 23. 10. 2012
2. **Spin Seebeck Insulator**
Niklas Roschewsky, Technische Universität München
20. 11. 2012

3. **Response and collective modes in non-cetrosymmetric superconductors**
   Nikolaj Bittner, Walther-Meißner-Institut
   27. 11. 2012
4. **Determination of the energy gap in superconductors via scanning tunneling spectroscopy**
   Andreas Walter, Technische Universität München
   04. 12. 2012
5. **Quantum coherent coupling of a mechanical oscillator to an optical cavity mode**
   Marco Bobinger, Technische Universität München
   11. 12. 2012
6. **Storing Quantum Information in Spin Systems – Concepts and Perspectives**
   Jochen Bissinger, Technische Universität München
   18. 12. 2012
7. **Inverse Spin Hall Effect**
   Johannes Mendil, Technische Universität München
   15. 01. 2013
8. **Electrical control of the ferromagnetic phase transition in cobalt at room temperature**
   Philipp Metzner, Technische Universität München
   22. 01. 2013

SS 2013:

9. **Preliminary discussion and assignment of topics**
   Rudolf Gross, Walther-Meißner-Institut, Garching
   16. 04. 2013, 23. 04. 2013
10. **How to write a bachelor thesis**
    Rudolf Gross, Walther-Meißner-Institut, Garching
    30. 04. 2013
11. **Nanoscale magnetic sensing and imaging**
    Hannah Schamoni, Technische Universität München
    28. 05. 2013
12. **Electronic readout of a single nuclear spin using a molecular spin transistor**
    Alexander Backs, Technische Unversität München
    11. 06. 2013
13. **Magnetization mapping with the anomalous Nernst effect (ANE)**
    Klara Beltinger, Technische Unversität München
    25. 06. 2013
14. **Organic superconductor as a low-temperature pressure gauge**
    Ismail Achmed-Zade, Technische Universität München
    25. 06. 2013
15. **Pressure sensors based on Carbon Nanotubes (CNTs)**
    Philipp Köhler, Technische Universität München
    02. 07. 2013
16. **Study of $BaFe_2As_2$ with applied hydrostatic pressure**
    Ali Özkü, Technische Universität München
    08. 07. 2013
17. **Effect of uniaxial pressure on the phase transition in $BaFe_2As_2$**
    Daniel Jost, Technische Universität München
    08. 07. 2013
18. **Photonic quantum simulators**
    Lujun Wang, Technische Universität München
    09. 07. 2013
19. **Magnetic Field Controlled Reconfigurable Semiconductor Logic**
    Andreas Wörfel, Technische Universität München
    16. 07. 2013
20. **Memristive Devices for Computing**
    Stephan Saller, Technische Universität München
    23. 07. 2013

WS 2013/2014:

21. **Preliminary discussion and assignment of topics**
    R. Gross, Walther-Meißner-Institut
    15. 10. 2013, 22. 10. 2013
22. **Heat Flux between Nanosystems and Entropy Produced by Thermal Fluctuations**
    Gustav Andersson, Technische Universität München
    12. 11. 2013
23. **Exciting Andreev pairs in a superconducting atomic contact**
    Sheng-da Wang, Technische Universität München
    19. 11. 2013
24. **Storing Information in Magnetic Skyrmions**
    Johannes Lang, Technische Universität München
    26.11.2013
25. **One Year Research in Alabama**
    Matthias Althammer, Walther-Meißner-Institut, Garching
    03. 12. 2013
26. **Bounding the pseudogap with a line of phase transitions in $YBa_2Cu_3O_{6+\delta}$**
    Vasileios Tzanos, Walther-Meißner-Institut, Garching
    10. 12. 2013
27. **Extremely Large Magnetoresistance in the Nonmagnetic Metal $PdCoO_2$**
    Ludwig Schaidhammer, Technische Universität München
    14. 01. 2014
28. **Ultrahigh Magnetoresistance at Room Temperature in Molecular Wires**
    Florian Schäble, Technische Universität München
    21. 01. 2014

Topical Seminar: Spin Caloritronics and Spin Pumping – WS 2012/2013, SS 2013

WS 2012/2013:

1. **Preliminary discussion and assignment of topics**
   Hans Hübl, Walther-Meißner-Institut
   17. 10. 2012, 24. 10. 2012
2. **Thermoelectric effects without a spin**
   Julia Winnerl, Technische Universität München
   05. 12. 2012
3. **Ferromagnetic Resonance**
   Andreas Rauscher, Technische Universität München
   19. 12. 2012
4. **Spin Hall effect**
   Friedrich Witek, Technische Universität München
   09. 01. 2013
5. **Spin Seebeck effect**
   Hans Hübl, Walther-Meißner-Institut
   16. 01. 2013
6. **Spin Peltier effect**
   Andreas Duensing, Technische Universität München
   23. 01. 2013

SS 2013:

7. **Preliminary discussion and assignment of topics**
   Hans Hübl, Walther-Meißner-Institut
   17. 04. 2013, 24. 04. 2013

8. **Electron Spin Resonance Spectrometers**
   Jonannes Ehrmaier, Technische Universität München
   16. 05. 2013
9. **Strong Coupling in Spin Ensembles**
   Kathrin Ganzhorn, Technische Universität München
   23. 05. 2013
10. **Equation of Motion of Paramagnetic Spin Systems**
    Kai Müller, Technische Universität München
    06. 06. 2013
11. **Spin Mechanics – The Static Limit**
    Malte Kremmser, Technische Universität München
    13. 06. 2013
12. **Torque Magnetometry with Quartz Tuning Forks**
    Stefan Klimesch, Technische Universität München
    13. 06. 2013
13. **Fabrication of Pyrochlore Iridate Thin Films**
    Michaela Lammel, Technische Universität München
    20. 06. 2013
14. **Strong Coupling in Exchange Coupled Spin Systems**
    Christian Vogl, Technische Universität München
    27. 06. 2013
15. **Transport in Graphene Nanoribbons**
    Markus Manz, Technische Universität München
    04. 07. 2013
16. **Impedance-Matched Electrical Study of Magnetization Dynamics**
    Korbinian Baumgärtl, Technische Universität München
    04. 07. 2013
17. **Determination of the Spin Diffusion Length in Ferromagnetic Insulator / Metal Thin Film Structures**
    Richard Schlitz, Technische Universität München
    11. 07. 2013
18. **Spin Hall Magnetoresistance in F/N/F Trilayers**
    Dominik Irber, Technische Universität München
    11. 07. 2013
19. **Fabrication of the Ferromagnetic Insulator / Normal Metal Hybrid Structures**
    Marc Schneider, Technische Universität München
    18. 07. 2013
20. **Fabrication of FMI/NM/FMI Trilayers**
    Felix Schade, Technische Universität München
    18. 07. 2013

Topical Seminar on Superconducting Quantum Circuits – WS 2012/2013, SS 2013 and WS 2013/2014

WS 2012/2013:

1. **Preliminary discussion and assignment of topics**
   F. Deppe, A. Marx, R. Gross, Walther-Meißner-Institut
   16. 10. 2012, 23. 10. 2012
2. **Hybrid circuit cavity quantum electrodynamics with a micromechanical resonator**
   Fredrik Hocke, Walther-Meißner-Institut, Garching
   13. 11 .2012
3. **Progress Report**
   Franz Sterr, Walther-Meißner-Institut, Garching
   20. 11. 2012
4. **Computing prime factors with a Josephson phase qubit quantum precessor**
   Stefan Zenger, Technische Universität München

27. 11. 2012

5. **Observation of Entanglement between Itinerant Microwave Photons and a Superconducting Qubit**
   Miriam Müting, Technische Universität München
   11. 12. 2012
6. **Stabilizing Rabi oscillations in a superconducting qubit using quantum feedback**
   Michael Fischer, Technische Universität München
   08. 01. 2013
7. **Quantum Simulation of Tunneling in Small Systems**
   Jan Goetz, Walther-Meißner-Institut, Garching
   22. 01. 2013
8. **Josephson junction embedded transmission-line resonators: from Kerr medium to in-line transmon**
   Friedrich Wulschner, Walther-Meißner-Institut, Garching
   05. 02. 2013
9. **A Josephson quantum electron pump**
   Ling Zhong, Walther-Meißner-Institut, Garching
   19. 02. 2013

SS 2013:

10. **Preliminary discussion and assignment of topics**
    F. Deppe, A. Marx, R. Gross, Walther-Meißner-Institut
    16. 04. 2013
11. **Vacuum Rabi Splitting in a Semiconductor Circuit QED Systems**
    Elisabeth Hoffmann, Walther-Meißner-Institut, Garching
    23. 04. 2013
12. **Realization of Deterministic Quantum Teleportation with Solid State Qubits**
    Peter Eder, Walther-Meißner-Institut, Garching
    30. 04. 2013
13. **Simulating accelerated atoms coupled to a quantum field**
    Jan Goetz, Walther-Meißner-Institut, Garching
    14. 05. 2013
14. **A wideband, low-noise superconducting amplifier with high dynamic range**
    Ling Zhong, Walther-Meißner-Institut, Garching
    28. 05. 2013
15. **Superconducting resonators for experiments with flux qubits / Setup of a microwave interferometer**
    Hans-Peter Gürtner, Stefan Gantner, Technische Universität München
    04. 06. 2013
16. **Nanoscale Josephson junction fabrication for flux qubits / Atomic force microscopy on nanoscale Josephson junctions**
    Edwar Xie / Dominik Müller, Walther-Meißner-Institut, Garching / Technische Universität München
    11. 06. 2013
17. **Probing Correlations, Indistinguishability and Entanglement in Microwave Two-Photon Interference**
    Karl Friedrich Wulschner, Walther-Meißner-Institut, Garching
    18. 06. 2013
18. **Catch and Release of Microwave Photon States**
    Udo Schaumburger, Technische Universität München
    25. 06. 2013
19. **Coherent state transfer between itinerant microwave fields and a mechanical oscillator**
    Matthias Pernpeintner, Walther-Meißner-Institut, Garching
    02. 07. 2013
20. **Multimode mediated qubit-qubit coupling and dark-state symmetries in circuit quantum electrodynamics**

Max Häberlein, Walther-Meißner-Institut, Garching
09. 07. 2013

21. **Towards on-chip superconducting interferometer**
Ferdinand Loacker, Walther-Meißner-Institut, Garching
16. 07. 2013

WS 2013/2014:

22. **Preliminary discussion and assignment of topics**
F. Deppe, A. Marx, R. Gross, Walther-Meißner-Institut
15. 10. 2013, 22. 10. 2013
23. **Progress Report**
Kirill Fedorov, Ling Zhong, Walther-Meißner-Institut, Garching
26. 11. 2013
24. **Electron spin resonance detected by a superconducting qubit**
Alexander Baust, Christoph Zollitsch, Walther-Meißner-Institut, Garching
10. 12. 2013
25. **Nonlinear optics quantum computing with circuit QED**
Edwin Menzel, Max Häberlein, Walther-Meißner-Institut, Garching
07. 01. 2014
26. **Dc SQUID coupled to mechanical oscillator**
Matthias Pernpeintner, Karl Friedrich Wulschner, Walther-Meißner-Institut, Garching
21. 01. 2014
27. **Towards Realizing a Quantum Memory for a Superconducting Qubit: Storage and Retrieval of quantum states**
Manuel Schwarz, Jan Goetz, Walther-Meißner-Institut, Garching
04. 02. 2014

C: Solid State Colloquium

The WMI has organized the Solid-State Colloquium of the Faculty of Physics in WS 2012/2013, SS 2013, and WS 2013/2014. The detailed program can be found on the WMI webpage: http://www.wmi.badw-muenchen.de/teaching/Seminars/fkkoll.html.

Staff of the Walther-Meißner-Institute

Director
Prof. Dr. Rudolf Gross

Deputy Director
Dr. Werner Biberacher

Technical Director
Dr. Achim Marx

Administration/Secretary's Office
Ludwig Ossiander

Emel Dönertas

Scientific Staff
Dr. Matthias Althammer
Dr. Frank Deppe
Priv.-Doz. Dr. habil. Dietrich Einzel
Prof. Dr. Andreas Erb
Dr. Kirill Fedorov
Dr. Stephan Geprägs
Priv.-Doz. Dr. habil. Sebastian Gönnenwein
Priv.-Doz. Dr. habil. Rudolf Hackl
Dr. Hans Hübl
Dr. Mark Kartsovnik
Dr. Edwin Menzel
Dr. Matthias Opel

Dipl.-Phys. Andreas Baum
Dipl.-Phys. Alexander Baust
Dipl.-Phys. Thomas Böhm
Dipl.-Phys. Nitin Chelwani
Dipl.-Phys. Peter Eder
Dipl.-Phys. Hans-Martin Eiter
Dipl.-Phys. Jan Goetz
Dipl.-Phys. Max Häberlein
Dipl.-Phys. Florian Kretzschmar
Dipl.-Phys. Michael Kunz
Dipl.-Phys. Johannes Lotze
Dipl.-Phys. Hannes Maier-Flaig
Dipl.-Phys. Sibylle Meyer
Dipl.-Phys. Matthias Pernpeintner
Dipl.-Phys. Michael Schreier
Dipl.-Phys. Manuel Schwarz
Dipl.-Phys. Karl Friedrich Wulschner
Dipl.-Phys. Edward Xie
Dipl.-Phys. Ling Zhong
Dipl.-Phys. Christoph Zollitsch

Technical Staff
Peter Binkert
Thomas Brenninger, M.Sc.
Dipl.-Ing. (FH) Ulrich Guggenberger
Dieter Guratzsch
Astrid Habel
Karen Helm-Knapp
Dipl.-Ing. (FH) Josef Höss
Julius Klaus

Robert Müller
Jan Naundorf
Georg Nitschke
Christian Reichlmeier
Alexander Rössl
Harald Schwaiger
Helmut Thies
Siegfried Wanninger

Assistants
Sybilla Plöderl

Brigitte Steinberg

Permanent Guests

Prof. Dr. B. S. Chandrasekhar
Dr. Robert Doll
Dr. Karl Neumaier
Dr. Kurt Uhlig
Dr. Christian Probst
Prof. Dr. Erwin Schuberth

Guest Researchers

1. Prof. Dr. B.S. Chandrasekhar
   permanent guest
2. Dr. Robert Doll
   permanent guest
3. Dr. Karl Neumaier
   permanent guest
4. Dr. Christian Probst
   permanent guest
5. Prof. Dr. Erwin Schuberth
   permanent guest
6. Dr. Kurt Uhlig
   permanent guest
7. Evgeniy Zamburg, Taganrog Institute of Technology, Southern Federal University, Taganrog, Russia
   01. 10. 2012 - 28. 02. 2013
8. Daniil Vakulov, Taganrog Institute of Technology, Southern Federal University, Taganrog, Russia
   19. 01. - 04. 02. 2013
9. David Zueco, Universidad de Zaragoza, Spain
   26. 01. - 03. 02. 2013
10. Isaac Fernando Quijandria Diaz, Universidad de Zaragoza, Spain
    26. 01. - 03. 02. 2013
11. Dr. Alexander Kemper, Lawrence Berkeley Laboratory, USA
    06. 02. - 09. 02. 2013
12. Dr. Elizabeth Nowadnick, Stanford University, Stanford, USA
    06. 02. - 09. 02. 2013
13. Dr. Neil D. Mathur, University of Cambridge, U.K.
    17. 02. - 18. 02. 2013
14. Julen Simon Pedernales, Universidad del Pais Vasco, Bilbao, Spain
    25. 02. - 09. 03. 2013, 14. 09. - 21. 09. 2013
15. Dr. Jorge Casanova, Universidad del Pais Vasco, Bilbao, Spain
    25. 02. - 09. 03. 2013
16. Akashdeep Kamra, Kavli Institute of Nanoscience, Delft University of Technology, Delft, The Netherlands
    08. 04. - 09. 06. 2013
17. Prof. Enrique Solano, Universidad del Pais Vasco, Bilbao, Spain
    17. 04. - 19. 04. 2013
18. Prof. Nikolei Sobolev, University of Aveiro, Portugal
    25. 04. - 26. 04. 2013
19. Roberto Di Candia, Universidad del Pais Vasco, Bilbao, Spain
    05. 05. - 12. 05. 2013, 26. 06. - 03. 07. 2013, 14. 09. - 21. 09. 2013
20. Prof. Lalit M. Kukreja, Raja Ramanna Centre for Advanced Technology, Indore, India
    26. 06. - 28. 06. 2013
21. Dr. Natasha Kushch, Institute of Problems of Chemical Physics, Chernogolovka, Russia
    26. 06. - 02. 07. 2013
22. Prof. Juan Poyato Ferrera, Instituto de Ciencia de Materiales, Sevilla, Spain

01. 07. - 30. 07. 2013

23. Dr. Brain Moritz, Stanford Institute of Materials and Energy Science, Stanford, USA
    23. 07. - 27. 07. 2013
24. Prof. Zoran Popovic, University of Belgrade, Belgrade, Serbia
    01. 09. - 07. 09. 2013
25. Dr. Nedad Lazarevic, University of Belgrade, Belgrade, Serbia
    01. 09. - 07. 09. 2013, 18. 11. - 23. 11. 2013
26. Prof. Vladimir Zverev, Institute of Solid Physics, Chernogolovka, Russia
    25.09. - 26.10.2013
27. Dr. Darko Tanaskovic, University of Belgrade, Belgrade, Serbia
    18. 11. - 23. 11. 2013
28. Milan Radonjic, University of Belgrade, Belgrade, Serbia
    18. 11. - 23. 11. 2013
29. Prof. Alfred Zawadowski, Budapest University of Technology and Economics, Budapest, Hungary
    01. 12. - 07. 12. 2013

Commission for Low Temperature Physics

Members of the Commission for Low Temperature Research of the Bavarian Academy of Sciences and Humanities:

Vollhardt, Dieter, chairman (Universität Augsburg)
Abstreiter, Gerhard, deputy chairman (Technische Universität München)
Bloch, Immanuel (Ludwig-Maximilians-Universität München)
Gross, Rudolf (Walther-Meißner-Institut)
Kaiser, Wolfgang (Technische Universität München)
Hänsch, Theodor (Max-Planck-Institut für Quantenoptik, Garching)
Schwoerer, Markus (Universität Bayreuth)
Weiss, Dieter (Universität Regensburg)